MULTICOMPONENT ADSORPTION OF PHENOLIC COMPOUNDS FROM AQUEOUS SOLUTION

A THESIS

Submitted in partial fulfilment of the requirements for the award of the degree of

DOCTOR OF PHILOSOPHY

in

CHEMICAL ENGINEERING

by

SURESH S.

M.G. CENTRAL LIBRARY
ACC.No. G21290
Date 26/4/12
I.I.T. ROORKEE

DEPARTMENT OF CHEMICAL ENGINEERING
INDIAN INSTITUTE OF TECHNOLOGY ROORKEE
ROORKEE-247 667 (INDIA)

JULY, 2010

©INDIAN INSTITUTE OF TECHNOLOGY ROORKEE, ROORKEE, 2010
ALL RIGHTS RESERVED

INDIAN INSTITUTE OF TECHNOLOGY ROORKEE

CANDIDATE'S DECLARATION

I hereby certify that the work which is being presented in the thesis entitled **MULTICOMPONENT ADSORPTION OF PHENOLIC COMPOUNDS FROM AQUEOUS SOLUTION** in partial fulfilment of the requirements for the award of the Degree of Doctor of Philosophy and submitted in the Department of Chemical Engineering of the Indian Institute of Technology Roorkee is an authentic record of my own work carried out during a period from July 2007 to July 2010 under the supervision of Dr. V. C. Srivastava, Assistant Professor, Department of Chemical Engineering and Dr. I. M. Mishra, Professor, Department of Chemical Engineering and Dean, Saharanpur Campus, Indian Institute of Technology Roorkee, Roorkee.

The matter presented in this thesis has not been submitted by me for the award of any other degree of this or any other Institute.

(SURESH S.)

This is to certify that the above statement made by the candidate is correct to the best of our knowledge.

Date: July 24 , 2010

Dr. I. M. MISHRA
Supervisor

Dr. V. C. SRIVASTAVA
Supervisor

The Ph.D. Viva-Voce Examination of **Mr. SURESH S.**, Research Scholar, has been held on ...10-12-10...

Signature of Supervisors

Signature of External Examiner

ABSTRACT

Phenol and its derivatives (P_s) and its associated compounds, like Aniline (AN), Phenol (P), 4-chlorophenol (CP), 4-nitrophenol (NP), catechol (C), resorcinol (R) and Hydroquinone (HQ) are emitted from industrial plants in the form of vapors in the air atmosphere and in aqueous effluents. P and its derivatives can also originate from diffuse emissions, e.g. from the tar coatings of the roads and pipes and from the use of pesticides including their transformation products, e.g. herbicides, fungicides. P and its derivatives are very important organic intermediates, used in the manufacture of many products in such units as drugs, rubber, pesticides, varnishes and also, dyestuffs, chemicals, petrochemicals, paper, wood, metallurgy and coking plants.

Phenols (P_s) constitute the 11th of the 126 chemicals, which have been designated as priority pollutants by the Environmental Protection Agency of USA [USEPA, 1987; Rodriguez et al., 2000]. USEPA has set a discharge limit of 0.1 mg/l of P in wastewater. The World Health Organization (WHO) has a 0.001 mg/l as the limit of P concentration in potable water [WHO, 1984].These compounds impart objectionable taste and odor to drinking water at concentrations as low as 0.005 mg/l. The Ministry of Environmental and Forests, Govt. of India has set a discharge limit of 1 mg/l for phenols in waste water.

Adsorption as a wastewater treatment process has aroused considerable interest during recent years. Granular activated carbon (GAC) is generally used as an effective adsorbent for controlling various organic and inorganic pollutants. Of all the methods proposed for the removal of P and its derivatives and associated compounds, adsorption appears to offer best prospects for overall treatment, especially for the effluents with moderate and low concentrations.

Unconventional adsorbents like bagasse fly ash, rice husk ash, brick kiln ask, carbon slurry, sewage sludge, kaolin, soil and clay, silica, peat, lignite, bagasse pith, wood, saw dust, molecular sieves, resins, montmorillonite, etc. have attracted the attention of several investigators [Viraraghavan and Alfaro, 1998; Rai, et al., 1999; Ng et al., 2002; Ravikumar et al., 2005; Chakraborty et al., 2006; Srivastava et al., 2006a; Shakir et al., 2008; Maiti et al., 2009; Rallapalli et al., 2010]. Various physico-chemical and biological treatment techniques are suggested for the treatment of P and its derivatives from

wastewaters, which include concentration followed by adsorption [Mall et al., 1996; Viraraghavan and Alfaro, 1998; Srivastava et al., 2006b], biodegradation [O'Neill et al., 2000; Kumar et al., 2005; Subramanyam and Mishra, 2008], catalytic oxidation [Garg et al., 2010], etc.

Much of the work on the adsorption of P_s by GAC has focused on the uptake of single component. Since industrial effluents can contain a number of components, it is necessary to study the simultaneous sorption of two or more compounds and also to quantify the interference of one compound with the sorption of the others. Thus, the studies on adsorption of P_s from binary and ternary systems are of prime importance. The equilibrium adsorption isotherm equations proposed for single component adsorption have been extended and modified to represent the binary and multi-component adsorption equilibria. The literature concerning multicomponent phenolic compounds adsorption from aqueous solutions on to GAC is scarce. Taguchi's method for optimal design of experiments is a very powerful method for studying the effect of various parameters and their interactions on the waste water treatment optimization [Roy, 1990]. Very little work has been done using the method for adsorption studies. No work is reported using Taguchi's method for the adsorption of P_s and their associated compounds from wastewater using batch and column systems.

The present study has been undertaken with the following objectives:

1. To characterize GAC, and to study its use in batch and column adsorption of P and its associated compounds.
2. To study the effects of various parameters viz. adsorbent dose (m), initial pH (pH_0), initial concentration (C_0 in the range 50–1000 mg/l), contact time (t) and temperature (T) (288–318 K) on the adsorption capacity in batch and column processes.
3. To study the kinetics, equilibrium adsorption and thermodynamics of the adsorption process.
4. To study multicomponent adsorption isotherm behavior of the competitive adsorption equilibria of P and its derivatives and associated compounds in binary and ternary systems.

5. The application of Taguchi's design of experimental methodology for the single, binary and ternary adsorption systems for P and its derivatives and associated compounds in batch and column system.
6. To study desorption of adsorbed species and disposal and management of spent GAC.

All the batch experiments were carried out at 30±1 °C. For each experimental run, 0.05 l of adsorbates solution of known C_0, pH_0 (2 - 12) and m, taken in a 0.25 l stoppered conical flask, was agitated in a temperature-controlled orbital shaker at a constant speed of 150 ± 5 rpm. Samples were withdrawn at appropriate time intervals and centrifuged using a research centrifuge. The residual P and its derivatives and its associated concentration (C_r) of the centrifuged supernatant were then determined.

Physico-chemical characterization including surface area, X-ray diffraction (XRD) analysis, scanning electron microscopy (SEM), energy dispersive X-ray spectroscopy (EDX) and Fourier transform infrared spectroscopy (FTIR) of the GAC before and after adsorption have been done to understand the adsorption mechanism.

The initial pH (pH_0) of the solution strongly affects the chemistry of P and its derivatives and its associated compounds and GAC in an aqueous solution. The point of zero charge (pH_{PZC}) of GAC lies at a pH_0 value of 10.3. Natural pH of 6.9, 6.0, 5.8, 6.0, 5.8, 5.6 and 6.1 were found to be optimum for the removal of AN, P, CP, NP, C, R and HQ, respectively. Optimum GAC dosages were found to be 10 g/l, for C_0 =500 mg/l of P and its derivatives and its associated compounds.

The pseudo-second-order kinetics represented the adsorption process well for all the adsorbates (single component). Equilibrium isotherms were analyzed by using different isotherm models viz. The maximum removal of the materials from the synthetic wastewaters was found in the range of 60 to 99% at higher and lower concentrations, respectively. Redlich-Peterson and Temkin isotherm models generally well represent the equilibrium adsorption of P and its derivatives and its associated compounds onto GAC. The heat of adsorption (ΔH^0) and change in entropy (ΔS^0) for adsorption on GAC were found to be in the range of 18-52 kJ/mol and 121-243kJ/mol K. The negative value of change in Gibbs free energy (ΔG^0) indicated the feasibility and spontaneity of adsorption on by GAC. The isosteric heat of adsorption calculated from the equilibrium adsorption data using the Clausius-Clapeyron equation was quantitatively correlated with the

fractional loading of compounds onto GAC. The surface energetic heterogeneity patterns of the GAC were described as functions of isosteric enthalpy. The higher heats of adsorption at low coverages were likely related to the presence of surface defects.

Batch studies for the removal of various components in binary and ternary systems by GAC were carried out using Taguchi's orthogonal array (OA) experimental design (DOE) methodology. Significant parameters, viz., concentration, temperature, adsorbent dose and contact time at three levels with a OA layout of L_{27} (3^{13}) were selected for the proposed experimental design for batch study. L_9 (3^4) OA was used column study. In all, 27 sets of experiments were conducted for the adsorption in binary and ternary systems. The removal efficiency was found to be in the range of ~90–95%.

The adsorption of P and its derivatives and associated compounds from the binary and ternary solutions onto GAC is generally found to be antagonistic in nature. Equilibrium isotherms for the binary and ternary adsorption have been analyzed by using non-modified Langmuir, modified Langmuir, extended-Langmuir, extended-Freundlich and Sheindorf–Rebuhn–Sheintuch (SRS) models. The competitive extended-Freundlich and SRS models fit the equilibrium data satisfactorily and adequately.

For the desorption experiments, several solvents (acids and alcohol, water) have been used. Among the various solvents, only NaOH was found to be better solvent for the desorption of P, CP, NP, C, R, HQ, while HNO_3 was found to be better solvent for the desorption of AN. Thermal desorption at 623 K was found to better as compared to solvent desorption. GAC worked well for at least five adsorption-desorption cycle, with continuous decrease in adsorption efficiency after each thermal desorption.

It is necessary to properly dispose of the spent-GAC and/or utilize it for some beneficial purpose, if possible. The dried spent-GAC can be used directly or by making fire-briquettes in the furnace combustors/incinerators to recover its energy value. Blank GAC has a heating value of about 8.26 MJ/kg. Thus, the GAC along-with the adsorbed P and other compounds can be dried and used as a fuel in the boiler furnaces/incinerators, or can be used for the production of fuel-briquettes. The bottom ash may be blended with clay to make fire bricks, or with cement-concrete mixture to make colored building blocks thus disposing of P and its derivatives and its associated compounds through chemical and physical fixation. Thus, spent-GAC could not only be safely disposed but also its energy value can be recovered.

ACKNOWLEDGEMENTS

I express my deep sense of gratitude to Dr. I. M. Mishra, Professor, Department of Chemical Engineering and Dean, Saharanpur campus and Dr. V. C. Srivastava, Assistant Professor, Department of Chemical Engineering, Indian Institute of Technology Roorkee for their precious guidance, suggestions and supervision at every level of this investigation. I am obliged forever for their kind inspiration, encouragement and wholehearted support without which it was not possible to complete this work.

I would like to take this opportunity to put on record my respects to Dr. I. D. Mall, Prof. and Head of the Department, for providing me various facilities during the course of the present investigation and Dr. B. Prasad, Associate Professor, Department of Chemical Engineering for his constant motivation and support.

My sincere and grateful thanks are also due to Prof. Surendra Kumar, Prof. Bikas Mohanty, Prof. Shri Chand, and Prof. V. K. Agrawal, Department of Chemical Engineering, IIT, Roorkee for their kind assistance and encouragement. I am thankful to Dr. Vineet Kumar, Dr. Shishir Shina, Dr. (Mrs) Shashi, Dr. Amit Kumar Dhiman, Dr. Prasenjit Mondal, Dr. Ram Prakash and Dr. Prakash Biswas for their moral support during my research. I am thankful to Prof. Kailash Chandra, and Prof. A. K. Chaudhary of the Institute Instrumentation Centre for their generous assistance and facilitation in the analysis of the samples.

I owe grateful thanks to my friends/senior/collegue, especially, Dr. Amit Keshav, Dr. Dilip Lataye, Dr. Anurag Garg, Dr. R. Subramanyam, Sachin Kumar Sharma, J.P. Kushwaha and many others who generously spent their precious time for my research work and helped me at crucial moments.

Special thanks are due to technical staff of the Department; Shri Ayodhya Prasad Singh, Mr. Rajendra Bhatnagar, Shri Suresh Chand, Shri Satpal Singh, Shri Harbans Singh, Shri Tara Chand, Shri Bhagwan Pal Singh, Shri Vipin Ekka, Shri Arvind Kumar, who helped me during the course of my experimental work. Thanks are also due to

Shri Shadab Ali, Shri S.P. Singh, Mrs. Anuradha, Shri Sudesh and other ministerial staff of the Department of Chemical Engineering for their assistance.

I am thankful to supporting staff Shri S. J. Sharma, Shri A.K. Saini, of the Institute Instrumentation Centre for their help in the analysis of the samples.

I felt highly privileged to be associated as a research scholar with Prof. I.M. Mishra and Dr. V.C. Srivastava, honest teachers, good researchers and dynamic persons. I am also thankful to Late Mrs. Geeta Mishra, Mrs. V.C. Srivastava and their family members who have been so cooperative and so kind to me, whenever I went to their residences.

I am also thankful to Shri Nagendra Datt Vyas, Shri P. Rajendra Prasad Vyas and Shri P. Rajiv Nayan Vyas who has given spiritual support for completion of my research work.

I fully understand that the research experience and knowledge which I have gathered during the course of my Ph.D. programme, would be highly useful for my academic profession. This work was possible due to contributions of many. I am thankful to all of them and extremely sorry if anyone has been hurt during the period of my research work.

I would deeply appreciate the encouragement and moral support of my parents and all my friends, without which it was not possible for me to complete my research work.

I thank God for encouraging me in every possible way and providing me strength to withstand the adversities during my past years.

SURESH S.

CONTENTS

Candidate's Declaration i

Abstract iii

Acknowledgement vii

List of Figures xiii

List of Tables xxi

Abbreviations and Notations xxv

Chapter – I: INTRODUCTION 1

1.1 General 1

1.2 P and its derivatives and associated compounds 6

1.3 Industrial and natural sources of P and its derivatives and associated compounds 10

1.4 Treatment processes for AN,P, CP,NP,C, R and HQ bearing wastewaters 11

1.5 Activated carbon (AC) as an adsorbent 12

1.6 Taguchi's experimental design 13

1.7 Objectives of the present study 14

Chapter – II: LITERATURE REVIEW 17

2.1 General 17

2.2 Treatment methods for aniline, phenol, 4-chlorophenol, 4-nitrophenol, catechol, resorcinol and hydroquinone bearing wastewaters 17

2.3 Adsorption studies using GAC and other adsorbents 28

2.4 Taguchi's design of experiments 77

2.5 Summary 81

Chapter – III: EXPERIMENTAL PROGRAMME 83

3.1 Materials 83

3.1.1 Adsorbent 83

3.1.2 Adsorbates and chemicals 83

3.2 Adsorbent characterization 83
3.2.1 Proximate Analysis 83
3.2.2 Particle Size 83
3.2.3 Bulk Density 84
3.2.4 Point of Zero Charge (pH_{PZC}) 84
3.2.5 X-Ray Diffraction (XRD) Analysis 84
3.2.6 Scanning Electron Microscopy (SEM) 84
3.2.7 Energy Dispersive Atomic X-ray (EDAX) Analysis 85
3.2.8 Pore Size Distribution Analysis 85
3.2.9 Fourier Transform Infra Red (FTIR) Spectral Analysis 85
3.3 Batch experimental programme 85
3.3.1 Kinetic Study 86
3.3.2 Adsorption Isotherm Study 87
3.3.3 Effect of Temperature and Estimation of Thermodynamic Parameters 87
3.4 Multi-Component Adsorption Study Using Taguchi's Method 88
3.4.1 Design of experiments (Phase I) 88
3.4.2 Batch adsorption experiments (Phase 2) 89
3.4.2.1 Batch binary/ternary adsorption experiments 89
3.4.2.2 Column ternary adsorption experiments 90
3.4.3 Analysis of experimental data and prediction of performance (Phase 3) 95
3.4.4 Confirmation experiment (Phase 4) 98
3.5 Multi-Component Isothermal Adsorption Study 98
3.5.1 Binary adsorbates system 98
3.5.2 Ternary adsorbates system 98
3.5.3 Analysis of adsorbate in aqueous solution and error analysis 99
3.6 Batch Desorption Study 100
3.7 Thermal Analysis of Spent-Adsorbent 100

Chapter – IV: RESULTS AND DISCUSSION 101
4.1 General 101
4.2 Characterization of adsorbent 101
4.2.1 Physico-chemical Characterization of GAC 101
4.2.2 Pore Size Distribution of GAC 104
4.2.3 FTIR spectroscopy of the GAC and various loaded-GAC 108

4.2.3.1 FTIR spectroscopy of the AN-, P-, CP-, NP- and HQ- loaded-GAC 108
4.2.3.2 FTIR spectroscopy of the C- and R- loaded-GAC 110
4.3 Batch Adsorption Study For Individual Adsorption 116
4.3.1 Effect of initial pH (pH_0) 116
4.3.1.1 Speciation diagram of adsorbates 116
4.3.1.2 Effect of pH_o on AN, P, CP and NP adsorption 117
4.3.1.3 Effect of pH_o on C, R and HQ adsorption 120
4.3.2 Effect of adsorbent dosage (m) 124
4.3.3 Effect of contact time and initial concentration (C_o) 125
4.3.4 Adsorption kinetic study 128
4.3.5 Adsorption diffusion study 135
4.3.6 Effect of Temperature 138
4.3.7 Adsorption isotherm modeling 141
4.3.8 Adsorption thermodynamics 150
4.3.8.1 Isosteric heat of adsorption 151
4.4 Multi-Component Batch Adsorption Study Using Taguchi's Method 158
4.4.1 Optimization of Parameters for Binary Systems 158
4.4.1.1 NP-P and AN-P binary systems 158
4.4.1.2 NP-C and NP-R binary systems 161
4.4.1.3 AN-C and AN-R binary systems 163
4.4.2 Optimization of Parameters for Ternary Systems 193
4.4.3 Summary 195
4.5 Multi-Component Batch Adsorption Isotherm Study 204
4.5.1. Binary Batch Isotherm Study 206
4.5.2 Ternary Batch Isotherm Study 234
4.5.2.1 Three-dimensional (3-D) adsorption isotherm surfaces 235
4.6 Multi-component column adsorption study using Taguchi's method 242
4.6.1 Optimization of Parameters for Ternary Column Adsorption Study 244
4.7 Desorption Study 257
4.7.1 Solvent desorption 257
4.7.2 Thermal desorption 257
4.8 Thermal oxidation of spent-GAC 258

Chapter – V: CONCLUSIONS AND RECOMMENDATIONS 263

5.1 Conclusions 263

5.2 Recommendations 265

REFERENCES 267

BIO-DATA

PUBLICATIONS FROM THESIS

LIST OF FIGURES

Figure No.	Title	Page No.
Figure 4.2.1.	X-ray diffraction of blank and various adsorbates loaded GAC.	105
Figure 4.2.2.	SEM of blank-GAC, AN-, P-, and CP-loaded GAC.	106
Figure 4.2.3.	SEM of NP-, C-, R- and HQ-loaded GAC.	107
Figure 4.2.4.	FTIR of blank-GAC.	111
Figure 4.2.5.	FTIR of pure-AN and AN loaded GAC.	111
Figure 4.2.6.	FTIR of pure-P and P loaded GAC.	112
Figure 4.2.7.	FTIR of pure 4CP and 4CP loaded GAC.	112
Figure 4.2.8.	FTIR of pure 4NP and 4NP loaded GAC.	113
Figure 4.2.9.	FTIR of pure HQ and HQ loaded GAC.	113
Figure 4.2.10.	FTIR of C, blank-GAC and C loaded GAC. 1: C ; 2: Blank-GAC; 3: C-GAC.	114
Figure 4.2.11.	FTIR of R, blank-GAC and R loaded GAC. 1: R; 2: Blank-GAC; 3: R-GAC.	115
Figure 4.3.1.	Point of zero charge (pH_{PZC}) for GAC.	118
Figure 4.3.2.	Distribution of AN, P, CP, NP, C, R and HQ as a function of pH	118
Figure 4.3.3.	Effect of pH_o on the adsorption of AN, P, CP, NP, C, R and HQ by GAC. T = 303 K, t = 24 h, m = 10 g/l.	123
Figure 4.3.4.	Effect of adsorbent dose on the adsorption of AN, P, CP, NP, C, R and HQ by GAC. T=303 K, t=24 h, C_o=0.91 mmol/l.	126
Figure 4.3.5.	Effect of contact time and initial concentration on adsorption of various adsorbates by GAC. T=303 K, m=1 g/1. Experimental data are given by data points whereas fitted line is due to pseudo-second order model.	129
Figure 4.3.6.	Weber and Morris intra-particle diffusion plot for the removal of AN, P, CP, NP, C, R and HQ by GAC. T=303 K, m=10 g/l.	140
Figure 4.3.7.	Equilibrium adsorption isotherms at different temperature. (a) AN-GAC system, lines fitted by R-P model; (b) P-GAC system, lines fitted by Tempkin model; (c) CP-GAC system, lines fitted by Tempkin model; and; (d) NP-GAC system, lines fitted by R-P model; (e) C-GAC system, lines fitted by Tempkin model; (f) R-GAC system, lines fitted by R-P model; and (g) HQ-GAC system lines predicted by Tempkin equation	145

Figure 4.3.8.	Van't Hoff Plot of adsorption equilibrium constant K for AN, P, CP and NP, C, R and HQ.	153
Figure 4.3.9.	Adsorption isosters for determining isosteric heat of adsorption for AN, P, CP, NP, C, R and HQ adsorption onto GAC.	154
Figure 4.3.10.	Variation of $\Delta H_{st,a}$ with respect to surface loading for AN, P, CP, NP, C, R and HQ adsorption onto GAC.	155
Figure 4.4.1.	Effect of process parameters on q_{tot} and S/N ratio for binary adsorption of NP and P onto GAC.	181
Figure 4.4.2.	Effect of process parameters on q_{tot} and S/N ratio for binary adsorption of AN and P onto GAC.	181
Figure 4.4.3.	Effect of process parameters on q_{tot} and S/N ratio for binary adsorption of NP and C onto GAC.	181
Figure 4.4.4.	Effect of process parameters on q_{tot} and S/N ratio for binary adsorption of NP and R onto GAC.	182
Figure 4.4.5.	Effect of process parameters on q_{tot} and S/N ratio for binary adsorption of AN and C onto GAC.	182
Figure 4.4.6.	Effect of process parameters on q_{tot} and S/N ratio for binary adsorption of AN and R onto GAC.	182
Figure 4.4.7.	Effect of process parameters on q_{tot} and S/N ratio for binary adsorption of NP and CP onto GAC.	183
Figure 4.4.8.	Effect of process parameters on q_{tot} and S/N ratio for binary adsorption of NP and AN onto GAC.	183
Figure 4.4.9.	Effect of process parameters on q_{tot} and S/N ratio for binary adsorption of NP and HQ onto GAC.	183
Figure 4.4.10.	Effect of process parameters on q_{tot} and S/N ratio for binary adsorption of AN and CP onto GAC.	184
Figure 4.4.11.	Effect of process parameters on q_{tot} and S/N ratio for binary adsorption of AN and HQ onto GAC.	184
Figure 4.4.12.	The interaction between A and B parameters at 3 levels on q_{tot} and S/N ratio for binary adsorption of NP and P onto GAC.	185
Figure 4.4.13.	The interaction between A and B parameters at 3 levels on q_{tot} and S/N ratio for binary adsorption of AN and P onto GAC.	185
Figure 4.4.14.	The interaction between A and B parameters at 3 levels on q_{tot} and S/N ratio for binary adsorption of NP and C onto GAC.	185

Figure 4.4.15.	The interaction between A and B parameters at 3 levels on q_{tot} and S/N ratio for binary adsorption of NP and R onto GAC.	186
Figure 4.4.16.	The interaction between A and B parameters at 3 levels on q_{tot} and S/N ratio for binary adsorption of AN and C onto GAC.	186
Figure 4.4.17.	The interaction between A and B parameters at 3 levels on q_{tot} and S/N ratio for binary adsorption of AN and R onto GAC.	186
Figure 4.4.18.	The interaction between A and B parameters at 3 levels on q_{tot} and S/N ratio for binary adsorption of NP and CP onto GAC.	187
Figure 4.4.19.	The interaction between A and B parameters at 3 levels on q_{tot} and S/N ratio for binary adsorption of NP and AN onto GAC.	187
Figure 4.4.20	The interaction between A and B parameters at 3 levels on q_{tot} and S/N ratio for binary adsorption of NP and HQ onto GAC.	187
Figure 4.4.21.	The interaction between A and B parameters at 3 levels on q_{tot} and S/N ratio for binary adsorption of AN and CP onto GAC.	188
Figure 4.4.22.	The interaction between A and B parameters at 3 levels on q_{tot} and S/N ratio for binary adsorption of AN and HQ onto GAC.	188
Figure 4.4.23.	Percent contribution of various parameters for q_{tot} for binary adsorption of NP and P onto GAC.	189
Figure 4.4.24.	Percent contribution of various parameters for q_{tot} for binary adsorption of AN and P onto GAC.	189
Figure 4.4.25.	Percent contribution of various parameters for q_{tot} for binary adsorption of NP and C onto GAC.	189
Figure 4.4.26.	Percent contribution of various parameters for q_{tot} for binary adsorption of NP and R onto GAC.	190
Figure 4.4.27.	Percent contribution of various parameters for q_{tot} for binary adsorption of AN and C onto GAC.	190
Figure 4.4.28.	Percent contribution of various parameters for q_{tot} for binary adsorption of AN and R onto GAC.	190
Figure 4.4.29.	Percent contribution of various parameters for q_{tot} for binary adsorption of NP and CP onto GAC.	191

Figure 4.4.30.	Percent contribution of various parameters for q_{tot} for binary adsorption of NP and AN onto GAC.	191
Figure 4.4.31.	Percent contribution of various parameters for q_{tot} for binary adsorption of NP and HQ onto GAC.	191
Figure 4.4.32.	Percent contribution of various parameters for q_{tot} for binary adsorption of AN and CP onto GAC.	192
Figure 4.4.33.	Percent contribution of various parameters for q_{tot} for binary adsorption of AN and HQ onto GAC.	192
Figure 4.4.34.	Effect of process parameters on q_{tot} and S/N ratio for ternary adsorption of P, CP and NP onto GAC.	200
Figure 4.4.35.	Effect of process parameters on q_{tot} and S/N ratio for ternary adsorption of C, R and HQ onto GAC.	200
Figure 4.4.36.	The interaction between A, B and C parameters at 3 levels on q_{tot} and S/N ratio for ternary adsorption of P, CP and NP onto GAC.	201
Figure 4.4.37.	The interaction between A, B and C parameters at 3 levels on q_{tot} and S/N ratio for ternary adsorption of C, R and HQ onto GAC.	202
Figure 4.4.38.	Percent contribution of various parameters for q_{tot} for ternary adsorption of P, CP and NP onto GAC.	203
Figure 4.4.39.	The interaction between A, B and C parameters at 3 levels on q_{tot} and S/N ratio for ternary adsorption of C, R and HQ onto GAC.	203
Figure 4.5.1.	Comparison of non-linearized adsorption isotherms of NP-CP binary system. [a] NP in the presence of increasing concentration of CP, [b] CP with increasing concentration of NP. $T = 30^0$C, t =12 h, GAC dosage = 10 g/l.	215
Figure 4.5.2.	Comparison of non-linearized adsorption isotherms of NP-AN binary system. [a] NP in the presence of increasing concentration of AN, [b] AN with increasing concentration of NP. $T = 30^0$C, t =12 h, GAC dosage = 10 g/l.	216
Figure 4.5.3.	Comparison of non-linearized adsorption isotherms of AN-P binary system. [a] AN in the presence of increasing concentration of P, [b] P with increasing concentration of AN. $T = 30^0$C, t =12 h, GAC dosage = 10 g/l.	217
Figure 4.5.4.	Comparison of non-linearized adsorption isotherms of AN-C binary system. [a] AN in the presence of increasing concentration of C, [b] C with increasing concentration of AN. $T = 30^0$C, t =12 h, GAC dosage = 10 g/l.	218

Figure 4.5.5.	Comparison of non-linearized adsorption isotherms of NP-C binary system. [a] AN in the presence of increasing concentration of C, [b] C with increasing concentration of AN. $T = 30^0$C, t =12 h, GAC dosage = 10 g/l.	219
Figure 4.5.6.	Comparison of non-linearized adsorption isotherms of NP-R binary system. [a] AN in the presence of increasing concentration of C, [b] R with increasing concentration of AN. $T = 30^0$C, t =12 h, GAC dosage = 10 g/l.	220
Figure 4.5.7.	Comparison of non-linearized adsorption isotherms of NP-HQ binary system. [a] NP in the presence of increasing concentration of HQ, [b] HQ with increasing concentration of NP. $T = 30^0$C, t =12 h, GAC dosage = 10 g/l.	221
Figure 4.5.8.	Comparison of non-linearized adsorption isotherms of AN-CP binary system. [a] AN in the presence of increasing concentration of CP, [b] CP with increasing concentration of AN. $T = 30^0$C, t =12 h, GAC dosage = 10 g/l.	222
Figure 4.5.9.	Comparison of non-linearized adsorption isotherms of NP-P binary system. [a] NP in the presence of increasing concentration of P, [b] P with increasing concentration of NP. $T = 30^0$C, t =12 h, GAC dosage = 10 g/l.	223
Figure 4.5.10.	Comparison of non-linearized adsorption isotherms of NP-R binary system. [a] NP in the presence of increasing concentration of R, [b] R with increasing concentration of NP. $T = 30^0$C, t =12 h, GAC dosage = 10 g/l.	224
Figure 4.5.11.	Comparison of non-linearized adsorption isotherms of NP-HQ binary system. [a] NP in the presence of increasing concentration of HQ, [b] HQ with increasing concentration of NP. $T = 30^0$C, t =12 h, GAC dosage = 10 g/l.	225
Figure 4.5.12.	Comparison of the experimental and calculated q_e values for NP-CP binary system. [a] NP, [b] CP.	226
Figure 4.5.13.	Comparison of the experimental and calculated q_e values for NP-AN binary system. [a] NP, [b] AN.	227
Figure 4.5.14.	Comparison of the experimental and calculated q_e values for AN-P binary system. [a] AN, [b] P.	228
Figure 4.5.15.	Comparison of the experimental and calculated q_e values for AN-R binary system. [a] AN, [b] C.	229
Figure 4.5.16.	Binary adsorption isotherms for NP-CP binary system. [a] NP, [b] CP. The surfaces are predicted by the extended Freundlich model and the symbols are experimental data.	230

Figure 4.5.17.	Binary adsorption isotherms for NP-AN binary system. [a] NP, [b] AN. The surfaces are predicted by the extended Freundlich model and the symbols are experimental data.	231
Figure 4.5.18.	Binary adsorption isotherms for AN-P binary system. [a] AN, [b] P. The surfaces are predicted by the extended Freundlich model and the symbols are experimental data.	232
Figure 4.5.19.	Binary adsorption isotherms for AN-C binary system. [a] AN, [b] C. The surfaces are predicted by the extended Freundlich model and the symbols are experimental data.	233
Figure 4.5.20.	Three-dimensional adsorption isotherm surfaces created using multicomponent SRS model for the P-CP-NP systems with $C_{e,NP}$, as a parameter. (a) The effect of P concentration on the equilibrium uptake of CP; (b) the effect of CP concentration on the equilibrium uptake of P (c) the effect of P and CP concentration on the equilibrium total uptake of P+CP onto GAC.	238
Figure 4.5.21.	Three-dimensional adsorption isotherm surfaces created using multicomponent SRS model for the P-CP-NP systems with $C_{e,CP}$, as a parameter. (a) The effect of P concentration on the equilibrium uptake of NP; (b) the effect of NP concentration on the equilibrium uptake of P (c) the effect of P and NP concentration on the equilibrium total uptake of P+NP onto GAC.	239
Figure 4.5.22.	Three-dimensional adsorption isotherm surfaces created using multicomponent SRS model for the C-R-HQ systems with $C_{e,C}$, as a parameter. (a) The effect of HQ concentration on the equilibrium uptake of R; (b) the effect of R concentration on the equilibrium uptake of HQ (c) the effect of R and HQ concentration on the equilibrium total uptake of R+HQ onto GAC.	240
Figure 4.5.23.	Three-dimensional adsorption isotherm surfaces created using multicomponent SRS model for the C-R-HQ systems with $C_{e,R}$, as a parameter. (a) The effect of HQ concentration on the equilibrium uptake of C; (b) the effect of C concentration on the equilibrium uptake of HQ (c) the effect of C and HQ concentration on the equilibrium total uptake of C+HQ.	241
Figure 4.6.1.	Breakthrough curves for simultaneous adsorption of P, CP and NP onto GAC for D=2 cm. (A) Expt. No. 1: Q=0.02 l/min, Z=30 cm; (B) Expt. No. 6: Q=0.04 l/min, Z=60 cm; (C) Expt. No. 8: Q=0.06 l/min, Z=45 cm.	250

Figure 4.6.2.	Breakthrough curves for simultaneous adsorption of P, CP and NP onto GAC for D=2.54 cm. (A) Expt. No. 2: Q=0.02 l/min, Z=45 cm; (B) Expt. No. 4: Q=0.04 l/min, Z=30 cm; (C) Expt. No. 9: Q=0.06 l/min, Z=60 cm.	251
Figure 4.6.3.	Breakthrough curves for simultaneous adsorption of P, CP and NP onto GAC for D=4 cm. (A) Expt. No. 7: Q=0.06 l/min, Z=30 cm; (B) Expt. No. 5: Q=0.04 l/min, Z=45 cm; (C) Expt. No. 3: Q=0.02 l/min, Z=60 cm.	252
Figure 4.6.4.	Breakthrough curves for simultaneous adsorption of C, R and HQ onto GAC for D=2 cm. (A) Expt. No. 1: Q=0.02 l/min, Z=30 cm; (B) Expt. No. 6: Q=0.04 l/min, Z=60 cm; (C) Expt. No. 8: Q=0.06 l/min, Z=45 cm.	253
Figure 4.6.5.	Breakthrough curves for simultaneous adsorption of C, R and HQ onto GAC for D=2.54 cm. (A) Expt. No. 2: Q=0.02 l/min, Z=45 cm; (B) Expt. No. 4: Q=0.04 l/min, Z=30 cm; (C) Expt. No. 9: Q=0.06 l/min, Z=60 cm.	254
Figure 4.6.6.	Breakthrough curves for simultaneous adsorption of C, R and HQ onto GAC for D=4 cm. (A) Expt. No. 7: Q=0.06 l/min, Z=30 cm; (B) Expt. No. 5: Q=0.04 l/min, Z=45 cm; (C) Expt. No. 3: Q=0.02 l/min, Z=60 cm.	255
Figure 4.6.7.	Effect of process parameters on q_{tot} for ternary adsorption of P, CP and NP in GAC packed-bed.	256
Figure 4.6.8.	Effect of process parameters on q_{tot} for ternary adsorption of C, R and HQ in GAC packed-bed.	256
Figure 4.7.1	Desorption efficiencies of AN, P, CP, NP, C, R and HQ by various desorbing agents. T=303 K t=24 h, C_0 (desorbing agents)=0.1 N, m=1 g/1.	259
Figure 4.7.2.	Thermal desorption efficiencies of AN, P, CP, NP, C, R and HQ in a sequence of adsorption/desorption cycle.	260
Figure 4.8.1.	DTA, DTG and %TG graphs of blank and AN-, P-, CP- and NP loaded GAC under oxidizing atmosphere.	261
Figure 4.8.2.	DTA, DTG and %TG graphs of C-, R- and HQ-loaded GAC under oxidizing atmosphere.	262

LIST OF TABLES

Table No.	Title	Page No.
Table 1.1.1	Health hazard information of various pollutants	3
Table 1.1.2	Discharge standards for liquid effluents from petrochemical and Petroleum oil refinery plants in India	4
Table 1.1.3	Physico-chemical properties and solvatochromic parameters.	8
Table 2.2.1.	Other treatment methods for the removal of AN, P, CP, NP, C, R and HQ from water and wastewater.	29
Table 2.2.2.	Adsorptive removal of AN, P, CP, NP, C, R and HQ from water and wastewater.	50
Table 3.4.1.	Process parameters for binary adsorption study of NP/AN and P or CP or NP or C or R or HQ onto GAC using Taguchi's L_{27} (3^{13}) orthogonal array.	92
Table 3.4.2.	Process parameters for ternary adsorption study of P, CP and NP or C, R and HQ onto GAC using Taguchi's L_{27} (3^{13}) orthogonal array.	92
Table 3.4.3.	Process parameters for ternary column adsorption study of P, CP and NP or C, R and HQ onto GAC using Taguchi's L_9 orthogonal array.	92
Table 3.4.4.	Column assignment for the various factors and one interaction in the Taguchi's L_{27} (3^{13}) orthogonal array for binary batch adsorption onto GAC.	93
Table 3.4.5.	Column assignment for the various factors and three interactions in the Taguchi's L_{27} (3^{13}) orthogonal array for ternary batch adsorption onto GAC.	94
Table 3.4.6.	Column assignment for the various factors in the Taguchi's L_9 orthogonal array for ternary adsorption onto GAC in column study.	95
Table 4.2.1.	Physico-chemical characteristics of blank and various adsorbates loaded.	103
Table 4.3.1.	Kinetic parameters for the removal of AN and P by GAC (t = 24 h, C_0 = 0.54-10.74; 0.53-10.63 mmol/l, m = 10 g/l, T= 303 K).	131
Table 4.3.2.	Kinetic parameters for the removal of CP and NP by GAC (t = 24 h, C_0 = 0.39-7.78; 0.36-7.19 mmol/l, m = 10 g/l, T= 303 K).	132
Table 4.3.3.	Kinetic parameters for the removal of C and R by GAC (t =24.0 h, C_0 =0.45-9.08 mmol/l, m =10 g/l, T=303 K).	133

Table 4.3.4.	Kinetic parameters for the removal of HQ by GAC (t=24.0 h, C_o=0.45-9.08 mmol/l, m=10 g/l, T=303 K).	134
Table 4.3.5.	Isotherm parameters for the adsorption of AN and P onto GAC at different temperature (t=24 h, m=10 g/l).	146
Table 4.3.6.	Isotherm parameters for the adsorption of CP and NP onto GAC at different temperature (t=24 h, m=10 g/l).	147
Table 4.3.7.	Isotherm parameters for the removal of C and R by GAC at different temperature (t=24 h, m=10 g/l).	148
Table 4.3.8.	Isotherm parameters for the removal of HQ by GAC at different temperatures (t=24.0 h, C_0=0.18-9.08 mmol/l, m=10 g/l, T=303 K).	149
Table 4.3.9.	Thermodynamic parameters for the adsorption of AN, P, CP, NP, C, R and HQ onto GAC.	156
Table 4.3.10.	Isosteric enthalpy of the adsorption of AN, P, CP, NP, C, R and HQ onto GAC.	157
Table 4.4.1.	Experimental q_{tot} and S/N ratio values for Taguchi's L_{27} (3^{13}) orthogonal array for NP-P and AN-P adsorption onto GAC.	167
Table 4.4.2.	Experimental q_{tot} and S/N ratio values for Taguchi's L_{27} (3^{13}) orthogonal array for NP-C and NP-R adsorption onto GAC.	168
Table 4.4.3.	Experimental q_{tot} and S/N ratio values for Taguchi's L_{27} (3^{13}) orthogonal array for AN-C, AN-R and AN-HQ adsorption onto GAC.	169
Table 4.4.4.	Experimental q_{tot} and S/N ratio values for Taguchi's L_{27} (3^{13}) orthogonal array for NP-AN, NP-CP and NP-HQ systems.	170
Table 4.4.5.	Experimental q_{tot} and S/N ratio values for Taguchi's L_{27} (3^{13}) orthogonal array for AN-CP and AN-HQ systems.	171
Table 4.4.6.	Average and main effects of q_{tot} values for raw and S/N data for NP-P and AN-P systems.	172
Table 4.4.7.	Average and main effects of q_{tot} values for raw and S/N data for NP-C and NP-R systems.	172
Table 4.4.8.	Average and main effects of q_{tot} values for raw and S/N data for AN-C and AN-R systems.	173
Table 4.4.9.	Average and main effects of q_{tot} values for raw and S/N data for NP-AN, NP-CP and NP-HQ systems.	173
Table 4.4.10.	Average and main effects of q_{tot} values for raw and S/N data for AN-CP and AN-HQ systems.	174

Table 4.6.3.	q_{tot} values in column study for P-CP-NP and C-R-HQ ternary systems.	248
Table 4.6.4	Average and main effects of q_{tot} values in column study for P-CP-NP and C-R-HQ ternary systems.	248
Table 4.6.5	ANOVA of q_{tot} values in column study for P-CP-NP and C-R-HQ ternary systems.	249
Table 4.6.6	Comparison of predicted optimal q_{tot} values, confidence intervals and results of confirmation experiments for P-CP-NP and C-R-HQ ternary systems in column study.	249

Table 4.4.11.	ANOVA of q_{tot} and S/N ratio data for NP-P and AN-P systems.	175
Table 4.4.12.	ANOVA of q_{tot} and S/N ratio data for NP-C and NP-R systems.	176
Table 4.4.13.	ANOVA of q_{tot} and S/N ratio data for AN-C and AN-R systems.	177
Table 4.4.14.	ANOVA of q_{tot} and S/N ratio data for NP-AN, NP-CP and NP-HQ systems.	178
Table 4.4.15.	ANOVA of q_{tot} and S/N ratio data for AN-CP and AN-HQ systems.	179
Table 4.4.16.	Comparison of predicted optimal q_{tot} values, confidence intervals and results of confirmation experiments for binary systems.	180
Table 4.4.17.	Experimental q_{tot} and S/N ratio values for Taguchi's L_{27} (3^{13}) orthogonal array for P-CP-NP and C-R-HQ ternary systems.	196
Table 4.4.18.	Average and main effects of q_{tot} values for raw and S/N data for P-CP-NP and C-R-HQ ternary systems.	197
Table 4.4.19.	ANOVA of q_{tot} and S/N ratio data for P-CP-NP and C-R-HQ ternary systems.	198
Table 4.4.20.	Comparison of predicted optimal q_{tot} values, confidence intervals and results of confirmation experiments for P-CP-NP and C-R-HQ ternary systems.	199
Table 4.5.1.	Binary isotherm parameter values for NP-CP and NP-AN systems.	210
Table 4.5.2.	Binary isotherm parameter values for AN-P and AN-C systems.	211
Table 4.5.3.	Binary isotherm parameter values for NP-C, NP-R and NP-HQ systems.	212
Table 4.5.4.	Binary isotherm parameter values for AN-CP and NP-P systems.	213
Table 4.5.5.	Binary isotherm parameter values for AN-R and AN-HQ systems.	214
Table 4.5.6.	Ternary isotherm parameter values for P-CP-NP and C-R-HQ systems.	237
Table 4.6.1.	Ternary column adsorption study using Taguchi's method for P-CP-NP system.	246
Table 4.6.2.	Ternary column adsorption study using Taguchi's method for C-R-HQ system.	247

ABBREVIATIONS AND NOTATIONS

ABBREVIATIONS

ACC	Activated carbon commercial grade
ACs	Activated carbons
AN	aniline
ANOVA	Analysis of variance
ATSDR	Agency for toxic substances and disease registry
BET	Brunauer-Emmett-Teller
BFA	Bagasse fly ash
BJH	Barrett-Joyner-Halenda
BOD	Bio-chemical oxygen demand
C	Catechol
COD	Chemical oxygen demand
CPCB	Central pollution control board
CV	Coefficient of variation
CP	4-Chlorophenol
DF/d.f	Degree of freedom
DOE	Design of experiments
DTA	Differential thermal analysis
DTG	Differential thermal gravimetery
DOF	Degree of freedom
ESR	Electron spin resonance spectra
FTIR	Fourier transform infrared spectroscopy
GAC	Granular activated carbon
HB	Higher-is-better
HPLC	High pressure liquid chromatography
HQ	Hydroquinone
HSDB	Hazardous substances data bank
HYBRID	hybrid fractional error function
IARC	International Agency for Research on Cancer
IAST	Ideal adsorption solution theory
IPCS	International programme on chemical safety
IRCH	Indiana relative chemical hazard
IRIS	Integrated risk information system
IUPAC	International Union of Pure and Applied Chemistry
LB	Lower-is-better
MCL	Maximum concentration limit
MINAS	Minimal national standard
MPSD	Marquardt's percent standard deviation

MW	Molecular weight
NB	Nominal-is-best
NOISH	National Institute of Occupational Safety & Health
NP	4-Nitrophenol
OME	Ontario Ministry of Environment
P	Phenol
P_s	Phenols
R	Resorcinol
RHA	Rice husk ash
SEM	Scanning electron microscopy
SSE	Sum of squares of error
TG	Thermal gravimetery
TGA	Thermo-gravimetric analysis
TLV	Threshold limit value
USEPA	United states environmental agency protection

NOTATIONS

$1/n$	mono-component (non-competitive) Freundlich heterogeneity factor of the single component, dimensionless
$1/n_i$	individual Freundlich heterogeneity factor of each component, dimensionless
a_R	constant of Redlich-Peterson isotherm, l/mg
a_{ij}	competition coefficients of component i by component j, dimensionless
A	adsorbate
$A(1)$	Level total due to parameter A at level L1
a_R	Constant of Redlich-Peterson isotherm, l/mg
Am	Projected area, nm^2
$A.S$	activated complex
B	Normalizing coefficient
B_{DR}	Dubinin and Radushkevich Isotherm Constant
B_T	Temkin Isotherm constant, related to the heat of adsorption
b	Temkin Isotherm constant
C	constant that gives idea about the thickness of boundary layer, mg/g
^oC	Degree Celsius
C_0	initial concentration of adsorbate in solution, mg/l
C_e	equilibrium liquid phase concentration, mg/l
C_S	adsorbent concentration in the solution
C_t	Equilibrium liquid phase concentration after time t, mg/l
CI_{POP}	confidence interval for the entire population

$C.F$	Correction factor.
C_0	initial concentration of adsorbate in solution, mg/l
$C_{0,i}$	initial concentration of each component in solution, mg/l
C_e	unadsorbed concentration of the single-component at equilibrium, mg/l
$C_{e,i}$	unadsorbed concentration of each component in the binary mixture at equilibrium, mg/l
D	Dipore moment
D1	One-dimensional diffusion model
D2	Two- dimensional diffusion model
D3	Three-dimensional diffusion
E	mean free energy of sorption per molecule of the sorbate, KJ/mol
E_a	Activation energy (kJ mol^{-1})
f	exchange of number of moles of water per mole of adsorbate at the adsorption site
$f_{L,N}$	total degree of an OA
f_T	total DOF
f_A	DOF of parameter A
$F(t)$	fractional uptake of adsorbate on adsorbent, $0 < F(t) < 1$
$F_i(C)$	positive fractional deviation of the synergistic Langmuir adsorption isotherm from the single component Langmuir isotherm for each component .
h	initial sorption rate, mg/g min
I	Constant that gives idea about the thickness of boundary layer, mg/g
i	Number of donor particles
k	Rate constant, min^{-1}
k	constant in Taguchi loss-function
k_{0B}	constant in Bangham equation
k_0	pre-exponential factor in Arrhenius equation
k_A	adsorption rate constant for the adsorption equilibrium
k_B	Boltzmann constant
k_D	desorption rate constant for the adsorption equilibrium
k_d	Distribution coefficient
k_f	rate constant of pseudo-first-order adsorption model, min^{-1}
k_{id}	intra-particle diffusion rate constant, $mg/g/min^{1/2}$
k_S	rate constant of pseudo-second-order adsorption model, g/mg min
K_F	constant of Freundlich isotherm, $(mg/g)/(l/mg)^{1/n}$
$K_{EL,i}$	constant of Extended-Langmuir isotherm for each component, l/mg
K_L	constant of Langmuir isotherm, l/mg

K_R	constant of Redlich-Peterson isotherm, g/l
K_F	mono-component (non-competitive) constant of Freundlich isotherm of the single component, $(mg/g)/(l/mg)^{1/n}$
$K_{F,i}$	individual Freundlich isotherm constant of each component, $(mg/g)/(l/mg)^{1/n}$
K_L	constant of Langmuir isotherm, l/mg
$K_{L,i}$	individual Langmuir isotherm constant of each component, l/mg
K_T	equilibrium binding constant (J/mol) corresponding to the maximum binding energy
m	mass of adsorbent per liter of solution, g/l
m_T	Target value at which the characteristic is set
L_N	OA designation
n	number of units in a given sample
n'	Order of thermal degradation reaction
$\bar{n}$	Avg. number of donor particle
n_m	number of measurements
n_p	number of parameters
N	number of data points
$N_i(Q)$	Number of sites having energy Q, dimensionless
P	Percentage contribution
pH_0	initial pH of the solution
pH_{PZC}	Point of zero charge
P_S	Steric Factor
q_e	equilibrium single-component solid phase concentration, mg/g
$q_{e,i}$	equilibrium solid phase concentration of each component in binary mixture, mg/g
$q_{e,cal}$	calculated value of solid phase concentration of adsorbate at equilibrium, mg/g
$q_{e,\exp}$	experimental value of solid phase concentration of adsorbate at equilibrium, mg/g
q_m	maximum adsorption capacity of adsorbent, mg/g
$q_{\max}$	constant in extended Langmuir isotherm, mg/g
q_t	amount of adsorbate adsorbed by adsorbent at time t, mg/g
Q	adsorption energy, J
R	universal gas constant, 8.314 J/K mol
R^2	Correlation coefficients
R_a	radius of the adsorbent particle assumed to be spherical, m

R_L	separation factor, dimensionless
SS_T	total sum of squares
S	active site on the adsorbent
S/N	Signal-to-noise ratio
$\overline{T}$	overall mean of response
t	time, min
T	absolute temperature, K
T_P	DTG peak temperature, K
T_T	total of all results
V	volume of the solution, l
V_A	Variance due to a parameter A
V_E	Variance due to error
V_I	Instrinic molar volume (cm^3/mol)
w	mass of the adsorbent, g
W_i	initial weight of the sample
$W\tau$	actual weight of the sample
W_f	final weight of the sample
x_i, y_i, z_i	multi-component (competitive) Freundlich adsorption constants of each component, dimensionless
X	Fractional thermal oxidation of adsorbent
X	Degree of transformation
X_{Ae}	fraction of the adsorbate adsorbed on the adsorbent under equilibrium
X	fractional thermal oxidation of adsorbent
y	Actual value of the characteristic
z	an integer

GREEK LETTERS

α'	Degree of transformation, Fractional pyrolysis of the adsorbent
α	Bangham constant (<1)
α_D	ratio of the isosteric enthalpy at zero coverage to that at monolayer coverage
α_i	constant in SRS model for each component, dimensionless
β_i	constant in multi-component Redlich-Peterson model for each component, dimensionless
β	constant of Redlich-Peterson isotherm ($0<\beta<1$)
β_D	pattern parameter
β_i	Slope or linear effect of the input factor x_i
ΔG	Gibbs free energy for active complex formation, kJ/mol

ΔG^0	Gibbs free energy of adsorption, KJ/mol
ΔH	Enthalpy for active complex formation, kJ/mol
ΔH^0	enthalpy of adsorption, KJ/mol
ΔH_w	heat of adsorption of water (normally assumed to be zero), KJ/mol
ΔH_{sol}	heat of solution, KJ/mol
$\Delta H_{st,0}$	isosteric heat of adsorption with zero coverage, KJ/mol
$\Delta H_{st,a}$	apparent isosteric heat of adsorption, KJ/mol
$\Delta H_{st,net}$	net isosteric heat of adsorption, KJ/mol
ΔS	Change in the entropy for active complex formation, k J/mol
ΔS^0	change in the entropy for adsorption, J/^{0}K/mol
ε	Dubinin-Radushkevich isotherm constant
λ_{vap}	heat of vaporization, KJ/mol
$\eta_{L,i}$	multi-component (competitive) Langmuir adsorption constant of each component, dimensionless
$\eta_{R,i}$	multi-component (competitive) Redlich-Peterson adsorption constant of each component, dimensionless
$\theta_i(Q)$	Coverage of each component at energy level Q, dimensionless
μ_D	Interaction energy of the adsorbed adsorbate molecules, KJ/mol
μm	Micron meter
ρ	Density, kg/m^3
τ	Inhibition function
χ	Transmission coefficient
2θ	Scattering angle
^{o}C	Degree Celsius

Chapter – I

INTRODUCTION

1.1 GENERAL

The explosive population growth and expansion of urban areas has exacerbated the adverse impacts on water resources. Up until 1950s, the discharge of waste in the environment was the way of eliminating them, until the self-purifying capacity of the environment was not sufficient. With the increasing concern for public health and environmental quality, the stringent limits on the acceptable environmental levels of organic pollutants have been recognized. The permitted levels have been vastly exceeded; causing such environmental contamination that our natural resources cannot be used for certain uses and their characteristics have been altered. The main problem stems from waste coming from industry and agriculture, despite the fact that the population also plays an important role in environmental contamination. It has now been realized that even trace quantities of organic contaminants in drinking water are hazardous, in particular aromatic and aliphatic hydrocarbons and their substituted compounds. A common problem in most industries is the disposal of large volumes of wastewater containing organic compounds.

Phenols (P_s) are extremely toxic to living species. Exposures to phenol (P) can occur in a workplace, from environmental media, contaminated drinking water or food stuff or from use of consumer products containing P [ATSDR, 1998]. P is absorbed through all routes readily: oral, inhalation, and dermal [Bruce et al., 1987]. P is a strong irritant to eyes and respiratory tract, corrosive to the eyes and skin upon direct contact. Human deaths have occurred following exposure due to ingestion P of through large areas of skin [ATSDR, 1998]. P is considered to be very toxic to humans through oral exposure. The minimum reported lethal dose (LD_{50}) in humans is 4.8 g or approximately 70 mg/kg body weight. Thus, the ingestion of this compound has been reported as lethal with symptoms including muscle weakness and tremors, loss of coordination, paralysis, convulsions and respiratory arrest [ATSDR, 1989].

P and its substituted compounds like 4-nitrophenol (NP), 4-chlorophenol (CP) are toxic and hazardous in nature (contact and exposure through all routes-oral, dermal, ingestion and inhalation). Resorcinol (R), catechol (C) and hydroquinone (HQ) have

higher toxicity than P [Othmer, 1981] and C is considered more toxic than R [Prager, 1997]. C and R are irritants for skin, eyes and mucous membranes. The toxicity of Catechols (C_s) for water flea, zebra fish, trout, rabbit, cat, rat and human cell lines are well demonstrated [Capasso et al., 1995]. C is strong irritant to eyes, skin, and respiratory tract, and it has been proven to cause DNA damage, vascular collapse and death. Acute intoxication with R and C occurs mainly by the oral route; symptoms are nausea, vomiting, diarrhea, pulmonary edema, tachypnea, and depression. Methemoglobinemia and hepatic injury may be noted within a few days after intoxication by R and C [Othmer, 1981]. HQ causes severe effects on the central nervous system and together with R it is carcinogenic [ATSDR, 1998]. Health hazards of various P_s are given in Table 1.1.1.

P_s constitute the 11th of the 126 chemicals, which have been designated as priority pollutants [USEPA, 1987; Rodriguez et al., 2000]. The European Union has also classified several P_s as priority contaminants [Rodriguez et al., 2000]. Due to the toxic nature of some of these compounds, the environmental protection agency (EPA) has set a water purification standard of less than 1 part per billion (ppb) of P in surface waters. In Italy, in agreement with the recommendations of the European Union, the limit for P_s in potable and mineral waters is 0.5 μg/l (0.5 ppb), while the limits for wastewater emissions are 0.5 mg/l (0.5 ppm) for surface waters and 1 mg/l for the sewerage system (law no. 152/2006). These compounds impart objectionable taste and odor to drinking water at concentrations as low as 0.005 mg/l. Therefore, World Health Organisation (WHO) is stricter on P_s regulation with a limit of 0.001 mg/l P_s in potable water [WHO, 1984]. P and associated compounds have been listed as priority-pollutants by the Ministry of Environment and Forests (MoEF), Government of India. MoEF has prescribed that concentration of P_s should not exceed 1.0 mg/l for their discharge into the surface waters and 5.0 mg/l for discharge into the public sewers, on land for irrigation and marine coastal areas. These limits have generally been defined on the basis of the total phenols measured as phenol present in the effluent. The Central Pollution Control Board [CPCB, 2006], India as well as the Bureau of Indian Standards (BIS) have set a discharge standard of 1.0 mg/l concentration of P_s in the industrial effluents for their safe discharge into the surface waters [CPCB, 2006; IS: 2490 (Part 3), 1974]. The discharge standards for certain parameters for liquid effluents from petrochemical and petroleum oil refinery units are shown in Table 1.1.2.

Table 1.1.1. Health hazard information of various pollutants. [Source: Scorecard, Pollution information site. http://www.scorecard.org/chemical-profiles/hazard-indicators accessed June 16, 2010].

Health hazard information	Aniline	
Inhalation	Blue lips or finger nails. Blue skin, Headache, Dizziness. Laboured breathing, Convulsions, Increased heartbeat. Vomiting. Weakness, Headache, Sneezing, abdominal pain and vomiting.	
Ingestion	Unconsciousness	
Skin and eyes	Redness and pain	
Health hazard information	**Phenol**	**Chlorophenol**
Inhalation	Sore throat, sensation, cough, Dizziness, Headache, Nausea, Vomiting, Shortness of breath, Laboured breathing.	Cough, Dizziness, Headache, Laboured breathing. Nausea. Sore throat, Vomiting, weakness
Ingestion	Corrosive, abdominal pain, convulsions, Diarrhoea. Shock or collapse. Sore throat, smoky, greenish-dark urine.	Abdominal pain, unconsciousness.
Skin and eyes	Serious skin burns, numbness, convulsion, collapse, coma and Death.	Redness, Blurred vision and pain.
Health hazard information	**Nitrophenol**	**Catechol**
Inhalation	Blue lips or finger nails. Blue skin, Headache, Dizziness. Laboured breathing, Convulsions, Increased heartbeat, Vomiting. Weakness, Unconsciousness. Weakness	Burning sensation, Diarrhoea, Vomiting
Ingestion	Abdominal pain, sore throat, vomiting.	Abdominal pain, Diarrhoea, Vomiting.
Health hazard information	**Resorcinol**	**Hydroquinone**
Inhalation	Abdominal pain, Blue lips or finger nails. Blue skin, confusion, convulsions, Cough, Dizziness, Headache, Nausea, sore throat, unconsciousness.	Cough, Laboured breathing
Ingestion	Abdominal pain	Dizziness, Headache, Nausea, Shortness of Breath, convulsions, vomiting, Ringing in the ears.

Table 1.1.2. Discharge standards for liquid effluents from petrochemical and Petroleum oil refinery plants in India [CPCB, 2006; MOEF, 2008]

Parameter	Concentration not to exceed, (mg/l) (except pH)	
	Petrochemical plants	Petroleum oil refinery plants
pH	6.5-8.5	6.5-8.5
Oil & Grease	-	5.0
BOD (3 days at 27°C)	50	15
Phenols	5	0.35
Sulphide as S	2	0.5
COD	250	125
Cyanide as CN	0.2	0.2
Ammonia as N	-	15.0
TKN	-	40.0
Fluoride as F	15	-
Total suspended solids	100	20
Chromium	-	-
Hexavalent	0.1	0.1
Total	2.0	2.0
Lead	-	2.0
Mercury	-	0.01
Zinc	-	5.0
Nickel	-	1.0
Copper	-	1.0
Vanadium	-	0.2
Benzene	-	0.1
Benzene (a)-pyrene	-	0.2

Aniline (AN) and P_s are found simultaneously in wastewaters. P_s and AN are mutagenic and also carcinogenic [Abrams and Sims, 1982; Ress et al., 2002]. AN reacts easily in the blood to convert haemoglobin into methaemoglobin, thereby preventing oxygen uptake [Khan et al., 1995]. AN is potentially toxic in the environment due to formation of carcinogenic azo-compounds and other oxidation products arising from interaction with soil enzymes or microflora [Raupach and Janik, 1988; Parris, 1980]. Health hazards of AN are given in Table 1.1.1.

AN is toxic by inhalation of the vapour, absorption through the skin or swallowing. It causes headache, drowsiness, cyanosis, and mental confusion, and, in severe cases, can cause convulsions. Prolonged exposure to the vapour or slight skin exposure over a period of time affects the nervous system and the blood, causing tiredness, loss of appetite, headache, and dizziness [Muir, 1971]. Oil mixtures containing rapeseed oil denatured with AN have been clearly linked by epidemiological and analytic chemical studies to the toxic oil syndrome that hit Spain in the spring and summer of 1981, in which 20,000 became acutely ill, 12,000 were hospitalized, and more than 350 died in the first year of the epidemic. The precise etiology though remains unknown. Some authorities class AN as a carcinogen, although the International agency for research on cancer (IARC) lists it in Group 3 (not classifiable as carcinogenic to humans) due to the limited and contradictory data available. AN dyes are a known risk factor for bladder cancer. Bladder cancer should always be in the differential diagnosis of a patient with hematuria and history of AN exposure. AN wastewater containing highly concentrated organic nitrogenous and aromatic structure is less biodegradable and very toxic to microorganisms [Chen, 2006]. Gheewala et al. [2004] reported that the derivatives of AN are difficult to be degraded and inhibit the biodegradation of other chemicals. Moreover, ammonia is one of the hydrolysis products during the biodegradation, which makes the water more toxic and leads to inhibitory effect.

Essentially there are three technological options available for the removal of P and its derivatives and associated compounds from industrial effluents; physical, chemical and biological treatment methods. These options are either used separately or in combination of each other, to meet the targeted P_s levels in the effluent.

1.2 PHENOL AND ITS DERIVATIVES AND ASSOCIATED COMPOUNDS (P_s)

Phenol and its derivatives and associated compounds (P_s) are very important organic intermediates, used in the manufacture of many products in such units as drugs, rubber, pesticides, varnishes and also, dyestuffs, chemicals, petrochemicals, paper, wood, metallurgy and coking plants [Ramade, 2000; Kumar et al., 2003; Wang et al., 2007].

P_s are defined as hydroxyl derivates of benzene. P, also known as carbolic acid, is a toxic, white with a slightly pink tinge, crystalline solid and is considered to be an extremely hazardous substance. Its chemical formula is C_6H_5OH and its structure is that of a hydroxyl group (-OH) bonded to a phenyl ring, making it an aromatic compound. P can be made from the partial oxidation of benzene, the reduction of benzoic acid, by the cumene process, or by the Raschig-Hooker process. It can also be found as a product of coal oxidation. P is also used in the preparation of cosmetics including sunscreens [Svobodova et al., 2003], hair dyes, and skin lightening preparations [DeSelms, 2008]. Compounds containing P moieties can be used to prevent ultraviolet light-induced damage to hair and skin due to the UV-absorbing properties of the aromatic ring of the P. It is also used in cosmetic surgery as an exfoliant, to remove layers of dead skin. It is also used in phenolization, a surgical procedure used to treat an ingrown nail, in which it is applied to the nail bed to prevent regrowth of nails. 5% P is sometimes injected near a sensory nerve in order to temporarily (up to a year) stop it from transmitting impulses in some intractable cases of chronic neuropathic pain [http://en.wikipedia.org/wiki/Phenol].

AN also known as phenylamine or aminobenzene, is an organic compound with the formula C_6H_7N. It is the simplest and one of the most important aromatic amines, being used as a precursor to more complex chemicals. Its main application is in the manufacture of polyurethane. Like most volatile amines, it possesses the somewhat unpleasant odour of rotten fish and also has a burning aromatic taste; it is a highly-acrid poison. It ignites readily, burning with a smoky flame. AN is a colorless compound. It slowly oxidizes in air giving a red-brown tint to aged samples. Chromic acid converts it into quinone, whereas chlorates, in the presence of certain metallic salts (especially of vanadium), give aniline black. Hydrochloric acid and potassium chlorate give chloranil. Potassium permanganate in neutral solution oxidizes AN to nitrobenzene, in alkaline solution to

azobenzene, ammonia and oxalic acid; and in acid solution to AN black. Hypochlorous acid gives 4-aminophenol and para-amino diphenylamine.

AN is widely used as a raw material in the manufacturing of a number of products. AN, has been used extensively in agriculture, drugs, resins, marking inks, perfumes, shoe polishes, dyes, conducting polymers and many other chemicals of current domestic and industrial interest. Derivatives of AN have been employed to produce herbicides, fungicides, insecticides, animal repellents, defoliants, antiknock compounds in leaded gasoline [Northcott, 1978; OME, 1980], and especially in the dye industry over many years. The US and China produce over 80,000 tonne/year and 457,000 tonne/year of AN, respectively [O'Neill et al., 2000; Qi et al., 2002]. The great commercial value of AN is due to the readiness with which it yields, directly or indirectly, dyestuffs. The discovery of mauve in 1856 by William Henry Perkin was the first of a series of an enormous range of dyestuffs, such as fuchsine, safranine and induline. In addition to its use as a precursor to dyestuffs, it is an intermediate for the manufacture of many drugs, such as paracetamol (acetaminophen, Tylenol). It is used to stain neural RNA blue in the Nissl stain. The largest market (~ 85%) for AN is in the preparation of methylene diphenyl diisocyanate (MDI). Other uses include rubber processing chemicals (9%), herbicides (2%), and dyes and pigments (2%) [http://www.the-innovation-group.com/ChemProfiles/Aniline.htm]. When polymerised, AN can be used as a type of nanowire for use as a semiconducting electrode bridge, most recently used for nano-scale devices such as biosensors. These polyaniline nanowires can be doped with a dopant in order to achieve certain semiconducting properties.

P_S and AN compounds are of great environmental concern because of their high toxicity, even at low concentrations [Razee and Masujima, 2002]. Table 1.1.3 gives physico-chemical properties and solvatochromic parameters of pollutants used in present study for their removal from aqueous solution.

Table 1.1.3. Physico-chemical properties and solvatochromic parameters.

Parameters	AN	P	CP	NP	C	R	HQ	References
Chemical Structure	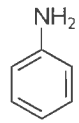	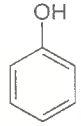	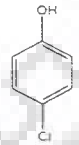	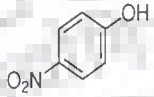	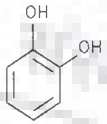	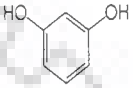		-
	C_6H_7N	C_6H_5OH	C_6H_5Cl	$C_6H_5NO_3$	$C_6H_6O_2$	$C_6H_6O_2$	$C_6H_4(OH)_2$	
Other names	Phenylamine Aminobenzene Benzenamine	Carbolic acid Phenic acid Hydroxybenzene	p-Chlorophenol 4-Chloro-1-hydroxybenzene, 4-Hydroxychlorobenzene	p-Nitrophenol 4-Hydroxynitrobenzene	Pyrocatechol 1,2-Benzenediol 1,2-Dihydroxybenzene	1,3-Dihydroxybenzene 1,3-Benzenediol 3-Hydroxyphenol Resorcin	p-Benzenediol; 1,4-Benzenediol; Dihydroxybenzene; 1,4-Dihydroxybenzene; Quinol	-
Colour	Colourless to yellow or light pink crystals, with characteristic odour	Colourless to yellow crystals, with characteristic odour	Colourless to pale yellow crystals	Colourless crystals, with characteristic odour. turns brown on exposure to air and light	White crystals. turns pink on exposure to air, light or on contact with iron	colourless crystals	Colourless oily liquid, with characteristic odour. turns brown on exposure to air or light	NIOSH [2005]
λ_{max} (nm)	230	269	279	317	275	273	289	[Yang et al., 2008; Richard et al.,2009; Mohamed et al., 2006]
Melting point (°C)	-6	43	43	113–114	10	110	172	Othmer, 1981]
Boiling point (°C) (101.3 kPa)	184	182	220	279	245.5	277	287	Othmer, 1981]
Flash point (°C)	70	79	121	169	127	127	165	[IPCS, 2005]
Auto-ignition temperature (°C)	615	715		490	510	607	515	[IPCS, 2005]

Table 1.1.3. (Contd.)

Parameters	AN	P	CP	NP	C	R	HQ	References
log Pow at 25 °C	0.94	1.46	2.39	1.91	0.88	0.79-0.93	0.59	[Beezer et al., 1980; Kamlet et al., 1988; IPCS, 2005]
Density g/cm^3	1.02	1.06	1.3	1.5	1.344	1.28	1.3	Yang et al., 2008; Kamlet et al., 1988]
Vapor pressure (at 20°C, Pa)		47	13	0.0032	4	0.065 (extrapolated); 0.027 (measured)	-	[Hoyer and Peperle, [1958]
MW,g/mol	93.13	94.11	128.56	139.11	110.11	110.11	110.1	[IPCS, 2005]
C_s,g/l at 25 ^{0}C	34	83	27	12.4	1100	1100	1100	[IPCS, 2005; Yalkowsky and Dannenfelser, 1992]
Molecular size	0.52 nm	0.42 nm			0.55 nm× 0.55nm	0.56nm × 0.47 nm		[Zhang et al., 2007; Huang et al., 2009;]
pK_a	4.63	9.95	9.38	7.15	9.25, 13	9.2, 10.9	9.9,11.6	[Fiore and Zanetti, 2009; Yang et al., 2008; EHC 157, 1994]
A_m, nm^2	0.47	0.437	0.482	0.519				[Laszlo et al., 2007; Caturla et al., 1988]
D, Debye	1.17	1.233	1.477	5.44	2.620	2.071	0.0	[Hatta et al. 1973; [Yogesh et al., 2008]
π	0.73	0.72	0.72	1.01	11.89±0.5x10^{-24}	59.11x 10^{-24}	0.21±0.02	[Yang et al., 2008; Kamlet et al., 1988]
V_I	0.567	0.536	0.625	0.685				[Yang et al., 2008; Kamlet et al., 1988]
α_s	0.16	0.61	0.67	0.93	0.85	1.10		[Yang et al., 2008; [Frich et al., 2003]
β_m	0.5	0.33	0.72	1.01	0.58	0.52		[Yang et al., 2008; Frich et al., 2003]

log Pow: Octanol/water partition coefficient ; MW= Molecular weight; (g/l) ;C_s =Water solubility; A_m=Projected area; D= Dipole moment; π=Polarity /Polarizability parameter; V_I= Intrinsic molar volume; α_s= hydrogen-bonding donor parameter; β_m= hydrogen-bonding acceptor parameter.

1.3. INDUSTRIAL AND NATURAL SOURCES OF P AND ITS DERIVATIVES AND ASSOCIATED COMPOUNDS.

AN, P, CP, NP, C, R and HQ are emitted from industrial plants in the form of vapors and in aqueous effluents. P_s are present in wastewater of various industries, such as refineries (6–500 mg/l), coking operations (28–3900 mg/l), coal processing (9–6800 mg/l), and manufacture of petrochemicals (2.8-1220 mg/l). P_s are also the main organic constituents present in condensate streams in coal gasification and liquefaction processes. Other sources of waste stream water containing P_s are pharmaceutical, plastics, wood products, paint, and pulp and paper industries (0.1–1600 mg/l) [Patterson, 1975; Mukherjee et al., 2007]. As a particular case, olive oil mill wastewaters, rich in P and polyphenol derivatives give rise to phytotoxicity. P_s contribute off-flavours in drinking and food processing waters [Busca et al., 2008]. Total P concentration in the wastewater of a typical Indian refinery processing 5.0 million tons of crude per year is ~135 mg/l and the wastewater discharge varies from 125 to 250 m^3/h with pH being in the range of 8.8–9.4 [Mukherjee et al., 2007]. The concentration of phenolic compounds in the wastewater from resin plants is typically in the range of 12–300 mg/l. Highest concentration of P (>1000 mg/l) is found in the wastewater generated from coke processing plants [Kumaran and Paruchuri, 1997]. Resin manufacture and processing produce wastewaters with a P concentration in the range of 12–300 mg/l [Patterson, 1975]. P and its derivatives can also originate from diffuse emissions, e.g. from the tar coatings of the roads and pipes and from the use of pesticides including their transformation products, e.g. herbicides, fungicides like CP, NP and dinitroorthocresol (DNOC), etc. C and HQ widely exist in industrial effluents, such as the waste from oil refineries, coal tar, plastic, leather, paint, steel and pharmaceutical industries [Terashima et al., 2002; Xiao and Xiao, 2007; Yu et al., 2009]. C, R and HQ were used widely as industrial solvents. C is also widely used to produce food additive agents, hair dyes, and antioxidants [Dellinger et al., 2001]. Similarly, R is used to produce dyes, plastics, and synthetic fibers [Merck, 1989; Milligan et al., 1998; Hays et al., 2005]. There are several methods to determine various types of P_s like using spectrometric detection [Lupetti et al., 2004], chromatography with different detectors [Rodriguez et al., 2000; Kojima et al., 2004]. However, only a few researchers have reported the concentration of P_s in air samples [Hanada et al., 2002; Pistonesi et al., 2004].

AN can enter into the environment from anthropogenic sources during any stage in its production, storage, transport, use, and disposal or from AN-containing materials such as coal tar and solutions arising as industry effluents. AN is the common substance found in the effluents of pharmaceutical, dyestuff, photographic, and agrochemical industries. Crude petroleum oils in north-eastern China contain more nitrogen compounds, compared to those of other countries, because of their geological origin [Wang and Zheng, 1999]. As a result, the wastewater produced from the treatment of such crude oils is rich in pentyl amine and AN. This complicates the effective treatment of such wastewaters. Such wastewaters are often treated using photo-decomposition, electrolysis, resin adsorption, or ozone oxidation but the cost of such treatments limits their application to small scale facilities [Qi et al., 2002; Gheewala et al., 2004].

Exposure of the population living near plants producing or utilizing P and its derivatives and associated compounds, is therefore, expected. Contamination of food and water is also possible. With the exception of the contamination of water supplies through accidental spillage, levels of exposure would generally be low. The highest potential for exposure is at the workplace, both through inhalation of vapor and contamination of the skin by liquid AN, P, CP, NP, C, R and HQ.

1.4 TREATEMENT PROCESSES FOR AN, P, CP, NP, C, R AND HQ BEARING WASTEWATERS

Several treatment methods including adsorption have been recommended for the treatment of wastewaters containing P_s and AN. Adsorption has been used by many investigators. The adsorption of P_s from aqueous solution onto activated carbon (AC) has been investigated extensively for decades [Zogorski et al., 1976; Salame and Bandosz, 2003; Ten Hulscher and Cornelissen, 1996; Khan et al., 1997; Swamy et al., 1997]. The adsorptive removal of phenolics like P, CP, NP, C, R and HQ from aqueous solutions using other adsorbents have also been studied [Kumar et al., 1987; Bhandari and Cho, 1999; Daifullah and Girgis, 1998; Ravi and Jasra, 1998; Srivastava et al., 2007; Richard et al., 2009, 2010; Rodriguez et al., 2008; Blanco-Martinez et al., 2009; Yildiz et al., 2005; Ayranci and Duman, 2005; Ahmaruzzaman and Sharma, 2005]. Adsorption of AN from aqueous solution have been reported by several authors [Orshansky and Narkis, 1997; Laszlo et al., 2007; Cotoruelo et al., 2007].

Detailed literature survey for removal of AN, P, CP, NP, C, R and HQ using adsorption is presented in Chapter II.

1.5 ACTIVATED CARBON (AC) AS AN ADSORBENT

AC has been used extensively in adsorption studies and in field-scale treatment of wastewaters. The adsorption capacity of AC depends on characteristics: texture (surface area, pore size distributions), surface chemistry (surface functional groups), and ash content. It also depends on adsorbate characteristics: molecular weight, polarity, pKa, molecular size, and functional groups. Finally, the solution condition is another factor to be taken into account. This includes pH, adsorbate concentration and presence of other possible adsorbates. AC is available in the market. However, its characteristics depends heavily on the source from which it has been manufactured and the process of its manufacture and activation. AC can be recycled, reactivated, or regenerated from spent AC.

The primary use for AC is the treatment of water, including potable water (24% of all use); wastewater (21%) and groundwater remediation (4%). AC has an extraordinarily large surface area and pore volume that gives it a unique adsorption capacity [Baker et al., 1990]. The surface area of commercial grade AC ranges between 300 and 2,000 m^2/g [Burdock, 2007]. Some have surface areas as high as 5,000 m^2/g. AC is also used as decolorizing agent; as taste- and as odor-removing agent; as purification agent in food processing. Food and beverage production accounts for only about 6% of the market for liquid-phase AC. Of this, the greatest use is decoloring sugar. More recent applications have enabled the production of xylose and its derivatives from complex cellulose sources via fermentation and activated charcoal [Mussatto and Roberto, 2001]. AC adsorption remains the most common method used to decolor vinegar [Achaerandio, et al., 2002]. Granular activated carbon (GAC) has been used for the adsorptive removal of phenolic compounds [Swamy et al., 1997; 1998; Srivastava et al., 2006a: Kumar et al., 2008], dyes [Mall et al., 2005; 2006], pyridine [Lataye et al., 2006], 2-picoline [Lataye et al., 2008, 2009] and heavy metals [Srivastava et al., 2006b, 2007, 2008a] from wastewaters. The Dye removal was also investigated using a hybrid adsorbent that was prepared by pyrolysing a mixture of carbon and fly ash [Ravikumar et al., 2005].

1.6 TAGUCHI'S EXPERIMENTAL DESIGN

Taguchi's experiments are, generally, conducted in such a manner as to optimize 'one-factor at-a-time'. This methodology overlooks the interactive effects of various factors on the sorption process. Fractional factorial design based on Taguchi's orthogonal array can be a very effective methodology to investigate the effects of multiple factors as well as potential interactions between these factors in a time and cost effective manner [Taguchi, 1986]. It has been used extensively in carrying out experiments and devising a strategy for quality control in the manufacturing industries. Recently, chemical and environmental engineers have started applying Taguchi's design of experimental methodology in various studies. Kim et al. [2004] optimized the experimental conditions based on the Taguchi robust design for the formation of nano-sized silver particles by chemical reduction method; Mohammadi et al. [2004] separated copper ions by electrodialysis; and Madaeni and Koocheki [2006] optimized the conditions for wastewater treatment using spiral-wound reverse osmosis element. Kaminari et al. [2007] used an electrochemical reactor for recovering heavy metals from acidified aqueous solutions for different process parameters as metallic ion concentration, current density and bed expansion. Plessis and Villiers [2007] applied Taguchi's method in the evaluation of mechanical flotation in waste activated sludge thickening. Moghaddama et al. [2006] used Taguchi's design methodology to determine the optimum purification conditions for minimizing the lead, cadmium, nickel and cobalt contents in the leaching solutions obtained from ammoniacal ammonium carbonate leaching of non-sulphide zinc ores. Srivastava et al. [2007] recently applied this methodology for multi-component adsorption of metal ions onto bagasse fly ash (BFA). Taguchi's methodology of optimal design of experiments for multicomponent adsorption has been described by Srivastava et al. [2007] and Lataye et al. [2008]. The method has been used in multicomponent adsorption of metal ions and pyridine and its derivatives by rice husk ash (RHA) [Srivastava et al., 2008b; Lataye et al., 2009] and bagasse fly ash (BFA) [Srivastava et al., 2007; Lataye et al., 2008]. In the present study, Taguchi's L_{27} (3^{13}) orthogonal array (OA) matrix, which incorporates five parameters experimental design is applied to investigate the effect of process parameters on the removal of AN, P, CP, NP, C, R and HQ from aqueous mixture solutions for binary and ternary system and L_9 orthogonal array (OA) matrix is applied to investigate the effect of process parameters namely flow rate (Q), bed height (Z) and

column diameter (D) for determine the breakthrough point and to determine the characteristic parameters of the column for the ternary aqueous system.

A survey of the literature as given in Chapter II shows that adsorption data for simultaneous adsorption of P and its derivatives and its associated compounds from binary and ternary is very meager. Also, no literature is available utilizing Taguchi's method for designing experiments on the simultaneous adsorption of P and its derivatives and associated compounds from aqueous solutions. Therefore, it is desirable to gather adsorption data for individual and simultaneous adsorption of P and its derivatives and its associated compounds onto GAC using batch and column study.

In the present study, Taguchi's L_{27} (3^{13}) orthogonal array (OA) matrix, which incorporates five parameters experimental design is applied to investigate the effect of process parameters on the removal of AN, P, CP, NP, C, R and HQ from aqueous mixture solutions for binary and ternary system and L_9 orthogonal array (OA) matrix is applied to investigate the effect of process parameters namely flow rate (Q), bed height (Z) and column diameter (D) for determine the breakthrough point and to determine the characteristic parameters of the column for the ternary aqueous system.

1.7 OBJECTIVES OF THE PRESENT STUDY

On the basis of the literature survey, the following aims and objectives have been set for the present work:

1. To characterize the GAC for its physico-chemical and adsorption properties before and after adsorption of adsorbates. These characteristics include the analysis of particle size, pore size distribution and proximate analysis. Determination of surface and functional characteristics of GAC by acid base titration, scanning electron microscopy (SEM), X-ray diffraction (XRD), Fourier Transform Infra-red (FTIR) spectroscopy and Thermogravimetric analyzer (TGA).
2. To study the effect of various parameters like initial pH (pH_0), adsorbent dose (m), contact time (t), initial concentration (C_0), and temperature (T) on the individual removal of AN, P, CP, NP, C, R and HQ from the aqueous solution by GAC in batch study.
3. To carry out kinetic and equilibrium adsorption studies of AN, P, CP, NP, C, R and HQ onto GAC and to analyze the experimental data using various

kinetic and isotherm models.

4. To understand the thermodynamics of adsorption and to estimate the isosteric heat of adsorption for AN, P, CP, NP, C, R and HQ adsorption using GAC as adsorbent.
5. To utilize Taguchi's optimization method for the design of experiments for estimating the effects of various adsorption parameters in binary, and ternary systems in the batch and column adsorption studies.
6. To carry out multi-component (binary and ternary) isotherm modelling for the adsorption of various adsorbates from multi-component mixtures.
7. To perform desorption study for the possible regeneration of GAC, and to develop a method for disposing off the spent GAC by fixing the (chemically or physically) AN, P, CP, NP, C, R and HQ.

Chapter – II

LITERATURE REVIEW

2.1 GENERAL

This chapter has been divided into three parts: the first part deals with the review of various studies on the treatment of synthetic wastewater containing aniline (AN), phenol (P), 4-chlorophenol (CP), 4-nitrophenol (NP), catechol (C), resorcinol (R) and hydroquinone (HQ). In the second part, a comprehensive review of literature on the removal of various types of adsorbates from aqueous solutions by adsorption using granular activated carbons (GAC) and other adsorbents has been reported. The third part reviews the application of Taguchi's design of methodology for adsorption studies.

2.2 TREATMENT METHODS FOR ANILINE, PHENOL, 4-CHLOROPHENOL, 4-NITROPHENOL, CATECHOL, RESORCINOL AND HYDROQUINONE BEARING WASTEWATERS

Several treatment technologies have been employed for the treatment of wastewaters containing phenols (P_s) and its derivatives/associated compounds (AN, P, CP, NP, C, R and HQ). Physico-chemical, biological, and thermal processes have been in use for the treatment. The physico-chemical treatment processes include adsorption, chemical precipitation, and ion exchange. Table 2.2.1 summarizes commonly used technologies for the treatment of wastewaters containing phenolic and its associated compounds.

All the methods have some advantages and some drawbacks. Because of the high cost and disposal problems, many of these conventional methods for treating P_s and its associated compounds in wastewaters have not been widely applied at a large scale in the coke-oven, resin, petrochemical, textile and paper industries. Biological treatment requires a large land area and is constrained by sensitivity toward diurnal variation as well as toxicity of some chemicals, and it has less flexibility in design and operation. Biological treatment does not provide satisfactory P_s removal with current conventional biodegradation processes [Ahmaruzzaman, 2005]. Although some organic molecules are amenable to biodegradation, many others are recalcitrant to biological treatment due to their complex chemical structure and synthetic organic origin as well as their toxicity at

higher concentrations. However, in the presence of other biodegradable compounds, even the recalcitrant compounds get degraded [Subramanyam and Mishra, 2008].

Conventional methods for the removal or destruction of P and its derivatives and its associated compounds from wastewaters include solvent extraction, biodegradation [O'Neill et al., 2000; Latkar et al., 2003; Kumar et al., 2005; Subramanyam and Mishra, 2007; Subramanyam and Mishra, 2008; Nasr et al., 2005; Chien et al., 2009], photocatalysis [Arana et al., 2005], catalytic oxidation [Barbier et al., 2002; Garg et al., 2010], membrane separation [Pithan et al., 2002; Devulapalli and Jones, 1999; Jadhav et al., 2001; Juang and Huang, 2009; Ivancev-Tumbasa et al., 2008; Lin et al., 2006], ultrasonic degradation [Jiang et al., 2006], supercritical water oxidation [Qi et al., 2002], and electrochemical oxidation [Brillas and Casado, 2002; Yang, 2004]. Solvent extraction usually produces liquid organic secondary waste, which may cause environmental problems. The biodegradation is not suitable to the wastewater with high concentration of P_s and salts.

Chemical methods include coagulation or flocculation combined with flotation and filtration, precipitation–flocculation with $Fe(II)/Ca(OH)_2$, electro-flotation, electrokinetic coagulation, conventional oxidation methods by oxidizing agents (ozone), irradiation or electrochemical processes. These chemical techniques are often expensive and accumulation of concentrated sludge creates a disposal problem [Ahmaruzzaman and Gayatri, 2010]. There is also the possibility that a secondary pollution problem will arise because of excessive chemical use. Recently, other emerging techniques, known as advanced oxidation processes, which are based on the generation of very powerful oxidizing agents such as hydroxyl radicals, have been applied with success for pollutant degradation. Although these methods are efficient for the treatment of wastewater contaminated with pollutants, they are very costly and commercially unattractive. The high electrical energy demand and the consumption of chemical reagents are common problems [Han et al., 2006; Ahmaruzzaman and Gayatri, 2010]. Different physical methods are also widely used, such as membrane-filtration processes (nanofiltration, reverse osmosis, electrodialysis, etc.) and adsorption techniques. The major disadvantage of the membrane processes is that they have a limited lifetime. Membrane fouling is a major problem and the cost of periodic replacement makes them of the economically unviable. Liquid-phase adsorption is one of the most popular methods

for the removal of pollutants from wastewaters. Proper design of the adsorption process produces high quality treated effluent. This process provides an attractive alternative for the treatment of contaminated waters, especially if the adsorbent is inexpensive and does not require an additional pre-treatment step before its application.

Adsorption has been found to be superior compared to other techniques for water reuse in terms of initial cost, flexibility and simplicity of design, ease of operation and insensitivity to toxic pollutants. Amongst all the adsorbent materials used, activated carbon is the most popular [Derbyshire et al., 2001; Babel and Kurniawan, 2003] In particular, the effectiveness of adsorption on GAC for the removal of a wide variety of phenolic compounds from wastewaters has made it an ideal alternative to other expensive treatment options.

Phenolic compounds are usually present in various forms [Srivastava and Tyagi, 1995], therefore, it is important to understand the competitive effects that can take place in such systems. Unfortunately, very few researchers have studied the competitive adsorption of ternary mixtures of P and its derivatives and its associated compounds in batch and column systems [Garcia-Araya et. al., 2003; Olgadehan and Susu, 2004].

Akaya et al. [2002] have reported studies on a cross-flow enzyme-immobilized membrane reactor for the removal of P and C from water. Crude enzyme extract was chemically immobilized onto a flat polyamide membrane with nominal pore size of 0.2μm. The highest P-degradation rate was 1.3μg/cm^2 s when C_o=500 μg/ml at the flux rate of 4.60 × 10^{-3} ml/cm^2 s and further performance can be increased at higher cross-flow velocities because the reaction is diffusion-controlled. In addition to this, optimum enzyme load and large membrane area contribute to better reactor performance. However, the hydrodynamic conditions in the vicinity of reaction media should be optimized because the shear rates existing during the cross-flow filtration can affect the reaction rates [Drioli and Giorno, 1999].

Solvent extraction [Wadekar and Sharma, 1981], adsorption, and membrane processes have been proposed as less energetically intensive separations for the removal and recovery of P and its derivatives and associated compounds from wastewater.

Liquid extraction has some drawbacks: when the concentration in the wastewater is very low or a polar solvent is used, recovery efficiencies are low; if a polar solvent is used, the wastewater becomes contaminated with the solvent because of its high solvent

solubility [Krishnakumar and Sharma, 1984]. The tendency to form stable emulsions of the two phases is a further problem of liquid extraction [Netke and Pangarkar, 1996]. The use of solid adsorbents such as AC [Orshansky and Narkis, 1997] or organobentonite [Zhu et al., 1998] avoids the problems of phase separation. However, adsorbent regeneration is required, and this operation often implies destruction of the compound [Orshansky and Narkis, 1997] or its dissolution in a liquid, thus requiring further treatment [Chiang et al., 2002]. The stability and loss of the adsorbent phase is also an issue.

P can be efficiently removed from polluted wastewaters by using a strong-base anion exchanger [Carmona et al., 2006]. A simple empirical model was able to reproduce the measured total uptake of P. The pH dependent equilibrium isotherms can be explained assuming that the uptake of P in the resin is accomplished by two ways: ion exchange and molecular adsorption. Adsorption of P onto IRA-420 is predominant at acidic pH, whereas both adsorption and ion exchange are important at alkaline pH. The theoretical model developed enabled the relation between P removal, pH and amount of resin to be determined.

Ozbelge et al. [2002] have investigated the removal of phenolic compounds from rubber–textile wastewaters by physico-chemical process using four different types of coagulants ($Al_2(SO_4)_3$, $Fe_2(SO_4)_3$, $FeSO_4$, $FeCl_3$) with or without lime ($Ca(OH)_2$) addition. The optimum results were obtained by using 50% $FeCl_3$ solution and lime at various dosages at 296K and pH=12.

Lu et al. [2005] studied the effect of chloride ions on AN oxidation in order to explore the mechanism of chloride ions inhibition. The inhibition effect by chloride ions could be overcome by extending the reaction time if the concentration of chloride ions is at a low level. At high concentrations of chloride ions, the oxidation of AN was inhibited, and was stopped due to the complexation of Fe–Cl. A greater amount of ferrous ions rather than hydrogen peroxide can break the inhibition originating from the chloride ions if the initial ferrous ion concentration is too low to overcome the complex effect. The inhibition effect of chloride ions on the AN reaction depended on the reaction pH; the extent of inhibition decreased with increasing initial pH when the pH<5. Consequently, the inhibition effect by chloride ions was primarily due to the complexation of iron species and chloride ions. The influence of chloride ions on AN oxidation due to the competition of hydroxyl radicals was not significant.

Thepsithar and Roberts [2006] studied the electrokinetic treatment to P contaminated soil combined with the addition of a chemical oxidant (permanganate) to the catholyte. It was found that the counter-current flow of the P (by electrosmosis) and permanganate (by electromigration) leads to a rapid oxidation of the P in the soil. After 5 days of treatment over 90% of the P (C_o=1 g/ kg dry soil) in a 15 cm long container of kaolin was removed by electrokinetic treatment with a voltage gradient of 1 V/cm and an initial concentration of $KMnO_4$ of 9 g/l in the catholyte. This level of treatment was achieved with an electrical energy consumption of less than 15 kWh/ m^3 of soil treated.

Kim et al. [2009] investigated the removal of P by catalytic wet oxidation (CWO) using mixed oxide ($Ce0.65Zr0.35O_2$) applied as a support of transition metal (Mn, Fe, Co, Ni, and Cu). The prepared catalysts showed an enhanced catalytic activity for CWO of P due to the excellent redox properties of ceria-zirconia mixed oxide. Among the prepared catalysts, the $CuOx/Ce0.65Zr0.35O_2$ was the most effective catalyst in view of catalytic activity and CO_2 selectivity. The leached copper ions seem to contribute to the higher conversion of P over the $CuOx/Ce0.65Zr0.35O_2$ via homogeneous catalysis. The characterization with XPS, and TPR experiments confirmed that the active copper species in the $CuOx/Ce0.65Zr0.35O_2$ is highly dispersed Cu^{2+} clusters. Although the $MnOx/Ce0.65Zr0.35O_2$ showed a high conversion of P and TOC, the converted P was mainly changed to carbon deposits on the surface of the catalyst resulting in catalyst deactivation.

Various researchers investigated the removal of P and its derivatives and its associated compounds by bisorption process. Kumar et al. [2009] have studied the removal of P, 2-chlorophenol (2CP) and CP on polyporus fungus from water. The adsorption capacity of the biosorbent was investigated as a function of pH, contact time, initial concentration of adsorbate and the amount of biomass employed. The adsorption process followed pseudo-first-order kinetic model. The maximum monolayer adsorption capacity of polyporus fungus for P, 2CP and CP were found to be 50 mg/g, 86 mg/g and 112 mg/g, respectively. Desorption of phenolic compounds was achieved using 0.1 M NaOH solution. The experimental results demonstrated that the polyporus fungus could be used as a sorbent for immobilizing phenolic compounds.

Villacanas et al. [2006] have reported the adsorption results for simple aromatic compounds on various ACs. The surface chemistry of AC plays a key role in the adsorption of

aromatic compounds because it affects both electrostatic and dispersive interactions. It was observed that the oxidative treatment of AC provides a material with a lower pH_{pzc} and electronic density; the thermal treatment eliminates the surface oxygen-containing groups, causing the opposite effect, that is, the increase of pH_{pzc} and electronic density in the basal planes. Dispersive interactions are favored in the thermally treated carbon. The electrostatic interactions were stronger than the dispersive ones only in the case of AN adsorption at pH=2. At this pH, there are anilinium cations in solution, and all the solid samples are charged positively (pH < pHpzc) except the acid sample.

Srivastava et al. [2006a] have reported the adsorption of P on bagasse fly ash (BFA) the BFA and activated carbon commercial grade (ACC) and laboratory grade (ACL). Batch studies were performed to evaluate the influences of various experimental parameters like initial pH (pH_0), contact time, adsorbent dose and initial concentration (C_o) on the removal of P. The initial concentration was varied in the range of $75 \leq C_o \leq 300$ mg/l for studies on the adsorption isotherm studies and the effect of temperature on adsorption. Optimum conditions for P removal were found to be $pH_0 \approx 6.5$, adsorbent dose $\approx$10g/l of solution and equilibrium time $\approx$5 h. Adsorption of P followed pseudo-second order kinetics with the initial sorption rate for adsorption on ACL being the highest followed by those on BFA and ACC. The effective diffusion coefficient of P is of the order of 10^{-10} m^2/s. Equilibrium isotherms for the adsorption of P on BFA, ACC and ACL were analysed by Freundlich, Langmuir, Temkin, Redlich–Peterson, Radke–Prausnitz and Toth isotherm models using non-linear regression technique. Redlich–Peterson isotherm was found to best represent the data for P adsorption on all the adsorbents. The change in entropy (ΔS_0) and heat of adsorption (ΔH_0) for BFA were estimated as 1.8 MJ/kg.K and 0.5 MJ/kg, respectively. The high negative value of change in Gibbs free energy (ΔG_0) indicated the feasible and spontaneous adsorption of P on BFA. The values of isosteric heat of adsorption varied with the surface loading of P.

Zhang et al. [2006] reported on the use of hypercrosslinked polymeric adsorbent NDA100 for separating NSA, P and AN from their aqueous solutions. The larger uptakes of AN was partly attributed to its greater electron density in the aromatic ring than P and NSA, which provides stronger dispersion interaction between adsorbate and adsorbent. The larger cooperative response factors of NSA are probably due to the greater acid–base interaction between the loaded NSA and AN molecules, which is more valuable for the loaded AN

molecules to attract NSA molecules in solutions. Similarly, the stronger acid–base interaction also causes more loaded AN molecules to be desorbed by NSA molecules in the solutions and results in the smaller cooperative response factor of AN in NSA/AN adsorption than in P/AN adsorption. A modified Langmuir model was developed to correlate binary adsorption equilibrium data using only single-component isotherm parameters and binary fitting parameters.

Podkoscielny and Laszlo [2007] used activated carbon (AC) for adsorption of AN from aqueous solutions. The Dubinin–Astakhov model and of Langmuir–Freundlich model seemed reliable for the experimental data. Increasing the pH gradually improved the strength of the interaction and uptake of AN from aqueous solutions. The most basic AC gave the maximum uptake of the AN in the molecular form (pH > pKa) for pH=12. They suggested that the adsorption energy of AN on AC is stronger (>19 kJ/mol) than that of water for the un-buffered solution.

The empirical model for the concentration in the liquid phase (D-H) provides a good description of the kinetics of aromatic compound adsorption onto AC [Cotoruelo et al., 2007]. This model has been used to determine q_m and q_t (achievable coverage at the maximum contact time and coverage at time t, respectively), which have been used in the driving force determination in the kinetic model for the concentration on the solid phase. The temperature effect on the adsorption of aromatics from water solutions is observed with an increase in the rate of adsorption, as a result of an increase in the diffusion coefficients with temperature increase.

Ko et al. [2007] reported sorption of NP, P and AN compounds by various organo-clays in terms of the concentration, solubility and log K_{ow} of sorbates, temperature, kinetic reaction time, and steric contour of organics. The suspension pH was found to have no significant influence on the sorption of P compounds by organo-clays through hydrophobic chemical reaction. The rate limiting step of the NP sorption reactions on organo-clays (i.e., 15A, 30B, 93A) was diffusion-controlled process, however, NP adsorbed by 10A showed the activation energy of 84.15 kJ/mol, indicating chemically-controlled processes.

Srivastava et al. [2008] investigated the adsorptive removal of P from synthetic aqueous solutions by BFA at 303 K under dynamic conditions in a packed bed. The effects of sorbent bed length (Z: 40-90 cm), flow rate (Q: 0.01-0.04 l/min), bed diameter (D: 2-4 cm), and initial concentration (C_o: 50-500 mg/l) on the sorption characteristics of P were investigated at an influent pH of 6.5. More than 99.5% of P was removed in the

column operated at C_o 100 mg/l of P. The column performance improved with increasing Z and decreasing Q. The Bohart-Adams, Thomas, Yoon-Nelson, Clark, and Wolborska models were applied to the experimental data to represent the breakthrough curves and determine the characteristic design parameters of the column. The bed depth service time model at 50% breakthrough provided a good fit to the experimental data, and the sorption capacity of the adsorbent was found to be close to the value predicted from a batch study. The sorption performance of the BFA columns could be well described by the Thomas, Yoon-Nelson, and Clark models at effluent-to-influent concentration ratios (C/C_o) > 0.08 and < 0.99. Application of the Wolborska model to the experimental data for C/C_o<0.5 enabled the determination of the kinetic coefficients for mass transfer in these systems. All of the models can be applied to describe the dynamic behavior of the column sorption with respect to bed length and flow rates. The sorptive capacity of BFA for P was found to be 9.93 mg/g.

The adsorption equilibrium characteristics for single and binary components of copper ion and P onto powdered activated carbon (PAC), alginate bead and alginate-activated carbon (AAC) bead were studied [Kim et al., 2008]. Adsorption equilibrium data of P and copper ion onto the adsorbents could be represented by Langmuir equation. The adsorption capacity of P was in the following order: PAC > AAC bead > alginate bead. Multi-component equilibrium data were correlated by three different models. The ideal adsorbed solution theory (IAST) gave the best fit to the experimental data.

Lin and Xing [2008] reported the adsorption of -OH substitution on P and found the adsorption in the following order: P < C < Pyrogallol onto CNTs over a wide range of pH (4.0-6.5). Sorption increased sharply from P to C and then to Pyrogallol, while their hydrophobicity decreased. Thus, the hydrophobic interaction can be ruled out as a major influencing factor regulating the sorption of these phenolics onto CNTs. Four possible solute sorbent interactions were considered: (a) hydrophobic interaction; (b) electrostatic attraction or repulsion; (c) hydrogen bonding between the -OH and the tube surface -OH or -COOH groups; and (d) -OH substitution-enhanced π-π interactions between the phenolics and the CNTs.

Patil and Shinde [1988] conducted experiments on the biodegradation of AN and/or nitrobenzene in AN plant wastewater. The effects of various parameters have been reported and critically discussed. The results are precise and afford simultaneous

determinations of AN and nitrobenzene. Patil and Shinde [1988] reported a systematic study on the biodegradation of AN and nitrobenzene in monosubstrate, binary substrate, and AN plant wastewater system by GC-FID using a Tenex column. This method was found to be rapid; the total analysis time being less than 10 min and provided direct determination of both nitrobenzene and AN. Peres et al. [1998] has reported that in a mixing through a three-reactor system a nitroreducing consortium and an AN-degrading Co-*mamonas acidovorans*, a mixed population was formed which was able to mineralize the nitroaromatic compound nitrobenzene via AN, its corresponding amino-aromatic compound. When aeration was optimum for growth, only 16% of the 0.5 mM nitrobenzene introduced was mineralized. Decreasing the aeration led to an increase in the amount of nitrobenzene reduced and decreased its volatilized fraction. A decrease in aeration did not slow down AN mineralization, although the latter is catalyzed by dioxygenases. This mixed population is thus able to remediate nitrobenzene and also AN, which is often found with the former in the environment.

Milligan and Häggblom [1998] Examined the anaerobic degradation of C (1, 2-dihydroxybenzene), R (1, 3-dihydroxybenzene), and HQ (1, 4-dihydroxybenzene). Anaerobic denitrifying enrichments were established with sediments from an estuarine tidal strait in New Jersey, USA. The three dihydroxybenzene isomers were provided as sole carbon source in separate enrichment series. R- and C-degrading consortia used their respective substrates over repeated feedings. Initial loss of HQ was observed, but activity could not be maintained. The degradation of R and C was coupled to denitrification and was dependent on nitrate or nitrite as an electron acceptor. Nitrate consumption and N_2 production corresponded to the stoichiometric values predicted for the oxidation of dihydroxybenzenes to CO_2.

O'Neill et al. [2000] investigated the degradation of AN by bacterial consortia under aerobic, fermentative, nitrate-reducing and sulphate-reducing conditions and a variety of salt concentrations (0.2, 4 and 7% NaCl w/v) and pH values (5 and 7). They found that the rate of bacterial growth decreased with increasing salinity. The bacterial consortium of each batch culture generally maintained its ability to degrade AN when salt concentrations and pH were changed; although often the lag-phase prior to growth was extended. Microbial populations in fixed film continuous reactors was able to tolerate changes in NaCl concentration. Increasing AN concentration (0.25±1 g/l) under 0.2%

NaCl (pH 5 and 7) conditions, resulted in AN removal without affecting growth rates. At the lower pH, cell yield was not adversely affected by an increase in AN concentration. However, at neutral pH, cell yield decreased with increasing AN concentration.

Kuscu and Sponza [2007] studied the anaerobic treatability of NP was investigated in an anaerobic/aerobic sequential reactor system under increasing organic loadings during operation period of 186 days. Lab-scale anaerobic migrating blanket reactor (AMBR)/completely stirred tank reactor (CSTR) system consisted of effective volumes of 13.5 and 9 l, respectively. Synthetic wastewater was obtained from constant NP concentration of 40 mg/l and a glucose concentration giving 3000 mg/l COD as primary substrate. The studies were carried out in continuous mode and the effluent of the AMBR reactor was used as the feed for the CSTR reactor. The AMBR/CSTR reactor system was operated at organic loading rates (OLRs) increasing from 0.31 to 3.25 kg/m^3.day. COD and NP removal efficiencies were decreased from 92% to 79% and from 94% to 86%, respectively, when the COD loading rates were increased from 0.31 to 3.25 kg/m^3 day in AMBR. The total COD and NP removal efficiencies were 94% and 91% in whole (AMBR/CSTR) reactor system, at a COD loading rate of 3.25 kg/m^3.day, respectively. The total gas and methane gas production increased with increased OLRs. The daily total and methane gas productions were 12.25 and 3.8 l/day at an OLR of 3.25 kg/m^3.day, respectively. Methane gas percentage was also found to be 31% at this loading rate.

A 79–92% of the NP transformed to p-aminophenol (p-AP) in anaerobic phase. The generation of P and ammonia (NH_4-N) was observed during the anaerobic degradation. A complete mineralization of p-aminophenol (E=100%) was found in the aerobic phase. The p-AP, P and NH_4-N were converted to nitrite (NO_2-N), nitrate (NO_3-N) and CO_2 as end products in the aerobic step.

The biodegradations of P and CP using the mutant strain CTM 2 obtained from *Candida tropicalis* was studied by Jiang et al. [2008]. The results showed that the capacity of the CTM 2 to biodegrade CP was increased up to 400 mg/l within 60 h. In the dual-substrate biodegradation, both velocity and capacity of the CTM 2 to degrade CP increased with low-concentration P. A total of 400 mg/l CP was completely degraded within 50.5 h in the presence of 300 mg/l P. The maximum CP biodegradation could reach to 440 mg/l with 120 mg/l P. Low-concentration of CP caused inhibition on the CTM 2 to degrade P.

Galindez-Mayer et al. [2008] evaluated the hydrodynamics and oxygen transfer characteristics of a fluidized bed reactor (FBR) and their performance in the continuous biodegradation of a P and CP-containing influent when the FBR was loaded with *Candida tropicalis* yeast immobilized onto GAC particles. The first part was carried out in terms of the behaviour of mixing time (t_{m95}), bubble diameter (d_B), gas hold-up (ε_G), gas–liquid interfacial area (a) and oxygen transfer coefficient (k_La) in biphasic (gas–liquid) and triphasic (gas–liquid–carbon) systems, both batch-wise operated in pseudo-homogeneous regime at superficial gas flow rates U_G below 1.72 cm/s. Mixing time was determined using a tracer technique, ε_G was measured by the volume expansion method; (d_B) was determined by the procedure reported by Poulsen and Iversen and k_La was determined by a transient gassing-in technique. Galindez-Mayer et al. [2008] found that hydrodynamic variables were severely influenced by GAC particles. The d_B values were smaller in triphasic than in biphasic system, with the consequent increase in the ε_G, a and k_La values.

These authors also studied the removal efficiencies of both P and CP in the bioreactor at increasing volumetric loading rate of pollutants. P and CP were determined by HPLC. The FBR was capable of efficiently removing P at volumetric loading rates as high as 60 mg P/l h when it was fed as the sole carbon source. Beyond this point, removal efficiencies drastically decreased. When operated with a feed consisting of a mixture of P and CP, the FBR was able to remove more than 98% of CP in the range of volumetric loading rates of 4.1 mg CP/l h and 55 mg P/l h with no apparent deterioration of the bioreactor performance.

The treatment of highly concentrated phenolic wastes is not a complex matter and often recovery techniques, in cases where such an approach is economically viable, or incineration technologies [Kaul et al., 1998], in the remaining cases, are used. When the concentration of organic material is lower, the choice of treatment technology is more difficult and several treatment processes compete [Lanonette, 1977]. The use of biological processes is normally recommended for the treatment of industrial wastes on the basis of economic considerations. However, phenolic compounds are highly toxic and biological processes are normally unsuitable for their treatment. For this reason, the treatment of low concentration phenolic wastes has to be carried out using non-biological technologies such as ozonation or chemical oxidation [Han et al., 1998]. Among these technologies, adsorption and electrochemical oxidation are frequently referred to in the literature [Teng and Hsie, 1998; Diez et al., 1999].

2.3 ADSORPTION STUDIES USING GAC AND OTHER ADSORBENTS

Adsorption process has been applied for separating and purifying mixtures of a large number of substances. ACs have, for long, been used as important adsorbents for the removal of various adsorbates from aqueous solutions. AC has many attractive properties such as high surface area (300 -1500 m^2/g), and high adsorption capacity for large number of adsorbates, organic chemicals, heavy metals, etc. In most instances physical adsorption has been found to prevail. Since AC can be manufactured from a variety of base materials (coal-bituminous to lignite, peat, wood, coconut shells, paper mill waste, molasses, petroleum coke, etc.) and different treatments, it has varying porous structure, physico-chemical and mechanical properties. The literature is full on the use of AC in powdered (PAC) and granular (GAC) forms as an adsorbent for the removal of various pollutants from wastewaters and aqueous solutions [Aksu and Kabasakal, 2004].

GAC adsorption is frequently used for the removal of hazardous organic pollutants from wastewater [Ramirez et al., 2000]. This technology achieves a rapid removal of the organic pollutants from the wastewater and retains them on the GAC surface. It has been reported [Kilduff and King, 1997] that activated carbon exhibits a high adsorption capacity for phenolic compounds and is cost-effective in their treatment.

Table 2.2.2 presents a summary of the recent adsorption studies using GAC in batch and/or column adsorbers for the removal of various adsorbates. Some studies relevant to the present investigation are also summarized.

Table 2.2.1. Other treatment methods for the removal of AN, P, CP, NP, C, R and HQ from water and wastewater.

Component/ pollutant	Treatment method	Process parameters, and brief description	Reference
P, CP and others	Coagulation	• Ferrate used as the coagulant, T=298K, pH=5.8-11. • Overall degradation by ferrate was found to be highly pH dependent and optimal pH: P/CP is 9.2. • Degradation was found to be highly pH dependent in presence of an increasing number of chlorine substituent atoms corresponds to an increasing reactivity of the undissociated compound, and a decreasing reactivity of the dissociated compound.	Graham et al. [2001]
AN, P and others	Coagulation	• Polyferric chlorides, poly-silicate-aluminium-ferric chloride, poly-aluminium-ferric chloride, poly-silicate-ferric chloride were used as coagulant, • T=ambient, pH=8-9 and optimum dosage~0.25 g/l. • Polysilicate ferric chloride was found to be most suitable for treatment of wastewater. COD removal efficiency was ~50-60%.	Yu-li et al. [2006]
C and others	Flocculation	• Removal of phenylamine and C by adsorptive micellar flocculation. laurylsulphate and α-olefinsulphonate, Al^{3+} were used as surfactant and coagulants. • T=298K, pH=11 and 14. An increase in pH from pH 3 to pH 4.5 causes, without affecting the flocculation of the surfactant, a decrease in the ratio C/SDS and also reduces the availability of Al^{3+} although within limits this would not affect surfactant flocculation. • C shows binding ratios up to 0.15, well above binding ratios up to 0.1 for P. and other properties similar, strong complexant C adsorbs much better than P. • Adsorptive micellar flocculation was found to be around 5-6 times > the ratios reported in the literature for micelle enhanced ultra filtration.	Almeida and Talens-Alesson [2006]
AN	Electro-Fenton and peroxi-coagulation	• O_2 and Ti/Pt was used as cathode and anode, C_o=1000 mg/l, T=313K, pH=3, electrode surface area=100 cm^2. • Electro-Fenton is total organic carbon=61% degradation after 2 h at 20 A. The peroxi-coagulation process with Fe anode has higher degradation power, allowing to remove >95% of pollutants at 20 A. • Both advanced electrochemical oxidation processes showed moderate energy costs, which increase with increasing electrolysis time and applied current.	Brillas and Casado [2002]
P	Electro-Coagulation	• Al and Fe used as electrodes, Fe and aluminium plates (4cmx4cm) T=294–295K, pH=4-7, V =250 cm^3 of wastewater solution different electrolysis times (1.0, 2.5, 5.0 and 7.5 min) at a constant cell voltage (12 V) and at a constant current (77.13 mA).	Ugurlu et al. [2008]

		• The removal capacities of the process using an Al electrode were 80% of lignin, 98% of P, 70% of BOD, and 75% of COD after 7.5 min. • Using a Fe electrode the removal capacities were 92%, 93%, 80% and 55%, respectively. It was found that removal of lignin, P, BOD and COD increased with increasing current intensity. • In the different current intensities, higher removal can be explained through a decrease in intra-resistance of solution and consequently an increase at the transfer speed of organic species to electrodes. • It was also found that Al electrode performs higher efficiency than Fe electrode except for COD removal.	
NP	Electro-Coagulation	• Fe, steel 310, Al and graphite anodes, and steel 304, graphite, Fe and Al cathodes were used as electrodes. The dimensions of electrodes were 40mm×70mm×2mm, pH=9, t=10 min, Current density=100 A/m^2 T=298 K, inter-electrode distance=15mm, area of each electrode=18.7cm^2 and stirring rate=400 rpm, C_0=20-300 mg/l, pH=9. • An increase in current density from 40 to 120 A/m^2 yields an increase in the efficiency of NP removal from 22.7 to 99.6%. Removal efficiency decreases from 99.9 to 88.7% by increasing the C_o from 15-35 mg/l. • The results showed that for 20 mg/l NP solution with COD of 40 mg O_2/l and NaCl concentration of 300 mg/l, NP and COD elimination of up to 99% and 65% were obtained respectively.	Modirshahla et al. [2008]
R	Electrochemical	• Ti/TiO_2-RuO_2-IrO_2 and graphite carbon are used as electrodes, T=310-324K, pH=5.5 to 7.5 and 8 to 8.5. The total effective surface area=0.28 dm^2 and 0.5 dm^2 for anode and cathode); C_o=400-800 mg/l, current density=1.78, 3.57, 5.36, 7.14 A/dm^2; charge input=10 Ah/l; chloride concentration=2500-3500 mg/l. • The maximum current efficiency was observed at higher R, higher chloride concentration and increasing current density. • The initial pH does not have significant effect on the removal of COD, but increase in chloride concentration and operating current density highly influences the treatment efficiency.	Rajkumar et al. [2004]
AN, NP and others	Electrochemical	• Novel beta-PbO_2 anode, T=ambient, pH=natural. Under current of 0.25A, the removal rate for organic compounds and COD of the wastewater in 2 h was around 75%-100%, and 22%-55%, respectively. • Higher current and initial organic compound concentration could enhance the wastewater treatment efficiencies. Benzoquinone, fumaric acid and oxalic acid were intermediates product.	Zhou et al. [2004]

P formaldehyde resin and oil refinery wastewater	Electrochemical	• $Ti/TiO_2–RuO_2–IrO_2$ (10 cm × 5 cm) and graphite are used as anode and cathode electrode, T=303K, pH=8.3, stirring rate=200 rpm. • The COD removal was 61.8% for the effluent as such and 82.4% for chloride added effluent after 24 Ah/l charge input with energy consumption of 161.2 and 102.1 kWh/kg of COD removal, respectively. The COD/TOC ratio was gradually reduced from 3.7 to 1.8 with a final TOC value of 83 mg/l (48% removal).	Rajkumar and Palanivelu [2004]
NP	Electrochemical	• Pb/PbO_2 anodes, current density=10, 20 and 30 mA/cm^2, T=293-333K, pH=8.5. • In alkaline media (0.1 M NaOH, pH 8.5), the most effective NP elimination (97%) was obtained at 333K, 20 mA/cm^2 and 420 min of electrolysis time, again with the production of p-benzoquinone and HQ (52.7 and 15.1%, respectively).	Quiroz et al. [2005]
C, R and HQ	Electrochemical	• Boron-doped diamond and stainless steel was used as the anode and cathode, area=78 cm^2 and both electrodes were circular (100 mm diameter) with a electrode gap of 9 mm, total V =500 ml, Flow rate=2500 cm^3/min, T=298K, pH=3. • It can be observed that carboxylic acids C_4 and C_2 are the main intermediates detected in the three cases and that the concentrations measured are low in comparison with the initial concentration of pollutant. The oxidation of C leads also to the formation of formic acid. • No aromatic intermediates were formed during the treatment except for the formation of *ortho*- and *para*-benzoquinone, whose presence is detected even previously to the oxidation process, due to the acid base equilibrium between the keto and the enolic forms of HQ and C.	Nasr et al. [2005]
CP	Electrochemical	• $Ti/IrO_2/RuO_2$ and carbon/polytetrafluoroethylene and Novel Pd/C used as anode and cathode gas-diffusion electrode; electrode surface area=16 cm^2, T=ambient, pH=7. • The removal efficiency of CP in terms of COD exceeded 70% after 120 min. • The analysis of HPLC identified that P was the dechlorination product, and HQ, benzoquinone, maleic, fumaric, crylic, malonic, oxalic, acetic and formic acids were the main oxidation intermediates.	Wang and Wang [2007]
P	Electrochemical	• Aluminum cathode and a horizontal aluminum screen anode, 2 g/l, pH: 7, time: 2 h, pH: 7, current density=19.3 mA/cm^2 and T: 293K. Removal of 97% of P after 2 h can be achieved. Removal of 97% of P after 2 h can be achieved at C_0=30 mg/l. • The percentage P removal was found to increase with increasing the number of screens per array.	Abdelwahab et al. [2009]
C	Electrochemical	• Glassy carbon and graphite are used as anode and cathode electrodes, T=298±274K, pH=6, C_0=0.5 mmol. The electrolysis was terminated the C when the decay of the current became more than 95%.	Khaleghi et al. [2009]
AN	Fenton oxidation	• [Fe (II) + H_2O_2] was used as reagent, T=298K , pH=4.5-5.5. The potential of the oxidation of various carcinogenic aromatic amines by Fenton's reagent [Fe(II) + H_2O_2] for liquid waste treatments was assessed.	Casero et al. [1997]

		• Complete removal took about 1 and 3 h of treatment overall for the formation of insoluble products and ring-cleavage products, respectively. • The iron (II) concentration was found to be crucial to the nature of the products, ring-cleavage products, CO_2.	
CP	Oxidation	• T=293K, pH=4, Degradation of CP was observed within 60 min reaction even if we increased the dosage of magnetite from 0.1 to 1.0 g/l. After one day's reaction, only 4.8% of CP was removed in the 1.0 g/l Fe_3O_4/H_2O_2 system. It seemed that degradation kinetic constant of CP in the iron oxides catalyzing Fenton-like system may be magnitude of per day. • Degradation of CP in a heterogeneous zero valent iron (ZVI)/H_2O_2 system was investigated. Initial pH was proven to have significant effect on the degradation and lower pH brought faster degradation rate. A scheme of CP degradation pathways in ZVI/H_2O_2 system was proposed and two pathways—4CC pathway (attacking by hydroxyl radical (•OH)) and ortho-parachlorophenolperoxyl radicals (ClPP•) pathway (participating by O_2) were expected to happen in the system. Both pathways would finally lead to the production of low molecule aliphatic organic acid.	Zhou et al. [2008]
NP	Oxidation	• MCM41-based catalysts incorporating Fe(III)-, Co(II)- and Ni(II)- cations were used for oxidizing 4-nitrophenol in water. In typical reaction conditions of temperature 353 K, time 300 min, catalyst load 2 g/l and 10^{-3} mol/l NP, the oxidation was 48.7, 52.2 and 55.2% with H_2O_2 and 42.5, 56.6 and 60.2% without H_2O_2 for Fe(III)-, Co(II)- and Ni(II)-MCM41, respectively. • Pseudo-first-order kinetics with kinetic constant of 2.0×10^{-3} to 5.5×10^{-3} l/g min was proposed along with a possible mechanism. 4-nitrocatechol, 4-nitropyrogallol, 1, 2, 4-trihydroxybenzene, hydroquinone, acrylic acid, malonic acid, and oxalic acid were identified in the oxidation products. The results suggest that the transition metal loaded MCM41 brings about a more effective interaction between nitrocatechol molecules and OH radicals.	Chaliha et al.[2008]
P	Oxidation	• Supported Cu(II) polymer catalysts were used for the catalytic oxidation of P at 303K and atmospheric pressure using air and H_2O_2 as oxidants. • The catalytic deactivation was evaluated by quantifying released Cu(II) ions in solution during oxidation, from where Cu–PVP25 showed the best leaching levels no more than 5 mg/l. • Results also indicated that Cu–PVP25 had a catalytic activity (56% of P when initial Cu(II) catalytic content was 200 mg/l) comparable to that of commercial catalysts (59% of P). Finally, the balance between activity and copper leaching was better represented by Cu–PVP25 due to the heterogeneous catalytic activity had 86% performance in the heterogeneous phase, and the rest on the homogeneous phase, while Cu–PVP2 had 59% and CuO/γ-Al_2O_3 68%.	Castroa et al. [2009]
NP	Photooxidation	• The aerobic visible-light-photosensitised irradiation of methanolic solutions of either of the p-phenylphenol , NP and P, and for two additional phenolic derivatives, namely CP and p-methoxyphenol (MeOP), used in some experiments, was carried out.	Haggi et al. [2004]

		• Employing the natural pigment riboflavin (R_f) as a sensitiser, the degradation of both the ArOH. A complex mechanism, common for all the ArOH studied, operates. It involves superoxide radical anion ($O_2^{\cdot-}$) and singlet molecular oxygen (O_2 ($^1\Delta g$)) reactions. • Maintaining R_f in sensitising concentrations levels (≈0.02 mM), the mechanism is highly dependent on the concentration of the ArOH. Kinetic experiments of oxygen and substrate consumption, static fluorescence, laser flash photolysis and time-resolved phosophorescence detection of O2($^1\Delta g$) demonstrate that at ArOH concentrations in the order of 10 mM, no chemical transformation occurs due to the complete quenching of R_f singlet excited state. When ArOH is present in concentrations in the order of mM or lower, $O_2^{\cdot-}$ was generated from the corresponding R_f radical anion, which is produced by electron transfer reaction from the ArOH to triplet excited R_f. • The determined reaction rate constants for this step show a fairly good correlation with the electron-donor capabilities for P, PP, NP, CP and MeOP. In this context, the main oxidative species was $O_2^{\cdot-}$, since O_2($^1\Delta g$) is quenched in an exclusive physical fashion by the ArOH. The production of $O_2^{\cdot-}$ regenerates R_f impeding the total degradation of the sensitiser. This kinetic scheme could partially model the fate of ArOH in aquatic media containing natural photosensitisers, under environmental conditions.	
C	Photooxidation	• T=300K, pH=2.5-5.5, C_0=50–1200 mg/l; The UV-lamp used in the study had wavelengths ranging from 250 to 273 nm. • Removal of C from aqueous solution by advanced photo-oxidation with hydrogen peroxide in presence of UV light. The effect of different process parameters, such as initial substrate concentration, H_2O_2 to substrate concentration ratio, addition of a solid catalyst (ferrous sulfate) has been studied. • The conversion attained within 5 min of adding of hydrogen peroxide in presence of UV light accounted for almost 90% of the total conversion achieved within a period of 1–2 h; almost 80–90% of the C present in the solution can be removed by the use of present process.	Mandal et al. [2004]
AN	Photolysis	• Metal halide light, *N. hantzschiana, C. vulgaris, C. sajao and A. cylindrical*, ≥350 nm, 250W, C_o =0.02-0.10 mmol/l and all had a pH of 6.7 ± 0.1 and 298K. • The photodegradation of AN was investigated using freshwater algae suspended in aqueous media under metal halide light (250 W). Four algal species were used: *Nitzschia hantzschiana, Chlorella vulgaris, Chlamydomonas sajao* and *Anabaena cylindrica*. Reactions were carried out under aerobic conditions. • The photodegradation rate of aniline was accelerated by the algae. In the *A. cylindrica* suspensions, with cell density ranging from 2.5×10^5 cells m/l to 6.5×10^6 cells m/l, the photodegradation rate of aniline was increased from 10% to 80% and rate constant k increased from 1.86×10^{-3} min^{-1} to 9.66×10^{-3} min^{-1}.	Wang et al. [2007]

		• Reactive oxygen species were thought to be the main reason for the degradation of aniline. Hydroxyl radicals and singlet oxygen photogenerated in the algal suspensions were detected. The maximum singlet oxygen yield was 75 μM in the presence of 1.0×10^6 cells m/l *C. sajao*. About 5 μM hydroxyl radicals were generated in the 4h reaction. • Oxygen played an important role in the formation of reactive oxygen species in the algal suspensions. The nature of the algae facilitating the photodegradation of AN was also investigated.	
C and others	Photolysis	• T=304-306K, pH=1-6, Emission maximum 313 nm, 1.3 10^7 Ein/s photon flux in the cells, and 2.6 x 10^{-5} Ein/l s photon flux per unit volume; maximum emission of the lamp (313 nm), expressed (1/M cm) units, are the following: 1-naphthol (2.3 x 10^3), naphthalene (1.1 x 10^2), nitrate (5.9). C and benzene do not absorb 313 nm radiation at an appreciable extent; 15/85 CH_3CN/buffer: C (3.80). • The pH effect on the photonitration of C, 1-naphthol, naphthalene, and benzene. The pH trend is influenced by the generation of HNO_2 and peroxynitrous acid (HOONO) upon nitrate photolysis. HNO_2 can be involved in a direct and an indirect nitration process. • Direct nitration follows the pH distribution of HNO_2 (~ 3). Indirect nitration, possibly involving nitrosation + oxidation, would be highest around pH 3. HOONO can be involved in electrophilic nitration, where the initial formation rate of the nitroderivatives is proportional to $[H^+]$, or take part in nitration directly, in which case a less important pH effect in photonitration is observed. The relative importance of the various nitration pathways for each substrate determines the resulting pH effect in photonitration upon nitrate photolysis.	Minero et al. [2007]
CP	Photodegradation	• Titanium dioxide (TiO_2) powder was mixed with varying concrete sealer formulations and applied to prepared concrete surfaces within PVC batch reactors. A solution of CP in de-ionized water, with an C_o=4 mg/l, was added to each open reactor. • The photocatalytic efficiency of each TiO_2-sealer was determined through bulk solution sampling while a reactor was exposed to continuous UV light. Through analysis of mean CP concentrations, the disappearance of CP from solution was attributed solely to the presence of TiO_2 in the sealed concrete surface of a UV exposed reactor. • The rate of disappearance increased when the mass percent of TiO_2 in the sealer was increased. The zero-order reaction rate constants ranged from 0.135 to 0.2873 mg/ l h.	Watts and Cooper [2008]
P	Photodegradation	• TiO_2/Ag_2S nanocomposites were prepared by a single-source decomposition method. • The best catalytic results, for P photodegradation, were obtained using a TiO_2/Ag_2S material with a surface Ti/Ag atomic ratio equal to 2.40. With this material the complete photodegradation of a 0.20 mM P solution was achieved within 90 min, which is considerably faster when compared with the use of TiO_2. • The TiO_2/Ag_2S nanocomposite materials have shown better P photocatalytic activity than TiO_2.	Neves et al. [2009]

P	Catalytic oxidation	• The catalysts tested were 35% CuO+65% ZnO; 5-15% CuO+85-95% Al_2O_3; 26% CuO+74% Cu Chromite.In the other laboratory, the catalysts tested included 35% CuO+65% ZnO; 5-10% Ba_2CO_3+<5% C+30-40% CuO+60-70% ZnO; and 8-15% Al_2O_3+1-5% C+35-45% CuO+40-50% ZnO. • With some of these catalysts depending on the operating conditions, complete P conversion could be obtained within 90 min. Under certain experimental conditions, the reaction underwent an induction period after which there was a transition to a much higher activity regime. The induction period may be due to an autocatalytic reaction system or to a very slow rate of formation of HQ and C which then readily oxidize to o- and p-benzoquinone. • An increase in the temperature and the oxygen partial pressure decreased the induction period, which increased as the catalyst to phenol ratio increased. 26% CuO+74% Cu Chromite and 8-15% Al_2O_3+1-5% C+35-45% CuO+40-50% ZnO were found to be the most active catalysts.An increase in the temperature and the oxygen partial pressure decreased the induction period, which increased as the catalyst to P ratio increased.	Akyurtlua et al. [1998]
NP	Catalytic oxidation	• A novel magnetically recoverable Au nanocatalyst was fabricated by the simple adsorption-reduction of Au(III) ions on chitosan-coated iron oxide magnetic nanocarrier. • Au nanoparticles with a mean diameter of 3.14 nm were well loaded on the surface of magnetic nanocarrier because chitosan layer provided an effective driving force in the formation and stabilization of Au nanoparticles. • The resultant magnetically recoverable Au nanocatalyst exhibited excellent catalytic activity to the reduction of NP with sodium borohydride. • The rate constants evaluated in terms of pseudo-first-order kinetic model increased with increasing the amount of Au nanocatalyst, decreasing the initial NP concentration, and increasing the temperature. Also, the kinetic data suggested that this catalytic reaction was diffusion controlled owing to the presence of chitosan layer.	Chang and Chen [2008]
C, R, HQ	Catalytic oxidation	• Abiotic degradation and mineralization of C, R, HQ catalyzed by birnessite (δ-MnO_2) was investigated. C_0=2.3 mmol, T=298K, pH=6-10, (200 mg) of δ-MnO_2 for 90 h under air; rate constants=15.4-26.8$\times10^{-6}$ 1/s. Birnessite; NaOH; HCl; 120 rpm. • Studies were carried out by monitoring changes of pE versus time and pH versus time of the reaction systems during the initial 10 h reaction period and release of CO_2 and associated reactions at the end of a 90 h reaction period. • The reactions under anoxic condition were compared with aeration condition. The reactions were carried out in suspensions at initial pH of 6.0 under air and N_2 atmosphere at room temperature and free of microbial activity.	Chien et al. [2009]

		• These results indicated that kinetic related changes of pE versus time and pH versus time were dependent on structural characteristics of phenolic compound and aeration or anoxic condition in the reaction system. The sequence of the mineralization of phenolic compounds catalyzed δ by δ-MnO_2 in presence of air expressed by CO_2 release was C> HQ>R and the differences were significant. However, under an N_2 atmosphere the amounts of CO_2 released were drastically reduced with insignificant differences among the three reaction systems. • Further, phenolic compound degradations, dissolved and adsorbed Mn, and oxidation state of Mn in δ-MnO_2 were also determined to elucidate the catalytic efficacy mediated by both O_2 and δ-MnO_2 in the reaction systems.	
AN	Photocatalytic degradation	• The degradation of AN has been investigated using aqueous TiO_2 suspensions containing carbonate ions as photocatalyst. • The addition of carbonate to Degussa P-25 increased the number of active adsorption sites at its surface. For the TiO_2 suspensions containing carbonate ions the intensity of adsorption of AN increased to 6.9×10^2 from 5.5×10^2 l/mol in case of bare TiO_2 suspensions. This in turn results in the increased interfacial interaction of the photogenerated charge carriers with the adsorbed AN and thus enhancing the rate of its photodecomposition to 6.5×10^{-6} mol/l s compared to 2.7×10^{-6} mol/l s in the absence of Na_2CO_3. • The maximum efficiency of this photocatalyst has been obtained upon addition of 0.11 mol/l of Na_2CO_3 at pH 10.8. The photocatalytic action is understood by the simultaneous interaction of intermediates, •OH and $CO_3^{\bullet-}$, and their reactivity with AN. Azobenzene, p-benzoquinone, nitrobenzene, and NH_3 have been identified as the major products of the photooxidation of AN. Both the reactant and products have been followed kinetically. • The photodegradation follows Langmuir–Hinshelwood Model. The mechanism of the occurring reactions has been analyzed and discussed. In the presence of Na_2CO_3, 3×10^{-3} mol/l of AN could be photodegraded completely in about 6 h while all organic intermediates decomposed completely within about 10 h.	Kumar and Mathur [2006]
P	Photocatalytic degradation	• Pr-doped TiO_2 nanoparticles was used as catalyst, T=298K, pH=6.5-6.8. Photocatalytic activity of the particles was studied in a batch reactor containing P solution with 400WUV irradiation. Parameters affecting photocatalytic process such as the catalyst crystallinity, light absorption efficiency, the dosage of catalyst, dopant and P concentrations were investigated. • The Pr-doped TiO_2 showed high activity for photocatalytic degradation of phenol. The presence of Pr ions in the TiO_2 particles would cause a significant absorption shift towards the visible region.	Chiou and Juang [2007]

		• The degradation process was optimized using 1 g/l Pr-doped TiO_2 with a Pr(III) concentration of 0.072 mol% after 2 h irradiation. It was shown that photodegradation followed a pseudo-first-order kinetics and the rate constant changed with phenol concentration. The degradation efficiencies are 93.6, 92.4, 89.9, and 81.9% in the first to fourth runs, respectively. The difference of apparent rate constant between C_0=12.5 and 200 mg/l was nearly nine-fold. • At a dosage of 1.0 g/l, 0.072 mol% Pr-doped TiO_2, about 99 and 50% of P was degraded after 2 h irradiation at an initial concentration of 12.5 and 200 mg/l, respectively. The present results demonstrated the promising photocatalysis potential of the Pr-doped TiO_2 particles, at least for P, due to their relatively faster degradation.	
CP	Photocatalytic degradation	• Synthesised nanosized titanium dioxide powder was used as catalyst, T=298K, pH=7 and 11. In the photocatalysis results, higher photodegradation efficiency of CP was observed at higher pH values. • Both CP and TOC reduction were significant for systems illuminated at 254 nm. Considering the direct photolysis effect at 254 nm where CP reduction is near 100% and TOC removal is nil, CdSe/TiO_2(RdH) exhibits a 50% photomineralization efficiency and a nearly four times faster reaction rate than the single TiO_2(RdH) semiconductor.	Lo et al. [2004]
NP	Photocatalytic degradation	• Synthesised TiO_2 nanoparticles was used, the TiO_2 nanoparticles incorporated with $CuInS_2$ clusters display higher photocatalytic activity with 99.9% of degradation ratio of NP after 2h irradiation. • In order to investigate the effect of the $CuInS_2$ clusters on the photocatalyticactivity of TiO_2 nanoparticles, diffusereflectance UV–Vis spectra, photoluminescence (PL) spectra, and photocurrent action spectra were measured. The results indicate that the enhanced photo catalytic activity is probably due to the interface between TiO_2 and $CuInS_2$ as a trap of the photogene rated electrons to decrease there combination of electrons and holes.	Kang et al. [2002]
C, R	Photocatalytic degradation	• The photocatalytic features of TiO_2 doped with ferric oxides or mixed with activated carbon (AC-TiO_2) are compared with those of the unmodified Degussa P-25 TiO_2. • These new catalysts show specific structural features that alter catechol and resorcinol photodegradabilities, according to their chemical structures. For instance, we have observed that Fe oxides located on the TiO_2 particle surface hamper these dihydroxybenzenes degradation. Likewise, AC-TiO_2 catalysts have shown improved catechol photodegradability with respect to that of TiO_2, while that of R is not altered. • These studies show that C and R adsorption patterns are different, i.e., they have different adsorption centres on the catalyst surface and are differently affected by photonic flux variations.	Arana et al. [2003]
HQ	Electro catalytic oxidation	• Mesoporous carbon (OMC-*x*) materials with different pore characteristics were prepared by templating SBA-15 mesoporous silica materials. • Using the ferricyanide system, the electrochemical behavior of OMC-0.6/GC electrode was found to be improved and the electrocatalytic oxidation of HQ is investigated with OMC-0.6/GC electrode.	Hou et al. [2008]

		• The results show that OMC-0.6/GC electrode could be a promising candidate for effectively electrochemical sensors for the detection of HQ due to its very low detection limit (0.3 nmol/l) and fast response.	
AN	Catalytic wet air oxidation (CWAO)	• T=473K, P=6.9 bar, pH=natural. Mesoporous MCM-41 based materials containing various transition metals (Cr, Cu and V) were used as catalyst. • Among the prepared materials, (Cu)MCM-41 showed a significant catalytic activity with an AN conversion after 2 h of 96% and a selectivity towards CO_2 formation of 76%. Although some leaching of the Cu was observed, the catalyst showed a good performance and stability after re-use in at least three consecutive cycles.	Gomes et al. [2005]
P	Catalytic wet air oxidation	• T=423K, P=3MPa, CeO_2-TiO_2 catalysts are used, a catalyst dosage of 4 g/l and C_0=2100 mg/l. In a batch reactor, COD and TOC removals are about 100% and 77% after 120 min in the CWAO of P over CeO_2-TiO_2 1/1 catalyst at reaction temperature of 423K, the total pressure of 3 MPa, P concentration of 1000 mg/l, and catalyst dosage of 4 g/l. In a packed-bed reactor using CeO_2-TiO_2 1/1 particle catalyst, over 91% COD and 80% TOC removals are obtained at the reaction temperature of 413K, the air total pressure of 3.5 MPa, the P concentration of 1000 mg/l for 100 h continue reaction. • Leaching of metal ions of CeO_2-TiO_2 1/1 particle catalyst is very low during the continuous reaction. CeO_2-TiO_2 1/1 catalyst exhibits the excellent activity and stability in the CWAO of P.	Yang et al. [2008]
P	Catalytic wet air oxidation	• P laden waste streams are not considered suitable for conventional biological treatment if P is present in amounts higher than 70 mg/l. • CWAO is one of the potential methods for treating waste streams containing such compounds. The present work investigated the degradation of synthetic wastewater contaminated with P (1 g/l) using a CWAO process in the presence of homogenous ($CuSO_4$) and heterogeneous ($LaCoO_3$, CuX and CuO-ZnO/CeO_2) catalysts. • The reaction was conducted at low temperature (363K) and atmospheric pressure, and at moderate operating conditions ($T \gtrsim$423K and total pressure $\lesssim$0.8 MPa). Among all the tested catalysts, $CuSO_4$, $LaCoO_3$ and CuX were used for WAO reactions performed at atmospheric pressure conditions, whereas the performance of CuO-ZnO/CeO_2 catalyst was tested in above atmospheric pressure studies. • At atmospheric conditions, homogeneous $CuSO_4$ was found to be the best showing ~90% P degradation and ~83% COD reduction after a 24 h reaction period. The above atmospheric studies with catalyst showed ~82% P reduction and 54% COD removal within 3 h reaction time.	Garg et al. [2010]
AN	Ozonation	• T=ambient, pH=2-8. Aqueous solutions of AN and p-chloroaniline were treated with ozone in order to study the reaction and oxidation by-products. AN solutions were ozonated at low and high pH, so as to compare both molecular and hydroxyl free radical mechanisms, respectively.	Sarasa et al. [2002]

		• The main identified aromatic by-products were nitrobenzene and azobenzene when the experiment was carried out at acid pH. Formation of nitrobenzene, azobenzene, azoxybenzene and 2-pyridine-carboxylic was observed when the ozonation was carried out at basic pH. • p-chloroaniline was treated with ozone only at high pH and the identified by-products were in accordance with those obtained in the ozonation of AN: p-chloronitrobenzene, 4, 4'-dichloroazobenzene and 4-chloro-2-pyridine-carboxylic acid. All the aromatic by-products found were less toxic than the raw materials. • The pseudo-first-order constants in AN concentration were calculated, whilst kinetic in p-chloroaniline concentration could not be adjusted to a first-order reaction.	
P	Ozonation	• Ozone concentration at a flow rate of 0.013 g/l. The pseudo first order rate constant was depending on the initial concentration of P solution. A comparison of TOC removal percentage. TOC removal efficiency was increased from 31% to 96% with decreasing from C_0=1000-100 mg/l. • The designed bubble column reactor was investigated for increasing the rate of mass transfer of ozone, the rate of oxidation of P in the solution, the solubility and decomposition rate of ozone in the distilled water were also studied at different flow rates. • The decomposition rate constants were calculated based on pseudo first order kinetics. The oxidation of P was investigated in order to provide the overall reaction rate constant for the reaction between ozone and P at 298K. The influence of the operating parameters like initial P concentration, ozone flow rate and pH for the destruction of P by ozonation were studied. The pseudo first order rate constant was depending on the initial concentration of P solution.	Matheswaran and Moon [2009]
CP	Ozonation	• T=295K, pH=7.5. H_2O_2 was detected during the ozonation of CP in aqueous solutions. Its formation and influence on the reaction mechanism were examined. Semi-batch experiments showed that hydrogen peroxide was formed during the direct reaction between molecular ozone and CP. • The detected hydrogen peroxide could reach 12.3% of the initial mole concentration of CP. Hydrogen peroxide reacts with ozone in neutral pH and leads to the appearance of the powerful oxidant, OH* radicals. An O(3)/OH* probe compound, succinate was then developed, and also included in the CP solution matrix. • The disappearance of succinate with time shows the amount of OH radicals. CP was transformed to para-quinone by ozone, and subsequently destroyed to formic acid and oxalic acid. Without scavengers of inactivation the OH• radicals, CP was destroyed to low molecular weight acid.	Pi et al. [2007]
R, AN and others	Ozonation	• T=ambient, pH=0-8, C_0=1x10^{-3} M; The COD change of various substituted aromatic compounds, namely benzoic acid, p-aminobenzoic acid, p-toluenesulfonic acid, sulfanilic acid, nitro benzene, R, p-cresol, o- cresol, o-toluidine, AN and 8-hydroxyquinoline were investigated at ozone doses of 5, 10, 15 and 20 mg O_3/min, respectively. • Percent COD removal of initial compounds after ozonation was compared with reported	Gu et al. [1999]

		biodegradation results. The pH change and percent removal of selected compounds were also evaluated in ozone does of 20 mg O_3/min up to 80 min. ozonation. • The results showed that high ozone doses are needed to obtain better elimination of initial compounds and also to improve further degradability of the ozonation products. ozone gas passing ozone gas at speeds of 5, 10, 15, 20 mg O_3 l/min; It was found that an 80 min. ozonation period with 20 mg O_3 /min was sufficient to degradate the with a high percentage of removal.	
P	Supercritical extraction	• T=3723K, P=334 bar. Supercritical fluid extraction (SFE) method for the isolation of phenols from olive leaf samples was examined. • Total P extracts were determined using the Folin-Ciocalteu reagent. Dried, ground, sieved olive leaf samples (30 mg) are subjected to SFE, using carbon dioxide modified with 10% methanol at 334 bar, 373K (CO_2 density 0.70 g/ ml) at a liquid flow-rate of 2 ml/ min for 140 min. • The extraction yield obtained was only 45%, using liquid methanol. supercritical fluid extracts were screened for acid compounds such as carboxylic acids and phenols using Electrospray-MS (in the negative ionization mode). • SFE was found to produce higher phenol recoveries than sonication in liquid solvents such as *n*-hexane, diethyl ether and ethyl acetate. However, the extraction yield obtained was only 45%, using liquid methanol.	Le Floch et al. [1998]
P, CP	Solid-phase extraction	• Tetrakis(*p*-carboxyphenyl) porphyrin (H2TCPP) was chemically bonded to porous polymeric XAD resins by ketone linkage. • The synthesized sorbent showed higher recoveries in tap water than commercially available sorbents such as XAD-2 and XAD-4. Tetrakis (p-carboxyphenyl) Porphyrin (H2TCPP) as extractant. • The preconcentration of a 25-ml tap water sample allowed determination of these compounds at microgram-per-liter levels, and the coefficient of variation was lower than 10%.	Kim et al. [1999]
AN, P and others	Supercritical water (SCW)	• T=798-973K, P=20 and 28 MPa, pH=natural. C_0=2.351x10^{-3} mol/l. P, AN and nitrobenzene were oxidized in supercritical water. • It was found that the COD removal efficiency of the organic compounds could be achieved 90% in short resident time at high enough temperature. Increasing temperature, pressure and residence time, the COD removal efficiency of the organic compounds increases. • It was found that temperature and resident time offer greater influence than pressure. The difficulty of oxidizing three compounds was in the order: nitrobenzene >AN>P. AN and nitrobenzene were difficult to be oxidized to CO_2 and H_2O when the temperature was less than 873K and 923K respectively. Only at the temperature of more than 873K and 923K, did the COD removal efficiency of aniline and nitrobenzene can be achieved 90%.	Chen et al. [2000]

AN	Extraction	• T=296K, pH=0-14. 3-aminobiphenyl and benzidine as extractant. A new procedure has been developed for the quantitation of aromatic amines in mainstream cigarette smoke. • Two solid-phase extraction (SPE) cleanup steps using different retention mechanisms are required to process the samples. The first step uses a cation-exchange cartridge, followed by a second step that uses a cartridge with a hydrophobic retention character. • The aromatic amines eluted from the second SPE cartridge are derivatized with heptafluorobutyric anhydride and analyzed with GC–MS selected ion monitoring in the negative chemical ionization mode. All cigarettes were conditioned at 60 and 62.5% relative humidity. The detection limits ranged from 0.02 ng/cigarette for tolidine to 1.41 ng/cigarette for AN and the recoveries were from 79 to 109%.	Smith et al. [2003]
C and others	Solid phase extraction	• A polymeric sorbent based on molecular imprinting technology has been synthesized and applied to selectively extract catechol from water samples with subsequent determination by differential pulse voltammetry (DPV). • The C and 4-vinylpyridine as template and monomer, Differential pulse voltammograms of C extracts were recorded from 0.3V to more positive potential at 40mV/s using pulse amplitude (ΔE) of 70mV at a glassy carbon electrode bare, $C_0=1.0\times10^{-5}$ mol/l., respectively. • The effect of the flow and chemical variables associated to the performance of the solid phase extraction procedure was investigated and optimized using a 2^{5-1} fractional factorial design as well as Doehlert design. • A study of selectivity was carried out percolating a standard aqueous solution, which contained a mixture of C and five phenolic compounds (4-chloro-2-methoxyphenol, 4-aminophenol, 2-cresol, 2-methoxyphenol and 4-chloro-2-metoxyphenol) through the polymer packed into a cartridge followed by the elution with methanol/acetic acid (4:1, v/v) solution. • Recovery higher than 95% was obtained for extraction of C even in the presence of structurally similar phenolic compounds. The procedure was further applied for catechol determination in aqueous effluent from paper mill industry and river water.	Tarley and Kubota [2005]
P, NP	Three-liquid-phase extraction	• T=298K, pH=4-10. Several new three-liquid-phase extraction systems containing ethylene oxide–propylene oxide (EOPO) random copolymers have been developed. • Results showed that P and NP could be unevenly and efficiently partitioned among the phases at pH 9.3, with about 80% P in the top phase and 95% NP in middle phase, respectively. • Separation factor of two compounds increased remarkably with the increase of pH 4-10. The separation factor was over 13 at pH 8.43.	Shen et al. [2006]
Phenolic compounds	Micro-solid phase extraction	• Methylacrylic acid , divinylbenzene has been prepared and used as molecularly imprinted micro-solid phase extraction (MIMSPE) procedure for the selectively preconcentration of phenolic compounds from environmental water samples.	Feng et al. [2009]

		• Various parameters for the extraction efficiency of the MIMSPE have been evaluated. The optimized MIMSPE method allowed the extraction of the analytes from the sample matrix followed by a selective washing step using acetonitrile containing 0.3% (v/v) acetic acid. • The characteristics of the MIMSPE method were valid by high performance liquid chromatography. The recoveries ranged between 88.9% and 102.5% for tap water, between 80% and 94% for river water, between 80.0% and 90.5% for sewage water fortified with 0.4mg/l of P, CP, 2, 4-dichlorophenol, pentachlorophenol (PCP) were obtained. methylacrylic acid, divinylbenzene as extractant.	
AN	Membrane process	• An emulsion liquid membrane process is developed to separate AN from dilute aqueous solution. Emulsion liquid membranes, 2% of kerosene, hydrochloric acid. • AN (amino-benzene) is a carcinogenic chemical common in industry and industrial wastewater. Due to aniline's high boiling point (465K) and low concentration in wastewater, more traditional methods of separation such as distillation are very energy intensive. • This emulsion process is offered as a low energy alternative. All separations occur in a Rushton stirred tank. The membrane phase consists of kerosene and the surfactant sorbitan monooleate. Hydrogen chloride solution is the internal phase. • This study also examines the effects of HCl concentration, AN concentration, and the amount of emulsion on separation. Up to 99.5% of the AN is removed from solutions containing 5000 ppm in as little as 4 min depending on process conditions.	Devulapalli and Jones [1999]
P, CP, NP, HQ and others	Membrane process	• Silicone rubber membrane tubing was used, T=323K and NaOH concentration 12.5 wt.%. • At steady-state, the total P concentration in the stripping solution can be orders of magnitude higher than in the wastewater, ensuring a high P recovery efficiency. • The work found P recovery efficiencies of over 94%, with a recovered organic-rich phase comprising 86.5 wt.% P, and the balance water. The van't Hoff–Arrhenius relationship for the temperature dependence of the permeability of the penetrant through the polymer gave excellent agreement with our experimental data.	Han et al. [2001]
NP	Liquid membrane process	• The research on treatment of wastewater containing nitrophenols was carried out by liquid membrane process. • The various parameters were selected for nitrophenols concentration 1050 mg/l in wastewater, such as the surfactant concentration in oil phase 2%, the NaOH concentration in the internal water phase 2%, the ratio of oil phase to internal water phase 2, the pH of external water phase 2 and the ratio of external water phase to emulsion phase 3. • The results indicate that the total NPs in influent can be reduced from 1050 to <1 mg/l and from 6700 to <2.2 mg/l via one-stage liquid membrane process. The removal rate of total NPs in wastewater was >99.9%.	Luan and Plaisier [2004]

petroleum effluents (Ps=COD)	Membrane process	• Ceramic membrane. P=100 kPa . The critical conditions of membrane separation were determined: TMP=100 kPa and v=5m/s. In these conditions, the permeate flux remained constant and high with a permeability about 10^{-3} l/h m^2 Pa (100 l/ h m^2 · bar). • The use of back pulsing enabled the permeate flux to increase by only 10%. On the other hand, back pulsing maintained a high constant permeate flux over several weeks. • The membrane bioreactor process was evaluated in terms of membrane performance and biological degradation. • No P was detected in the permeate although a large quantity of P (50 g/day) was degraded. The absence of suspended matter, the removal of a substantial amount of P and a good performance on organic substance removal show the excellent performances of MBR.	Barrios-Martinez et al. [2006]
R and others	Membrane process	• The effective membrane area was 46.2 cm^2, T=298K, P=0.48 MPa, pH=3-10; The average permeate flux for NF70 was found to be 2.5 ml/min (9.02m^3/m^2 s); concentration of DOC in the permeate increased with time for R and phloroglucinol, and the rejection ratios for R and phloroglucinol were measured at 79 and 80%; phloroglucinol and R (having similar rejection about 80%). to determine the rejection ratios of disinfection by-products (DBPs) precursors including R, phloroglucinol, 3-hydroxybenzoic acid, and tannic acid solution in the presence of calcium by nanofiltration with NF70 membrane. • The rejections of these model compounds also were studied at various compositions of a feed solution by changing pH and concentrations of model compounds. • It was found that the model compound rejection and membrane permeability increase with pH due to the conformational transformation of ionizable molecules and electric interaction between the model compounds and NF70 membrane. The interactions of model compounds with calcium have no significant effect on model compounds retentions. Because of the complexation of calcium with model compounds, calcium rejection rises with the presence of model compounds and with an increase of pH.	Lin et al. [2006]
AN	Combined photocatalysis and ozonation	• The combination of TiO_2-assisted photocatalysis and ozonation in the degradation of AN in aqueous solution is investigated. From the experimental results obtained it is observed that the ozonation pretreatment followed by photocatalysis strongly increases the yield of TOC removal in comparison to either ozonation or photocatalysis carried out separately. • The opposite sequence (photocatalysis pretreatment followed by ozonation) does not enhance the efficiency of AN degradation. Nevertheless, the highest TOC removal was achieved by simultaneous ozonation and photocatalysis. • A mechanism involving the formation of an ozonide anion radical previous to the generation of OH radicals is suggested to explain the synergic effect between ozone and TiO_2 under illumination. It	Sanchez et al. [1998]

		was observed that the ozonation pretreatment followed by photocatalysis strongly increases the yield of TOC removal in comparison to either ozonation or photocatalysis carried out separately. The opposite sequence (photocatalysis pretreatment followed by ozonation) does not enhance the efficiency of AN degradation. Nevertheless, the highest TOC removal was achieved by simultaneous ozonation and photocatalysis. A mechanism involving the formation of an ozonide anion radical previous to the generation of OH radicals is suggested to explain the synergic effect between ozone and TiO_2 under illumination.	
CP and others	Photolysis and Ozonation	• Synergistic effects including TOC elimination, ozone consumption and microtoxicity reduction for combination of photolysis and ozonation compared to those of direct photolysis and ozonation alone on destruction of chlorophenols including 2CP, CP and 2, 4-dichlorophenol were studied. • It was found that the synergistic effects of combination of photolysis and ozonation increased obviously with increasing initial pH of solution to basic pH levels. • Photolytic ozonation under the conditions imposed was notable with mineralization rate enlarging more than 100%, oxidation index decreasing 50%, and microtoxicity being reduced by 30%, indicating that the potentialities of photolytic ozonation compared to direct photolysis and ozonation alone was remarkable for treatment of industrial wastewater containing chlorophenols.	Kuo [1999]
NP and others	Photocatalysis and membranes	• Tests of degradation in a photocatalytic membrane system with the lamp immersed in the suspension inside the photoreactor have been carried out by using polycrystalline TiO2 (Degussa P25) as catalyst and humic acids, organic dyes, as pollutants. NF-PES-010 (Celgard, Germany) of polyethersulphone and NTR-7410 (Nitto-Denko, Japan) of sulphonated polyethersulphone were used. C_o=200 mg/l solution. • The system was able to maintain at steady-state conditions pollutant concentrations lower than 5 and 2 mg/l in the retentate and in the permeate, respectively. Despite the fluxes ranged between 20 and 40 l/(hm^2) in operating conditions at 6 bar and these values are interesting for application purposes, the rejections of NTR-7410 nanofiltration membrane, obtained during operation of the membrane photoreactor in the degradation of humic acids, patent blue dye and NP, were significantly lower than those obtained in the absence of photodegradation probably because of the small molecular size of by-products and intermediate species generated during the photodegradation process. This means that in order to select a suitable membrane, rejection should be determined during operation of the photoreactor.	Molinari et al. [2002]
C	Photocatalytic oxidation + ozonation	• Carbon black-modified nano-TiO_2; Al sheet; Tetrabutyl titanate; n-propyl alcohol. Flow rates of oxygen=0-200 ml/min. T=ambient, pH=acidic. • The photocatalytic activity of the carbon-black-modified nano-TiO_2 (CB-TiO_2) thin films was 1.5 times higher than that of TiO_2 thin films in degrading Reactive Brilliant Red X-3B.	Li et al. [2002]

		• Photocatalytic oxidation and ozonation of catechol over CB-TiO_2 thin films supported on Al sheet was investigated. The experiments showed that ozone concentrations had an important effect on TOC removal. • The combined photocatalysis with UV irradiation and ozonation (TiO_2/UV/O_3) process considerably increased TOC removal rate compared to combined photocatalysis with UV irradiation and oxygen oxidation (TiO_2/UV/O_2) process, ozonation alone (O_3) process, combined ozonation and UV irradiation (UV/O_3) process. • The complete mineralization of C followed pseudo-zero-order kinetics dependent upon ozone (oxygen) concentration and indicated C concentration did not affect the kinetics during UV/O_3 and TiO_2/UV/O_3 (O_2) processes. • The kinetic study showed that the rate constants in the complete mineralization of C with TiO_2/UV/O_3 are 1.32–1.80 times higher than that of UV/O_3 with the same concentration of ozone. The rate constants are 2.56–5.36 times higher than the maximal rate constants of TiO_2/UV/O_2 and 4.68–9.8 times higher than the maximal rate constants of TiO_2/UV.	
C, R, HQ	Up flow anaerobic fixed-film fixed-bed reactors	• Anaerobic degradation of three dihydric P_s, viz., C, R, HQ was studied in mono and binary substrate systems in three upflow anaerobic fixed-film fixed-bed reactors of similar dimensions. In order to predict the metabolic pathways existing in the microbial consortia for anaerobic degradation of these compounds, downstream intermediates of reductive and carboxylation pathways for P were fed to the three reactors acclimated to the three dihydric phenols. • C and HQ acclimated reactors demonstrated marginal degradation of the downstream intermediates of the reductive pathway for P, viz., cyclohexanol and cyclohexanone. However, the same reactors could degrade benzoic acid, which is the downstream intermediate of the carboxylation pathway for P, to the extent of 83%. This indicates good expression of the carboxylation pathway in these two reactors. • The R acclimated reactor, on the other hand, degraded cyciohexanol, cyciohexanone and benzoic acid with poor efficiency suggesting that the majority of resorcinol is catabolized by a hitherto unknown pathway. Binary mixture studies revealed that utilization of C and HQ from the binary mixed feed in R acclimated reactor was poor. In the C acclimated reactor, C aided better utilization of R when compared to that of HQ. • In the HQ acclimated reactor, high R utilization efficiency was seen from the R-C mixed feed. The study highlights the biochemical specificity acquired by microbial consortia when exposed to different substrates for acclimation.	Latkar and Chakrabarti [2003]
C, R, HQ	Up flow anaerobic fixed-film fixed-bed reactors	• Biodegradation of R and C was studied in upflow anaerobic fixed film-fixed bed reactors of uniform dimensions in mono and multisubstrate matrices. • Cross feeding studies have revealed that phenol was poorly degraded in R acclimated reactor	Swaminathan et al. [1999]

		whereas it was readily degraded in C acclimated reactor. Addition of R along with P in a COD ratio 1:3 in R reactor increased P removal efficiency to 95% indicating that resorcinol induces phenol degradation. • When both R and C were fed to the R acclimated reactor, it was observed that R degradation was inhibited by C. C acclimated reactor could degrade phenol readily when added as mono substrate indicating that it may be an intermediate in C degradation. • In binary mixture studies also C reactor could degrade P, R and HQ to 90%. C acclimated reactor exhibits relaxed substrate specificity whereas R acclimated reactor exhibits rigid substrate specificity for P as well as other isomers.	
P	Biodegradation	• The P degradation kinetics could be explained by the Briggs-Haldane equation using the model equations developed under different immobilized cell concentration. • Variation in the initial immboilized cell concentration is found to have the little effect on the time taken for degration of P.Iit is also observed that the effectiveness factor decreases parabolically as the initial immobilized cell concentration increase.	Swamy et al. [1997]; Swamy [1998]
AN, chlorinated AN, and AN blue	Biodegradation	• *Fusarium sp.* utilized 70% of 10mmol AN and produced 3.55mM ammonia during 30 days. *Rhizopus sp.* utilized 65% of 10 mmol AN during 30 days. *Rhizopus sp. and Fusarium sp.* utilized only 2-chloroaniline and 3-chloroaniline as nitrogen source in the presence of glucose, with production of C, ammonium and chloride. • The utilization of 2-chloroaniline was better than 3- chloroaniline, by *Fusarium sp. and Rhizopus sp. Cladosporium sp.* was the best isolate which could use AN blue as the only source of nitrogen. This fungus reduced 89% of aniline blue, and ammonia is produced as the result of aniline blue biodegradation by *Cladosporium sp.*	Emtiazi et al.[2001]
P, C, 2-4 dichlorophenol, 2, 6-dimethylphenol	Biodegradation	• The ability of the fungus *Aspergillus awamori* NRRL 3112 to degrade mixtures of some common phenolic compounds, namely P, C, 2, 4-dichlorphenol and 2, 6-dimethoxyphenol was investigated. • For all combinations in which dichlorophenol was incorporated, it took 4 days for the nearly complete degradation of the compound 4 days. • P was decomposed almost completely (99.5%) in a combination with dimethoxyphenol, to a lesser extent (88%) in a combination with C and to the least degree (25%) in the presence of 2, 4-dichlorophenol. C experienced a more substantial biotransformation (64%) when mixed with P and weaker (45%)—in a combination with dichlorophenol. 2, 6-Dimethoxyphenol was better decomposed (69%) in mixtures containing P, while its biodegradation in a combination with 2, 4-dichlorophenol was considerably poor (only 5%).	Stoilova et al. [2006]

C	Biodegradation	• The C was successfully mineralized in an UASB reactor in which microbial granulation was achieved with only glucose as the substrate. • The reactor showed 95% COD removal efficiency with 500–1000 mg/l C concentration in the feed and a glucose concentration of 1500 mg l/1 as a co-substrate. • Similar efficiency was obtained at a constant C concentration of 1000 mg/1 with 500–1000 mg/l glucose concentration. Once the reactor got acclimatized with C, higher concentrations of C can be mineralized with a minimum amount of glucose as the co-substrate without affecting the performance of the UASB reactor.	Subramanyam, and Mishra [2007]
CP	Biodegradation	• Removal of CP achieved at optimum HRT and substrate: co-substrate ratio was 88.3 ± 0.7%. Removal of CP occurred through dehalogenation and caused increase in chloride ion concentration in the effluent by 0.23–0.27 mg/mg CP removed. • The ring cleavage test showed the ortho mode of ring cleavage of CP. Change in the elemental composition of the anaerobic biomass of UASB reactors was observed during the study period. • Concentration of Ca^{2+} increased in the biomass and this could be attributed to the biosoftening. Specific methanogenic activity of the sludge of control and test UASB reactor was 0.832 g CH_4 COD/g VSS.d and 0.694 g CH_4 COD/g VSS d, respectively.	Majumder and Gupta [2008]
NP	Biodegradation	• Kinetic tests were performed in a sequencial batch reactor (2-l volume) operated in both conventional one- and two-phase configurations, with the two-phase system showing a significant improvement in the process kinetics in terms of reduced inhibition and increased removal rate.	Tomei et al. [2008]
C	Biodegradation	• The specific methanogenic activity of the sludge showed an increase in trend with an increase in the organic loading rate and the C concentration in the SWW. • The settling velocity of individual granules in the size range of 0.5–2.5 mm was found to be in the range of 30–75 m/h. The ash content in the sludge was 11.7% with a sludge volume index of 18– 20 ml/g.	Subramanyam and Mishra [2008]
C and R	Biodegradation	• The study involved biodegradation of a mixture of C and R in different ratios in an UASB reactor. When the R concentration was increased to have a R/C ratio of 1/4, the COD removal efficiency and the biogas production increased to the maximum levels. • Pseudo steady state condition for COD removal was achieved at each of the stepped-up loading condition. • An increase in the R/C ratio above 1/4 in the binary feed solution led to a decrease in the COD removal efficiency and the biogas production rate.	Subramanyam and Mishra [2008]
AN	Adsorption and Biodegradation	• T=298K, pH=7.2. The use of powdered activated carbon treatment (PACT), based on simultaneous adsorption and biodegradation, is effective for treating organic toxic pollutants, present in industrial wastewaters.	Orshansky and Narkis [1997]

		• Removal of P and AN from aqueous solutions by biological treatment alone, by adsorption on PAC alone and by simultaneous adsorption and biodegradation were compared. In the adsorption experiments, Langmuir adsorption isotherms were obtained, from which Q^{o}, the limiting adsorption capacities, and b, the constant related to the energy of adsorption, were determined. Q^{o} values of P and AN were found to be similar, while the energy-related constant for AN was five times higher than for P. Addition of mineral nutrients, needed for the biological treatment, and inactivated microbial cells increased the limiting adsorption capacities and significantly decreased the energy related constants. • In biological treatment alone, kinetic studies showed that AN was more resistant to biodegradation than P. In the simultaneous adsorption and biodegradation process, the PAC presence differently affected the biooxidation of P and AN. While the PAC enhanced the microbial respiration in the P bioreactor, it significantly reduced the microbial respiration in the AN bioreactor. • Different organic removal mechanisms are suggested in PAC for P and AN, due to their different energy of adsorption. The respirometric studies are recommended as an adequate tool for prediction of toxic organics removal capabilities from industrial wastewaters by PACT.	
P, R and other	Aerobic Bio-Oxidation and Aerobic Bio-Oxidation with Ozonation	• COD=500-3600 mg/l, BOD=150-1100 mg/l and total P=5- 50 mg/l. • Process water and phenols' balances for the two processes of oil shale thermal treatment, Kiviter (in vertical retort) and Galoter (with solid heat carrier) were compiled. Options of wastewater treatment in the Kiviter process were analyzed in more detail. Laboratory experiments of biological oxidation of the process water after the dephenolation stage without other effluents and municipal wastewater were carried out. • Experiments indicated that the oil shale P_s are generally quite easily degradable when the need for phosphorus is covered by added reagents. The experiments indicated that, compared to conventional aerobic bio-oxidation, the combined process, namely aerobic bio-oxidation with ozonation in re-circulation system, enabled to increase the efficiency of purification at relatively low ozone dosages. • Application of ozone at moderate doses (up to 30 mg/l) improved the rate of pollutant removal. Injection of ozone at small dose – 2 mg/l – into the activated sludge in the bioreactor increased the sludge activity: the specific oxygen uptake increased about 15–20%. The biologically treated wastewater can be used as some kind of technological water (cooling water) after chemical precipitation and reduction of sulphate content. • It can also been discharged to nature, but only after additional treatment to reduce nitrogen content and after filtration to remove the residual suspended solids. 60% for COD reduction and 93% for BOD, the removal of phenolic compounds achieved 85%.	Kamenev et al. [2003]

AN from hypersaline effluents	Combined adsorption/bio-regeneration	• Treatment of AN hypersaline wastewater with a combined physical–biological method was investigated in this study. • This method consisted of the physical adsorption of AN from hypersaline effluents by resins and the biodegradation of the adsorbate and the regeneration of the adsorbent in the subsequent stage. The XDA-1 resin, selected from five commercial products, could separate AN from salt effectively. The adsorption rate increased with the increase of salinity. • Biodegradation of the AN desorbed from the exhausted resin could be realized easily without salt interference. During the repetitive six combined operations, the percentage regeneration and NaCl separation efficiency of XDA-1 were 92.3% and 98.3%, respectively. • No obvious difference could be found in pore size distribution between virgin XDA-1 and samples repeated six regeneration cycles. The PR of specific surface area and total pore volume of the bio-regenerated XDA-1 resin were 94.5% and 97.2%, respectively. • It was indicated that XDA-1 could be bio-regenerated successfully and the regenerated resin could be re-utilized. The adsorption and bioregeneration process repeated for up to six cycles, the PR and NaCl SE of XDA-1 remained 92.3% and 98.3%, respectively. • The bio-regeneration process did not destroy the pore structure and the surface properties of XDA-1 resin. The static studies showed that the combined adsorption/bioregeneration process could treat AN hypersaline wastewaters efficiently.	Gu et al. [2008]
nitrocellulose industry wastewater	Combined photocatalytic and fungal processes	• The delignification effluent originating from the delignification industry and evaluate the combination of the fungus and photocatalytic process (TiO_2/UV system) for the treatment of this effluent. • The delignification effluent has proven harmful to the environment because it presents high color (3516 CU), total P (876 mg/l) and TOC (1599 mg/l) and is also highly toxic even in a low concentration. • The results of photocatalysis were 11%, 25% and 13% higher for reductions in color, total P and TOC, respectively. The combined treatments presented benefits when compared to the non-combined treatments. • Fungus and photocatalysis in combination proved to be the best treatment, reducing the color, total P, toxicity (inhibition of *Escherichia coli* growth) and TOC by 94.2%, 92.6%, 4.9% and 62%, respectively.	Barreto-Rodrigues et al. [2009]

Table 2.2.2. Adsorptive removal of AN, P, CP, NP, C, R and HQ from water and wastewater.

Adsorbates	Adsorbents	Operating conditions	Process parameters and brief description	References
			Phenol (P)	
P, R, and other	RHA	Batch	• Rice husk ash (RHA) obtained from a rice mill in Kenya has been used as an inexpensive and effective adsorbent (and reagent) for the removal (and detection) of some phenolic compounds in water. The abundantly available rice mill waste was used in dual laboratory-scale batch experiments to evaluate its potential in: (i) the removal of P, R and 2-chlorophenol from water; and (ii) the detection of 1, 2-dihydroxybenzene (pyrocatechol) and 1, 2, 3-trihydroxybenzene (pyrogallol) present in an aqueous medium. T=298,323K, pH=10 ±0.2. • % adsorption with time and that the recorded % adsorptions of P, 2CP and R by the 60th minute were 72, 52 and 48%, respectively. From these results, we can conclude that RHA has a higher affinity for P than R. • RHA exhibits reasonable adsorption capacity for the phenolic compounds and follows both Langmuir and Freundlich isotherm models. Adsorption capacities of 1.53×10^{-4}, 8.07×10^{-5}, and 1.63×10^{-6} mol/g were determined for P, R and 2CP, respectively. Nearly 100% adsorption of the Phenolic compounds was possible and this depended on the weight of RHA employed. • For the detection experiments, pyrocatechol and pyrogallol present in water formed coloured complexes with RHA, with the rate of colour formation increasing with temperature, weight of RHA, concentration of the phenolic compounds and sonication.	Mbui et al. [2002]
P	RHA	Batch	• C_0=500 μg/l of P in 100 ml of solution, T=298K, pH=5-11, minimum dosage of 0.3 g of rice husk ash is required for 96% removal of P. But, with this condition by rice husk, the removal efficiency is 27%. When the initial P concentration was increase from 150 μg/l to 350 μg/l on rice husk and C_0=500 μg/l to 1300 μg/l on rice husk ash, the loading capacity increased from 1.56×10-6 mg/mg to 1.96×10^{-6} mg/mg of rice husk, and from 2.7×10^{-4} mg/mg to 6.15×10^{-4} mg/mg of rice husk ash. • Adsorption equilibrium of rice husk and rice husk ash was reached within 6 h for phenolic concentration 150-500 μg/l and 3 h for C_0=500-1300 μg/l, respectively. • Kinetics of adsorption obeyed a first-order rate equation. The adsorption of P increases with increasing the solution pH value. • The results showed that the equilibrium data for all the P-sorbent systems fitted the Freundlich model best within the concentration range studied. A comparative study showed that rice husk ash is very effective than rice husk for P removal.	Mahvi et al. [2004]

C, R, HQ	RHA	Batch	• The RHC is a good sorbent for the removal of phenolic compounds from aqueous solution in the concentration range of 1.0×10^{-4} to 3.0×10^{-3} mol/l for HQ, 2.0×10^{-4} to 5×10^{-2} for C and 1.0×10^{-4} to 5×10^{-2} mol/l for R with adsorbent dose of 0.5 g/l at pH<6 under the minimum equilibration time of 0.5 h. There was a sharp decrease in adsorption when pH >7.0 and the adsorption in the higher pH range was negligible. • The results showed that the adsorption mainly took place on the external surface and was controlled by chemisorption and increased with the total density of carboxylic and lactonic. T=298K, pH=2-7.	Qi et al. [2004]
P and other	Sewage sludge		• The sorbent preparation from sewage sludge using experimental design methodology. Series of carbonaceous sorbents have been prepared by chemical activation with sulfuric acid. • Carbonaceous sorbents developed from sludge allow copper ion, P and dyes (Acid Red 18 and Basic Violet 4) to be removed from aqueous solution as well as VOC from gas phase. Indeed, according to experimental conditions, copper adsorption capacity varies from 77 to 83 mg/g, phenol adsorption capacity varies between 41 and 53 mg /g and VOC adsorption capacities (acetone and toluene) range from 12 to 54 mg/ g. Each response has been described by a second-order model that was found to be appropriate to predict most of the responses in every experimental region. The most influential factors on each experimental design response have been identified. • Regions in which optimum values of each factor were achieved for preparation of activated carbons suitable for use in wastewater and gas treatments have been determined using response surfaces methodology. In order to have a high mass yield and to minimize the energetic cost of the process, the following optimal conditions, 1.5 g of H_2SO_4 l/g of sludge, 973K and 145 min are more appropriate for use of activated carbon from sludge in water and gas treatments. 500 mg of chemically • activated sludges are continuously stirred (300 rpm) in 1L of aqueous solutions with an initial concentration of 100 mg/l for copper or phenol adsorption experiments	Rio et al. [2005]
P	flue dust	Batch and column	• Batch experiments have been carried out to study P removal from a synthetic phenol solution by adsorption onto blast furnace flue dust from a steel plant and slag generated in chrome alloy plants. Removal efficiencies attained after 8 h were observed to be more than 90 and 75% for the blast furnace flue dust and slag, respectively. • The adsorption processes for both adsorbents follow first-order kinetics, Freundlich and Langmuir adsorption isotherms, decreasing with increasing temperature and decreasing particle size. Intraparticle diffusion studies indicate that adsorption of the substrate takes place rapidly by external mass transfer, followed by intraparticle diffusion. • Column experiments indicate that the amount of P adsorbed decreases with increasing flow rate and decreasing bed height. The break-through time and bed-depth data show applicability of the	Das and Patnaik [2005]

M. G. CENTRAL LIBRARY
ACC No. G 21280
Date
I.I.T. ROORKEE

			bed-depth service time (BDST) model. C_0=20-50 mg/l. Blast furnace flue dust from steel plants and slag from chrome alloy plants can be used as effective adsorbents for removal of P from industrial effluents, being able to remove more than 90% and 75% of the P. T=975K, pH=5.0, 6.2, 7.0 and 8.2.	
P	Samla coal	Batch and column	• The adsorption capacity was found to be 51.54 mg/g. Adsorption capacity of residual coal treated with phosphoric acid was found to be 142.8, 256.4, and 243.9 mg/g for P, NP, and CP, respectively. pH=2-12,C_0=1000 mg/l • The results showed that the equilibrium data for all the P–sorbent systems fitted the Redlich–Peterson model best. • Kinetic modeling of removal of P was done using the Lagergren first-order rate expression. A series of column experiments were performed to determine the breakthrough curves.	Ahmaruzzaman and Sharma [2005]
P, HQ, NP	ACC	Batch	• Adsorption of P, HQ, m-cresol, p-cresol and NP from aqueous solutions onto high specific area activated carbon cloth. The effect of ionization on adsorption of these ionizable phenolic compounds was examined by studying the adsorption from acidic, basic and natural pH solutions. • Kinetics of adsorption was followed by in situ UV-spectroscopy over a period of 90 min. First-order rate law was found to be valid for the kinetics of adsorption processes and the rate constants were determined. The highest rate constants were obtained for the adsorption from solutions at the natural pH. The lowest rate constants were observed in basic solutions. • The rate constants decreased in the order NP>m-cresol >p-cresol >HQ>P. Adsorption isotherms were derived at 303K and the isotherm data were treated according to Langmuir, Freundlich and Tempkin isotherm equations.	Ayranci and Duman [2005]
P and other			• The objective of this study was the reuse of waste for industrial wastewater treatment, the adsorption properties of the ACs were tested towards pollutants representative of industrial effluents: P, the dye Acid Red 27 and Cu^{2+} ions. Chemical activation by phosphoric acid seems the most suitable process to produce fibrous AC from cellulose fiber. • Different fibrous ACs were prepared from natural precursors (jute and coconut fibers) by physical and chemical activation. • Physical activation consisted of the thermal treatment of raw fibers at 1223K in an inert atmosphere followed by an activation step with CO_2 at the same temperature. • In chemical activation, the raw fibers were impregnated in a solution of phosphoric acid and heated at 1173K in an inert atmosphere.	Phan et al. [2006]

			• The characteristics of the fibrous ACs were determined in the following terms: elemental analysis, pore characteristics, SEM observation of the porous surface, and surface chemistry. • This method leads to an interesting porosity (S_{BET} up to 1500 m^2/g), which enables a high adsorption capacity for micropollutants like P (reaching 181 mg/g). Moreover, it produces numerous acidic surface groups, which are involved in the adsorption mechanisms of dyes and metal ions.	
P	AC	Batch	• Batch kinetics and isotherm studies were carried out to evaluate the effect of contact time, initial concentration, and desorption characteristics of AC. • The equilibrium data in aqueous solutions was represented by the isotherm models. Desorption studies to recover the adsorbed P from activated carbon performed with NaOH solution. It is necessary to propose a suitable model to gain a better understanding on the mechanism of P desorption. • The diffusivity rate (D/r^2) and first-order desorption rate (k_D) constants were determined as 6.77×10^{-4} and 3.924×10^{-4} 1/s, respectively. The two- and three-parameter in the adopted adsorption isotherm models were obtained using a non-linear regression with the help of MATLAB package program. • It was determined that best-fitted adsorption isotherm models were determined to be in the order: Langmiur>Toth> Redlich–Peterson > Freundlich isotherms. C_0=10–200 mg/l. the first-order kinetic model represented the data for NaOH desorption more suitable fitting than the pore diffusion model. • The results also demonstrated that the Langmiur model fitted the experimental data a little better than the three parameter models, Redlich–Peterson and Toth.	Ozkaya [2006]
P	AC, BFA	Batch	• Three carbonaceous materials, activated carbon (AC), bagasse ash (BA) and wood charcoal (WC), as adsorbents for removal of P from water. 30 and 50 mg/l, with an adsorbent (AC, BA or WC) dosage of 50 g/l. 98% P removal was achieved when AC dosage was 10 g/l and C_0=30 mg/l. But for BA and WC, P removal increased from 86% to 90% when their dosages increased from 10 to 60 g/l under the same other conditions. • P removal efficiencies of BA at C_0=20-100 mg/l were about 92% and 80%, respectively. For WC, when the C_0 increased from 20-100 mg/l the P removal efficiency decreased from 91% to 79.5%.	Mukherjee et al. [2007]
P	AC	Batch	• The production yield was observed to decrease with increase in activation temperature. Adsorption behavior of P onto the porous carbon was studied by varying the parameters such as agitation time, P concentration, pH and temperature. • Studies showed that the adsorption decreased with increase in pH and temperature. The sorption process was found to be exothermic in nature.	Kennedy et al. [2007]

			• The kinetic models such as pseudo first order, pseudo second order and intra particle diffusion model were fitted to identify the mechanism of adsorption process. • The isotherm data were fitted to Langmuir and Freundlich models. The maximum uptake of phenol was found to be 2.35×10^{-4} mol/g at 293K and final pH 2.7.The K_F values were observed to decrease with increase in pH and temperature due to the decrease in the adsorption capacity. The highest K_F values were found as 0.329 at the condition of final pH 2.5 and temperature 293K.	
P and NP	GAC	Batch	• Batch studies were carried out for studying the adsorption behaviour of P and NP on GAC from a basal salt medium (BSM) at pH ≈7.1 and T=303K • Based on maximum deviations and correlation coefficients, Langmuir gave the poorest fit for both compounds; Redlich–Peterson, Radke–Prausnitz, and four parameter model of Fritz–Schlunder could represent the data with similar accuracy, i.e. with R^2 value of 0.98 and maximum deviation ≈12%. However, for P, two parameter model of Freundlich may be recommended because of ease in its parameter estimation and better accuracy. • NP was found to be more adsorbed than P, which is consistent with the result found in literature. The kinetics of the adsorption was found to be intra-particle diffusion controlled with diffusion coefficient values of the order of 10^{-13} m^2/s. Three distinct phases of kinetics – rapid, medium, and slow – have been observed.	Kumar et al. [2007]
P and o-cresol	GAC	Batch	• The AC was utilized for the adsorptive removal of P and *o*-cresol from dilute aqueous solutions T=288, 298, 308 and 318 K, pH=4, 7, and 9. • The Langmuir monolayer adsorption capacities were found to be 0.7877 and 0.5936 mmol/g, respectively, for P and *o*-cresol. Kinetic studies performed indicate that the sorption processes can be better represented by the pseudo-second order kinetics. • The processes were found to be endothermic and the thermodynamic parameters were evaluated. Desorption studies performed indicate that the sorbed P molecules can be desorbed with dil. HCl.	Vasu [2008]
P	AC	Batch	• The kinetic study showed that the maximum of adsorption is reached after 60 min of contact T=293-333K, pH=5.5. • The effect of pH on the yield adsorption has been carried in a range of 2–10, the maximum of adsorption is obtained towards a value of 5.5. • The temperature is practically without any influence in P elimination; consequently, tests of adsorption will be carried out at the ambient temperature. The method of simplex has been applied to determining optimum values yield of elimination, the two parameters to be optimized are the speed stirring and the initial concentration of the adsorbent. The best P elimination obtained is 86%.	Hannafi et al. [2008]

P	AC	The flasks were mechanically shaken for 9 days	• Seven Erlenmeyer flasks were used, each one of them containing 0.03, 0.05, 0.08, 0.1, 0.13, 0.15, and 0.18 g of AC and 200 ml of the stock solution. To study the kinetics of P adsorption, a 100 ml stock solution of P was prepared T=288, 298, 308 and 318 K, pH=4, 7 and 9. • Six Erlenmeyer flasks were used, each containing 100ml of the stock solution and 0.2 g of rice husk AC. maximum loadings of 27.58 and 24.68 mg P/g AC, respectively. K_F=0.4080, 0.3414 for AC from rice husk and AC from sugarcane bagasse and qe=19.455, 12.33 mg/g for AC from rice husk and AC from sugarcane. bagasse; 1/n=0.4303, 0.5435 for AC from rice husk and AC from sugarcane bagasse and Kl=1.8423, 2.4727 for AC from rice husk and AC from sugarcane bagasse	Kalderis et al. [2008]
P and other	AC	Batch	• The phosphoric acid AC was derived from waste wooden pallets. T=ambient, pH=2-12, C_0=100-4000 mg/l, the adsorption of P by PAC and F400 reached equilibrium after 1-18 h, respectively. • The adsorption kinetics of MB was slower than that of P on both ACs. Whereas the adsorption PAC=222.2 mg/g was less than that of F400=370.4 mg/g. Batch studies were conducted to evaluate • The MB and P adsorption capacity of PAC and F400 and their dependence on pH, contact time, and initial adsorbate concentration. Experimental results showed that the solution pH slightly influenced the adsorption of MB and P on F400, whereas it had no effect on their adsorption on Phosporic AC. • Equilibrium adsorption data were fitted with an Langmuir isotherm equation. In comparison with F400, PAC showed a higher adsorption capacity for MB but lower for P. Given the comparable physical properties of PAC and F400 and the polar nature of MB and phenol, surface chemistry of the two carbons appeared to determine the adsorption mechanism and capacity. • The strongly negative surface of PAC, due to phosphoric acid activation, facilitated the adsorption of positively charged MB, whereas the presence of oxygen-containing functional groups on Phosporic AC inhibited P adsorption.	Liu et al. [2008]
P and other	AC	Batch	• The adsorption equilibrium characteristics for single and binary components of copper ion and phenol onto powdered activated carbon, alginate bead and alginate-activated carbon (AAC) bead. • The amounts of the adsorbents were varied (0.001–0.25 g), and the volume of the solution was 200 ml of 1.06 mol/m^3 in single and binary components test, T=298K, pH=3, 7 and 10, C_0=1.06 mol/l. • The adsorption capacity of Cu2+ onto different adsorbents was in the following order: alginate bead > AAC bead > powdered activated carbon (PAC). On the other hand, that of phenol was: PAC > AAC bead > alginate bead.	Kim et al. [2008]

			• Multi-component equilibrium data were correlated by three different models. Among them the ideal adsorbed solution theory (IAST) gave the best fit to our data. And the adsorption amount of Cu^{2+} onto AAC bead was greater than that of phenol in the binary components.The maximum adsorption amount of P onto AAC bead at pH 3, 7 and 10 was 1.24, 1.02, 1.01 mol/kg, respectively.	
P	AC	Batch	• The adsorption of P onto coconut shell-based AC. Coconut shell was converted into high quality AC through physiochemical activation at 1123K under the influence of CO_2 flow. Beforehand, the coconut shell was carbonized at 973K and the resulted char was impregnated with KOH at 1:1 weight ratio. • In order to evaluate the performance of CS850A, a series of batch adsorption experiments were conducted with C_0=100 to 500 mg/l, adsorbent loading of 0.2 g and the adsorption process was maintained at 303K. The adsorption isotherms were in conformation to both Langmuir and Freundlich isotherm models. • Chemical reaction was found to be a rate-controlling parameter to this P-CS850A batch adsorption system due to strong agreement with the pseudo-second-order kinetic model. Adsorption capacity for CS850A was found to be 205.8 mg/g.	Din et al. [2009]
P and CP	AC	Batch and column	• Process parameter were T=ambient, pH=5.96 and 6.02. different particle size (1.3, 1.7, 2.3, 2.9, and 3.6 m); A comparison of P and CP adsorption in aqueous solution on mineral activated carbon columns with different particle size (1.3, 1.7, 2.3, 2.9, and 3.6 mm) was studied. • The percentage saturation values of the columns at the break point were evaluated for carbon columns for the removal of P and CP. • It was concluded that P and CP retention and the carbon saturation percentage in column systems depended on the pore volume and surface area of the mineral AC.	Garcia-Mendieta et al. [2009]
P	AC	Batch	• Process parameter were T=303K, pH=7, C_0=100-500 mg/l; The liquid-phase adsorption of P onto coconut shell-based AC. • Coconut shell was converted into high quality activated carbon through physiochemical activation at 1123K under the influence of CO(2) flow. Beforehand, the coconut shell was carbonized at 973K and the resulted char was impregnated with KOH at 1:1 weight ratio. • In order to evaluate the performance of CS850A, a series of batch adsorption experiments were conducted with initial phenol concentrations ranging from 100 to 500 mg /l, adsorbent loading of 0.2g and the adsorption process was maintained at 303K. • The adsorption isotherms were in conformation to both Langmuir and Freundlich isotherm models. Chemical reaction was found to be a rate-controlling parameter to this phenol-CS850A batch adsorption system due to strong agreement with the pseudo-second-order kinetic model. Adsorption capacity for CS850A was found to be 205.8 mg/ g.	Din et al. [2009]

P	AC	Fixed bed reactor	• Steam-activated carbons from oil-palm shells were prepared and used in the adsorption of P. The activated carbon had a well-developed non-micropore structure which accounted for 55% of the total pore volume. The largest Brunauer–Emmett-Teller (BET) surface area of the activated carbon was 1183m^2/g with a total pore volume of 0.69cm^3/g using N_2 adsorption at 77 K. • Experimental tests on the adsorption of P by the activated carbons were carried out in a fixed bed. The aqueous phase adsorption isotherms could be described by the Langmuir equation. • The effects of the operation conditions of the fixed bed on the breakthrough curve were investigated. A linear driving force model based on particle phase concentration difference (LDFQ model) was used to simulate the fixed bed adsorption system. The model simulations agreed with the experimental data reasonably well.	Lua and Jia [2009]
P	AC	Batch	• The adsorption of P and MB on modified ACs. 10 mg of activated carbon with 10 ml of a solution of P or dye at concentration 100 mg/l. • The maximum adsorption capacities calculated from the Langmuir isotherm model were 161.8 and 216.4 mg/g for P and MB. T=298K. • Adsorption kinetic data were tested using pseudo-first-order, pseudo-second-order and intraparticle diffusion models. • Equilibrium data were analyzed by Langmuir and Freundlich isotherm models. The maximum adsorption capacities calculated from the Langmuir isotherm model were 161.8 and 216.4 mg/.g for phenol and MB, respectively. The different uptakes obtained are discussed in relation to the chemical properties of the adsorbents. • The results show that surface chemistry of the activated carbon plays a key role in P and dye adsorption. Finally, activated carbon from date pits with appropriate preparations can rich a high adsorption capacity.	Belhachemi et al. [2009]
P	manganese nodule leached residue	Batch	• Manganese nodule leached residue is a good adsorbent T=ambient, pH=3. • Adsorption of P on water washed manganese nodule leached residue (WMNLR), waste materials from manganese nodules processing plant, has been investigated. The adsorbent (WMNLR) used for the removal of phenolic compounds were characterized by EDX, FTIR, SEM and BET surface area measurement before and after the adsorption process. • Adsorption experiments were carried out to study the effect of various parameters like adsorbent dose, pH, adsorbate concentration, reaction time, temperature and calcination temperature. WMNLR calcined at 673K showed highest adsorption capacity. • The equilibrium adsorption data for P was analyzed by using Langmuir isotherm model. The	Parida and Pradhan [2010]

			maximum adsorption of P was obtained at pH 3 (about 95% for adsorbent dose 1 g/l and 30 mg/l adsorbate concentration). • The increase in percentage of adsorption with increase in temperature indicates that adsorption is endothermic in nature. The pseudo-second-order kinetics was followed in the adsorption process.	
P	AC	Batch	• Cherry stone based AC derived from a canning industry was evaluated for its ability to remove phenol from an aqueous solution in a batch process. • A comparative adsorption on the uptake of P by using commercial AC (Chemviron CPG-LF), and two non-functional commercial polymeric adsorbents (MN-200 and XAD-2) containing a styrene–divinylbenzene macroporous hyperreticulated network have been also examined. • Equilibrium studies were conducted for C_0=25 mg/l, 6.5–9 solution pH and at temperature of 303K. The experimental data were analyzed by the Langmuir and Freundlich isotherm models. Besides, the cherry stone based activated carbons were carried out by using zinc chloride and KOH activation agents at different chemical ratios (activating agent/precursor), to develop carbons with well-developed porosity. • The cherry stone AC prepared using KOH as a chemical agent showed a high surface area. According to the results, ACs had excellent adsorptive characteristics in comparison with polymeric sorbents and commercial activated carbon for the P removal from the aqueous solutions. T=303K, pH=6.5–9.	Beker et al. [2010]
			Aniline (AN)	
AN, PCA	Montmorillonite	Batch	• The adsorption of AN and p-chloroaniline (PCA) from montmorillonite saturated with different cations (i.e. Na^+, K^+, Ca^{2+}, Mg^{2+}, Cu^{2-}, Fe^{3+} and Al^{3+}). • In all cases PCA was absorbed to a greater extent than AN. The shapes of the isotherms depend on the adsorbate and on the exchangeable cation and are interpreted in terms of adsorption mechanisms. • The enthalpy changes (ΔH) calculated from the temperature coefficient of the equilibrium constant are exothermic, but the exothermicity decreases as the polarizing power of the exchange cation increases. The adsorption of the amines on Na^+, K^+ and Ca^+, Mg^+ montmorillonite gives rise to an entropy loss which is higher for the divalent cations. This result is in good agreement with desorption curves obtained after several washings which indicated for the nature of the organo-clay complexes the decreasing order of stability, viz $Mg^{2+} > Ca^{2+} > K^+ > Na^+$. T=313K, pH=natural.	Moreale and Bladel [1979]
AN	AC	Batch	• The adsorption of model aromatic compounds (P, AN, nitrobenzene) on modified ACs. T=ambient, pH=2-12. Dosage=50 mg of crushed sample. Three aromatic • compounds it can be observed that, for the same equilibrium concentration, the amount adsorbed	Villacanas et al. [2006]

			increases from nitrobenzene > AN>P, which is related with the solubility effect on adsorption The best uptake for all the adsorptives under most of the pH conditions used corresponded to the basic sample, which means that dispersive interactions are the most important in this process.	
AN, 4MA	Polymeric resin	Batch	• Synthesized bifunctional polymeric resin (LS-2) was used for removal of AN and 4-methylaniline in aqueous solutions, T=288-318K, C_0=200-1000 mg/l. • Freundlich model gives a perfect fitting to the isotherm data. Although the specific surface area of LS-2 is lower than that of Amberlite XAD-4, the adsorbing capacities for these two adsorbates on LS-2 are higher than those on Amberlite XAD-4 within the temperature range 288–318K, which is contributed to microporous structure and the polar groups on the network of LS-2 resins. The adsorption for AN or 4-methylaniline on LS-2 was proved to be an endothermic process and increasing temperature was favorable. • From the studies on the adsorption thermodynamics, static equilibrium adsorption, and the desorption conditions, an important conclusion can be drawn that the adsorption for AN or 4-methylaniline on the LS-2 is a coexistence process of physical adsorption and chemical transition.	Jianguo et al. [2005]
AN	ACC	Plexiglass reactor	• Activated carbon fibers (ACC) used as aosrbent for removal of AN with a fixed adsorbent (25±0.5 mg/100ml) at range of pH=3-11. • The adsorption/electrosorption of AN on ACFs follow pseudo-first-order adsorption kinetics, and the adsorption rate improves with increasing bias potential. • The electrosorption isotherms, which exhibit a variety of responses depending on bias potential, electrolyte and pH, follow the two classical models of Langmuir and Freundlich. With electrosorption of AN from aqueous solution, a two-fold enhancement of adsorption capacity is achievable. • These experimental results suggest that the electrochemical polarization of ACFs can effectively improve the adsorption rate and capacity of AN, which may be due to the enhanced affinity between AN and ACFs instead of the oxidation on the surface of ACFs or in the solution.	Han et al. [2006]
AN	AC	Batch	• The interaction of P and AN with the surface of highly microporous ash-free carbon was systematically studied in aqueous solutions in the pH range 3–11 under oxic conditions. T=293K. P and AN are adsorbed most strongly in unbuffered conditions. Due to competitive adsorption of water and the buffer ions only part of the surface area is utilized. According to thermal desorption measurements, physisorption takes place in the whole pH range studied. Chemisorption was detected only when electrostatic interaction is possible. Thermal desorption removes only part of the adsorbed species, leaving behind a morphologically and chemically modified surface.	Laszlo et al. [2007]
AN	AC	Batch	• The heterogeneity of ACs prepared from different precursors is investigated on the basis of adsorption isotherms of aniline from dilute aqueous solutions at various pH values. The APET carbon prepared from polyethyleneterephthalate (PET), as well as, commercial ACP carbon	Podkoscielny and Laszlo [2007]

			prepared from peat were used. Besides, to investigate the influence of carbon surface chemistry, the adsorption was studied on modified carbons based on ACP carbon. • Its various oxygen surface groups were changed by both nitric acid and thermal treatments. The Dubinin–Astakhov equation and Langmuir–Freundlich one have been used to model the phenomenon of AN adsorption from aqueous solutions on heterogeneous carbon surfaces. • Adsorption-energy distribution functions have been calculated by using an algorithm based on a regularization method. Analysis of these functions for activated carbons studied provides important comparative information about their surface heterogeneity.	
AN	CNT	Batch	• 3M nitric acid (NA) and 0.3MKMnO4 (PP) (NA-MWNT and CA-MWNT) were used as adsorbent, T=298, 323 and 348 K, pH=natural 50 mg MWNT sample, 25ml AN solution with a known C_0=10-60 mg/l was added into each flask results show that the CNTs treated by citric acid possess favorable performance for AN adsorption at high temperature. • Among the samples, NA-MWNT and CA-MWNT exhibit higher adsorptive capacities at 298 and 348 K, respectively, which have been checked as 11.5 and 28.3 mg/g. • The AN adsorption reactions are considered as spontaneous process because of the negative adsorption standard free energy together with positive standard entropy change. • The average standard enthalpy changes of pristine MWNTand PP-MWNT samples are negative while they are positive in the other two samples. It suggests that nitric acid and citric acid increase the amounts of carboxylic groups of MWNT, which induce the endothermic chemical adsorptions.	Xie et al. [2007]
AN, PNA	AC	Batch	• The adsorption processes of several aromatic chemicals onto ACs, C_0=30-500 mg/l, T=278, 308 K, pH=6.8-7.2. Adsorption isotherms data were fitted to the Freundlich and Fritz-Schlunder equations. • The values of ΔH, ΔG, and ΔS were calculated and these indicate that the process is exothermic in nature in all the examined cases. the adsorption capacity approximate order can be written as follows: toluene> Nitrobenzene > benzene > p-nitrotoluene > p-nitroaniline > AN.	Cotoruelo et al. [2007]
AN	organo-clays	Batch	• Organo-clays (i.e., Cloisite-10A, Cloisite-15A, Cloisite-30B and Cloisite-93A), to remove NP, P and AN of organic pollutants. 50 mg of organo-clay were placed in 50ml. T=288, 298, 308 and 318 K, pH=4, 7, and 9. The d-spacings (0 0 1) of the XRD peak of Cloisite-10A, Cloisite-15A, Cloisite-30B and Cloisite-93A are 1.98, 2.76, 1.93 and 2.64 nm, respectively. The d(0 0 1)-spacings of XRD indicated that these NP, P and AN could penetrate into the interlayer of clays and expand the d(0 0 1)-spacings. • The parabolic diffusion and power-function of kinetic models were employed to describe properly the kinetic experiments. The linear sorption isotherm of constant partition was employed to describe the sorption isotherms of phenols sorbed by organo-clays through hydrophobic–hydrophobic chemical reactions.	Ko et al. [2007]

			• The parabolic diffusion and power-function of kinetic models were employed to describe properly the kinetic experiments. The rate limiting step of the NP sorption reactions on organo-clays were diffusion-controlled processes (i.e., 15A, 30B, 93A) and chemicalcontrolled process for 10A organo-clays. The pre-exponential factor of the NP sorbed by four organo-clays showed the trend as follows: 10A > 30B > 93A > 15A.	
AN	Cr-bentonite	Batch	• The sorptions of AN on Cr-bentonite prepared using synthetic wastewater containing chromium were investigated in a batch system at 303K. • Adsorption efficiencies of aniline are high and stable under acidic and neutral pH conditions and decrease with the increase of pH value under alkaline pH conditions. • The AN removal efficiency decreased from 97.80% to 89.46% as the C_0 was increased from 20-200 mg/l. The experimental data were analyzed by the Langmuir and Freundlich, and Temkin models of sorption. • The sorption isotherm data were fitted well to Langmuir isotherm and q_e was found to be 21.60 mg/g at 303K. Dubinin–Redushkevich (D–R) isotherm was applied to describe the nature of AN uptake and it was found that it occurred chemically. The experimental data fitted very well the pseudo second-order kinetic model. Intraparticle diffusion affects AN uptake. • The results indicate that there is significant potential for Cr-bentonite as an adsorbent material for AN removal from aqueous solutions.	Zheng et al. [2008]
AN, CA and NA	Multiwalled	Batch	• Aqueous adsorption of a series of Ps and anilines by a multiwalled carbon nanotube material (MWCNT15), T=298K, pH=4-7. P or AN substitution with more groups has higher adsorption affinity, and nitro, chloride, or methyl groups enhanced adsorption in the following order: nitro group > chloride group > methyl group. All adsorption isotherms of nondissociated Ps and anilines are nonlinear and fitted well by the Polanyi-theory based Dubinin-Ashtakhov (DA) model. • Linear quantitative relationships combining DA model parameters (E and b) with solute solvatochromic parameters were developed to evaluate the adsorptive behaviors of nondissociated species. Strong H-bonding interaction between solutes, as hydrogen-bonding donors, and carbon nanotubes observed in this study indicates that the solutes with H-bonding donor ability have higher adsorption affinity than the ones without H-bonding donor ability in relatively low concentrations.	Yang et al. [2008]
AN	AC	Batch	• The adsorption of three selected aromatic compounds (AN, sulfanilic acid and benzenesulfonic acid) on AC at different solution pH. T=ambient, pH=3, 7, 11. Dosage=50 mg AC C_0=10–500 mg/l. • The Freundlich model was used to fit the experimental data. T • The AN uptake is significantly lower at pH=3 than at pH=7 and 11. At pH=7 and pH=11, AN in aqueous solution is mainly in its molecular form Higher uptakes are attained when the compounds are present in their molecular form.	Faria et al. [2008]

AN	H-Beta zeolite	Batch catalytic oxidation setup	• H-Beta zeolite was used for removal of AN by ion-exchange process to enhance its catalytic activity, T=2987K, pH=5-11. C_0=50 and 3000 mg/l. Experimental results indicated an AN adsorption level of approximately 106–114 mg/g for each of the unmodified H-Beta, the 0.5% (w/w) Cu-Beta or the 1.4 % (w/w) Cu-Beta zeolites. • The adsorption processes followed the Langmuir model and the level of AN adsorbed was largely unaffected by a change in temperature. • Assessment of the aqueous stability of the exchanged copper on the Beta zeolites indicated minimum copper leaching in the range pH 5–11 thus providing a stable working pH range for both the 0.5% (w/w) and 1.4% (w/w) Cu-Beta adsorbent materials. Catalytic oxidation studies on the adsorbed AN indicated that the presence of copper in the zeolites significantly enhanced the degradation of AN to predominantly carbon dioxide, water and nitrogen. Five successive adsorption/catalytic oxidation cycles did not diminish the AN adsorption capacity of the copper loaded zeolites but there was a small loss in the efficacy of the catalytic oxidation of the adsorbed AN by the end of the 5th cycle.	O'Brien et al. [2008]
AN	Macroporous kaolin	Batch	• The interactions of P, AN and NP, adsorbed from aqueous solutions, with the surface of two activated carbons (with and without oxygen surface groups) were followed by temperature programmed desorption, thermogravimetry and analysis by mass spectrometry. (1 g weighted to the nearest 0.1 mg). C_0=100-10,000 mg/ml. • The results indicate that the dynamic and levels of adsorption of these molecules is not controlled by differences in molecular size. The nature of substituents on the AN ring plays an important role on the adsorption. The incorporation of oxygen as a methoxy group in the ortho or para position enhances the adsorption, while the incorporation of alkyl groups has mixed effects on this phenomenon, decreasing the adsorptivity when the group in placed in the ortho position.	Lopez-Linares et al. [2008]
AN+P	HSAG and AC	Batch	• 0.1 g of carbons and 2 ml of bidistilled water were placed in contact with 20 ml of water solutions of different known concentrations of P, AN and the different mixtures of P and AN (25/ 75, 50/50 and 75/25 molar ratios) pH=6.5-9.5. • All the adsorption isotherms of P and on HSAGs are adequately fitted by Freundlich type isotherms, while on ACs, the extended Langmuir equation provides a better description of the experimental results. This fact reveals the importance of the textural characteristics (i.e., pore sizes) on the adsorption behavior. The presence of oxygen surface groups affects the adsorption behavior. Their effect depends on the amount of these groups that are present on the adsorbent surface and on the nature of the adsorbate molecule. • In the case of HSAG, AN is adsorbed to a larger extent than P for all the studied P–AN mixtures. The opposite trend was found for ACs. Elimination of oxygen groups, originally present in larger amounts on the HSAG surface than on AC, produces an inversion in the selectivity adsorption of	Nevskaia et al. [2004]

			the mixtures. That is more P than AN is adsorbed on the surface of heat-treated HSAG (HSAGT).	
AN+P, AN+2-naphthalenes	Polymeric resin	Batch	• C_0=0.15 to 2 mmol/l with a 1/1 molar ratio of P/AN mixtures or NSA/AN mixtures. • The experimental uptakes of adsorbates in the test binary-component systems are obviously larger than the corresponding ones predicted from Extended Langmuir model postulating no lateral interaction between the loaded molecules, which is assembly due to the cooperative effect mainly arisen from the acid–base interaction between the loaded aromatic acid (P, NSA) and aromatic base (AN) molecules. • The newly modified model, with single-component adsorption isotherm parameters and binary-component fitting parameters, generally showed a marked improvement in the correlation of binary adsorption equilibrium compared to the Extended Langmuir model, which used only single-component isotherm parameters.	Zhang et al. [2006]
AN+P	Polymeric resin	Batch	• The adsorption equilibria of P and AN on nonpolar polymer adsorbents (NDA-100, XAD-4, NDA-16 and NDA-1800) were investigated in single- and binary-solute adsorption systems at 313 K. Adsorbent weight=50 mg, C_0=0.3–8 mmol/l. • The results showed that all the adsorption isotherms of P/AN on these adsorbents can be well fitted by Freundlich and Langmuir equations, and the experimental uptake of P and AN in all binary-component systems is obviously higher than predicted by the extended Langmuir model, arising presumably from the synergistic effect caused by the laterally acid–base interaction between the adsorbed P and AN molecules. • A new model (MELM) was developed to quantitatively describe the synergistic adsorption behavior of P/AN equimolar mixtures in the binary-solute systems and showed a marked improvement in correlating the binary-solute adsorption of P and AN by comparison with the widely used extended Langmuir model. The newly developed model confirms that the synergistic coefficient of one adsorbate is linearly correlated with the adsorbed amount of the other, and the larger average pore size of adsorbent results in the greater synergistic effect of P/AN equimolar mixtures adsorption.	Zhang et al. [2007a]
AN+P	Polymeric resin	Batch	• Adsorption equilibria of P and AN onto nonpolar macroreticular adsorbents were investigated in single and binary-solute aqueous systems at 293 K and 313 K. • All adsorption isotherms can be well represented by the Langmuir equation. Larger uptake of AN than P onto all the adsorbents probably results from the higher hydrophobicity of the former compound as well as the greater electronic density of the aromatic ring of AN. • It is interestingly observed that at a relatively high loading, the total uptake of P and AN in a binary system is remarkably higher than those in a single system. Such uptake difference was elucidated by the cooperative effect arising from the lateral acid-base interaction between the loaded P and AN molecules. Moreover, larger average pore size of the adsorbent is found to result	Zhang et al. [2007b]

			in a greater cooperative coefficient, as observed from the equimolar P/AN adsorption system.	
			4-chlorophenol (CP)	
P, CP	montmorillonite	Batch	• Sorption of P and 2-, 3- and CP from water by tetramethylammonium (TMA)-smectite and tetramethylphosphonium (TMP)-smectite was studied. • Sorption of the phenolic compounds appeared to occur on the aluminosilicate mineral surfaces between neighboring organic cations (TMA or TMP). TMP-smectite was a better sorbent than TMA-smectite, which did not measurably adsorb any of the phenolic compounds. • This disparity in sorption efficiency was attributed to differences in hydration of the interlayer cations. Apparently, hydration occurred to a greater extent in TMA-smectite that in TMP-smectite, causing the interlayer pore size to be smaller for TMA-smectite than for TMP-smectite. TMP-smectite showed selective sorption within the group of chlorinated phenols studied. P and CP were effectively sorbed by TMP-smectite, whereas 2-and 3-chlorophenol were not sorbed. The selectivity appeared to be size- and shape-dependent, and not strongly influenced by water solubility.	Lawrence et al. [1998]
P and CP	GAC	Batch	• The adsorption of P and CPs on four GAC was investigated by batch experiment to correlate with the structure of activated carbons. Physical properties including surface area, average pore diameter and micropore volume and chemical structure of the activated carbons were characterized by N_2 adsorption experiment, SEM., XRD , elemental analysis, X-ray photoelectron spectroscopy (XPS) and FT-IR spectroscopy. To calculate the adsorption parameters, adsorption isotherm data were fitted to the Freundlich equation. From the correlation between the characterization and the Freundlich parameters, it is concluded that the adsorption behavior of P and CPs on ACs is controlled by the dispersion force between the π-electrons in ACs and those in phenol molecules. T=298K, pH=3	Jung et al. [2001]
P, CP, NP	Amberlite XAD-4	Batch and Column study	• Amberlite XAD-4 polymeric resin was chemically modified with an acetyl group, which enables the resin to be used directly without a wetting process. • The modified resin was comparatively evaluated using four phenolic compounds, P, p-cresol, CP, and NP. The capacities of equilibrium adsorption for all four phenolic compounds from their aqueous solutions increased around 20% on the acetylated resins within temperature range of 283–323 K. • Freundlich isotherm equations, as well as the relative adsorptive capacities and isosteric adsorption enthalpies for the four Phenolic compounds, indicate a physical and multiple-layer adsorption process on the Amberlite XAD-4 resins either with or without the chemical modification. • Mini-column adsorption studies showed that the breakthrough adsorption capacity and the total adsorption capacity at designated conditions for all four phenolic compounds also increased over 20% after chemical modification.	Li et al. [2001]

P, CP	Amberlite XAD-16 resin	Batch and column study	• Removal of P and CP from synthetic single and bisolute aqueous solutions at 303.15K through adsorption on Amberlite XAD-16 resin under batch equilibrium and dynamic column experimental conditions were investigated. • The equilibrium adsorption data from single component solutions were fitted to Langmuir and Freundlich adsorption isotherm models to evaluate the model parameters and the parameters in turn were used to predict the extent of adsorption from bisolute aqueous solutions using Ideal Solution Adsorption (IAS) model. • The effect of pH on removal of P and CP from single and bisolute systems was studied. The breakthrough capacity and total capacity of the resin for the adsorbates at different concentrations were evaluated through column adsorption studies. • Attempts were made to regenerate the resin by solvent washing using methanol as an eluent. The limited number of adsorption–desorption cycles indicated that the adsorption capacity of the resin remained unchanged.	Abburi [2003]
P, CP	Ca-montmorillonite	Batch	• Adsorption of P, 2CP, and 2, 4-dichlorophenol on Ca-montmorillonite was studied with batch experiments at 298K. The results from the experiments show that the amount of the adsorption of the phenolic compounds increases with chlorination, i.e., P< 2CP < 2, 4-dichlorophenol. • This adsorption trend is due to the differences in the affinity of the phenolic compounds between the adsorbent and water, that is more affinity to water leads to less adsorption. • The adsorption of P is unrecognizable, while 2, 4-dichlorophenol is showing the highest adsorption density despite the repulsion between dissociated dichlorophenol anions and montmorillonite surface. • Freundlich model fits moderately well to the adsorption isotherm of 2CP and 2, 4-dichlorophenol. The calculated model parameters are n=1.50, 0.49 and logkF=0.51, 1.09 for 2-chlorophenol and 2, 4-dichlorophenol, respectively.	Yu et al. [2009]
P, CP	cationic surfactants hexadecyltrimethyl ammonium bromide	Batch	• P and CP on pumice modified with the cationic surfactants hexadecyltrimethyl ammonium bromide (HDTMA) and benzyldimethyl tetradecylammonium chloride (BDTDA) was investigated. • Experimental studies indicate that HDTMA-pumice and BDTDA-pumice have the capability to remove P and CP from aqueous solution. The influence of initial concentration and adsorbent dosage was studied. • The adsorption of P and CP increased with increasing initial concentration and decreased with increasing amount of adsorbent used. The Freundlich adsorption isotherm was found to describe well the equilibrium adsorption data. The parameters of the Freundlich model have been	Akbal [2005]

			determined using the adsorption data.	
CP	Amberlite XAD-4 resin	Batch	• Redlich–Peterson > Langmuir > Toth > Freundlich isotherms T=298, 308 and 318K, pH=6.8 and 6.9. • The pseudo-second-order kinetic model provided the best correlation to the experimental results. • Results of the intra-particle diffusion model show that the pore diffusion is not the only rate limiting step. The lower correlation of the data to the Bangham's equation also represents that the diffusion of the adsorbate into pores of the sorbent is not the only rate-controlling step. • The thermodynamic constants of adsorption phenomena; ΔG°, $\Delta H^{\circ}$and ΔS° were found as −4.17 (at 298K) kJ/mol, −42.01 kJ/mol, and −0.127 kJ/(mol K), respectively. The results showed that adsorption of CP on Amberlite XAD-4, a nonionic polymeric resin was exothermic and spontaneous.	Bilgili [2006]
P, CPs	modified natural zeolite	Batch	• P and CP by surfactant-modified zeolite. Batch studies were performed to evaluate the effects of various experimental parameters such as t, m, C_0, and temperature on the removal of P and CP. • The sorption kinetics was tested for intraparticle diffusion, Elovich, and pseudo-second order reaction and rate constants of kinetic models were calculated. • Equilibrium isotherms for the adsorption of P were analyzed by Freundlich, Langmuir, and Tempkin isotherm models. Freundlich isotherm was found to best represent the data for P and CP adsorption. • Equilibrium isotherms for the adsorption of P were analyzed by Freundlich, Langmuir, and Tempkin isotherm models. • Freundlich isotherm was found to best represent the data for P and CP adsorption. The P removal efficiencies reached up to 71% and 73% for HDTMA-zeolite and BDTDA-zeolite and the CP removal efficiencies reached up to 81% and 89% for HDTMA-zeolite and BDTDA zeolite after 24 h. T=293-313K	Kuleyin [2007]
CP	AC	Batch	• The adsorption studies of CP from aqueous solution on AC derived from rattan sawdust (RSAC) have been analyzed in the range of 25–200 mg/l initial CP concentrations and at temperature 300K. • Different experimental parameters like initial pH, contact time and initial concentration on the adsorption of CP were evaluated. • Equilibrium data fitted very well with the Langmuir isotherm model. • The rates of adsorption were found to obey the rules of pseudo-second order model with good correlation. Results of the intra-particle diffusion model show that the pore diffusion is not the only rate limiting step.T=301K, pH=1-14	Hameed et al. [2007]
P, CPs	natural zeolite	Batch	• The adsorption isotherms of P, 2CP, CP, 2, 4-dichlorophenol, and 3, 5- dichlorophenol onto natural zeolite were obtained at pH values of 4.0, 6.0, pKa of Ps, and 10.5. • A simple two-site Langmuir model was used to fit the experimental data where two types of	Yousef and El-Eswed [2009]

			interaction were quantified by the model. • The first is the pH independent interaction of Ps with hydrophobic sites of zeolite. The second is the pH-dependent phenolate complexation with hydrophilic sites of zeolite (metal ions). • The adsorption was enhanced with increasing pH values due to the increase of phenolates complexation with metal ions on zeolite surface. • The number of hydrophobic sites of zeolite available for Ps was found to be greater than that of the hydrophilic sites. On the other hand, the affinity constants of the hydrophilic sites were found to be much greater than those of the hydrophobic sites. Moreover, the adsorption process of ps onto zeolite was found to be independent on the ionic strength.	
			4-nitrophenol (NP)	
NP, P and other	polymeric resins	Batch and column	• A water-compatible hypercrosslinked polymeric adsorbent (NJ-8) for adsorbing and removing phenolic compounds from their aqueous solutions was prepared. This product can be used directly without a wetting process. Its adsorption property toward four phenolic compounds, P, p-cresol, CP, and NP was tested using the commercial Amberlite XAD-4 as a reference. • The capacities of equilibrium adsorption for all four phenolic compounds on the NJ-8 from their aqueous solutions are around two times as high as that of Amberlite XAD-4 within the temperature range 283–323K, which may contribute to their micropore structure and the partial polarity on the network. • Freundlich isotherm equations, as well as relative adsorption capacities and isosteric adsorption enthalpies for the four phenolic compounds, indicate that the adsorption of phenolic compounds on the NJ-8 resin is a physical adsorption process. • Mini-column adsorption studies for phenol on Amberlite XAD-4 and NJ-8 resins show that the breakthrough adsorption capacities are 0.54 and 0.99 mmol/ml, and the total capacities are 0.62 and 1.37 mmol/ml, while no extra acetone was needed to remove the adsorbed phenol from NJ-8 as from Amberlite XAD-4.	Li et al. [2002]
NP, Benzoic acid	AC	Column study	• Three series of batch tests at 298K were performed to determine the benzoic acid and NP binary adsorption isotherms onto GAC in the aqueous solutions and the experimental data were fitted to the extended Langmuir isotherm model successfully. • The experimental data and the isotherm model parameters showed that the GAC used in this study had a higher affinity to NP than benzoic acid. Three column tests were performed to determine the breakthrough curves and effluent solution pH with varying feed compositions. According to the experimental results, the weakly adsorbed BA exhibited an intermediate zone of effluent concentration higher than its feed one; the effluent solution pH could serve as a good indicator for breakthrough. • The breakthrough curves with varying feed compositions could be predicted by the non-linear wave	Chern and Chien [2003]

			propagation theory satisfactorily. Only the adsorption isotherm models were required to construct the composition path diagram with which the breakthrough curves could be predicted.	
NP	AC	Column	• Carbon fixed-beds are usually used to remove organic contaminants. Adsorption in a carbon filter is a dynamic, non-steady process which is not yet completely understood. The objective of this paper is to establish a methodology to simplify the study of this process based on the wave theory, rapid small-scale column test and experimental design/surface response analysis. • The constant pattern wave hypothesis was confirmed by the experimental data. The influence of the inlet concentration of NP and the flow rate on dynamic adsorption was studied at 293K following a central composite design using a second-order model. • Both parameters have an important influence on the response variables studied. The methodology used is a useful tool for studying the dynamic process and shows interactions that are difficult to verify by the classical step-by-step method.	Sabio et al. [2006]
NP, CP	AC	Batch	• Static and kinetic studies on adsorption of nitrobenzene, NP and CP on two mesoporous carbons are performed. The carbon properties are analyzed by means of nitrogen adsorption. • The adsorption experiments are performed in acidic buffer solutions in a wide range of concentrations.The static experiments are analyzed by means of Langmuir–Freundlich and Freundlich isotherms. • The Lagergren, pseudo second- order, intraparticle-diffusion and multi-exponent equations are used in the analysis of kinetic equilibria.	Marczewski et al. [2007]
NP	ACC	Batch	• The adsorption of NP onto ACF was investigated in simulated wastewater in a batch system to evaluate the effects of solution pH, presence of sodium chloride, m and T. • It was found that PNP adsorption amount depended on pH, sodium chloride content, adsorbent doses and temperature. Langmuir and Freundlich models were applied to describe the adsorption isotherms. • Freundlich model agreed with experimental data well, indicating the possibility of more than just one monomolecular layer of coverage. SEM photographs of ACF before and after adsorption revealed that it was in part with multimolecular layers of coverage on ACF surfaces. The change of free energy, enthalpy, and entropy of adsorption were also evaluated for the adsorption process. • The pseudo-first-order and pseudo-second-order kinetic models were used to describe the kinetic data. • The experimental data fitted very well the pseudo-second-order kinetic model. Attempts were made to desorb NP from ACF using dilute NaOH solution and water, and desorption efficiency was obtained to the extent of 92.7% with 0.025M NaOH and water at 368 K.	Tang et al. [2007]
NP	XAD-4	Batch	• Chloromethylated styrene-divinylbenzene copolymers were post-crosslinked through Fredel–Crafts alkylation reaction and a water-compatible hypercrosslinked resin HJ-1 was developed successfully. It can be wetted directly by water and can be used without any wetting process. It	Huang et al. [2009]

			was applied to remove NP in aqueous solution in comparison with the commercial Amberlite XAD-4 resin T=300, 305, and 310 K, pH=Neutral. • Their adsorption behaviors for NP were conducted and it was found the adsorption dynamics obeyed the pseudo-second-order rate equation and the intra-particle diffusion was the rate-limiting step. • The adsorption isotherms can be correlated to Freundlich isotherm and the adsorption capacity onto HJ-1 resin was much larger than XAD-4. • The maximum adsorption capacity of NP for HJ-1 resin was measured to be 179.4 mg/g with the equilibrium concentration at 178.9 mg/l and the maximum removal percentage was predicted to be 98.3%. • The adsorption thermodynamic parameters were calculated and the adsorption was mainly driven by enthalpy change. The micropore structure, the size matching between the pore diameter of HJ-1 resin and the molecular size of NP, and polarity matching between the formaldehyde carbonyl groups of HJ-1 resin and NP bring the larger adsorption capacity and higher adsorption affinity.	
			C, R and HQ	
CP and others	TiO_2	Batch	• The experiments with wide range of dosage 0.5- 10 g/l at 24 has a equilibrium time 24-36 h; C_0=1 x 10^{-5} to 5 x 10^{-3} M; 1 g/l. T=ambient, pH=2-11. • They are found that, at ≥10 g/l are high as 90% adsorption removal also carried out the experiments with wide range of pH (2-11) at optimum dosage (1 g/l) and total ligand concentration (optimum 5 x 10^{-5} M). • The adsorption is typically diminished at very high pH (where OH- effectively competes with the deprotonated ligand for surface sites) and at low pH (where neutral surface sites are converted into protonated sites and ligand molecules become successively protonated).	Vasudevan and Stone [1996]
C and R	AC	Batch (0.25 l)	• For both R and C, 10 g/ l was required to remove 95% of the initially present (C_o=1000 mg/ l). T=29.9±0.3 °C, pH=7.1. • The adsorption behavior of R and C on granular activated carbon from a basic salt medium (BSM) at pH=7.1 and temperature=303K. • The isotherm data were correlated with six isotherm models, namely Langmuir, Freundlich, Redlich–Peterson, Radke–Prausnitz, Toth, and Fritz–Schlunder's using a nonlinear regression technique.It is observed that the C isotherm data may be represented by Redlich–Peterson, Radke–Prausnitz, Toth, and Fritz–Schlunder models with similar accuracy (max. dev. 12%). R data may be represented by Freundlich, Redlich–Peterson, Radke–Prausnitz, and Fritz–Schlunder models equally well (max. dev. 15%). Freudlich being a simple model is recommended for R. At the conditions investigated in this study, C is adsorbed to a greater extent than R. This is due to the compound's solubility and position of the –OH group on the benzene aromatic ring.	Kumar et al. [2003]

			• The kinetics of adsorption has been found to be diffusion controlled and the value of effective particle diffusion coefficients is of the order of 10^{-13} m /s. Three distinct phases of kinetics rapid, medium, and slow have been observed. These results should be useful for the design of adsorbers for removing these pollutants.	
C	Waste Fe(III)/Cr(III) Hydroxide	Polythene bottles (0.25 l)	• 500 mg/50 ml; 160 rpm; C_o=10, 20, 30, 40 mg/l. The percent C removal at equilibrium decreased from 80% to 65% as the concentration was increased from 10 to 40 mg/l. T=32-60 °C, pH=3.5-10. • The adsorption of C onto "waste" Fe(III)/Cr(III) hydroxide was investigated to assess the possible use of this adsorbent. The influence of various parameters such as agitation time, C concentration, adsorbent dose, pH, and temperature has been studied. Equilibrium adsorption data followed both Langmuir and Freundlich isotherms. • Adsorption followed second order rate kinetics. The q_m was found to be 4.0 mg/g of the adsorbent. Acidic pH was favorable for the adsorption of C. Desorption studies showed that chemisorption seems to be the major mode of the adsorption process.	Namasivayam and Sumithra [2007]
HQ	RHA	Batch	• The removal of phenolic compounds from aqueous medium by rice husk-based active carbons (RHCs) was first demonstrated. Factors of influence on the RHCs adsorbability were examined in detail. Two series of RHCs were derived by KOH-activation and NaOH-activation at different temperatures for various time, respectively. • The difference in the adsorption performance for phenolic compounds were compared and elucidated by their pore size distribution, surface functional groups and the electric capacity, the results showed that the adsorption mainly took place on the external surface and was controlled by chemisorption and increased with the total density of carboxylic and lactonic.	Qi et al. [2004]
P, NP and others	GAC	Batch	• Competitive adsorption of some priority pollutants, namely P, omicron-cresol, NP, m-methoxyphenol, benzoic acid and salicylic acid from their aqueous solutions onto GAC column was studied. Experiments were carried out to determine the breakthrough curves for adsorbates when present in aqueous solutions as single-, bi- and tri-solute system to evaluate the competitive adsorption phenomenon. • Results indicate that in single-solute-GAC systems, NP is most strongly adsorbed as compared to other P derivatives studied. • The substituted Ps were found to adsorb to a greater extent than P itself. The GAC-bisolute and GAC-trisolute systems clearly show the competitive or preferential adsorption of one solute over the other, as the solutes are competing for the available GAC surface for adsorption. Initially, all the adsorbates are taken up by the GAC surface, but near the breakthrough point the more adsorbable solute is able to desorb the less adsorbable one.	Singh and Yenkie [2004]

C and R	Polymeric resin	Batch (0.25 l)	• aminated hypercrosslinked polymers (AH-1, AH-2 and AH-3) were prepared on the basis of the conventional chloromethylated low-crosslinked macroporous styrene–divinylbenzene copolymers by controlling the postcrosslinking reaction and surface modification with dimethylamine C_0=100-1000 mg/l; 200 rpm for 24 h; 0.100 g/100 ml. T=283-323K. • Adsorption behaviour of R and C from aqueous solution onto the above aminated hypercrosslinked polymers and the hypercrosslinked polymeric adsorbent NDA-100 without amino groups was compared. • It was found that the aminated hypercrosslinked polymers had higher adsorption capacities than NDA-100 due to the Lewis acid–base interaction between the phenolic compounds and the tertiary amino groups on the polymer matrix. Specific surface area and micropore structure of the adsorbent, in company with tertiary amino groups on the polymer matrix mutually affect the adsorption performance towards the both phenolic compounds. Additionally, more C is adsorbed than R due to the affinity towards water and position of the hydroxyl group on the benzene ring of the compound. Besides, thermodynamic study was carried out to interpret the adsorption mechanism. • Kinetic study testified that the tertiary amino groups on the polymer matrix could decrease the adsorption rate and increase the adsorption apparent activation energy.	Sun et al. [2005]
HQ	ACC	Batch	• The rate constants decreased in the order NP~m-cresol > *p*-cresol > HQ~P. Adsorption isotherms were derived at 303K and the isotherm data were treated according to pH=7.4. • Langmuir, Freundlich and Tempkin isotherm equations. The goodness of fit of experimental data to these isotherm equations was tested and the parameters of equations were determined. The possible interactions of compounds with the carbon surface were discussed considering the charge of the surface and the possible ionization of compounds at acidic, basic and natural pH conditions.	Ayranci and Duman [2005]
R, P, HQ and others	AC	Batch	• 0.25 g/50ml of carbon; sawdust was used as a source material to prepare ACs by chemical activation with sulphuric acid. Texture properties of these carbons were determined by measuring the adsorption of nitrogen at 77K and of carbon dioxide at 29 K. • The nitrogen adsorption isotherms were interpreted by BET equation and αs-method while Co_2 adsorption results were interpreted by applying the D–R equation. The nature of carbon surface functionalities was studied by FTIR spectroscopy and Boehm titration method. • The adsorption of P, HQ, R and C from aqueous solution at 298K on to these carbons has been investigated. FTIR shows that the carbon surface acquires an acidic character with carboxylic groups were essentially fixed along with lactonic and phenolic groups. • The equilibrium data fit well the Langmuir isotherm. The amounts of Ps adsorbed, without exception decrease with increasing the concentration of acid groups on the carbon surface. Moreover, for each carbon, the amount of P adsorbed follows the order P > HQ > R > C.	Mohamed et al. [2006]

P, CP and others	GAC	Batch	• P, 2CP, and CP biosorption on *Sargassum muticum*, an invasive macroalga in Europe, has been investigated. The efficiency of this biosorbent was studied measuring the equilibrium uptake using the batch technique. • A chemical pre-treatment with $CaCl_2$ has been employed in this study in order to improve the stability as well as the sorption capacity of the algal biomass. • The influence of pH on the equilibrium binding and the effect of the algal dose were evaluated. The experimental data at pH=1 have been analysed using Langmuir and Freundlich isotherms. It was found that the maximum sorption capacity of CPs, $q_{(max)}$=251 mg/g for CP and $q_{(max)}$=79 mg/g for 2CP, as well as that of a binary mixture of both CPs, q(max)=108 mg/g, is much higher than that of P, $q_{(max)}$=4.6 mg/g. Moreover, sorption kinetics have been performed and it was observed that the equilibrium was reached in less than 10 h. • Kinetic data have been fitted to the first order Lagergren model, from which the rate constant and the sorption capacity were determined. Finally, biosorption of the Pic compounds examined in the present study on *Sargassum muticum* biomass was observed to be correlated with the octanol-water partitioning coefficients of the Ps. This result allows us to postulate that hydrophobic interactions are the main responsible for the sorption equilibrium binding.	Rubin et al. [2006]
R, C, P, and others	TiO_2 Degussa P-25	Stirred glass vessels (0.25 l)	• The photocatalytic behaviour of different phenolic compounds (C, R, P, *m*-cresol and *o*-cresol), their adsorption and interaction types with the TiO_2 Degussa P-25 surface were studied. Langmuir and Freundlich isotherms were applied in the adsorption studies. • The obtained results indicated that catechol adsorption is much higher than those of the other phenolics and its interaction occurs preferentially through the formation of a catecholate monodentate. R and the cresols interact by means of hydrogen bonds through the hydroxyl group, and their adsorption is much lower than that of C. • Finally, P showed an intermediate behaviour, with a Langmuir adsorption constant, K_L, much lower than that of C, but a similar interaction. The interaction of the selected molecules with the catalyst surface was evaluated by means of FTIR experiments, which allowed us to determine the probability of •OH radical attack to the aromatic ring. C_0=10–150 mg/l; $K_L^C >> K_L^P > K_L^R > K_L^{m\text{-cresol}} > K_L^{o\text{-cresol}}$; $n_F^C >> n_F^P > n_F^R > n_F^{m\text{-cresol}} > n_F^{o\text{-cresol}}$. T=25 °C, pH=5	Arana et al. [2007]
Phenolic compounds	GAC	Batch	• The adsorption equilibrium isotherms of five phenolic compounds, P, 2CP, CP, 2, 4-dichlorophenol, and 2, 4, 6-trichlorophenol, from aqueous solutions onto granular activated carbon were studied and modeled. In order to determine the best-fit isotherm, the experimental equilibrium data were analyzed using thirteen adsorption isotherm models with more than two-	Hamdaouia and Naffrechoux 2007

			parameter; nine three-parameter equations – the Redlich–Peterson, Sips, Langmuir–Freundlich, Fritz–Schlunder, Radke–Prasnitz (three models), Tóth, and Jossens isotherms – three four-parameter equation – the Weber–van Vliet, Fritz–Schlunder, and Baudu isotherms – and one five-parameter equation – the Fritz–Schlunder isotherm. • The results reveal that the adsorption isotherm models fitted the experimental data in the order: Baudu (four-parameter) > Langmuir–Freundlich (three-parameter) > Sips (three-parameter) > Fritz–Schlunder (five-parameter) > Tóth (three-parameter) > Fritz–Schlunder (four-parameter) > Redlich–Peterson (three-parameter). The influence of solution pH on the adsorption isotherms of CP was investigated. • It was shown that the solution pH has not an effect on the adsorption isotherms for pH < pK_a. The pH at which the uptake decreased was found to be dependent on the adsorptive pK_a and the pH_{PZC}.	
C, R, P and others	CNT	Batch	• Adsorption of R and other phenolic derivatives on pristine multi-walled carbon nanotubes (MWCNTs) and HNO_3 treated MWCNTs has been investigated in attempt to explore the possibility to use MWCNTs as efficient adsorbents for pollutants. • MWCNTs showed higher adsorption ability in a rather wide pH range of 4–8 for R, while decreased uptake capacity was found for acid-treated MWCNTs. Other Phenolic derivatives such as P, C, HQ and pyrogallol were employed to study the influence of the number and position of hydroxyl groups on the adsorption capacity. • The amounts adsorbed by MWCNTs increased with the increasing number of hydroxyl. The substitution of P with a hydroxyl in meta-position leads to a much higher absorption ability than substitution in ortho- or para-position, which suggested that MWCNTs possess a great potential in removal of R from water, as well as the other phenolic derivatives.The uptake of R was 19.7 mg/ml within 1 min, which was about 60% of the total amounts adsorbed when adsorption reached equilibrium; The uptake of the adsorbates follows the order: pyrogallol > C > P, pH=4-8.	Liao et al. [2008]
C	CTAB-B	Batch	• Contact time=0.016–4.16 h, C_o=0.8–15.3 mmol/l; 0.25 g of CTAB-B; % adsorption increases from 81.5 to ~100. T=30, 40, 50±1 °C, pH=5-12. The equilibrium data fit well into the Langmuir and Freundlich adsorption isotherms over a wide range of concentration. • Both the Langmuir and Freundlich models fit well to adsorption data obtained (at 303, 313 and 323K). The steep rise exhibited by both isotherms. At low concentrations of C indicates a high affinity of CTAB-B for C, whereas the almost levelling off of the isotherms in the region of saturation suggests that the overall capacity can be taken advantage of in a wide range of equilibrium concentration of the adsorbate in the aqueous phase.	Shakir et al. [2008]
Phenolic compounds	GAC	Column	• Mathematical modeling of liquid phase adsorption of Ps in fixed beds of granular activated carbon was investigated. The model considered the effects of axial diffusion in the fluid, the external film and internal diffusional mass transfer resistances of the particles, and the nonlinear adsorption	Aribike and Olafadehan [2008]

			isotherm of Freundlich. • It was shown that the analysis of a complex multicomponent adsorption system could be simplified by converting it into a pseudo single-component adsorption system. This was achieved by lumping the concentrations of the components together as one single parameter, chemical oxygen demand. • The resulting model equations were solved using the orthogonal collocation method and third-order semi-implicit Runge-Kutta method combined with a step-size adjustment strategy. Excellent agreement between simulated results and pilot plant data was obtained. Also, the breakthrough profiles revealed the formation of a primary monomolecular layer on the adsorbent surface.	
C and others	AC	Batch	• 0.5 g of active charcoal; removal: 90% at 5 h; total time: 35–40 h to reach the equilibrium. T=25 °C, pH=6-13. Adsorption of polyfunctional phenols encountered in olive oil mill waste waters was carried out on an active charcoal at 293 K. • The relation between the structure of the P and its adsorption capacity was discussed. Different isotherm equations were considered for modelling the experimental data and their parameters and standard deviations were determined. • Freundlich equation was found to provide the best fit except for the C.	Richard et al. [2009]
C and R	polymeric resin	Batch	• 0.150 g/25 ml of resin; C or R (C_0=200, 400, 600, 800, 1000, and 1200 mg/l); adsorption capacity of C > R. T=293-313K. water-compatible hypercrosslinked resin HJ-1 was developed for adsorbing C and R in aqueous solution in this study. • Its adsorption performances for C and R were investigated in aqueous solution by using the commercial Amberlite XAD-4 as a reference. • The adsorption dynamic curves were measured and the adsorption obeyed the pseudo-second-order rate equation of Boyer and Hsu. • The adsorption isotherms were scaled and Freundlich isotherm model characterized the adsorption better. The adsorption thermodynamic parameters were calculated and the adsorption was an exothermic, favorable, and more ordered process. • The fact that the adsorption capacity of C was larger than R and the adsorption enthalpy of C was more negative than R can be explained in terms of the solubility and the polarity of two adsorbates.	Huang et al. [2009]
C	AC	Column	• The sensitivity of the model for the prediction of the critical time to the different parameters is discussed and it is found to be mostly dependant upon the mass-transfer coefficient K_f and the adsorbant mean particle diameter dP. In addition, the critical time has been proved to increase with the adsorption capacity q_{max}. • The existence of an optimal flow of polluted effluent through the column to achieve the removal of the pollutant with the highest efficiency is observed.	Richard et al. [2009]

P, NP, CP (binary)	GAC	Batch	• A series of equilibrium experiments have been conducted to assess the capactiy of GAC to adsorb three bisolute contaminants of Ps including NP/P, CP/P acid CP/NP. The observed equilibrium data are analyzed and compared with four existing models, i.e, Langmuir competitive model, extended three-parameter isotherm, ideal adsorbed solution theory and modified ideal adsorbed solution theory. • The mutual interferences of phenolic adsorption onto GAC are prominent by experimental observation and the bisolute adsorption isotherm curves can be represented by ideal adsorbed solution theory for all three binary phenolic mixtures. Furthermore, modified ideal adsorbed solution theory can reduce the deviations between the experimental and calculated values. • The determination of the sorbent capacity will offer the accurate description of bisolute equilibrium behavior for designing the activated carbon adsorber to remove P pollutants from wastewater.	Wang and Yang [1997]
P and others	GAC	Batch	• The impact of the presence of molecular oxygen on multicomponent adsorption is evaluated in this study. Adsorption equilibria for binary mixtures of P/o-cresol and ternary mixtures of P/o-cresol/3-ethylphenol on GAC are determined at 296K using three different initial-concentration combinations. • Experiments were conducted under conditions where molecular oxygen is present (oxic adsorption) and under conditions where oxygen was excluded from the adsorbate solution and the GAC particles (anoxic adsorption). • The ideal adsorbed solution theory, using the Myers equation for correlating the single-solute anoxic isotherms, is found to accurately describe the competitive adsorption behavior of these phenolic mixtures under anoxic conditions. When the Freundlich equation was used to describe the single solute behavior, increased deviations were observed. • Poor model predictions for the oxic isotherms are attributed to the presence of molecular oxygen, which promotes the polymerization of the adsorbates on the surface of GAC.	Sorial et al. [1993a]
P and others	GAC	Batch	• The impact of the presence of molecular oxygen in the test environment is further evaluated for adsorption behavior of a mixture of phenolic compounds on fixed-bed GAC adsorbers. Adsorption breakthrough curves are obtained for the single-solute system P, o-cresol, and 3-ethylphenol; the binary solute system of P and o-cresol; and the ternary solute system of P, o-cresol, and 3-ethylphenol. • The plug-flow homogeneous surface diffusion model is evaluated as a predictor of adsorber performance for these systems. • The binary and ternary solute calculations of the model are performed using kinetic parameters determined for the single-solute system. The ideal adsorbed solution theory is used to describe the equilibrium on the surface of the adsorbent particle. • The model predictions for the single-solute system agree very well with the experimental breakthrough curves conducted under anoxic conditions, with exceptions to the later portion of	Sorial et al. [1993b]

			the o-cresol breakthrough, where tailing of the experimental breakthrough has been noticed due to the presence of limited concentrations of dissolved oxygen in the feed. The model predictions for the binary and ternary solute systems agree well with the experimental data collected under anoxic conditions.	
Fu-Ph-CP	AC	The experiments were carried out in QVF glass column of 50 mm (I.D.) and 50 cm in height	• For a multicomponent competitive adsorption of furfural and phenolic compounds, a mathematical model was built to describe the mass transfer kinetics in a fixed bed column with activated carbon. • The effects of competitive adsorption equilibrium constant, axial dispersion, external mass transfer, and intraparticle diffusion resistance on the breakthrough curve were studied for weakly adsorbed compound (furfural) and strongly adsorbed compounds (CP and P). • The results show that the mathematical model includes external mass transfer and pore diffusion using nonlinear isotherms and provides a good description of the adsorption process for furfural and phenolic compounds in a fixed bed adsorber.	Sulaymon and Ahmed [2008]
P+2-butanol + tert-amyl alcohol	AC	Column	• A computational procedure is presented for solving the set of stiff hyperbolic and parabolic partial differential equations describing the simultaneous adsorption of a ternary system in a column packed with adsorbent particles using nonlinear adsorption isotherms of Fritz and Schluender. • The model equations account for the effects of axial diffusion in the fluid and in the film and internal diffusional mass-transfer resistances of the particles. Orthogonal collocation and Michelsen's modified third-order semiimplicit Runge-Kutta methods combined with a step size adjustment strategy are used to solve the general form of the resulting 6N coupled ordinary differential equations for simultaneous adsorption of 2-butanol, tert-amyl alcohol, and phenol in fixed beds. Simulated results obtained from this model are compared with experimental data. • Excellent agreement between simulated results and previously published experimental data is obtained in 0.41- and 0.82-m adsorbers when the film mass-transfer coefficients are reduced by 15% and 12.5%, respectively.	Olafadehan and Susu [2004]

2.4 TAGUCHI'S DESIGN OF EXPERIMENTS

Conventional optimization procedures involve altering of one parameter at a time and keeping all other parameters constant. These methods enable one to assess the impact of those particular parameters on the process performance. These procedures are time consuming, cumbersome, require more experimental data sets and cannot provide information about the mutual interactions of the parameters [Beg et al., 2003]. Taguchi's method of orthogonal array (OA) experimental design (DOE) involves the study of any given system by a set of independent variables (factors) over a specific region of interest (levels) [Mitra, 1998]. Unlike traditional DOE, which focuses on the average process performance characteristics, Taguchi's method concentrates on the effect of variation on the process characteristics [Phadke, 1989] and makes the product or process performance insensitive to variation by proper design of parameters. This approach also facilitates to identify the influence of individual factors, establishing the relationship between variables and operational conditions and finally establish the performance at the optimum levels obtained with a few well-defined experimental sets [Joseph and Piganatiells, 1988]. This method also determines the optimum levels of the important controllable factors based on the concept of robustness and S/N ratio [Mitra, 1998; Tong, 2004]. In this methodology, the desired design is sought by selecting the best performance under conditions that produces consistent performance [Roy, 2001] and the conclusions drawn from the small-scale experiments are valid over the entire experimental region spanned by control factors and their setting levels [Phadke and Dehnad, 1988; Srivastava et al., 2007].

Analysis of the experimental data using the ANOVA (analysis of variance) and factor effects give the output that are statistically significant in finding the optimum levels. This approach not only helps in considerable saving in time and cost but also leads to a more fully developed process by providing systematic, simple and efficient methodology for the optimization of the near optimum design parameters with only a few well defined experimental sets [Taguchi, 1986].

Its application created significant changes in several industrial organizations in Japan and USA in manufacturing processes and total quality control [Taguchi, 1986; Ross,

1996]. More recently, it has been applied for the optimization of a few biochemical techniques [Han, 1998] and bioprocess applications [Rao, 2002].

Barrado et al. [1996] developed a method for the precipitation of metals as magnetic ferrite from the alkalinized solution containing Fe(II). The working conditions were optimized by using a Taguchi L_9 (3^4) experimental design in order to minimize the total residual concentration (TRC) of metal ions in solution. A statistical analysis of the experimental data revealed the most influential factor to be the Fe(II)/metal concentration ratio (F), with a 29.5% contribution, followed by pH (5.2%) and time (2.3%). On the other hand, temperature (T) had little effect on the purification efficiency (1.0%), whereas noise ($KMnO_4$) was found to contribute by as much as 22.1%. Maximal purification efficiency (99.99%) is achieved when wastewater samples are treated for 21 h at 50°C and pH 10.0 in the presence of Fe(II) in a ratio Fe(II)/total metal of 15.

Rao et al. [2002] optimized the parameters for xylitol production by *Candida* sp. using L_{18} OA layout. Optimal levels of physical parameters and key media components namely temperature, pH, agitation, inoculum size, corn steep liquor (CSL), xylose, yeast extract and KH_2PO_4 were determined. Among the physical parameters, temperature and agitation were found to contribute higher influence. Media components CSL, xylose concentration and KH_2PO_4 were found to play an important role in the conversion of xylose to xylitol. The yield of xylitol under optimal conditions was 78.9%.

Srivastava et al. [2007] optimized various parameters for the simultaneous removal of Cd, Ni, and Zn metal ions from aqueous solutions using BFA by Taguchi design methodology. The effect of such parameters as the $C_{o,i}$, temperature, initial pH, adsorbent dosage (m), and contact time on the adsorption of the aforementioned metal ions has been studied at three levels to determine their effect on the selected response characteristic (the total amount of metal adsorbed on BFA, in terms of mg/g of BFA (q_{tot})). The Pareto analysis of variance showed that m was the most significant parameter, with a 53.14% and 31.25% contribution to the q_{tot} and signal-to-noise (S/N) ratio data. The contribution of interactions between the $C_{o,i}$ values was also significant. Confirmation experiments were performed to prove the effectiveness of the Taguchi technique after the optimum levels of process parameters were determined.

Srivastava et al. [2008b] optimized various batch parameters for the simultaneous removal of cadmium (Cd(II)), nickel (Ni(II)) and zinc (Zn(II)) metal ions from aqueous solutions by RHA using Taguchi's optimization methodology. The parameter *m* was found to be the most significant parameter with 47.38 and 37.78% contribution to the *q*tot and S/N ratio data. It is also observed that the interactions between $C_{o,i}$'s (i.e. $C_{o,Cd} \times C_{o,Ni}$, $C_{o,Cd} \times C_{o,Zn}$ and $C_{o,Ni} \times C_{o,Zn}$) contribute significantly to both raw and S/N ratio data for simultaneous metal ions removal by RHA. All the parameters and their interactions considered are found to be statistically significant at 95% confidence level for the desired response characteristic, q_{tot}. The study showed that the Taguchi's method is suitable to optimize the experiments for total metal ions removal. The total optimum adsorptive removal of metal ions was obtained with $C_{o,i}$=0–100 mg/l, *T*=40°C, pH=6, *m*=10 g/l and *t*=60 min. The results showed that a multi-staged adsorptive treatment may be necessary to meet the minimal discharge standards of metal ions in the effluent.

Engin et al. [2008] applied Taguchi experimental design to determine optimum conditions for colour removal from textile dyebath house effluents in a zeolite fixed bed reactor. After the parameters were determined to treat real textile wastewater, adsorption experiments were carried out. The breakthrough curves for adsorption studies were constructed under different conditions by plotting the normalized effluent colour intensity (C/C_o) versus time (min) or bed volumes (BV). The chosen experimental parameters and their ranges are: C_o, 1–7.5 g/l; HTAB feeding flow rate (Q_b), 0.015–0.075 l/min; textile wastewater flowrate (Q), 0.025–0.050 l/min and zeolite bed height (H), 25–50 cm, respectively. Mixed orthogonal array L_{16} for experimental plan and the larger the better response category were selected to determine the optimum conditions. The optimum conditions were found to be as follows: C_o=1 g/l, feeding Q=0.015 l/min, textile wastewater flow rate (Q_{dye})=0.025 l/min and Z=50cm. Under these conditions, the treated wastewater volume reached a maximum while the bed volumes (BV) were about 217. While C_o, Z, cm (D) and Q were found to be significant parameters, respectively.

Lataye et al. [2009] dealt with the simultaneous removal of Pyridine (Py), α-picoline (αPi) and γ-picoline (γPi) from aqueous solutions by sorption onto RHA

and GAC. Optimal design of experiments using Taguchi's methodology was applied to study the effects of various parameters, viz adsorbent dose, initial pH, contact time, initial concentrations, and temperature on the simultaneous removal of Py, α Pi, and γ Pi. 3^{13} orthogonal array of Taguchi design was used for parameter optimization for the sorption q_{tot} of Py, α Pi, and γ Pi, by RHA and GAC. The ANOVA showed that the initial concentration of α Pi was the most significant parameter with 27.6% and 27.8% contribution to the q_{tot} for raw and S/N ratio data, respectively, for RHA. For GAC, the adsorbent dose (*m*) was found to be the most significant parameter with 32.2% and 17.5% contribution to the q_{tot} for raw and S/N ratio data, respectively. The interactions between initial concentrations also contributed significantly to the overall sorption. Using the optimum conditions obtained from Taguchi's experimental design, the respective removal of Py, α Pi, and γ Pi was found to be ~49%, ~71%, and ~88% by RHA, and ~42%, ~61%, and ~71% by GAC. They recommended that spent RHA and GAC can be used as fuels in furnaces.

Kaushik and Thakur [2009] studied that the ability of five different types of bacterial strains isolated from a distillery mill site for decolorization of distillery spent wash. 16S rDNA based denaturing gradient gel electrophoresis (DGGE) and amplified random DNA restriction analysis (ARDRA) were used to characterize the bacterial strains. One of the isolates had higher capability to reduce color (21%) and chemical oxygen demand (COD) (30%) was finally identified by 16S rDNA sequence analysis as *Bacillus sp.* Different parameters such as pH, temperature, aeration, % carbon, % nitrogen, inoculum size and incubation time were optimized by the Taguchi approach to achieve maximum decolorization of distillery spent wash by the *Bacillus sp.* Reduction in color (85%) and COD (90%) was observed within 12 h after optimization by the Taguchi method. The significant factor in the optimization process was duration followed by inoculum size to attain maximum color reduction. The Taguchi approach proved to be a reliable tool in optimizing culture conditions and analyzing interaction effects of process parameters in achieving the best possible combination for maximum decolorization of the distillery spent wash.

2.5 SUMMARY

The literature review shows that there is a need for systematic studies on removal of phenol and its derivatives and its associated compounds using granular activated carbon (GAC), as an adsorbent. The following recommendations are suggested for future work.

- There exist a large number of phenols and their removal by adsorption is based on various factors which include adsorbate–adsorbent relationships (interactions), size of adsorbate molecules and role of functional groups on both adsorbate as well as adsorbent. Most work is needed to study the effect of various interactive factors and their correlation, if any.
- Most of the investigators have used Freundlich and Langmuir isotherms to fit equilibrium adsorption data irrespective of the surface heterogeneity of the adsorbent. While temperature also plays significant role in adsorption but the effect of temperature on adsorptive capacity has not been studied by most of the researchers in detail for compounds like hydroquinone.
- Using standard protocol, GAC should be used for adsorption of different phenols and their derivatives. Pore size distribution of adsorbent, size of phenol molecules, functional groups present on the surface of the adsorbent, solution pH, temperature, etc. should be used to discuss the adsorption characteristics. Column studies should be carried out to understand the breakthrough characteristics.
- As the phenolic effluents contain several pollutants, attention has to be given to adsorption of various components from mixtures. A survey of the literature shows that adsorption data for simultaneous adsorption of P and its derivatives and its associated compounds from binary and ternary is very meager. It is necessary to use optimal design of experiments to understand the interactive effects of various parameters on the adsorption of different components.
- The main drawback in adsorption by GAC is its high cost and hence, in spite of its good efficiency and applicability for adsorption of a wide variety of pollutants/chemicals, its use can sometimes be restricted due to economic considerations. It is therefore, necessary to regenerate GAC for further use. None of the earlier studies reported on the desorption of phenolic compounds from GAC which is very essential considering the high cost of GAC.

Chapter – III

EXPERIMENTAL PROGRAMME

This chapter deals with the materials and methods of analysis, and the experimental procedures adopted to collect the experimental data.

3.1 MATERIALS

3.1.1 Adsorbent

Granular activated carbon (GAC) was used as an adsorbent. It was obtained from S. D. Fine Chemicals, Mumbai, India.

3.1.2 Adsorbates and chemicals

All the chemicals used as the adsorbates in the study were of analytical grade reagent (AR) grade. AN, P, CP, NP, C, R and HQ were supplied by Qualigens Fine Chemicals, Mumbai, Ranbaxy Fine Chemicals, New Delhi, S.D. Fine Chemicals Ltd., Mumbai and Hi Media Laboratories Pvt. Ltd., Mumbai, India and were used for the preparation of synthetic aqueous solutions. KNO_3, NaOH, HNO_3 were supplied by Hi Media Laboratories Pvt. Ltd., Mumbai, India.

3.2 ADSORBENT CHARACTERIZATION

The physico-chemical characteristics of the GAC were determined by following standard procedures as discussed below:

3.2.1 Proximate Analysis

Proximate analyses of the GAC was carried out using the procedure given in the Bureau of Indian Standards (BIS) IS 1350:1984.

3.2.2 Particle Size

Particle size analysis of the adsorbent was carried out as per IS 2720 (part-4): 1985 using standard sieves.

3.2.3 Bulk Density

Bulk density of the GAC was determined by using MAC bulk density meter.

3.2.4 Point of Zero Charge (pH_{PZC})

The point of zero charge of the GAC was determined by the solid addition method [Balistrieri and Murray, 1981; Srivastava et al., 2006a]. 45 ml of KNO_3 solution of known strength was transferred to a series of 100 ml conical flasks maintained at 303 K. The initial pH (pH_0) values of the solution were roughly adjusted between 2 and 12 by adding either 0.1 N HNO_3 or 0.1 N NaOH. The total volume of the solution in each flask was made up to 50 ml exactly by adding the KNO_3 solution of the same strength. The pH_o of the solutions was then accurately noted. One g of the GAC was added to each one of the flasks, which were securely capped immediately. The suspensions were then manually shaken and allowed to equilibrate for 48 h with intermittent manual shaking. The pH values of the supernatant liquid were then noted. The differences between the initial and final pH (pH_f) values ($\Delta pH = pH_0 - pH_f$) were plotted against the pH_0. The point of intersection of the resulting curve at which $\Delta pH = 0$ gave the pH_{PZC}. The procedure was repeated for different concentrations of KNO_3. All the experiments were conducted at 303 K.

3.2.5 X-Ray Diffraction (XRD) Analysis

The structure of GAC was studied with the help of a X-ray diffractometer (Bruker AXS, Diffraktometer D8, Germany) available in the Institute Instrumentation Centre (IIC), IIT, Roorkee, India. The XRD analysis was done using Cu-Kα as a source and Ni as a filter. Goniometer speed was kept at 2 °/ min. The range of scanning angle (2θ) was kept at 10-90°. The intensity peaks indicate the values of 2θ, where Bragg's law is applicable. The identification of compounds was carried out by using the ICDD library.

3.2.6 Scanning Electron Microscopy (SEM)

To understand the morphology of the GAC, before and after the adsorption of AN, P, CP, NP, C, R and HQ, the SEM micrographs were taken using LEO, Model 435 VP, UK. The particles were first gold-coated using Sputter Coater, Edwards S150, to provide conductivity to the samples. The SEM micrographs were taken thereafter.

3.2.7 Energy Dispersive Atomic X-ray (EDAX) Analysis

To understand the chemical composition of the GAC surface before and after the adsorption of AN, P, CP, NP, C, R and HQ, the EDAX analysis was carried out using LEO, Model 435 VP, UK.

3.2.8 Pore Size Distribution Analysis

Textural characteristic of GAC was determined by nitrogen adsorption at 77.15 K to determine the specific surface area and the pore diameter using an ASAP 2010 Micromeritics instrument and its software. Brunauer-Emmett-Teller (BET) method [Brunauer et al., 1938] was used for the purpose. Nitrogen was used as the cold bath (77.15 K). The Barrett-Joyner-Hanlenda (BJH) method [Barret et al., 1951] was used to calculate the mesopore distribution.

3.2.9 Fourier Transform Infra Red (FTIR) Spectral Analysis

FTIR spectrometer (Thermo Nicolet, NEXUS, USA) was employed to determine the presence of functional groups in the GAC before and after the adsorption of AN, P, CP, NP, C, R and HQ at room temperature. Pellet (pressed-disk) technique has been used for this purpose. The pellets were prepared with KBr. The sample and KBr are mixed thoroughly in grinding equipment and keep and press it in the pressure gauge and then pellet will form. The spectral range was from 4000 to 400 cm^{-1}. The study was used to determine the functional groups participating in the adsorption process.

3.3 BATCH EXPERIMENTAL PROGRAMME

An incubator-cum- shaker (Metrex Scientific Instruments, New Delhi) was used for the batch adsorption study. The temperature range for the studies was from 288 to 318 K. All the batch studies were performed at the constant shaking speed of 150 revolutions per minute (rpm). For each experimental run, 100 ml aqueous solution of the known concentration of the respective adsorbates (AN or P or CP or NP or C or R or HQ or mixture thereof) was taken in a 250 ml Erlenmeyer flask containing a known mass of the GAC. Capped flasks were agitated at a constant shaking rate in a temperature-controlled orbital shaker maintained at a constant temperature. To check whether the equilibrium has

been attained, the samples were withdrawn from the flasks at different time intervals, centrifuged using a Research Centrifuge (Remi Instruments, Mumbai) at 10000 rpm for 5 min and then the supernatant liquid was analyzed for residual concentration of the respective adsorbates (AN or P or CP or NP or C or R or HQ or mixture thereof) using a double beam UV/Vis spectrophotometer (Lambada 35; PerkinElmer, MA 02451, USA) for single adsorbate solutions.

The required quantity of the adsorbate was accurately weighed and dissolved in a small amount of distilled water and subsequently made up to 1 litre in a measuring flask by adding double distilled water. Fresh stock solution as required was prepared every day and was kept at ambient conditions. The C_o was ascertained before the start of each experimental run accordingly.

The removal of adsorbate (%) and equilibrium adsorption uptake in solid phase, q_e (mg/g), were calculated using the following relationships:

Adsorbate removal (%) = $100(C_0 - C_t)/C_0$ (3.3.1)

Amount of adsorbate adsorbed per g of solid, $q_t = (C_0 - C_t)V/w$ (3.3.2)

where, C_o is the initial adsorbate concentration (mg/l), C_t is the equilibrium adsorbate concentration (mg/l), V is the volume of the solution (l) and w is the mass of the adsorbent (g).

3.3.1 Kinetic Study

To determine the time necessary for adsorption of a particular adsorbate by GAC, 100 ml of the aqueous solution containing 50-1000 mg/l of the given adsorbate (AN or P or CP or NP or C or R or HQ or a mixture thereof) was taken in a series of conical flasks. Pre-weighed amount of the GAC was added to different flasks. The flasks were kept in a temperature-controlled shaker and the aqueous solution-GAC mixtures were stirred at a constant speed of 150 rpm. At the end of the predetermined time (t) the flasks were withdrawn, their contents were centrifuged, and the supernatant was analyzed for adsorbate concentration. Adsorption kinetics was followed for 24 h and it was observed that after 1 h, there was gradual but very slow removal of the adsorbate from the mixture/solution. In order to investigate the kinetics of adsorption of the adsorbate on the

GAC, various kinetic models, like pseudo-first-order, pseudo-second-order and intra-particle diffusion models were used.

3.3.3 Adsorption Isotherm Study

For adsorption isotherms, experiments were carried out at natural pH_0 of the samples by contacting a fixed amount of GAC with 100 ml of the adsorbate solutions having C_0 in the range of 20-1000 mg/l. After 24h contact time, the mixture was centrifuged and the adsorbate concentration in the supernatant solution and on/in the GAC was estimated. Two-parameter models, viz., Langmuir, Freundlich and Tempkin, and one three-parameter model, viz., Redlich-Peterson (R-P) have been used to correlate the experimental equilibrium adsorption data.

Two error functions namely Marquardt's percent standard deviation (MPSD) [Marquardt, 1963] and sum of square of errors (SSE) were employed in this study to find out the most suitable kinetic and isotherm models to represent the experimental data. These error functions are given as

$$MPSD = 100\sqrt{\frac{1}{n-p}\sum_{i=1}^{n}\left(\frac{(q_{e,\exp} - q_{e,calc})}{q_{e,\exp}}\right)_i^2} \tag{3.3.3}$$

$$SSE = \sum_{i=1}^{n}(q_{e,\exp} - q_{e,cal})_i^2 \tag{3.3.4}$$

The MPSD is similar in some respects to a geometric mean error distribution modified according to the number of degrees of freedom of the system. The most commonly used error function, SSE, has one major drawback in that it will result in the calculated isotherm parameters providing a better fit at the higher end of the liquid phase concentration range. This is because of the magnitude of the errors, which increase as the concentration increases.

3.3.4 Effect of Temperature and Estimation of Thermodynamic Parameters

The effect of temperature on the sorption characteristics was investigated by determining the adsorption isotherms at 288, 303 and 318 K for AN, P, CP, NP, C, R and HQ. Apparent and net isosteric heats of adsorption at various surface coverages have been

determined using classical thermodynamic equations. C_o was varied from 20 mg/l to 1000 mg/l, but the natural pH_0 of the solutions was maintained.

3.4 MULTI-COMPONENT ADSORPTION STUDY USING TAGUCHI'S METHOD

Taguchi's methodology has been used extensively in carrying out experiments and devising a strategy for quality control of the products in the manufacturing industries. Taguchi's method to improve quality of the products depends heavily on designing and testing a system based on engineer's judgment of selected materials, parts and nominal product / process parameters based on current technology [Taguchi and Wu, 1979]. While system design helps to identify the working levels of the design parameters, process parameter design seeks to determine the parameter levels that produce the best performance of the product/process under study. The optimum condition is selected so that the influence of uncontrollable factors (noise factors) causes minimum variation to the system performance. The orthogonal arrays (OA), variance and signal to noise (S/N) analysis are the essential tools of the parameter design.

Taguchi's methodology as adopted in this study consisted of four phases (with various steps) viz., planning, conducting, analysis and validation. The design of experiments (DOE) involves establishment of a large number of experimental situations described as OAs to reduce experimental errors and to enhance the efficiency and reproducibility of the laboratory experiments. Each phase has separate objectives which are interconnected sequentially to achieve the overall optimization process.

3.4.1 Design of experiments (Phase I)

Phase 1 starts with the identification of the various factors which need to be optimized in batch experiments that have critical effect on the simultaneous adsorptive removal of NP/AN and P or CP or C or R or HQ and ternary mixture (P, CP, NP) and (C, R and HQ) from aqueous solutions by GAC. Factors are selected and the ranges are further assigned on the basis of the detailed experiments for adsorbate removal by GAC [Srivastava et al., 2007; Lataye et al., 2009]. Based on the experience in our laboratory, five process parameters that exerted significant influence on the adsorbate adsorption have been

selected for the present experimental design. These process parameters, their designations and levels are given in Table 3.4.1 and 3.4.2. Table 3.4.3 gives the conditions for process parameters, their designations and levels used for ternary column adsorption study.

Since the initial concentration of one adsorbate ($C_{o,i}$) significantly affects the adsorption of the other adsorbates during simultaneous adsorption of adsorbates, it was decided to study one and two parameter interactions between the initial concentrations of the adsorbates, i.e., $C_{0,NP}$ x $C_{0,P}$, and $C_{0,P}$ x $C_{0,NP}$ and three parameter interactions between the initial concentrations of the adsorbates, i.e., $C_{0,P}$ x $C_{0,CP}$ x $C_{0,NP}$, and $C_{0,C}$ x $C_{0,R}$ x $C_{0,HQ}$.

The next step in phase 1 is the design of the matrix of experiments and to define the data analysis procedure. Taguchi provides many standard OAs and corresponding linear graphs for this purpose. The OA selected must satisfy the following inequality:

Total degrees of freedom (DOF) of the OA ≥ Total degrees of freedom required for the experiment. Thus, the appropriate OAs for the control parameters to fit a specific study was selected.

It was decided to study each selected process parameter at three levels to account for non-linear behaviour (if any) of the parameters of a process [Byrne 1987]. For binary adsorption study, with five parameters each at three levels and one second order interaction, the total degree of freedom (DOF) required is 14 [= 5 x (3 – 1) + 1 x 4], since a three level parameter has 2 DOF (number of levels - 1) and each two-parameter interaction term has 4 DOF (2 x 2). Hence, an L_{27} (3^{13}) OA (a standard 3-level OA) has been selected for this phase of work. Table 3.4.4 and 3.4.5 show the L_{27} OA with assignment of parameters and interactions for binary and ternary adsorption experiments, respectively. The parameters and interactions have been assigned to specific columns of the OA using the triangular table [Ross 1996]. Table 3.4.6 shows the L_9 OA with assignment of parameters and interactions for ternary column adsorption experiments.

3.4.2 Batch adsorption experiments (Phase 2)

3.4.2.1 Batch binary/ternary adsorption experiments: Binary or ternary batch adsorption experiments were performed for simultaneous adsorbate removal by GAC

employing selected 27 experimental trials in combination with five or six process factors at three levels (Table 3.4.4 and 3.4.5). For each experimental run, 100 ml aqueous solution having 50 ml of each adsorbate solution (viz. NP/AN and P or CP or C or R or HQ) of known concentration was taken in a 250 ml stoppered conical flask containing specific amount of GAC. These flasks were agitated at a constant shaking rate of 150 rpm in a temperature-controlled orbital shaker (Metrex Scientific Instruments, New Delhi) maintained at 288, 303 and 313 K. The samples were withdrawn after appropriate contact time and were centrifuged using Research Centrifuge (Remi Instruments, Mumbai) at 10000 rpm for 5 min. Then the supernatant liquid was analyzed for the residual concentration of adsorbates. The removal of adsorbate from the solution and the equilibrium adsorption uptake in the solid phase, q_{tot} (mg/g), was calculated using the following relationship:

$$q_{tot} = \sum_{i=1}^{2} (C_{0,i} - C_{e,i}) / m \qquad (3.4.1)$$

where, $C_{0,i}$ is the initial adsorbate concentration (mg/l), $C_{e,i}$ is the equilibrium adsorbate concentration (mg/l), and m is the adsorbent dose (g/l).

3.4.2.2 Column ternary adsorption experiments: Plexiglass columns with inside diameters (D) of 2, 2.54, and 4 cm and a length of 110 cm were used for the column sorption studies. The columns were provided with a feed port at the bottom centre of the column. The lower portion of the column was filled with pieces of 0.3-0.5 cm diameter glass rods to a height of approximately 10 cm, and this portion was used for the uniform distribution of the solution across the whole cross section of the column and to dampen the fluctuating flow phenomenon induced by the peristaltic pump. This portion was attached to the main column through two flanges with O-ring rubber seals and a sintered metal disc in between. The column was packed with GAC up to different lengths, viz., 30, 45 and 60 cm from the bottom, and was loaded with aqueous solution of phenol using a peristaltic pump (Miclins PP20). The solution flowed upward. Sampling ports were provided at 30, 45 and 60 cm from the bottom. Samples were withdrawn from different ports at different time intervals. The column assembly was kept in a temperature-controlled chamber maintained at 303±1 K by use of a thermostatic heating device. All experimental runs

were performed with C_o = 500 mg/l. The length of the bed, Z, was varied from 30 to 60 cm, and the flow rate, Q, was varied between 0.02 and 0.06 l/min. In most of the experimental runs, the breakthrough point was taken at C/C_o=0.10, i.e., at $t_{0.1}$.

Table 3.4.5 gives the L_9 Taguchi design and process parameter. The synthetic pollutant (P, CP, NP, C, R and HQ) stock solutions were prepared as a 500 mg/l concentration of P or CP or NP (for a mixture of P+CP+NP), C or R or HQ (for a mixture of C+R+HQ). Then these solutions were mixed with equal proportion (say 1500 mg/l each). The obtained concentrations were 500 mg/l. The solutions were diluted with DDW to make solution of other concentration.

The removal of adsorbates from the solution and the adsorption uptake in the solid phase in column study, q_{tot},(mg/g), was calculated using the following relationship:

$$q_{tot} = \frac{\sum_{N=1}^{3}\left[QC_0\int_0^{t_b}\left(1-\frac{C_i}{C_0}\right)dt\right]_N}{\frac{\pi}{4}D^2 Z\rho_{BD,ads}} \qquad (3.4.2)$$

where, C_0 is the initial adsorbate concentration (mg/l), C_t is the residual adsorbate concentration at time t (mg/l), t_b is the breakthrough time (min), Q is the flow rate (l/min), D is the diameter of the column (cm) and Z is the bed height (cm), $\rho_{BD,ads}$ is the bulk density of the adsorbent, and N is the number of adsorbates.

Table 3.4.1. Process parameters for binary adsorption study of NP/AN and P or CP or NP or C or R or HQ onto GAC using Taguchi's L_{27} (3^{13}) orthogonal array.

	Parameters		Units	Levels		
				0	1	2
A:	Initial concentration of NP/AN	$C_{0,NP/AN}$	(mg/l)	0	250	500
B:	Initial concentration of P or CP or NP or C or R or HQ	$C_{0,P}$	(mg/l)	0	250	500
C:	Temperature	T	(^{0}C)	15	30	45
D:	GAC dose	m	(g/l)	2	10	18
E:	Contact time	t	(min)	60	360	660

Table 3.4.2. Process parameters for ternary adsorption study of P, CP and NP or C, R and HQ onto GAC using Taguchi's L_{27} (3^{13}) orthogonal array.

	Parameters		Units	Levels		
				0	1	2
A:	Initial concentration of P/C	$C_{0,P/C}$	(mg/l)	0	250	500
B:	Initial concentration of CP/R	$C_{0,CP/R}$	(mg/l)	0	250	500
C:	Initial concentration of NP/HQ	$C_{0,NP/HQ}$	(mg/l)	0	250	500
D:	Temperature	T	(^{0}C)	15	30	45
E:	GAC dose	m	(g/l)	2	10	18
F:	Contact time	t	(min)	60	360	660

Table 3.4.3. Process parameters for ternary column adsorption study of P, CP and NP or C, R and HQ onto GAC using Taguchi's L_9 orthogonal array.

	Parameters		Units	Levels		
				0	1	2
A:	Flow rate	Q	(l/min)	0.02	0.04	0.06
B:	Bed height	Z	(cm)	30	45	60
C:	Column diameter	D	(cm)	2	2.54	4

Table 3.4.4. Column assignment for the various factors and one interaction in the Taguchi's L_{27} (3^{13}) orthogonal array for binary batch adsorption onto GAC.

Exp. no.	1	2	3	4	5	6	7
	A	B	AxB	AxB	C	D	E
1	0	0	0	0	15	2	60
2	0	250	1	1	15	2	60
3	0	500	2	2	15	2	60
4	250	0	1	2	15	10	660
5	250	250	2	0	15	10	660
6	250	500	0	1	15	10	660
7	500	0	2	1	15	18	360
8	500	250	0	2	15	18	360
9	500	500	1	0	15	18	360
10	0	0	0	0	30	10	360
11	0	250	1	1	30	10	360
12	0	500	2	2	30	10	360
13	250	0	1	2	30	18	60
14	250	250	2	0	30	18	60
15	250	500	0	1	30	18	60
16	500	0	2	1	30	2	660
17	500	250	0	2	30	2	660
18	500	500	1	0	30	2	660
19	0	0	0	0	45	18	660
20	0	250	1	1	45	18	660
21	0	500	2	2	45	18	660
22	250	0	1	2	45	2	360
23	250	250	2	0	45	2	360
24	250	500	0	1	45	2	360
25	500	0	2	1	45	10	60
26	500	250	0	2	45	10	60
27	500	500	1	0	45	10	60

Table 3.4.5. Column assignment for the various factors and three interactions in the Taguchi's L_{27} (3^{13}) orthogonal array for ternary batch adsorption onto GAC.

Exp. order	1	2	3	4	5	6	7	8	9	10	11	12
	A	B	AxB	AxB	C	AxC	AxC	BxC	D	BxC	E	F
1	0	0	0	0	0	0	0	0	15	0	2	60
2	0	0	0	0	250	1	1	1	30	1	10	360
3	0	0	0	0	500	2	2	2	45	2	18	660
4	0	250	1	1	0	0	0	1	30	2	10	660
5	0	250	1	1	250	1	1	2	45	0	18	60
6	0	250	1	1	500	2	2	0	15	1	2	360
7	0	500	2	2	0	0	0	2	45	1	18	360
8	0	500	2	2	250	1	1	0	15	2	2	660
9	0	500	2	2	500	2	2	1	30	0	10	60
10	250	0	1	2	0	1	2	0	30	0	18	360
11	250	0	1	2	250	2	0	1	45	1	2	660
12	250	0	1	2	500	0	1	2	15	2	10	60
13	250	250	2	0	0	1	2	1	45	2	2	60
14	250	250	2	0	250	2	0	2	15	0	10	360
15	250	250	2	0	500	0	1	0	30	1	18	660
16	250	500	0	1	0	1	2	2	15	1	10	660
17	250	500	0	1	250	2	0	0	30	2	18	60
18	250	500	0	1	500	0	1	1	45	0	2	360
19	500	0	2	1	0	2	1	0	45	0	10	660
20	500	0	2	1	250	0	2	1	15	1	18	60
21	500	0	2	1	500	1	0	2	30	2	2	360
22	500	250	0	2	0	2	1	1	15	2	18	360
23	500	250	0	2	250	0	2	2	30	0	2	660
24	500	250	0	2	500	1	0	0	45	1	10	60
25	500	500	1	0	0	2	1	2	30	1	2	60
26	500	500	1	0	250	0	2	0	45	2	10	360
27	500	500	1	0	500	1	0	1	15	0	18	660

Table 3.4.6. Column assignment for the various factors in the Taguchi's L_9 orthogonal array for ternary adsorption onto GAC in column study.

Expt. No.	Run Order	Factors		
		A	B	C
1	9	0.02	30	2
2	4	0.02	45	2.54
3	7	0.02	60	4
4	8	0.04	30	2.54
5	2	0.04	45	4
6	1	0.04	60	2
7	3	0.06	30	4
8	5	0.06	45	2
9	6	0.06	60	2.54

3.4.3 Analysis of experimental data and prediction of performance (Phase 3)

The experimental data were processed with higher-is-better quality characteristic to (i) determine the optimum conditions for the adsorption, (ii) to identify the influence of individual factors on adsorption, and (iii) estimate the performance (q_{tot}) at the optimum conditions.

Taguchi defines the loss-function L(y) as a quantity proportional to the deviation from the nominal quality characteristic and found the following quadratic form to be a practical workable function, viz.

$$L(y) = k\,(y - m_T)^2 \qquad (3.4.3)$$

where, k denotes the proportionality constant, m_T the target value and y the experimental value obtained for each trial.

In case of 'higher-is-better' quality characteristic, the loss function can be written as $L(y) = k\,(1/y)^2$ and the expected loss function can be represented by [Srivastava et al., 2007].

$$E[L(y)] = k\,E\left(\frac{1}{y^2}\right) \tag{3.4.4}$$

where, $E(1/y^2)$ can be estimated from a sample of R as

$$E(1/y^2) = \frac{\sum_{i=1}^{R}[1/y_i^2]}{R} \tag{3.4.5}$$

Taguchi created a transform for the loss function as the signal-to-noise (S/N) ratio, which considers at two characteristics of a distribution and rolls these characteristics into a single number or figure of merit. The S/N ratio combines the mean level of the quality characteristic and the variance around this mean into a single metric [Barker, 1990]. A high value of S/N ratio implies that the signal is much higher than the random effects of noise factors. Process operation consistent with highest S/N ratio always yields optimum quality with minimum variation.

The S/N ratio consolidates several repetitions (at least two data points are required) into one value. The equation for calculating S/N ratios for higher-is-better (HB) type of characteristic is [Ross 1996]:

$$(S/N)_{HB} = -10\log\left(\frac{1}{R}\sum_{i=1}^{R}\frac{1}{y_i^2}\right) \tag{3.4.6}$$

where, y_i is the value of the characteristic in an observation i and R is the number of observations or the number of repetitions in a trial. From amongst the methods suggested by Taguchi for analyzing the data, the following methods have been used in the present work: (i) Plot of average response; (ii) ANOVA for raw data; and (iii) ANOVA for S/N data.

The plot of average response at each level of a parameter indicates the trend. It is a pictorial representation of the effect of a parameter on the response. The change in the response characteristic with the change in levels of a parameter can easily be visualized from these curves. Typically, ANOVA for OA's is conducted in the same manner as other structured experiments [Ross, 1996]. The S/N ratio is treated as a response of the experiment, which is a measure of the variation within a trial when noise factors are present. A standard ANOVA can be conducted on the S/N ratio which will identify the significant parameters (mean and variation).

After determination of the optimum condition, the mean of the response (μ) at the optimum condition is predicted. This mean is estimated only from the significant parameters. The ANOVA identifies the significant parameters. Suppose, parameters A and B are significant and A_2, B_2 (second level of A = A_2, second level of B = B_2) are the optimal treatment conditions. Then, the mean at the optimal condition (optimal value of the response characteristic) is estimated as:

$$\mu = \bar{T} + (\bar{A}_2 - \bar{T}) + (\bar{B}_2 - \bar{T}) = \bar{A}_2 + \bar{B}_2 - \bar{T} \tag{3.4.7}$$

where, $\bar{T}$ is the overall mean of the response, and $\bar{A}_2$ and $\bar{B}_2$ represent average values of response at the second level of parameters A and B, respectively.

Taguchi suggested two types of confidence intervals with regard to the estimated mean of the optimal treatment condition [Ross, 1996]:

(i) Around the estimated average of a treatment condition predicted from the experiments. This type of confidence interval is designated as CI_{POP} (confidence interval for the population).

(ii) Around the estimated average of a treatment condition used in a confirmation experiment to verify predictions. This type of confidence interval is designated as CI_{CE} (confidence interval for a sample group).

The difference between CI_{POP} and CI_{CE} is that CI_{POP} is for the entire population, i.e., all parts ever made under the specified conditions, and CI_{CE} is for a sample group only, made under the specified conditions. Because of the smaller size (in confirmation experiments) relative to the entire population, CI_{CE} must be slightly wider. The expressions for computing the confidence interval are given below [Roy, 1990]:

$$CI_{POP} = \sqrt{\frac{F_\alpha\,(1, f_e)\,V_e}{n_{eff}}} \tag{3.4.8}$$

$$CI_{CE} = \sqrt{F_\alpha\,(1, f_e) V_e \left[\frac{1}{n_{eff}} + \frac{1}{R}\right]} \tag{3.4.9}$$

where, $F_\alpha\,(1,f_e)$= the F-ratio at a confidence level of (1-α) against DOF 1 and error DOF f_e.

V_e= error variance (from ANOVA)

$$n_{eff} = \frac{N}{1 + [\textit{total DOF associated in the estimate of the mean}]} \tag{3.4.10}$$

where, N is the total number of results and R is the sample size for confirmation experiment.

It can be seen that as R approaches infinity, i.e., the entire population, the value 1/R approaches zero and $CI_{CE} = CI_{POP}$. As R approaches 1, the CI_{CE} becomes wider.

3.4.4 Confirmation experiment (Phase 4)

The confirmation experiment is the crucial and the final step in verifying the conclusions drawn from the previous round of experiments. The optimum conditions are set for the significant parameters (the insignificant parameters are set at economic levels) and a selected number of tests are conducted under constant specified conditions. The average of the results of the confirmation experiments is compared with the anticipated average based on the parameters and levels tested.

3.5 MULTI-COMPONENT ISOTHERMAL ADSORPTION STUDY

3.5.1 Binary adsorbates system

In binary mixture-GAC systems, for each initial concentration of NP solution: viz., 50, 100, 250, 500, 1000 mg/l, the concentrations of AN, P, CP, C, R and HQ were varied in the range of 50-1000 mg/l. Isothermal experiments were conducted at 303 K. For experimental run, 100 ml mixture of known C_0, and an optimum amount of the GAC were taken in a 250 ml glass-stoppered conical flask. This mixture was agitated in a temperature-controlled orbital shaker at a constant speed of 150 rpm at 303 ± 1 K. Samples were withdrawn after 12 h. Due to suspension of particles, all the samples were centrifuged (Research Centrifuge, Remi scientific works, Mumbai) at 10,000 revolution per minute (rpm) for 5 min at the desired temperature and the supernatants were analyzed for the residual adsorbates concentration using a HPLC (Waters (India) Pvt. Ltd., Bangalore).

3.5.2 Ternary adsorbates system

Ternary adsorption was studied for P-CP-NP and C-R-HQ mixtures. In ternary mixture-GAC systems, for each C_0 of P or C solutions: viz., 50, 100, 250, 500, 1000 mg/l; the CP (or R) and NP (or HQ) C_0 were varied in the range of 50-1000 mg/l. Isothermal experiments were conducted at 303 K. For each experimental run, 150 ml mixture of adsorbates of known C_o, and an optimum amount of the GAC were taken in a 250 ml glass-stoppered conical flask. This mixture was agitated in a temperature-controlled orbital shaker at a constant speed of 150 rpm at 303 ± 1 K. Samples were withdrawn after 12 h and centrifuged. The supernatant was analyzed for the residual adsorbate concentration using a HPLC (Waters (India) Pvt. Ltd., Bangalore).

3.5.3 Analysis of adsorbate in aqueous solution and error analysis

The concentration of AN, P, CP, NP, C, R and HQ in the aqueous solution was determined at 285 nm wavelength [US EPA Method 604; www.dionex.com], using high performance liquid chromatograph (HPLC) supplied by Waters (India) Pvt. Ltd., Bangalore. Symmetry, C_{18} column having size (4.6 mm x 150 mm) was used in the analytical measurement of P, CP, NP and C, R, HQ ternary mixture. Methanol-water mixture was used as the solvent for P, CP, NP, C, R and HQ analysis. The mixture of methanol-water composed of 40% methanol and 60% Milli-Q purification system (millipore) water and 1% acetic acid was used as a solvent for their examination keeping flow rate 0.5 ml/min as per specification given in user manual with the instruments. The calibration curves of P, CP, NP and C, R, HQ were plotted as peak area versus concentration.

The $q_{e,i}$, individual adsorption yield (Ad_i%) and total adsorption yields (Ad_{Tot}%) can be calculated by using the following expressions:

$$q_{e,i} = (C_{0,i} - C_{e,i})V / w, \quad \text{(mg of adsorbate/g of adsorbent)} \tag{3.5.1}$$

$$Ad_i\% = 100(C_{0,i} - C_{e,i}) / C_{0,i} \tag{3.5.2}$$

$$Ad_{Tot}\% = 100 \sum (C_{0,i} - C_{e,i}) / \sum C_{0,i} \tag{3.5.3}$$

where, V is the volume of the adsorbate containing solution (l) and w is the mass of the adsorbent (g). Equilibrium isotherms for the binary or ternary adsorption have been analyzed by using non-modified, modified and extended-Langmuir models; non-modified and modified R-P models; and Sheindorf–Rebuhn–Sheintuch (SRS) models. The isotherm parameters of all the multicomponent models can be found by using the MS Excel 2002 for Windows by minimizing Marquardt's percent standard deviation (MPSD). This error function is given as:

$$MPSD = 100 \sqrt{\frac{1}{n_m - n_p} \sum_{i=1}^{n_m} \left(\frac{\left(\sum_{i=1}^{N} q_{e,i,\exp} \right) - \left(\sum_{i=1}^{N} q_{e,i,cal} \right)}{\sum_{i=1}^{N} q_{e,i,\exp}} \right)_i^2} \tag{3.5.4}$$

In the above equation, the subscript 'exp' and 'calc' represent the experimental and calculated values, and n_m the number of measurements, n_p the number of parameters in the model, and N is number of adsorbates.

3.6 BATCH DESORPTION STUDY

For batch solvent desorption experiments, a series of 250 ml Erlenmeyer flasks containing 50 ml of aqueous solution of HCl, H_2SO_4, HNO_3, distilled water, NaOH, CH_3COOH, CH_3OH and C_2H_5OH of known concentration or water was contacted with the adsorbate-loaded GAC (0.5 g) at 30 ± 1 ^{0}C. The mixtures were agitated at 150 rpm for 24 h in an orbital shaker. Thereafter, the mixture was centrifuged and the supernatant was analyzed for the adsorbate released into the solvent.

In the thermal desorption study, the GAC utilized for the adsorption was separated from the solution and dried in an oven at 373 K for 2 h. After that it was placed in a furnace at 623 K for 3 h. The furnace was flushed with nitrogen in order to avoid combustion atmosphere. The samples were taken out from the furnace and kept in a desiccator having silica gel. The loaded samples were again used for adsorption in the next trial. This adsorption-desorption procedure was repeated five times.

3.7 THERMAL ANALYSIS OF SPENT-ADSORBENT

The thermal degradation characteristic of the blank and spent GAC was studied using the thermo-gravimetric analysis (TGA). The thermal degradation of GAC was carried out non-isothermally at the Institute Instrumentation Centre, IIT, Roorkee using the TGA analyzer (Perkin Elmer, Pyris Diamond).

For TGA, the operating pressure was kept slightly positive. The samples were prepared carefully after crushing and sieving so as to obtain homogeneous material properties. The sample was uniformly spread over the crucible base in all the experiments and the quantity of the sample was 5-10 mg in all the runs. The oxidation runs were taken at a heating rate of 25 K/min under an oxidizing atmosphere (flowing moisture-free air) for gasification. The tests were conducted over a temperature range (ambient temperature to 1000 ^{0}C). Flow rate of nitrogen/air was maintained at 200 ml/min. The weight loss, during heating was continuously recorded and downloaded using the software, Muse, Pyris Diamond. The instrument also provided the continuous recording of the differential thermal gravimetry (DTG) and differential thermal analysis (DTA) data as a function of sample temperature and or time. The TGA, DTG and DTA curves obtained in each case were analyzed to understand the behavior of thermal degradation.

Chapter – IV

RESULTS AND DISCUSSION

4.1 GENERAL

This chapter presents the results and discussion pertaining to adsorption of AN (AN), phenol (P), 4-chlorophenol (CP), 4-nitrophenol (NP), catechol (C), resorcinol (R) and hydroquinone (HQ) from aqueous solutions onto granular activated carbon (GAC). This chapter has been divided into the following sections:

1. Characterization of adsorbent,
2. Batch adsorption study for individual adsorption,
3. Multi-component batch adsorption study using Taguchi's method,
4. Multi-component batch adsorption isotherm study,
5. Multi-component column adsorption study using Taguchi's method,
6. Desorption of AN, P, CP, NP, C, R and HQ from spent adsorbent, and
7. Thermal oxidation study of spent adsorbent.

4.2 CHARACTERIZATION OF ADSORBENT

The GAC was used as procured without any pretreatment. The physico-chemical characteristics of GAC such as proximate, bulk density, surface area, etc. were carried out. X-ray diffraction (XRD) and scanning electron microscopy (SEM) analyses were used to study the structural and morphological characteristics of the GAC before and after adsorption.

4.2.1 Physico-chemical Characterization of GAC

The physico-chemical characteristics of the GAC are presented in Table 4.2.1. Proximate analysis showed the presence of 9.04% moisture, 12.09% volatile matter and 78.87% fixed carbon in blank-GAC; 1.62% moisture, 10.54% volatile matter and 87.84% fixed carbon in AN-GAC; and 1.34% moisture, 12.18% volatile matter and 86.48% fixed carbon in P-GAC. The analysis of other adsorbates-GAC systems are given in Table 4.2.1. Bulk density and heating value of GAC were found to be 725 kg/m^3 and 8.26 MJ/ kg, respectively.

The particle size distribution of GAC was obtained as: < 1.18 mm (0.11%), 1.18-1.4 mm (0.02%), 1.4-1.7 mm (0.1%), 1.7-2.26 mm (7.7%), 2.36-3.34mm (55.3%), 3.34-4 mm (24.8%), 4-4.75 mm (10.9%) and > 4.75 mm (0.95%). The average particle size was found to be 3.16 mm. The GAC as procured was used in the batch experiments.

EDX was conducted to study the distribution of elements before and after adsorption of various adsorbates onto GAC (Table 4.2.1). Blank-GAC was found to contain 90.41% carbon, 9.01% oxygen, and rest others. AN- and P-loaded GAC were found to contain 88.28% and 91.08% carbon, 6.30% and 7.28% oxygen, respectively, and rest others. Thus, the amount of carbon increased in GAC after the loading of P whereas it decreased in AN-loaded GAC. AN- and NP-loaded GAC showed presence of 3.85% and 2.96% nitrogen, respectively, whereas CP-loaded GAC showed presence of 3.18% chlorine. Thus, the distribution of elements in various adsorbates loaded GAC depended on the elemental distribution in original adsorbates.

Boehm titration method helps in determining the numbers of carboxylic, lactonic, and phenolic groups present on GAC surface. GAC was found to have 0-4 mmol/g carboxylic (COOH), 1.8 mmol/g lactonic (-COO) and 3.3 mmol/g phenolic (-OH) groups. The amount of these groups per nm^2 of GAC surface was calculated using the relation:

$$FG_D = 10^{-21} FG_C \frac{N_A}{S} \tag{4.2.1}$$

where, FG_D is the density of the functional group on adsorbent surface (number of molecules/nm^2), FG_C is the surface concentration of functional groups (mmol/g), N_A=6.023 x 10^{23} is Avogadro number (number of molecules/mol) and S is pore surface area (m^2/g). Thus, the amount of carboxylic, lactonic and phenolic groups present on the GAC surface were 0.246, 1.108 and 2.032 molecule/nm^2, respectively. Total basic sites on the GAC surface were 1.302 mmol/g or 0.801 molecule/ nm^2. Thus, it is inferred that the GAC which was used in the present study contained more acidic groups; and among these groups,-OH group was found to be predominant.

Table 4.2.1. Physico-chemical characteristics of blank and various adsorbates loaded GAC.

Characteristics	GAC	AN-GAC	P-GAC	CP-GAC	NP-GAC	C-GAC	R-GAC	HQ-GAC
Proximate analysis								
Moisture (%)	9.04	1.62	1.34	1.72	1.24	1.52	1.84	2.87
Volatile matter (%)	12.09	10.54	12.18	11.17	10.71	10.13	11.11	12.01
Fixed Carbon (%)	78.87	87.84	86.48	87.11	88.05	88.35	87.05	85.01
Bulk density (kg/m^3)	725	-	-	-	-	-	-	-
Heating value (MJ/kg)	8.26	14.3	8.89	9.84	10.45	-	-	9.12
Average particle size (mm)	3.161	-	-	-	-	-	-	-
EDX analysis								
C (%)	90.41	88.28	91.08	92.14	89.67	92.22	92.05	91.15
O (%)	9.01	6.30	7.28	4.08	3.89	6.03	7.28	8.13
N (%)	-	3.85	-	-	2.96	0.40	0.25	0.21
Cl (%)	-	-	-	3.18	-	0.69	0.24	0.34
Al (%)	0.15	0.52	0.55	0.13	0.44	0.44	0.44	0.44
Mg(%)	0.26	0.35	0.44	0.2	0.58	0.58	0.58	0.58
Surface area of pores (m^2/ g)								
(i) BET	977.65	-	-	-	-	-	-	-
(ii) BJH								
(a) adsorption cumulative	45.03	-	-	-	-	-	-	-
(b) desorption cumulative	47.63	-	-	-	-	-	-	-
BJH cumulative pore volume (cm^3/ g)								
(i) Single point total	0.4595[a]	-	-	-	-	-	-	-
(ii) BJH adsorption	0.0717[b]	-	-	-	-	-	-	-
(iii) BJH desorption	0.0789[b]	-	-	-	-	-	-	-
Average pore diameter (Å)		-	-	-	-	-	-	-
(i) BET	18.79	-	-	-	-	-	-	-
(ii) BJH adsorption	63.72[b]	-	-	-	-	-	-	-
(iii) BJH desorption	66.24[b]	-	-	-	-	-	-	-
pH_{PZC}	10.31	-	-	-	-	-	-	-

[a] Pores less than 5666 Å; [b] Pores between 17 and 3000 Å diameter.

For structural and morphological characteristics, XRD and SEM analyses were carried out. X-ray diffraction patterns for blank and various adsorbates loaded GAC are shown in Fig. 4.2.1. The broad peak in the XRD indicates amorphous nature of GAC. Diffraction peaks corresponding to crystalline carbon were not observed in GAC. All adsorbates loaded GAC show diffraction pattern similar to blank-GAC.

The SEM micrographs as obtained are shown in Fig. 4.2.2 for blank and AN-, P-, and CP-loaded GAC; and Fig. 4.2.3 for NP-, C-, R- and HQ-loaded GAC. GAC shows random type of pores with cracks and crevices. At low magnification, the surface texture of blank and various adsorbates-loaded GAC were found to be similar with very little difference. However, at high magnification, adsorbates-loaded GAC showed same bright spots which may be due to the pore filling by the adsorbates.

4.2.2 Pore Size Distribution of GAC

Barrett-Joyner-Halenda (BJH) method is the most popular method used for the evaluation of the meso-pore size distribution. Pore sizes are classified in accordance with the classification adopted by the International Union of Pure and Applied Chemistry (IUPAC) [IUPAC, 1982], that is, micro-pores (diameter (d) < 20 Å), meso-pores (20 Å < d < 500 Å) and macro-pores (d > 500 Å). Micro-pores can be divided into ultra micro-pores (d < 7 Å) and super micro-pores (7 Å < d < 20 Å). Because of the larger sizes of liquid molecules, the adsorbent for liquid phase adsorbates should have predominantly meso-pores in the structure.

Results of pore size distribution of GAC are given in Table 4.2.1. The pore size, surface area and pore volume characterization were done by using a Micromeritics Instruments. The BET surface area of GAC was found to be 977.05 m^2/g, whereas BJH adsorption/desorption surface area of pores is 45.03/47.63 m^2/g. The single point total pore volume was found to be 0.4595 cm^3/g, whereas cumulative adsorption/desorption pore volume of the pores (17 Å < d < 3000 Å) is 0.0717/0.0789 cm^3/g, respectively. The BET average pore size was 18.79 Å, whereas the BJH adsorption/desorption average pore size was 63.72/66.24 Å. In accordance with the IUPAC classification [IUPAC, 1982], the GAC is found to be predominantly consisting of mesopores (20 Å < d < 500 Å).

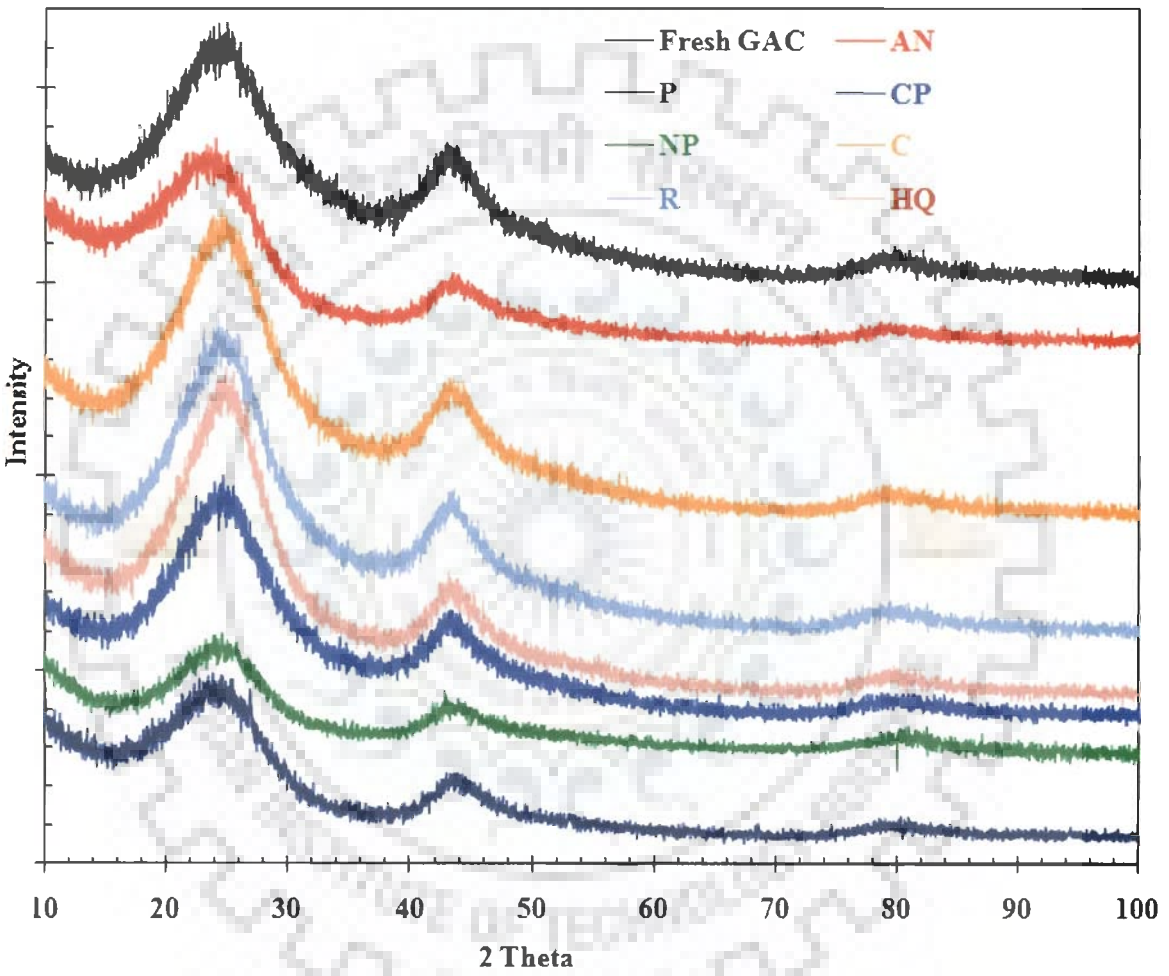

Fig. 4.2.1. X-ray diffraction of blank and various adsorbates loaded GAC.

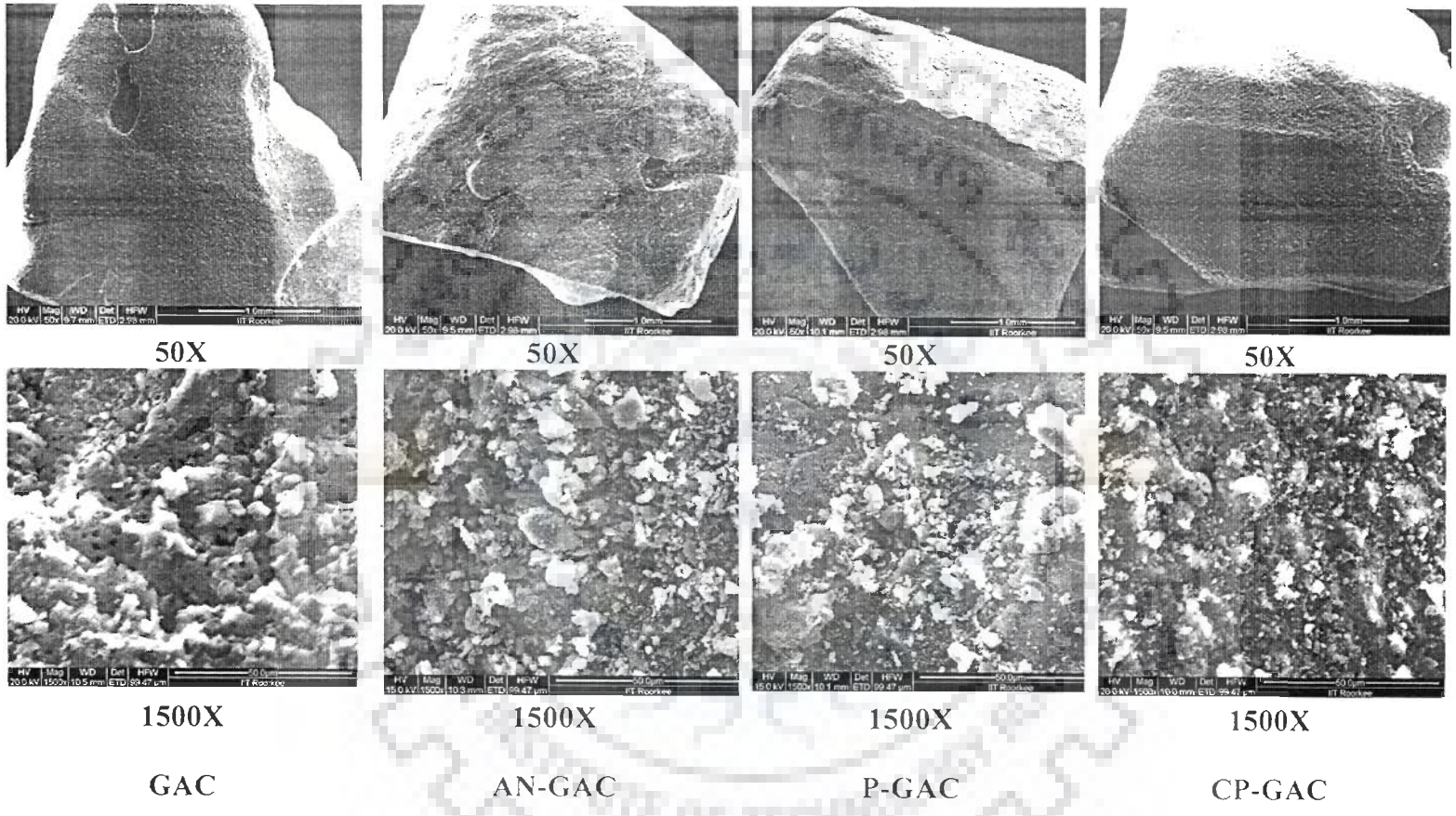

Figure 4.2.2. SEM of blank-GAC, AN-, P-, and CP-loaded GAC.

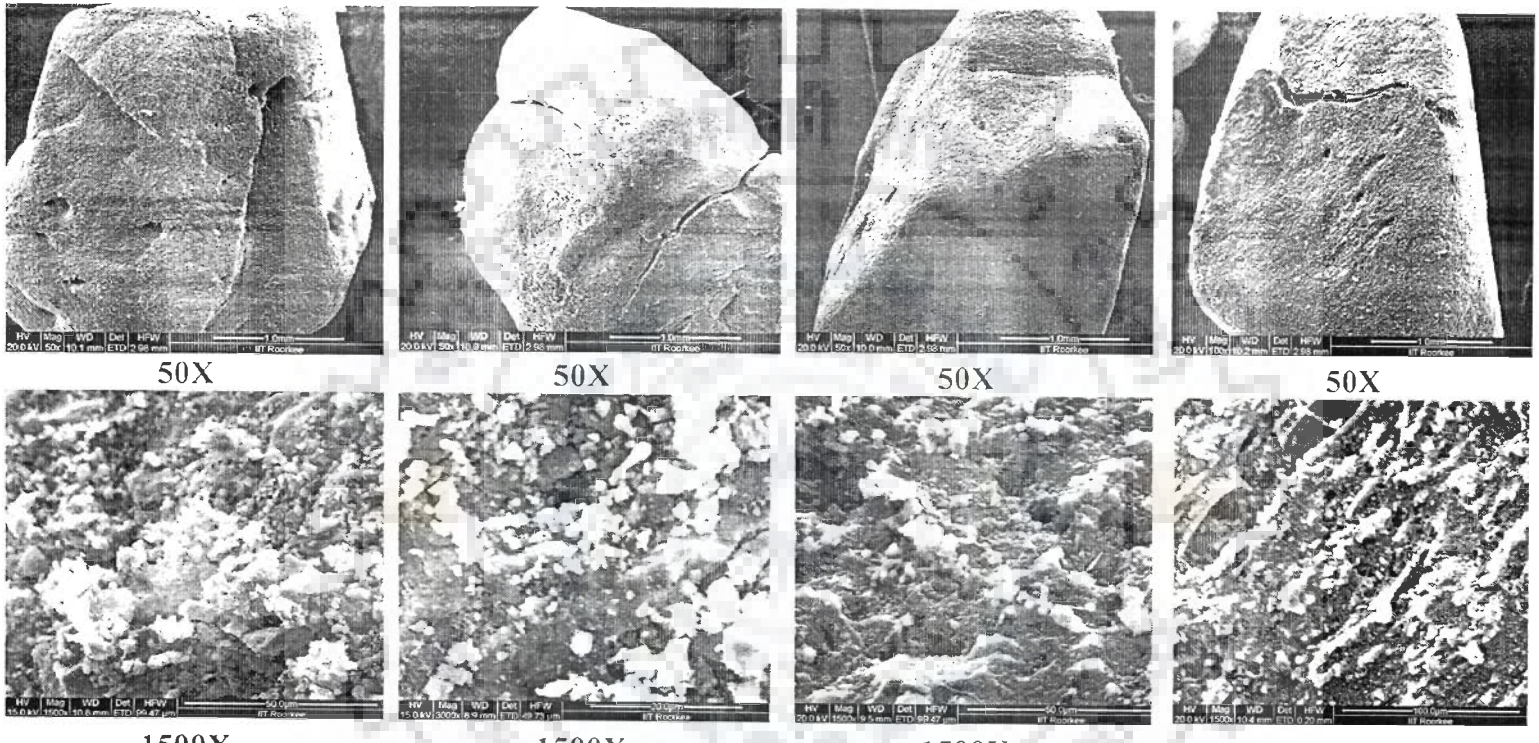

50X 50X 50X 50X

1500X 1500X 1500X 1500X

NP-GAC C-GAC R-GAC HQ-GAC

Figure 4.2.3. SEM of NP-, C-, R- and HQ-loaded GAC.

4.2.3 FTIR spectroscopy of the GAC and various loaded-GAC

The chemical structure of GAC is of vital importance in understanding the sorption process. The adsorption capacity of GAC is strongly influenced by the chemical structure of their surface. The carbon-oxygen functional groups are by far the most important structures that influence the surface characteristics and surface behavior of GAC. The functional groups suggested most often are (I) carboxyl groups, (II) phenolic hydroxyl groups, (III) carbonyl groups (e.g. quinone-type), and (IV) lactone groups (e.g. fluorescein-type) [Ricordel et al., 2001]. The nature of interaction between various adsorbates with functional groups present on the GAC surface was assessed through FTIR spectral analysis.

The infrared spectra of blank-GAC is shown in Fig. 4.2.4. Blank-GAC shows a broad band with centre at 3450 cm^{-1} indicative of the presence of both free and hydrogen bonded OH groups on the GAC surface. The FTIR spectrum of blank GAC shows weak and broad peak in the region of 1620 cm^{-1}. The broad peak in the region of 1602 cm^{-1} indicates the presence of CO group stretching from aldehydes and ketones. The band at 1600 cm^{-1} may also be due to conjugated hydrocarbon bonded carbonyl groups. The FTIR spectra also show transmittance around ~1115 cm^{-1} region due to the vibration of the CC group in lactones and due to –COH stretching and –OH deformation.

4.2.3.1 FTIR spectroscopy of the AN-, P-, CP-, NP- and HQ- loaded-GAC: Fig. 4.2.5 shows the pure AN and AN-loaded-GAC spectrum. The spectrum of AN can be assigned as: a band at 3347.95 cm^{-1} for stretching vibration of $-NH_2$ group. A ring stretching with a contribution of the NH_2 scissoring band is appeared at 1610.96 cm^{-1}. The mode at 1276.71 cm^{-1} is assigned as partly to C-N stretching and partly to the ring stretching vibration [Ibrahim and Koglin, 2005; Galinos and Zafiropoulos, 1978]. Fig. 4.2.6 shows the FTIR spectra of pure P and after P adsorption onto GAC. The peak in pure P at 3331.51 cm^{-1} and 3041.10 cm^{-1} were assigned to OH stretching and aromatic C-H stretching. The peaks at 1468.49, 1364.38, 805.48 and 690.41 cm^{-1} were diminished, while the absorbance band of hydroxymethyl and methylene groups increased. The peaks at 1468.49 cm^{-1} corresponded to the C=C aromatic ring vibrations. The peaks at 1364.38 cm^{-1}

corresponded to the C-H bending in plane, while the 690.41 cm^{-1} peaks belonged to the C-H out of plane vibrations. Similar peaks were observed by Poljansek and Krajnc [2005] and Bardakci [2007]. The strong band at 1589.82, 1489.02 cm^{-1} in the spectrum of pure CP (Fig. 4.2.7) can be attributed to C=C stretching. This band was observed as 1590 cm^{-1} by other researchers for the interaction between activated carbon (AC) surfaces and adsorbed P derivatives [Paku et al, 2005]. The band at 1369.86 cm^{-1} was attributed to the in-plane bending of C-H bonds. The band at 1090.36 cm^{-1} is assigned to a C-Cl vibration. The band at 810.96 cm^{-1} was attributed to mostly out- of-plane bending of the ring C-H vibration [Zierkiewicz et al, 2000; Pandit et al, 2001; Bardakci, 2007]. Fig. 4.2.8 shows the FTIR spectra of pure NP and after NP adsorption onto GAC. Bands appearing in pure NP spectra at 3429 cm^{-1} and 2966.52 cm^{-1} were assigned to OH stretching and C–H stretching of aromatics. The variation in intensity of the bands at 3421.38 and 3084.93cm^{-1} shows the adsorption of NP. The bands at 1923.29, 1614.28, 750.68 and 629.16cm^{-1} were due to C≡C stretching, C=O stretching of carboxylic group, methylene rocking band and ≡C–H bending mode, respectively. Out of these, carboxylic and hydroxyl groups played a major role in the removal of NP. Bands at 1499.42 and 1384.38cm^{-1} were typical of NO_2 group indicating the adsorption of NP. The presence of a medium peak at 750.68cm^{-1} further confirmed the adsorption of para-substituted benzene product [Ahmaruzzaman and Gayatri, 2010]. The infrared spectra of HQ and HQ-GAC are shown in Fig. 4.2.9. The peaks corresponding to O-H stretching at 3262.3 cm^{-1}, C--H stretching for aromatic ring at 3027.03 cm^{-1}, C-C- stretching at 1517.0 cm^{-1}, O-H bending at 1384.4 cm^{-1}, C-O stretching at 1191.6 cm^{-1}, C-H bending at 758.6 cm^{-1} are found for pure HQ and HQ loaded GAC.

It may be seen that few peaks appear in AN-, P-, CP-, NP- and HQ- loaded GAC and few of the peaks originally present in GAC get shifted. Also the transmittance of the peaks gets increased after the loading of AN, P, CP, NP and HQ signifying the participation of these functional groups in the adsorption. Although some inference can be drawn about the surface functional groups participating in the adsorption of AN, P, CP, NP and HQ onto the GAC from FTIR spectra, the weak and broad bands do not provide any authentic information about the actual mechanism of the adsorption process, although

it seems that the adsorption of AN, P, CP, NP and HQ is chemisorptive in nature. However, the nature of adsorption will be further tested later.

4.2.3.2 FTIR spectroscopy of the C- and R- loaded-GAC: FTIR analysis was done to evaluate the nature of interaction between C and R with functional groups presents on the GAC surface. The infrared spectra of the OH stretching region of C, GAC and C-GAC, and R, GAC and R-GAC are shown in Figs. 4.2.10(a) and 4.2.11(a), respectively. The infrared spectra of C and R display many peaks in the region 3610-3730 cm^{-1} and 3610-3671 cm^{-1}, respectively. These bands are assigned to OH stretching vibrations of the P unit [Zhou et al., 2007]. Blank-GAC shows peaks at ~3365, ~3440 and ~3536 cm^{-1}. First peak may be due to the water-hydrogen bonded OH units and second and third peaks may be due to the non-hydrogen bonded OH units. The infrared spectra of GAC with adsorbed C show peaks in similar positions to that of C only. The peaks found for blank-GAC disappeared completely in C-GAC and R-GAC spectra. This may be due to the utilization of these peaks during the adsorption process. Figs. 4.2.10(b) and 4.2.11(b) show FTIR spectra of C, GAC, and C-GAC and R, GAC, and R-GAC in the wave numbers range of 1200-1800 cm^{-1}, respectively. This IR region was selected to emphasize the variation of OH and C=C vibrations after the adsorbate-adsorbate interaction. OH vibration band modifications or disappearance reveals that the compound interaction is by means of a hydrogen bond or the formation of catecnate or resorcinate. C and R spectra show peaks at ~1385 cm^{-1} and ~1632 cm^{-1} to OH deformation and stretch of C=C aromatic rings, respectively [Terzyk, 2001; Zhou et al., 2007]. The band at 1636 cm^{-1} in GAC is assigned to water bending modes of the water in the hydration sphere within the carbon interlayer. The intensity of this band decreases with R and C loading. In the C-GAC and R-GAC spectra, only small band shifts are observed such as that for OH (from 1385 to 1388 cm^{-1}) and C=C (from 1632.42 to 1632.86 cm^{-1}) vibrations. These results suggest that the interaction of C and R to GAC occurred through hydrogen bond [Arana et al., 2007].

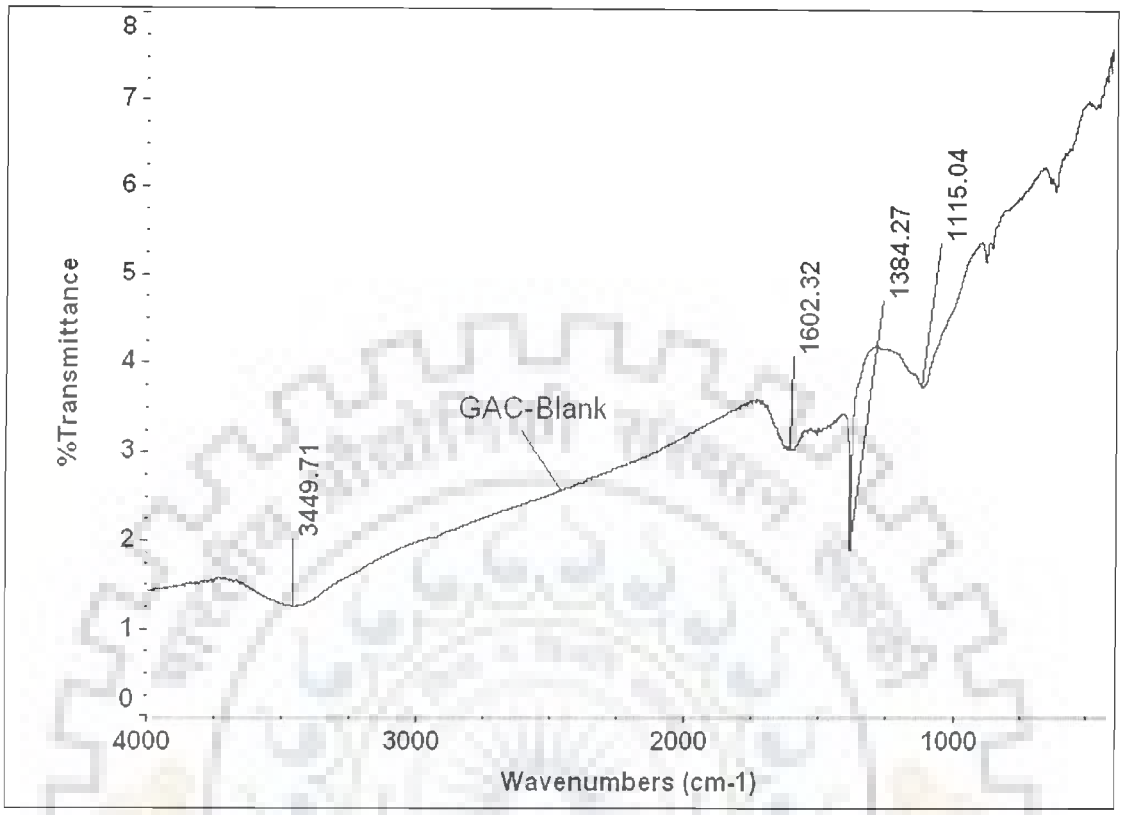

Figure 4.2.4. FTIR of blank-GAC.

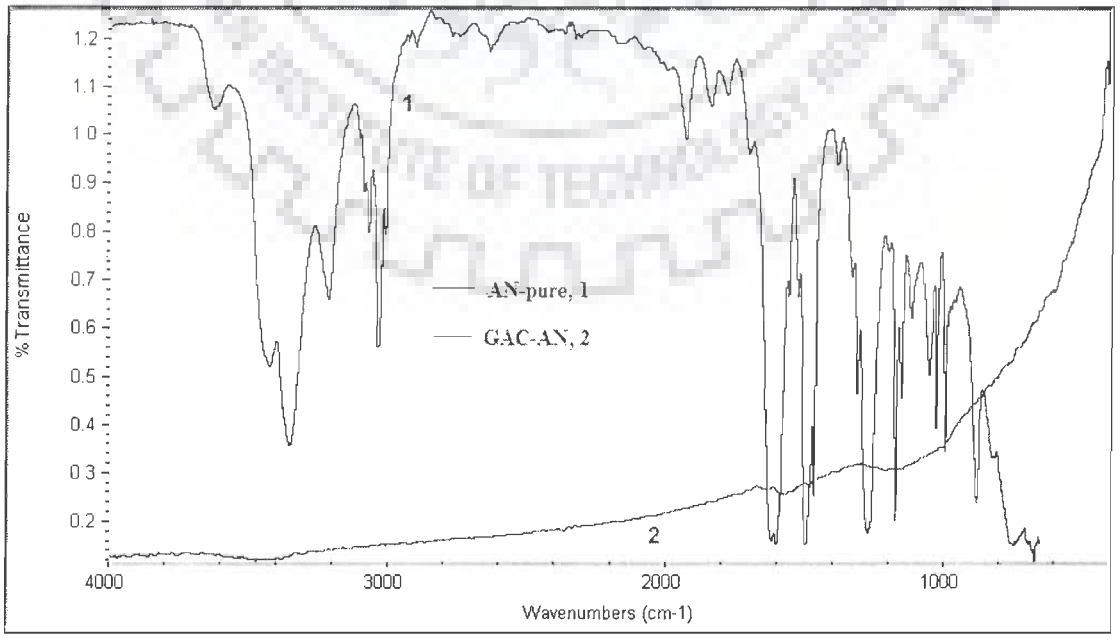

Figure 4.2.5. FTIR of pure-AN and AN loaded GAC.

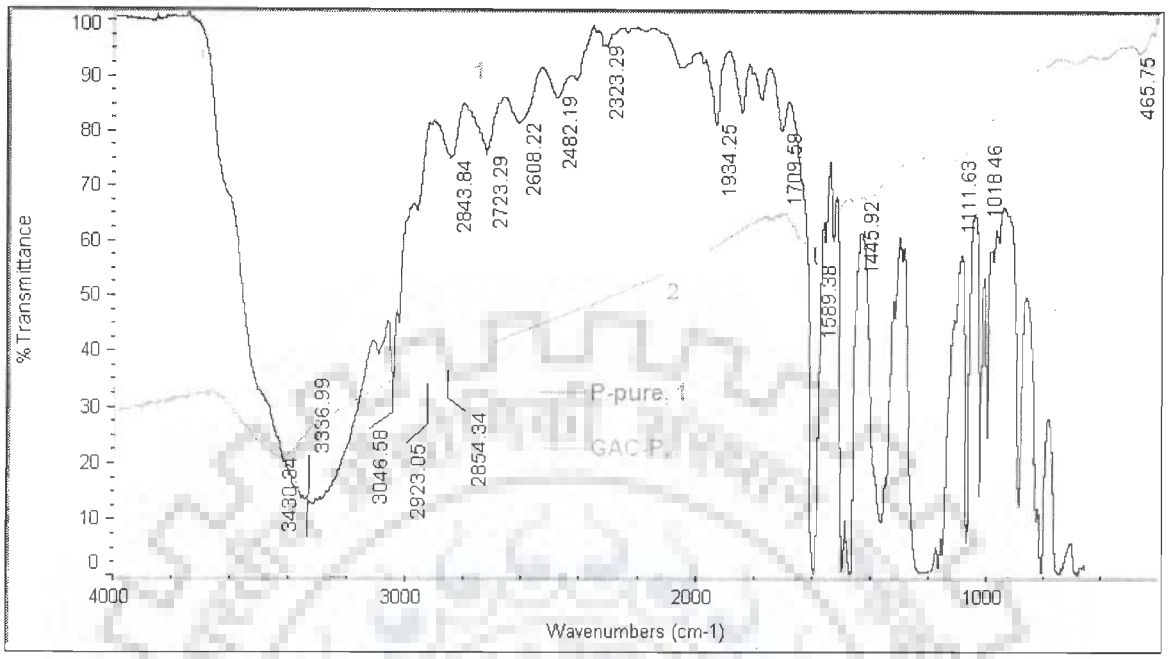

Figure 4.2.6. FTIR of pure-P and P loaded GAC.

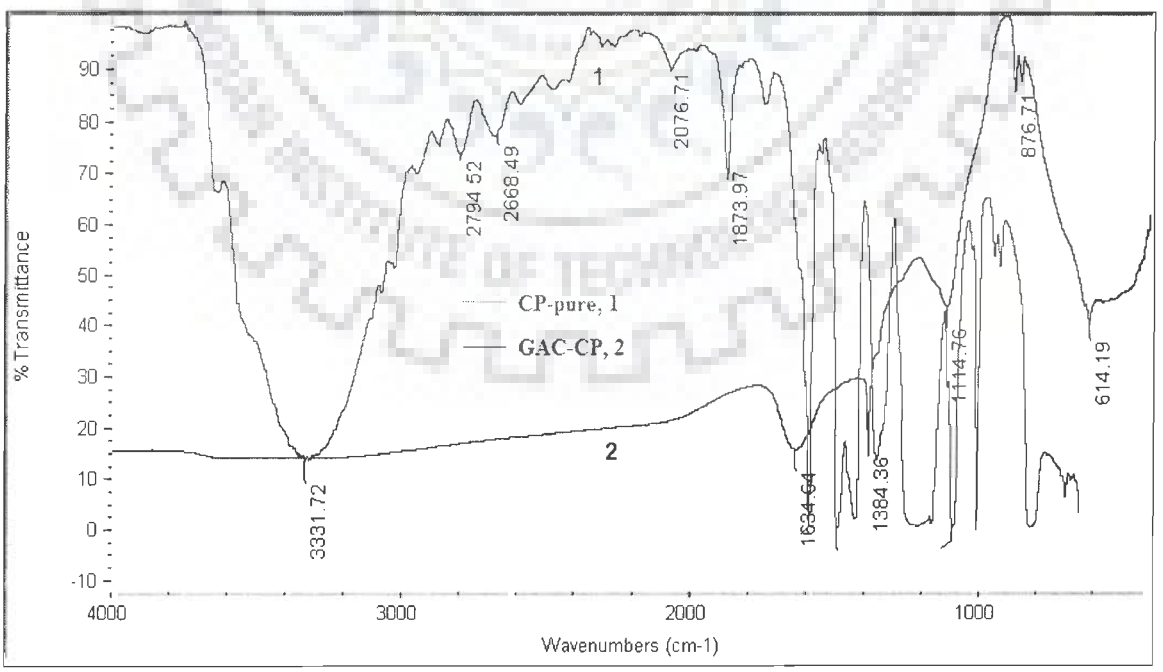

Figure 4.2.7. FTIR of pure CP and CP loaded GAC.

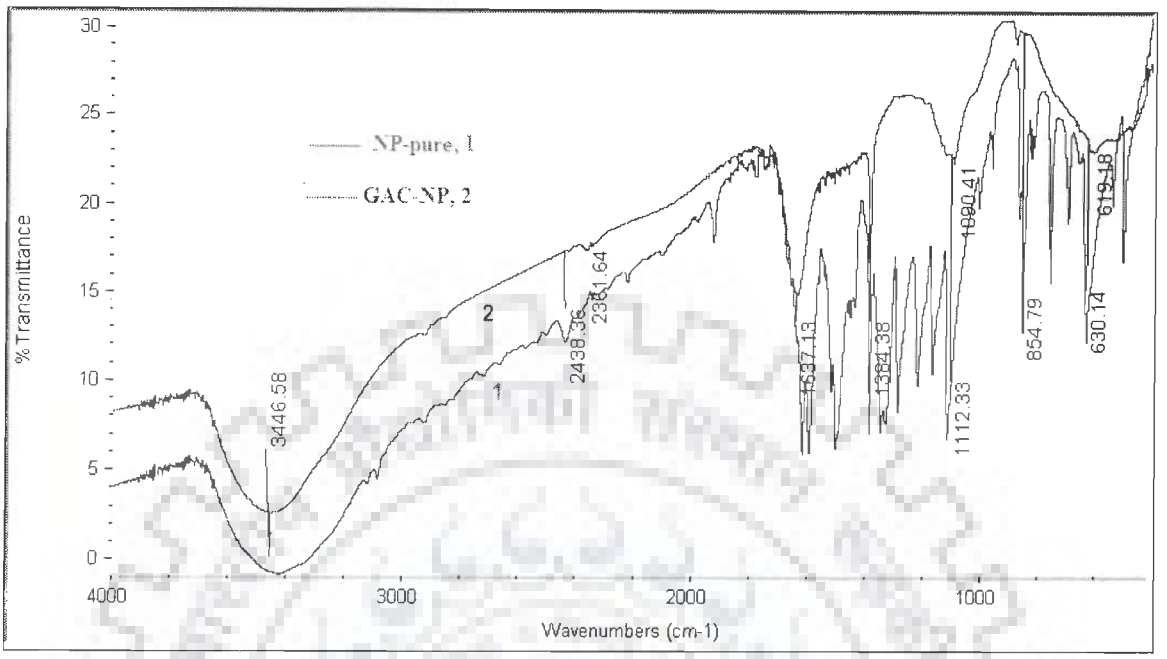

Figure 4.2.8. FTIR of pure NP and NP loaded GAC.

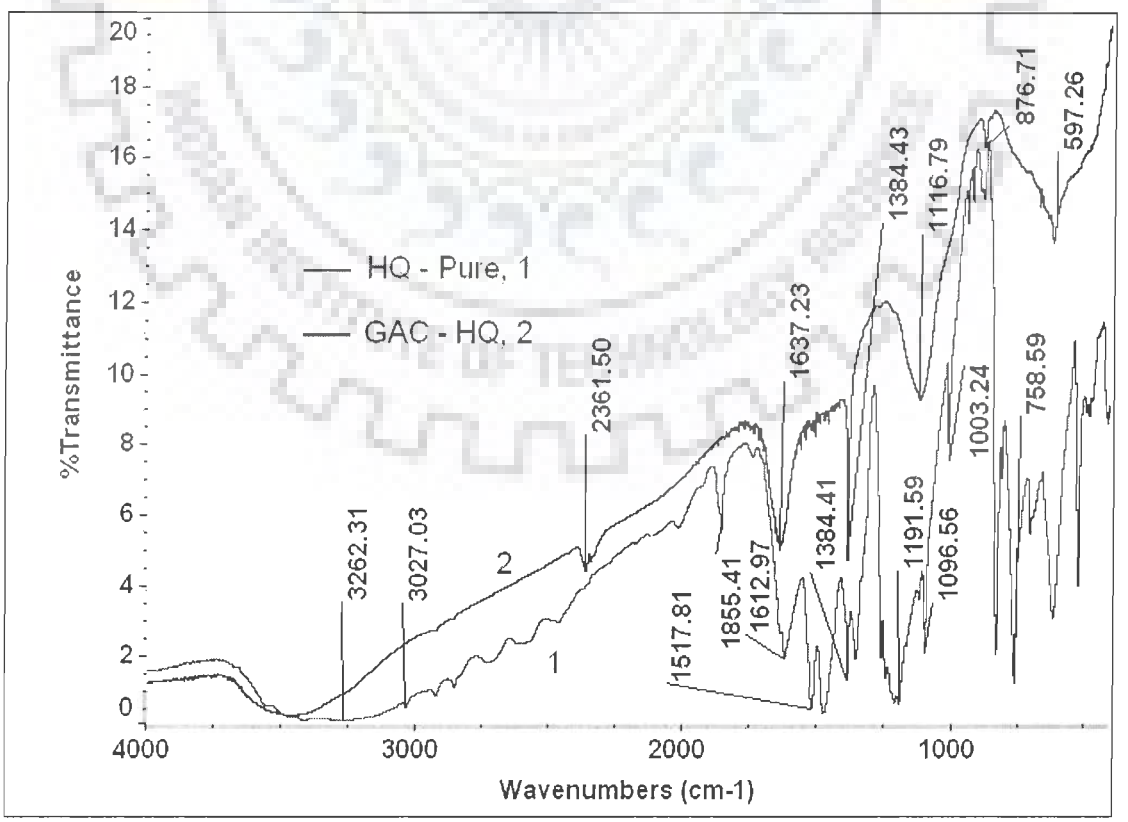

Figure 4.2.9. FTIR of pure HQ and HQ loaded GAC.

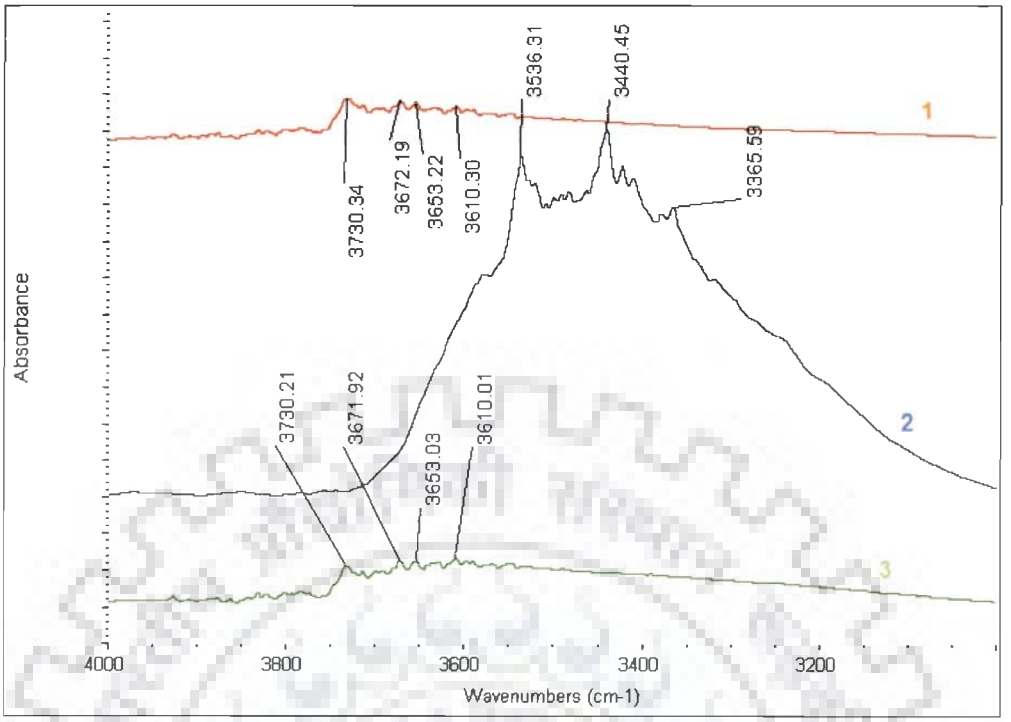

(a) 3000-4000 cm^{-1}

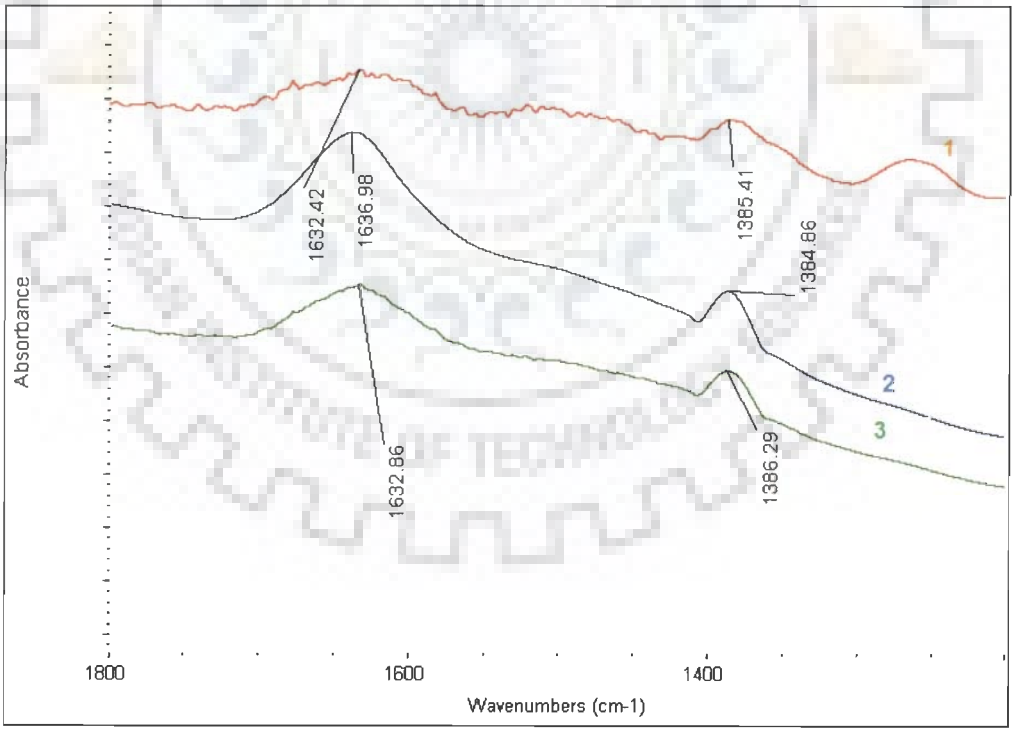

(b) 1200-1800 cm^{-1}

Figure 4.2.10. FTIR of C, blank-GAC and C loaded GAC. 1: C; 2: Blank-GAC; 3: C-GAC.

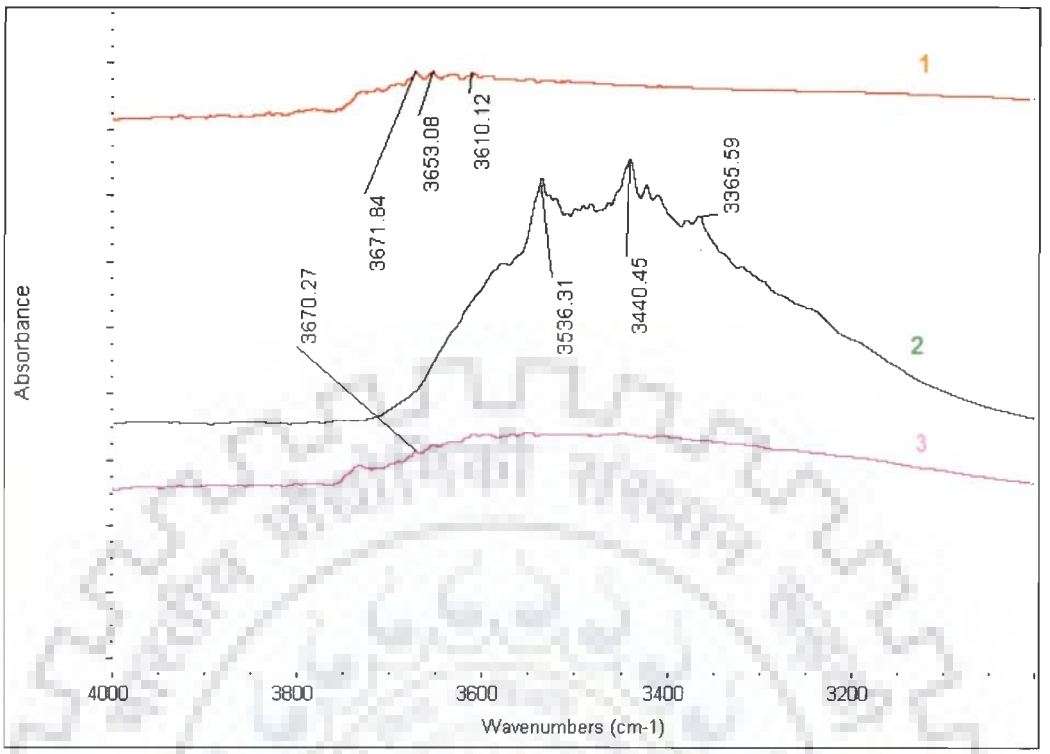

(a) 3000-4000 cm^{-1}

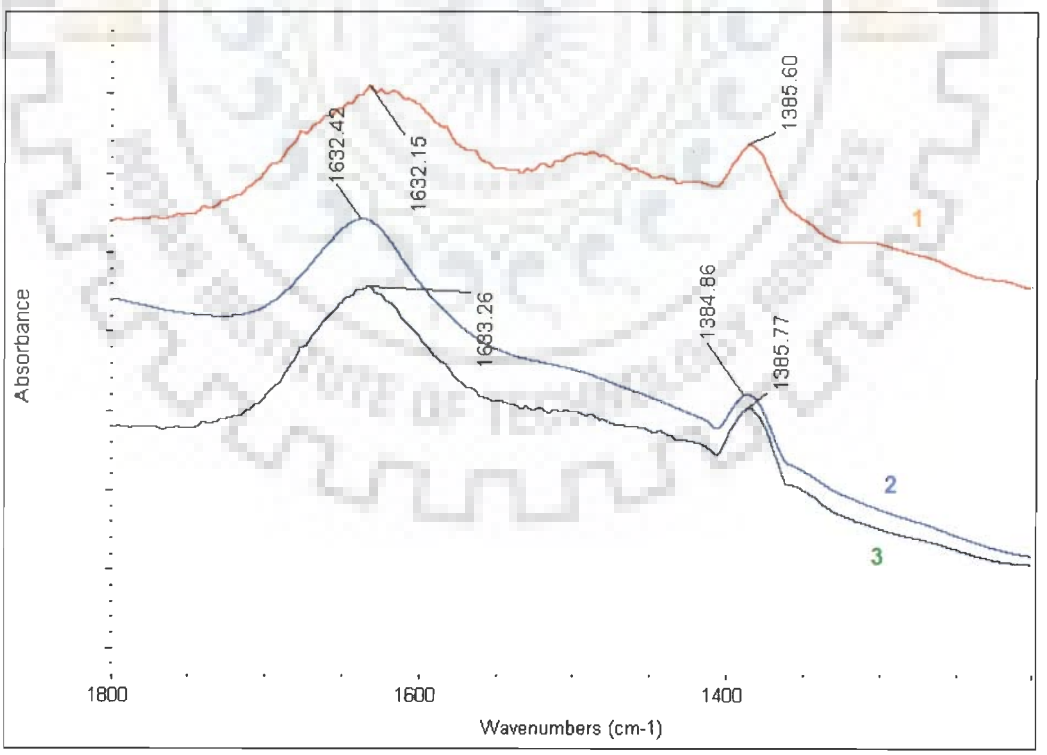

(b) 1200-1800 cm^{-1}

Figure 4.2.11. FTIR of R, blank-GAC and R loaded GAC. 1: R; 2: Blank-GAC; 3: R-GAC.

4.3 BATCH ADSORPTION STUDY FOR INDIVIDUAL ADSORPTION

4.3.1 Effect of initial pH (pH_o)

System pH affects the adsorption process through dissociation of functional groups on the active sites of the adsorbent surface. This pH change affects the kinetics and equilibrium characteristics of the adsorption process. To understand the adsorption mechanism, the point of zero charge (pH_{PZC}) of the GAC was estimated. Fig. 4.3.1 shows that for all the concentrations of KNO_3, the zero value of ΔpH and hence pH_{PZC} for GAC lies at the pH_0 value of 10.3. Kumar et al. [2008] and Srivastava et al. [2008] have reported pH_{PZC} value of 10.33 and 8.50, respectively for GAC. At low pH (e.g., pH < pH_{PZC}), most ACs are positively charged, at least in part as a consequence of donor/acceptor interactions between the carbon graphene layers and the hydronium ions [Leon y Leon et al., 1992]. The adsorption of cations is favored at $pH > pH_{PZC}$, while the adsorption of anions is favored at $pH < pH_{PZC}$.

4.3.1.1 Speciation diagram of adsorbates: The pK_1 values of AN, P, CP and NP are 4.63, 9.95, 9.38 and 7.15, respectively [Yang et al., 2008; Fiore and Zanetti, 2009]. The percentage of hydrolytic products of AN, P, CP and NP was calculated from the following stability constants.

$C_6H_5NH_3^+ + H_2O \approx C_6H_5NH_2 + H_3O^+$ pKa=4.63 (4.3.1)

$C_6H_5OH + H_2O \approx C_6H_5O^- + H_3O^+$ pKa=9.95 (4.3.2)

$C_6H_4ClOH + H_2O \approx C_6H_4ClO^- + H_3O^+$ pKa=9.38 (4.3.3)

$C_6H_4(NO_2)OH + H_2O \approx C_6H_4(NO_2)O^- + H_3O^+$ pKa=7.15 (4.3.4)

The speciation of AN, P, CP and NP in deionized water is presented in Fig. 4.3.2(a). The $pK_{a,1}$ and $pK_{a,2}$ values of C are 9.25 and 13.0, respectively [Schweigert et al., 2001]. C species are found to be present in deionized water in the form of $C(OH)(O)^-$, $C(O)^{2-}$ [Blanco et al., 2005]. The concentration of the hydrolyzed C species depends on the total C concentration, and the solution pH. The speciation of C in deionized water is presented in Fig. 4.3.2(b). The percentage of C hydrolytic products was calculated from the following stability constants:

$C(OH)_2 + H_2O \rightleftharpoons C(OH)(O)^- + H_3O^+$ $pK_{a,1} = 9.25$ (4.3.5a)

$C(OH)(O)^- + H_2O \rightleftharpoons C(O)^{2-} + H_3O^+$ $pK_{a,2} = 13$ (4.3.5b)

The $pK_{a,1}$ and $pK_{a,2}$ values of R are 9.4 and 12.3, respectively [Blanco-Martinez et al., 2009]. The distribution of various R species as a function of pH as calculated from the following equations has been presented in Fig. 4.3.2(c).

$$R(OH)_2 + H_2O \rightleftharpoons R(OH)(O)^- + H_3O^+ \qquad pK_{a,1} = 9.20 \qquad (4.3.6a)$$

$$R(OH)(O)^- + H_2O \rightleftharpoons R(O)^{2-} + H_3O^+ \qquad pK_{a,2} = 10.90 \qquad (4.3.6b)$$

The $pK_{a,1}$ and $pK_{a,2}$ values of HQ are 9.9 and 11.5, respectively [EHC 157, 1994; Blanco-Martínez et al., 2009]. The distribution of various HQ species as a function of pH as calculated from the following equations has been presented in Fig. 4.3.2(d).

$$HQ(OH)_2 + H_2O \rightleftharpoons HQ(OH)(O)^- + H_3O^+ \qquad pK_{a,1} = 9.9 \qquad (4.3.7a)$$

$$HQ(OH)(O)^- + H_2O \rightleftharpoons HQ(O)^{2-} + H_3O^+ \qquad pK_{a,2} = 11.5 \qquad (4.3.7a)$$

where, $C(OH)_2$, $R(OH)_2$ and $HQ(OH)_2$ are neutral C, R, HQ; $C(OH)(O)^-$, $R(OH)(O)^-$ and $HQ(OH)(O)^-$ are the catecnate, resorcinate and hydroquinate monoanion, respectively; and $C(O)^{2-}$, $R(O)^{2-}$ and $HQ(O)^{2-}$ are the catecnate and resorcinate and hydroquinate dianions, respectively. At pH > $pK_{a,1}$, the phenolic compounds like C, R and HQ are mainly in the form of negatively charged phenoxyions, while at pH< $pK_{a,1}$, the phenolic compounds are predominantly in the neutral molecular form [Richard et al., 2009].

4.3.1.2 Effect of pH_o on AN, P, CP and NP adsorption: The effect of pH_o on the adsorption of AN, P, CP and NP (C_o=1.07mmol/l, 1.06 mmol/l, 0.78mmol/l and 0.72 mmol/l, respectively) onto GAC was studied at a temperature of 303 K by varying the pH_0 in the range of 2-12. Natural pH of AN, P, CP and NP solution at C_o=1.07mmol/l, 1.06 mmol/l, 0.78mmol/l and 0.72 mmol/l were 6.9, 6.0, 5.8 and 6.0, respectively. Results of the experiments are presented in Fig. 4.3.3(a). This figure shows that removal of the AN, P, CP and NP slightly increased with an increase in pH_o of the solution from 2 to natural pH. The percentage adsorption were found to be ~97%,~94.3%,~97.4% and ~87.62% for AN, P, CP and NP, respectively, at pH_o = 4; and ~99.3%, ~98.2%, ~98.7% and ~94.8%, respectively at natural pH. Percentage adsorption decreased sharply for $pH_o \geq 6$ for AN, P, CP and NP. However, decrease in removal efficiency for NP and CP was much sharper than as compared to that for AN and P.

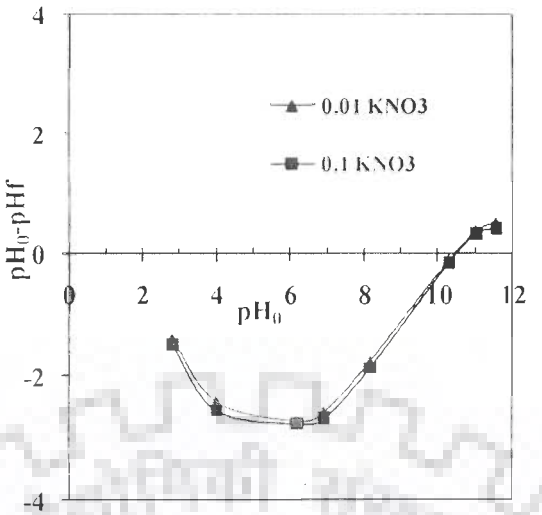

Fig. 4.3.1. Point of zero charge (pH_{PZC}) for GAC.

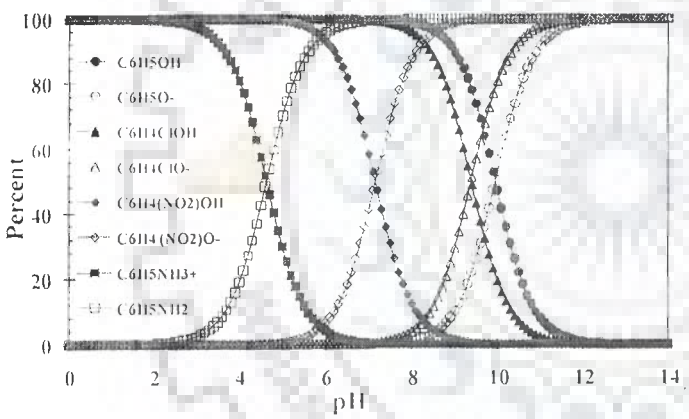

(a) AN, P, CP and NP

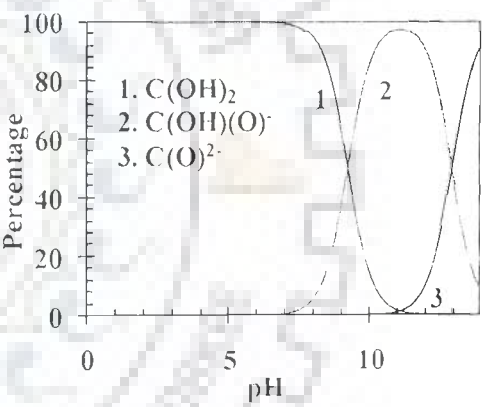

(b) C

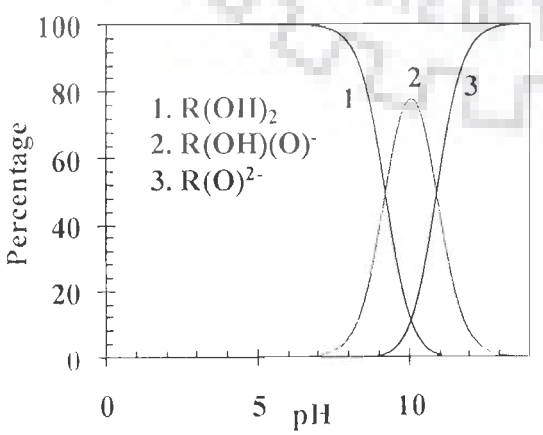

(c) R

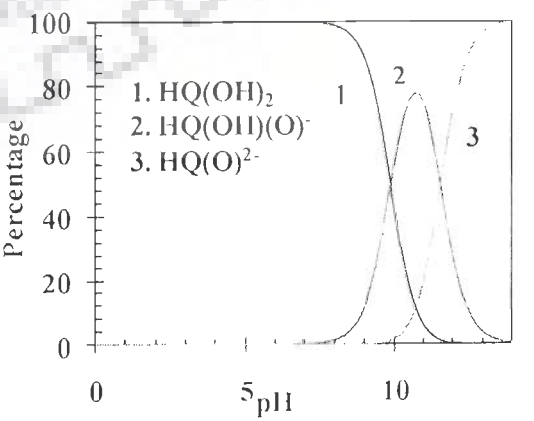

(d) HQ

Figure 4.3.2. Distribution of AN, P, CP, NP, C, R and HQ as a function of pH .

The pH affects the protonation equilibria of ligands in solution and the protonation level of individual surface sites [Vasudevan and Stone, 1996]. When pH < p*K*a, the non-dissociated species and the dissociated species (bases form cations by protonation at pH) are dominated for organic acids and organic bases, respectively; whereas, when pH > p*K*a, the dissociated species (anion) is dominant for organic acids and the non-dissociated species is dominant for organic bases [Yang et al., 2008].

At low pH, owing to its charge and resultant hydration the interaction between anilinium cations and the positively charged surface results in electrostatic repulsion and greatly reduced adsorption [Conway, 1995]. With increasing pH, protonation of AN becomes less and less pronounced, enhancing the uptake. Adsorption of neutral AN is preferred over the cationic form owing to its reduced hydrophilicity [Niu and Conway, 2002]. Zhang et al. [2009] adsorption of AN onto Cr-bentonite. They found that adsorption efficiencies of AN are high and stable under acidic and neutral pH conditions and decrease with the increase of pH value under alkaline pH conditions. Lower sorption of AN at alkaline pH is probably due to the presence of excess OH^- ions competing with AN for hydrogen bond formed with water molecules. Faria et al. [2008] reported that the AN uptake is significantly lower at pH=3 than at pH_o=7. At pH_o=7, AN in aqueous solution is mainly in its molecular form. In this case adsorption is believed to occur mainly through dispersive interactions between the aromatic ring and the π-electrons of the graphitic structure of the AC [Faria et al., 2008]. Dispersive interactions are more predominant at $pH_o \approx 7$ because the NH_2 is an activant group [Villacanas et al., 2006].

At low pH, the GAC surface is protonated and is thus positively charged. Surface protonation has a double effect: (i) protonated oxygen-containing functional groups act as centers for water cluster formation [Villacanas et al., 2006; Franz et al., 2000], which cover the adsorption sites and reduce access of the aromatics by blocking the entrance of the micropores; (ii) protonation of the basal plane disturbs the π– π interaction with the aromatic ring of the pollutants. Effects (i) and (ii) both reduce the dispersive interaction between the protonated P and the surface. Moreover, hydrogen bonds between P molecules and surface groups may block the entrances of fine pores [Terzyk, 2003]. The uptake of P, CP and NP by GAC is low at pH 3.

At $pH \approx pK_a$, the phenolic compouds are predominantly in the neutral molecular form. The increasing removal efficiency of P, CP and NP by GAC within pH 3-6 suggests the insignificant involvement of hydrogen bond between the phenolics and GAC [Chen et al., 2007]. At $pH_o \leq pH_{PZC}$, the GAC surface is positively charged, and the species adsorbed at pH (6-7) are neutral molecules. In these conditions, the dispersive or Van der waals interactions determine the adsorption process [Blanco-Martinez et al., 2009; Shakir et al., 2008]. The increased surface acidity of GAC at $pH \approx 6$ favors the donor acceptor interaction between the electrons of the aromatic ring and the surface. This leads to an increase of the removal efficiency [Blanco-Martinez et al., 2009]. Liu and Pinto [1997] also observed an increase of P sorption by AC from pH 3.1 to 6.3 due to decreased proton adsorption on carbonyl oxygen sites, which increases P adsorption on these sites. Therefore, in this work, the pH of the solutions of P and CP were not adjusted and were 5.96 and 6.02, respectively.

For $pH > pK_a$, the compounds are mainly in the form of negatively charged phenoxy ions, while the functional groups of the carbon surface are de-protonated and negatively charged, thus, the electrostatic repulsion lead to a decrease of the removal efficiency at higher $pH > pK_a$ [Blanco-Martinez et al., 2009]. It may be noted that the dissociation of the phenolics would increases their hydrophilicity, which may also decrease the adsorption for $pH > pK_a$ [Vasudevan and Stone, 1996]. In addition, the dissociation of -OH groups on the phenolics at high pH may inhibit the formation of hydrogen bonds the GAC and phenolic molecules and thus reduce the adsorption as well.

4.3.1.3 Effect of pH_o on C, R and HQ adsorption: The effect of pH_o on the adsorption of C, R and HQ onto GAC was studied at a temperature of 303 K by varying the pH_0 in the range of 2-12. Natural pH of C, R and HQ solution were 5.8, 5.6 and 6.1, respectively. Results of the experiments are presented in Fig. 4.3.3(b). This figure shows that removal of the C and R slightly increased with an increase in pH_o of the solution from 2 to natural pH. Further increase in pH_o from natural pH to 12 led to sharp

decrease in the C, R and HQ removal efficiency. The percentage adsorption were found to be ~94% and ~90% for C and R, respectively, at $pH_o = 4$; and ~97% and ~94%, respectively at natural pH. Percentage adsorption decreased sharply for $pH_o \geq 6$ for both C and R. However, decrease in removal efficiency for R was much sharper than as compared to that for C. For HQ, the removal efficiency of HQ was constant at ~65% for $8 \leq pH \leq 10$ but lower than that at $pH \approx 6$ (~95%).

The adsorption mechanisms of P_s on AC have been studied earlier. The GAC graphene surface is highly polarizable and may show amphoteric nature attracting π-acceptors to the electron-rich graphene surface area near edges and π-donors to the central regions which are relatively electron poor [Zhu and Pignatello, 2005]. The main contributions to organics adsorption onto GAC are π–π dispersion interactions [Coughlin and Ezra, 1968], hydrogen-bonding interactions [Franz et al., 2000] and donor–acceptor interactions [Mattson et al., 1969]. The substituents on benzene ring provide different inductive and resonance effects, and their relative electron donating properties are well-known [Star et al., 2003]. Hydroxyl is an electron-donating functional group [Hansch et al., 1991] which can increase the π-donating strength of the host aromatic ring. Thus, -OH can increase the adsorption affinity of the phenolic compounds to the GAC graphene surfaces [Lin and Xing, 2008]. It is obvious that π–π dispersive interactions will be stronger with the increase of the number of hydroxyl. Therefore, the number of hydroxyl has positive effect on the adsorption of phenolic derivatives. The substitution of P with a hydroxyl in *meta*-position results in a much higher adbsorption amount than substitution in the *ortho*- and *para*-position [Blanco-Martinez et al., 2009].

It may be seen in Fig. 4.3.3(b) that adsorption gets diminished at very high pH (where OH^- effectively competes with the deprotonated ligand for surface sites) and at low pH (where neutral surface sites are converted into protonated sites and ligand molecules become successively protonated). It may be noted as earlier that the dissociation of the phenolics would increases their hydrophilicity, which may also decrease the adsorption for $pH > pK_{a1}$ [Vasudevan and Stone, 1996]. In addition, the dissociation of -OH groups on the phenolics at high pH may inhibit the formation of hydrogen bonds the GAC and

phenolic molecules and thus reduce the adsorption as well. At $pH < pK_{a1}$, the phenolic compouds are predominantly in the neutral molecular form. The increased surface acidity of GAC at $pH \approx 6$ favor the donor–acceptor interaction between the electrons of the aromatic ring and the surface. This leads to an increase of the removal efficiency [Blanco-Martinez et al., 2009]. Increasing adsorption of these polar aromatics to GAC with increasing pH before their pK_{a1} may be due to the change of GAC properties with pH. At $pH_o \leq pH_{PZC}$, the GAC surface is positively charged, and the species adsorbed at pH (5.6-5.8) are neutral molecules. In these conditions, the dispersive or Van der waals interactions determine the adsorption process [Blanco-Martinez et al., 2009; Shakir et al., 2008].

The decrease in removal efficiency for HQ and R was sharper for $pH > 6$. It may be seen in Fig. 4.3.2 that formation of $C(OH)(O)^-$, $R(OH)(O)^-$ and $HQ(OH)(O)^-$ start at nearly same pH ~8. However, formation of $C(O)^{2-}$ starts at $pH \approx 11.5$ whereas formation of $R(O)^{2-}$ and $HQ(O)^{2-}$ starts at pH ~10 itself. For $8 \leq pH_o \leq 10$, the removal efficiency of HQ and R were constant at ~65% and ~73% but lower than that at $pH_0 \approx 6$. At the intermediate pH (8-10), C, R and HQ exists in solution in both the neutral and anionic forms. Hence, it seems judicious to assume that at this pH, C, R and HQ are adsorbed via both electrostatic and van der Waals interaction [Shakir et al., 2008]. For $pH_0 \geq 10$, the HQ and R removal efficiency decreased sharply. This sharp decrease in R and HQ removal efficiency were due to high repulsive force between negatively charged GAC and negatively charged $R(O)^{2-}$ and $HQ(O)^{2-}$ formed at $pH_0 \geq 10$. No sharp decrease in C removal efficiency was observed which may be due to the fact that $C(O)^{2-}$ gets formed at $pH_0 > 11.5$, and thus, the repulsive force for C adsorption is not that active as it is for R adsorption.

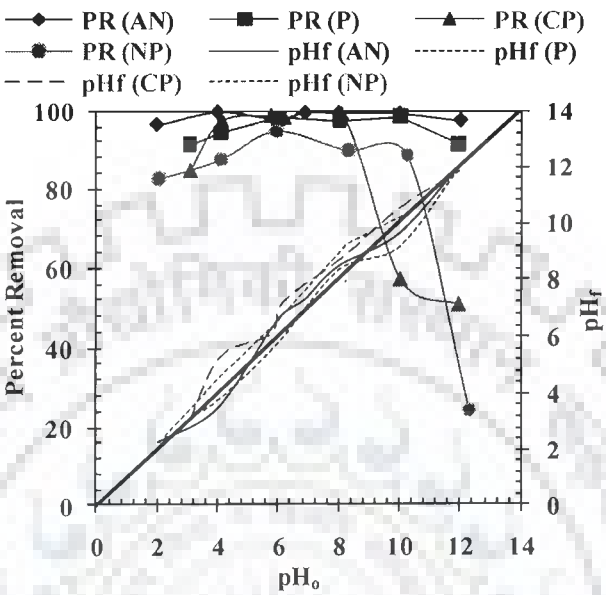

(a) AN, P, CP and NP

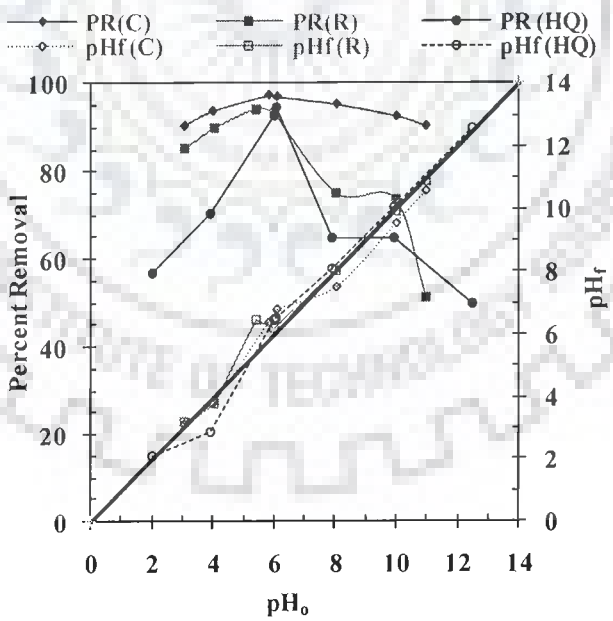

(b) C, R and HQ

Figure 4.3.3. Effect of pH_o on the adsorption of AN, P, CP, NP, C, R and HQ by GAC. T = 303 K, t = 24 h, m = 10 g/l.

4.3.2 Effect of adsorbent dosage (m)

Fig. 4.3.4 (a-g) show the AN, P, CP, NP, C, R and HQ removal efficiency as a function of GAC dosage. The AN, P, CP, NP, C, R and HQ removal efficiency increased from 29.2%, 38.3%, 23.4%, 47.07%, 22%, 28% and 35% at m=1 g/l to 86.47%, 90.74%, 96.69%, 87.8%, 74%, 72% and 89% respectively, at m=5 g/l. For $m \geq 10$ g/l, AN, P, CP, NP, C, R and HQ removal efficiencies became constant at ~95.8%, ~97.3%, ~98.56%, ~98.4%,~98%,~97% and ~99%, respectively. The increase in adsorption of AN, P, CP, NP, C, R and HQ with an increase in m upto 10 g/l was due the presence of greater number of adsorbent sites at enhanced m. However for $m \geq 10$ g/l, the AN, P, CP and NP removal efficiency become less dependent on m.

Adsorption efficiency of AN and CP increased with the increase of m upto 10 g/l remain almost constant onto XAD-4 and Cr-bentonite [Bilgili, 2006; Zheng et al., 2008]. Similar results were reported for 4-hydroxyphenol sorption on Cr-bentonite from aqueous solution [Zheng et al., 2008]. Kumar et al. [2003] reported 10 g/l as optimum dosage for adsorption of C and R onto GAC with > 95% removal efficiency. Mondal and Balomajumder [2007] reported 69.74% R removal efficiency by *Pseudomanas putida* immobilized GAC at optimum dosage of 10 g/l. The difference in removal efficiencies in present study to that reported earlier by Kumar et al. [2003] is due to the lower surface area of GAC used by Kumar et al. [2003]. However, m=10 g/l was the optimum dosage. Varying amounts of AC were contacted with the BSM containing 1000 mg/l of P or NP to optimize the dose of adsorbent. Kumar et al. [2007] reported that NP showed more adsorbability than P. Only 6 g/l of AC dose was required in case of NP as against 10 g/l of AC dose to effect the same amount of P, i.e. 95%, showing a good interaction between -nitro group of NP and functional groups present on AC surface. After 95% removal, the AC dose is not much effective suggesting that the whole of the P and NP present in the wastewater cannot be reduced in a single stage batch reactor.

The optimum value of m=10 g/l was used in all further experiments in the present study.

4.3.3 Effect of contact time and initial concentration

The effect of contact time on the q_t values for various C_o of AN, P, CP, NP, C, R and HQ at m=10 g/l and T= 303 K is shown in Fig. 4.3.5. The adsorption was followed over a period of 24 h. These durations are considered to be approximately the equilibration times for the adsorption process. It may be seen that in the first 1 h, the adsorption of the adsorbates was fast and, thereafter, the adsorption rate decreased gradually and the adsorption reached equilibrium. For $C_o \leq 2.68$ mmol/l, the residual concentrations at 5 h contact time were found to be higher by a maximum of ~2% than those obtained after 24 h contact time. Therefore, after 5 h contact time, a steady state approximation was assumed and a quasi-equilibrium situation was accepted for $C_o \leq 2.68$ mmol/l.

For AN adsorption onto GAC, equilibrium adsorption time were found to be 5 h (96.5%), 5 h (97.7%), 8 h (97.8%), 16 h (98.6%) and 20 h (92.4%) respectively, at C_o values of 0.54, 1.07, 2.68, 5.37 and 10.74 mmol/l. For P adsorption onto GAC, equilibrium adsorption time was found to be 5 h (97.2%), 5 h (97.3%), 8 h (97.2%), 5 h (98.6%) and 5 h (99.2%) respectively, at C_o values of 0.53, 1.06, 2.66, 5.31 and 10.63 mmol/l. For CP adsorption onto GAC, equilibrium adsorption time was found to be 2 h (97.9%), 3 h (98.5%), 5 h (98.3%), 5 h (99.5%) and 3 h (99.1%), respectively, at C_o values of 0.39, 0.78, 1.94, 3.89 and 7.78 mmol/l and for NP adsorption onto GAC, equilibrium adsorption time was found to be 3 h (98.1%), 5 h (96.5%), 5 h (97.5%), 8 h (95.6%) and 12 h (94.1%), respectively, at C_o values of 0.36, 0.72, 1.80, 3.59 and 7.19 mmol/l. For C adsorption onto GAC, equilibrium adsorption time was found to be 5 h (96.4%), 5 h (98.8%), 5 h (97%), 12 h (96.6%) and 12 h (89.8%) respectively, at C_o values of 0.45, 0.91, 2.27, 4.54 and 9.08 mmol/l. The respective equilibrium adsorption time for R adsorption was 2 h (90.55%), 5 h (93.2%), 5 h (95.56%), 12 h (95%) and 12 h (98.1%). For 2.27 mmol/l < $C_0 \leq 9.08$ mmol/l, a quasi-equilibrium situation may be assumed after 12 h for both C and R. Similar values can be computed for HQ adsorption. For HQ adsorption onto GAC, equilibrium adsorption time (and corresponding equilibrium adsorption) was found to be 5 h (98.7%), 2 h (99%), 12 h (96%), 8 h (99.5%) and 12 h (99.9%) respectively, at C_o values of 0.45, 0.91, 2.27, 4.54 and 9.08 mmol/l.

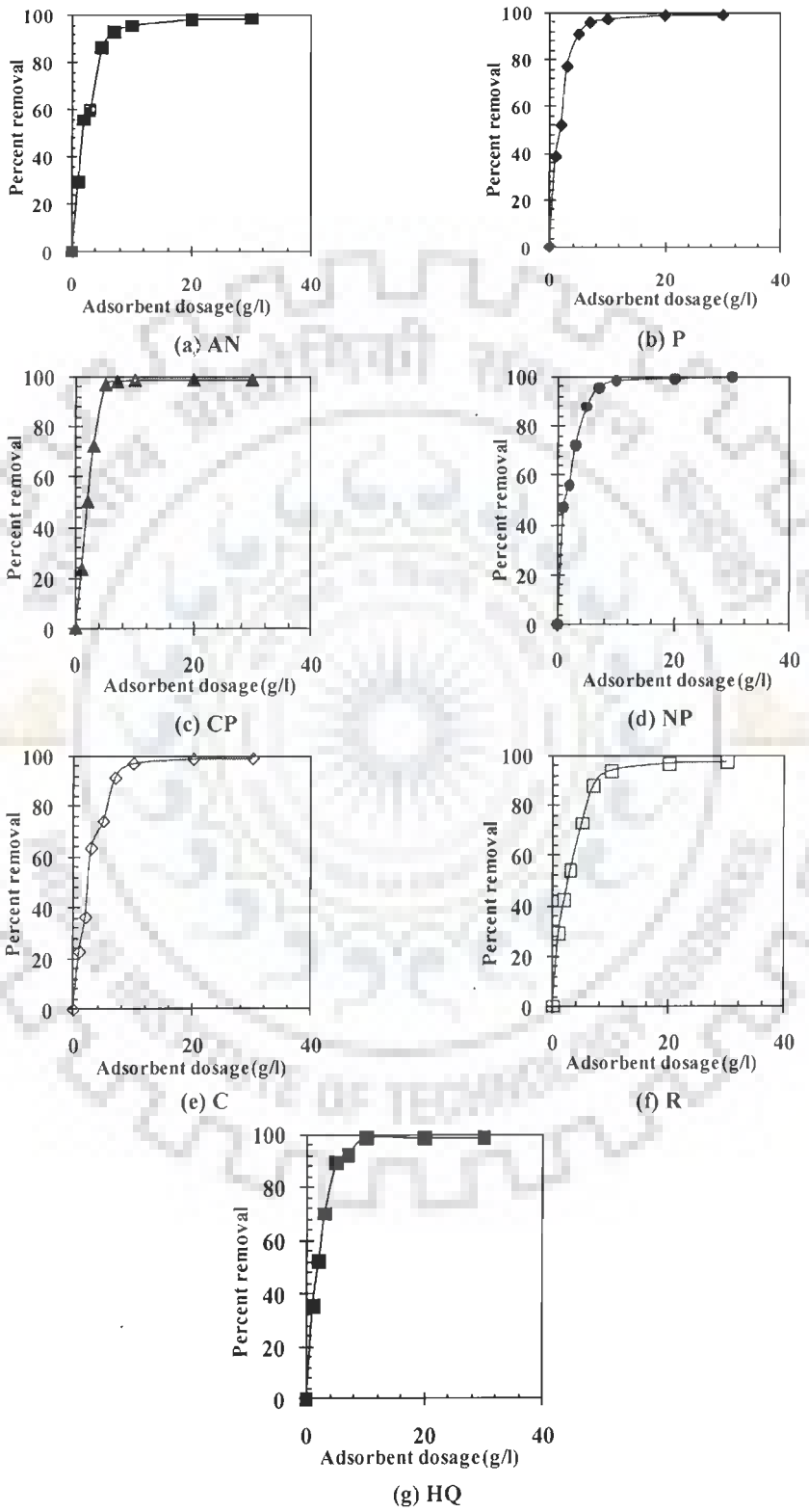

Figure 4.3.4. Effect of adsorbent dose on the adsorption of AN, P, CP, NP, C, R and HQ by GAC. T =303 K, t =24 h, C_o =0.91 mmol/l.

The rate of adsorbate removal by GAC is fast for first 1 h. This is obvious from the fact that a large number of vacant surface sites are available for the adsorption during the initial stage and with the passage of time, the remaining vacant surface sites were difficult to be occupied due to repulsive forces between the solute molecules on the solid phase and in the bulk liquid phase. Also, the adsorbates get adsorbed into the mesopores of GAC that get almost saturated during the initial stage of adsorption. Thereafter, the adsorbates have to traverse farther and deeper into the pores encountering much larger resistance. This results in the slowing down of the adsorption during the later period of adsorption.

Zheng et al. [2009] reported that the C_o provides an important driving to overcome all mass transfer resistances of the AN between the aqueous and solid phases. Hence, a higher initial concentration of AN will enhance the sorption process. AN adsorbed per unit mass of adsorbent increased from 1.96 to 17.89 mg/g as the AN concentration was increased from 20 to 200 mg/l. The equilibrium conditions were reached in about 15 min for low concentration (≤120 mg/l), while the rate of sorption was slower for concentration ranging from 160 to 200 mg/l (~30 min). When initial concentration of AN is 20 mg/l, maximum sorption efficiency on Cr-bentonite was attained as 97.80% at 30 °C. Li et al. [2008] found that the adsorption curves of 2-nitroaniline varying with contact time at four different temperatures had similar trends. The curves could be divided into three parts. In the first 25 min, almost 70% of the adsorption occurred at temperatures of 25, 35 and 45 °C, and 50% of the adsorption did at temperature of 15 °C. In the second part (25 min < t < 60min), the slopes became gentle as 20% adsorption occurred. In the third part (t > 60 min), the adsorption amount q_t was steady and the adsorption reached equilibrium. The slower adsorption at the end is probably due to the saturation of active sites and decrease of 2-nitroaniline concentrations [Li et al., 2008]. Akbal [2005] reported that an increase in initial P and CP concentration would increase the mass transfer driving force, and therefore, the rate at which P and CP molecules pass from the solution to the particle surface. This would result in higher P and CP adsorption. However, Banat et al. [2000] found that the percentage adsorption of P and CP decreased as C_o increased. Chen et al. [2009] studied the removal of NP and P from aqueous solution onto MgAl-mixed oxide. They found that it takes 10-12 h for adsorption of NP to reach the equilibrium at room temperature while the equilibrium time is 20-25 h for P adsorption. q_e increased with an increase of C_o.

The equilibration time reported in the literature for C and R adsorption onto various types of adsorbents vary appreciably. Sun et al. [2005] have reported equilibrium contact time of 80 min for the removal of C and R by various polymeric adsorbents. Shakir et al [2008] reported 6 h as equilibrium time for C adsorption onto bentonite. In comparison to these values, 12 h quasi-equilibrium contact time for C and R adsorption onto GAC in the present study is much higher. However, few authors have reported higher equilibrium contact time as compared to that reported in present paper. Bayram et al. [2009] reported 17 h and 25 h, respectively, as equilibrium contact time for C and R adsorption onto AC cloth. Kumar et al. [2003] reported equilibrium contact time of 24 h for C and R adsorption onto GAC. Richard et al. [2009] reported 35 h equilibrium time for C adsorption onto active charcoal. The difference in equilibrium contact time may be due the difference in adsorbent properties and C_o value used to study the effect of contact time.

The C_o provided the necessary driving force to overcome the resistance for mass transfer of AN, P, CP, NP, C, R and HQ between the aqueous phase and the solid phase. The increase in C_o also enhances the interaction between adsorbate molecules and the vacant sorption sites on the GAC and the surface functional groups. Therefore, an increase in C_o enhances the adsorption uptake of AN, P, CP, NP, C, R and HQ.

4.3.4 Adsorption kinetic study

Two kinetic models namely pseudo-first-order [Lagergren, 1898] and the pseudo-second-order model [Ho and McKay, 1999] were applied to kinetic data in order to investigate the adsorption behavior of AN, P, CP, NP, C, R and HQ onto GAC in the present study.

The adsorption of adsorbates from aqueous phase to the solid phase can be considered as a reversible process with equilibrium being established between the solution and the solid phase. Assuming non-dissociating molecular adsorption of adsorbates on GAC particles with no adsorbates initially present on the adsorbent, the uptake at any instant (t) is given as [Lagergren, 1898]

$$q_t = q_e\left[1-\exp\left(-k_f t\right)\right] \tag{4.3.8}$$

where, q_e = amount of the adsorbate adsorbed on the adsorbent under equilibrium condition and k_f is the pseudo-first order rate constant.

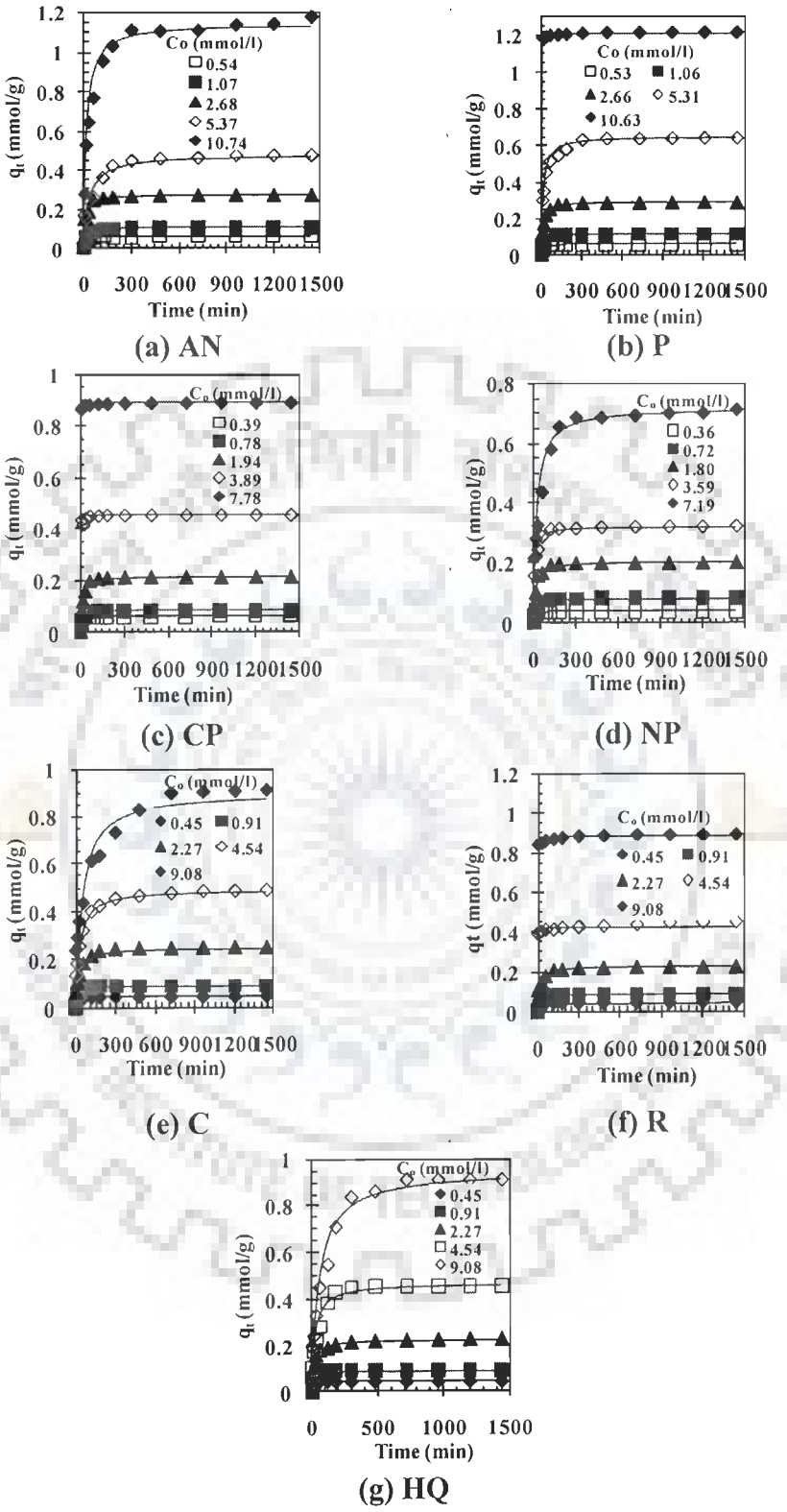

Figure 4.3.5. Effect of contact time and initial concentration on adsorption of various adsorbates by GAC. T=303 K, m=1 g/1. Experimantal data are given by data points whereas fitted line is due to pseudo-sencond order model.

The pseudo-second-order model is represented as: [Ho and McKay, 1999]

$$q_t = \frac{tk_S q_e^2}{1 + tk_S q_e} \tag{4.3.9}$$

The initial adsorption rate, h (mg/g min), at $t \rightarrow 0$ is defined as

$$h = k_S q_e^2 \tag{4.3.10}$$

The results of the fit of these models are given in Tables 4.3.1 through 4.3.4. The fit of experimental data to the pseudo first-order and the pseudo-second-order equations seemed to be quite good when correlation coefficients (R^2) obtained from non-linear regression analyses were examined. However, it was very difficult to decide which model represents the experimental data better, just on the basis of R^2. A better criterion to find the best model for the experimental data is MPSD parameter. It is known that the lower the MPSD value, the better is the fit. When the MPSD values given in Tables 4.3.1 through 4.3.4 are examined, it can be seen that they are much smaller for the pseudo-second-order model as compared to that for the pseudo-first-order model, leading to the conclusion that the kinetic data of adsorption of AN, P, CP, NP, C, R and HQ onto GAC fit to the pseudo-second order model better than the pseudo-first-order model. Similar conclusions were made by various researchers [Cotoruelo et al., 2007; Jianguo et al., 2005; Alzaydien and Manasreh, 2009; Hameed et al., 2008] for removal of AN, 4-methylaniline, and 4-nitroaniline and CP onto various types of AC. The fitting of pseudo-second order model is shown by lines in Fig. 4.3.5.

Table 4.3.1. Kinetic parameters for the removal of AN and P by GAC (t = 24 h, C_0 = 0.54-10.74; 0.53-10.63 mmol/l, m = 10 g/l, T = 303 K).

Equations	AN-GAC adsorption system					P-GAC adsorption system				
	0.54	1.07	2.68	5.37	10.74	0.53	1.06	2.66	5.31	10.63
Pseudo 1st order										
k_f (min^{-1})	0.0456	0.0465	0.0649	0.0255	0.0427	0.1214	0.0680	0.0601	0.0522	0.7792
$q_{e,cal}$ (mmol/g)	0.0594	0.1049	0.2599	0.4440	1.1112	0.0568	0.1109	0.2881	0.6399	1.2111
$q_{e,\exp}$ (mmol/g)	0.0599	0.1057	0.2748	0.4718	0.2748	0.0580	0.1119	0.2907	0.6436	1.2160
R^2 (non-linear)	0.9860	0.9921	0.9524	0.9566	0.9675	0.9791	0.9871	0.9847	0.9620	0.9996
MPSD	26.94	15.79	43.18	58.38	43.54	22.49	23.14	26.87	42.04	2.82
Pseudo 2nd order										
k_s (g/mmol.min)	1.9799	0.5523	0.2836	0.0589	0.0489	2.8506	1.3643	0.3330	0.1188	8.4584
h (mmol/g.min)	0.0072	0.0064	0.0219	0.0139	0.0645	0.0096	0.0172	0.0287	0.0501	12.3765
$q_{e,cal}$ (mmol/g)	0.0603	0.1078	0.2780	0.4854	1.1487	0.0581	0.1123	0.2937	0.6496	1.2110
R^2 (non-linear)	0.9893	0.9986	0.9747	0.9809	0.9929	0.9983	0.9971	0.9972	0.9856	0.9998
MPSD	17.16	12.29	24.13	38.13	19.13	5.74	7.53	10.18	21.82	2.41
Weber Morris										
K_{id1} (mmol/g. $min^{1/2}$)	0.0055	0.0081	0.0155	0.0273	0.0596	0.0049	0.0067	0.0251	0.0143	0.0013
I_1	0.0116	0.0169	0.0998	0.0572	0.3037	0.0175	0.0429	0.2739	0.1292	1.1947
R^2	0.9163	0.8752	0.8956	0.9358	0.9978	0.9533	0.8925	0.9011	0.9227	0.9581
K_{id2} (mmol/g. $min^{1/2}$)	0.00008	0.0002	0.0002	0.0014	0.0032	0.00007	0.0002	0.0005	0.0002	0.0002
I_2	0.0572	0.0991	0.2685	0.4217	1.0431	0.0554	0.2843	0.6257	0.2843	1.2122
R^2	0.7614	0.6151	0.9035	0.9231	0.7773	0.869	0.7309	0.7585	0.7309	0.6982

Table 4.3.2. Kinetic parameters for the removal of CP and NP by GAC (t = 24 h, C_0 = 0.39-7.78; 0.36-7.19 mmol/l, m = 10 g/l, T = 303 K).

Equations	CP-GAC adsorption system					NP-GAC adsorption system				
	0.39	0.78	1.94	3.89	7.78	0.36	0.72	1.80	3.59	7.19
Pseudo 1st order										
k_f (min^{-1})	0.1158	0.0752	0.0555	0.6498	0.7462	0.1298	0.0584	0.0495	0.1355	0.0212
$q_{e,cal}$ (mmol/g)	0.0599	0.0800	0.2113	0.4545	0.8889	0.0368	0.0793	0.1952	0.3115	0.6876
$q_{e,\exp}$ (mmol/g)	0.0605	0.0804	0.2125	0.4552	0.2125	0.0371	0.0796	0.1973	0.3199	0.1973
R^2 (non-linear)	0.9421	0.9831	0.9945	0.9963	0.9998	0.9885	0.9956	0.9952	0.9667	0.9815
MPSD	23.00	21.06	17.55	5.27	1.77	15.02	16.25	17.26	26.96	50.64
Pseudo 2nd order										
k_s (g/mmol.min)	12.0762	2.3940	0.4796	10.7915	8.9857	4.7908	1.1609	0.3068	0.4513	0.0594
h (mmol/g.min)	0.0441	0.0156	0.0221	2.2303	7.1063	0.0066	0.0075	0.0125	0.0459	0.0305
$q_{e,cal}$ (mmol/g)	0.0604	0.0808	0.2145	0.4546	0.8893	0.0372	0.0806	0.2018	0.3190	0.7167
R^2 (non-linear)	0.9935	0.9941	0.9965	0.9974	0.9999	0.9990	0.9982	0.9931	0.9962	0.9845
MPSD	9.34	10.82	10.87	4.29	1.18	4.57	6.87	10.53	9.96	36.07
Weber Morris										
K_{id1} (mmol/g. $min^{1/2}$)	0.002	0.0045	0.002	0.0046	0.0015	0.0003	0.0055	0.0114	0.0132	0.0409
I_1	0.0425	0.0356	0.0425	0.4082	0.8697	0.0131	0.0233	0.0711	0.17	0.1168
R^2	0.9837	0.862	0.9837	0.7122	0.7732	0.8758	0.8286	0.8147	0.9634	0.9958
K_{id2} (mmol/g.$min^{1/2}$)	0.00004	0.00002	0.00007	0.00004	0.0002	0.00002	0.00009	0.0001	0.0003	0.0013
I_2	0.059	0.0795	0.2098	0.4528	0.8863	0.0363	0.0764	0.1926	0.3062	0.6610
R^2	0.9686	0.8355	0.8406	0.9431	0.9868	0.8904	0.7726	0.741	0.9197	0.9116

Table 4.3.3. Kinetic parameters for the removal of C and R by GAC (t=24.0 h, C_o=0.45-9.08 mmol/l, m=10 g/l, T=303 K).

Equations	C-GAC adsorption system					R-GAC adsorption system				
	0.45 mmol/l	1.06 mmol/l	2.78 mmol/l	4.78 mmol/l	9.08 mmol/l	0.45 mmol/l	1.06 mmol/l	2.78 mmol/l	4.78 mmol/l	9.08 mmol/l
Pseudo 1st order										
k_f (1/min)	0.061	0.0697	0.0364	0.0383	0.8980	0.0447	0.0342	0.0362	0.5106	0.7733
$q_{e,cal}$ (mmol/g)	0.0457	0.0862	0.2417	0.4604	0.0111	0.0425	0.0830	0.2352	0.4846	1.0141
$q_{e,\exp}$ (mmol/g)	0.047	0.087	0.245	0.482	0.912	0.044	0.084	0.238	0.513	1.033
R^2 (non-linear)	0.9821	0.9742	0.9663	0.9525	0.9448	0.9920	0.9821	0.9332	0.9821	0.9960
MPSD	21.40	20.51	37.46	46.94	83.50	17.64	33.17	42.03	14.35	7.47
Pseudo 2nd order										
k_s (g/ mmol min)	2.6019	1.8743	0.1887	0.0774	0.0243	1.8539	0.6558	0.2891	4.7945	3.8657
h (mmol/g min)	0.0056	0.0142	0.0157	0.0185	0.0199	0.0036	0.0047	0.0168	1.1291	4.0573
$q_{e,cal}$ (mmol/g)	0.0465	0.0871	0.2494	0.4884	0.9056	0.0438	0.0851	0.2412	0.4853	1.0245
R^2 (non-linear)	0.9940	0.9880	0.9920	0.9921	0.9584	0.9920	0.9702	0.9643	0.9860	0.9980
MPSD	9.32	11.37	18.42	20.35	56.12	12.71	34.64	22.00	12.30	5.28
Weber-Morris										
K_{id1} (mmol/g min$^{1/2}$)	0.0043	0.0052	0.0150	0.0269	0.0344	0.0047	0.0075	0.0108	0.0026	0.0033
I_1	0.0093	0.0343	0.0444	0.0860	0.1723	0.0027	0.0059	0.0924	0.4446	0.9684
R^2	0.9584	0.00739	0.9293	0.9332	0.9487	0.9702	0.7868	0.8949	0.8537	0.9781
K_{id2} (mmol/g min$^{1/2}$)	0.00005	0.00003	0.0003	0.0016	0.0047	0.00006	0.0002	0.0003	0.0015	0.0003
I_2	0.0445	0.0856	0.2353	0.4245	0.7468	0.0413	0.0774	0.2292	0.4584	1.0228
R^2	0.8668	0.6988	0.8409	0.8574	0.5013	0.8668	0.5270	0.8612	0.9101	0.8779

Table 4.3.4. Kinetic parameters for the removal of HQ by GAC (t = 24.0 h, C_o = 0.45-9.08 mmol/l, m = 10 g/l, T = 303 K).

Equations	0.45 mmol/l	1.06 mmol/l	2.78 mmol/l	4.78 mmol/l	9.08 mmol/l
Pseudo 1st order					
k_f (1/min)	0.2243	0.0342	0.0346	0.0225	0.0113
$q_{e,cal}$ (mmol/g)	0.0449	0.0910	0.2132	0.4528	0.9074
$q_{e,\exp}$ (mmol/g)	0.0450	0.0907	0.2234	0.4534	0.2234
R^2 (non-linear)	0.9778	0.9304	0.9875	0.9882	0.9853
MPSD	15.59	59.36	32.74	42.69	68.22
Pseudo 2nd order					
k_s (g/ mmol.min)	9.0334	2.3715	0.2619	0.0865	0.0185
h (mmol/g min)	0.0184	0.0197	0.0130	0.0187	0.0167
$q_{e,cal}$ (mmol/g)	0.0451	0.0911	0.2231	0.4649	0.9504
R^2 (non-linear)	0.9946	0.9949	0.9946	0.9920	0.9900
MPSD	7.17	9.79	16.65	26.26	43.83
Weber Morris					
K_{id1} (mmol/g min$^{1/2}$)	0.0026	0.0048	0.0226	0.029	0.0456
I_1	0.0249	0.0453	0.0117	0.0543	0.0778
R^2	0.9638	0.771	0.8413	0.9909	0.99
K_{id2} (mmol/g min$^{1/2}$)	1E-05	3E-05	0.0006	0.0002	0.0037
I_2	0.0446	0.0897	0.2002	0.4468	0.7824
R^2	0.7127	0.9645	0.9756	0.8045	0.7753

4.3.5 Adsorption Diffusion Study

It is well established that adsorption of an adsorbate from the aqueous phase onto an adsorbent involves broadly following basic steps: (1) transport of the adsorbate from the bulk of the solution to the exterior surface of the liquid film surround the adsorbent particle (external transport), (2) transport across the film to the exterior surface of the adsorbent (film diffusion), (3) the transport of the adsorbate within the adsorbent either by pore diffusion and/or by surface diffusion, and (4) the adsorption onto the surface of the adsorbent.

The overall adsorption process may be controlled either by one or more steps, e.g. film or external diffusion, pore diffusion, surface diffusion and adsorption on the pore surface, or a combination of more than one step. In a rapidly stirred batch adsorption process, the first and fourth of the above steps are considered to be fast enough [Weber, 1972], thereby rendering the other two responsible for determining the overall rate of adsorption. Either one or both of these two steps can be rate controlling. The rate of uptake is limited by several characteristics of the adsorbate, adsorbent and the solution phase. Particle size of the adsorbent, concentration of the adsorbate, diffusion coefficient of the adsorbate in the bulk phase and the pores of the adsorbent, affinity towards adsorbent and degree of mixing are some of the important factors [Kumar et al., 2003]. For adsorption process, the external mass transfer controls the sorption process for the systems that have poor mixing, dilute concentration of adsorbate, small particle sizes of adsorbent and higher affinity of adsorbate for adsorbent. Whereas, the intra- particle diffusion controls the adsorption process for a system with good mixing, large particle sizes of adsorbent, high concentration of adsorbate and low affinity of adsorbate for adsorbent [Aravindhan et al., 2007].

In the present study, experiments were conducted at well-mixed condition for AN, P, CP, NP, C, R and HQ adsorption onto GAC. In general, external mass transfer is characterized by the initial solute uptake [McKay et al., 1981] and can be calculated from the slope of plot between C/C_o versus time. The slope of these plots can be calculated either by assuming polynomial relation between C/C_o and time or it can be calculated based on the assumption that the relationship was linear for the first initial rapid phase (in the present study first 30 min).

In the present study, the second technique was used by assuming the external mass transfer occurs in the first 30 min. The initial adsorption rates (K_S) (min^{-1}) were quantified as (C_{30min}/C_0)/30. For AN adsorption onto GAC, the calculated K_S values were found to be 0.00722, 0.0103, 0.01139, 0.0168 and 0.0185 min^{-1} for C_o values of 0.54, 1.07, 2.68, 5.37 and 10.74 mmol/l, respectively. For P adsorption onto GAC, the calculated K_S values were found to be 0.0069, 0.0076, 0.0096, 0.01028 and 0.00075 min^{-1} for C_o values of 0.53, 1.06, 2.66, 5.31 and 10.63 mmol/l, respectively. For CP adsorption onto GAC, the calculated K_S values were found to be 0.0038, 0.0072, 0.0089, 0.00357 and 0.00045 min^{-1} for C_o values of 0.39, 0.78, 1.94, 3.89 and 7.78 mmol/l, respectively. For NP adsorption onto GAC, the calculated K_S values were found to be 0.0040, 0.0067, 0.0075, 0.00908 and 0.01866 min^{-1} for C_o values of 0.36, 0.72, 1.80, 3.59 and 7.19 mmol/l, respectively. For C adsorption onto GAC, the calculated K_S values were found to be 0.0092, 0.0079, 0.0155, 0.0161 and 0.021 min^{-1} for C_o values of 0.45, 0.91, 2.27, 4.54 and 9.08 mmol/l, respectively. The respective values for R adsorption were 0.011, 0.013, 0.012, 0.0042 and 0.0021 min^{-1}.

In the present study because of use of well-mixed condition, it is expected that the rate of uptake would be governed by the intraparticle or surface diffusion transport. The possibility of intra-particle diffusion was explored by using the intra-particle diffusion model [Weber and Morris, 1963].

$$q_t = k_{id} t^{1/2} + I \tag{4.3.11}$$

where, k_{id} is the intra-particle diffusion rate constant, and values of I give an idea about the thickness of the boundary layer. If the plot of q_t versus $t^{0.5}$ satisfies the linear relationship with the experimental data, then the sorption process is supposed be controlled by intra-particle diffusion only. However, if the data exhibit multi-linear plots, then two or more steps influence the sorption process.

Fig. 4.3.6 presents the plots of q_t versus $t^{0.5}$ for all the adsorbates and the parametric values are given in Tables 4.3.1 through 4.3.4. In this figure, the data points are related by two straight lines. The curvature from the origin to the start of the first straight portion (not shown in figure) represents the boundary layer diffusion and/or external mass transfer effects [Crank, 1965; McKay et al., 1980]. The first straight portion depicts

macro-pore diffusion and the second represents meso-pore diffusion. These show only the pore diffusion data. Extrapolation of the linear portions of the plots back to the y-axis gives the intercepts which provide the measure of the boundary or film layer thickness. The first linear portion is attributed to the gradual equilibrium stage with intra-particle diffusion dominating. The second portion is the final equilibrium stage for which the intra-particle diffusion starts to slowdown due to the extremely low adsorbate concentration left in the solution [Reichenberg, 1953; Crank, 1965]. The deviation of straight lines from the origin indicates that the pore diffusion is not the sole rate-controlling step. Therefore, the adsorption proceeds via a complex mechanism [Chaturvedi et al., 1988] consisting of both surface adsorption and intra-particle transport within the pores of GAC. It can be inferred from the Fig. 4.3.6 that the diffusion of adsorbates from the bulk phase to the external surface of GAC, which begins at the start of the adsorption process, is the fastest. The slope of the linear portions are defined as a rate parameters ($k_{id,1}$ and $k_{id,2}$) and are characteristics of the rate of adsorption in the region where intra-particle diffusion is rate controlling.

It seems that the intra-particle diffusion of adsorbates into meso-pores (second linear portion) is the rate-controlling step in the adsorption process. The portion of the plots are nearly parallel ($k_{id,2} \approx$ 0.00008–0.0032 mg/g $min^{0.5}$ for AN, 0.00007–0.0032 mg/g $min^{0.5}$ for P, 0.00002–0.0002 mg/g $min^{0.5}$ for CP, 0.00002–0.0013 mg/g $min^{0.5}$ for NP, 0.001–0.013 mg/g $min^{0.5}$ for C and R, 0.00005–0.0037 mmol/g. $min^{0.5}$ for HQ), suggesting that the rate of adsorption AN, P, CP, NP, C, R and HQ into the meso-pores of GAC is comparable at all C_o. Slopes of first portions ($k_{id,1}$) are higher for higher C_o for which corresponds to an enhanced diffusion of adsorbates through macro-pores. This is due to the greater driving force at higher C_o.

The multi-phasic nature of intra-particle diffusion plot confirms the presence of both surface and pore diffusion. In order to predict the actual slow step involved, the kinetic data were further analysed using Boyd kinetic expression which is given by [Boyd et al., 1947; Skelland, 1974]:

$$F = 1 - \frac{6}{\pi^2}\exp(-B_t) \text{ or } B_t = -0.4977 - \ln(1-F) \qquad (4.3.12)$$

where, $F(t) = q_t/q_e$ is the fractional attainment of equilibrium at time t, and B_t is a mathematical function of F. Above Eq. was used to calculate B_t values at different time t. The linearity of the plot of B_t versus time was used to distinguish whether surface

and intra-particle transport controls the adsorption rate. It was observed that the relation between B_t and t (not shown here) was non-linear (R^2 = 0.828–0.991 for AN, 0.900–0.999 for P, 0.796–0.959 for CP, 0.764–0.994 for NP, 0.599–0.974 for C, and R^2 = 0.637–0.897 for R) at all concentrations, confirming that surface diffusion is the not the sole rate-limiting step. Thus, both surface and pore diffusion seem to be the rate-limiting step in the adsorption process and the adsorption proceeds via a complex mechanism.

Applying Vermeulen's approximation [Vermeulen, 1953] to the solution of the simultaneous set of differential and algebric equations [Reichenberg, 1953] leads to the calculation of effective particle diffusivity by following eq.:

$$\ln\left[\frac{1}{(1-F^2(t))}\right] = \frac{\pi^2 D_e t}{R_a^2} \tag{4.3.13}$$

where, D_e is the effective diffusion coefficient of adsorbate in the solid phase (m^2/s), R_a is radius of the adsorbent particle assumed to be spherical (m), and t is the time (min). Thus, the slope of the plot of $\ln[1/(1-F^2(t))]$ versus t gives the value of D_e. The values of effective diffusion coefficient (D_e) as calculated from Eq. (4.3.6). Average values of D_e were found to be 2.24×10^{-10}, 2.43×10^{-10}, 3.65×10^{-10}, 2.89×10^{-10}, 2.94×10^{-10}, 2.24×10^{-10} and 3.19×10^{-10} m^2/s, respectively, for the adsorption of AN, P, CP, NP, C, R and HQ onto GAC. This shows that CP has little higher overall pore diffusion rate. Similar average values of D_e (0.388×10^{-10}) were reported by Srivastava et al. [2006] for adsorption of P onto AC.

4.3.6 Effect of temperature

Fig. 4.3.7 show the plots of adsorption isotherms, q_e versus C_e, for AN, P, CP, NP, C, R and HQ adsorption onto GAC at three different temperatures 288, 303 and 318 K. It is found that the adsorption of all the adsorbates increases with an increase in temperature. The adsorptive uptake, q_e rises sharply at a low C_e value and then the rise in q_e is gradual with an increase in C_e. When the temperature of the adsorption system was increased from 288 K to 318 K. q_e increases from 1.29 to 2.15 mmol/g (for AN), 1.40 to 1.51 mmol/g (for P), 1.4 to 1.8 mmol/g (for CP), 1.21 to 1.35 mmol/g (for NP), 1.09 to 1.41 mmol/g (for C), 1.21 to 1.27 mmol/g (for R) and 0.94 to 1.23 mmol/g (for HQ). It

may be seen that the effect of temperature is most pronounced for AN, where ~ 67% increase in equilibrium uptake q_e has been observed.

Many investigators have given different reasons for endothermic nature of adsorption of phenolics onto ACs. An increase in temperature increases the chemical potential of the organic molecules to penetrate to the surface of GAC and thereby increasing the possibility of bonding between the dsorbates and the functional groups present on the adsorption sites of GAC. Also, adsorption processes which are diffusion (intraparticle transport-pore diffusion) controlled show an increase in adsorption capacity increase with an increase in temperature due to the endothermicity of the diffusion process. This is due to the increased mobility of the adsorbate and decreased retarding forces acting on the diffusing at higher temperature. These result in the enhancement in the adsorptive capacity of the GAC [Srivastava et al., 2006]. However, the diffusion of the AN, P, CP, NP, C, R and HQ into the pores of the adsorbent is not the only rate-controlling step (details not given here), and the diffusion resistance can be ignored with adequate contact time. Therefore, the increase in adsorptive uptake of the AN, P, CP, NP, C, R and HQ with an increase in temperature can be attributed to chemisorption [Namasivayam and Sumithra, 2004]. In later studies, it is shown that the desorption of AN, P, CP, NP, C, R and HQ from the spent (loaded) GAC using various solvents (acids, bases and water) is not significant confirming chemisorptive nature of the adsorption process. These together results in the enhancement in the adsorptive capacity of the GAC at higher temperatures. An increase in the P adsorption capacity of the carbonaceous adsorbents with an increase in temperature has also been reported by other investigators [Banat et al., 2000; Vijayalakshmi et al., 1998].

A rise in adsorption temperature weakens the hydrogen bonds formed among water molecules and between water molecules and the adsorbate or adsorbent [Costa et al., 1988] and enhances the pore diffusion [Garcia-Araya et al., 2003; Terzyk, 2004]. Therefore, an increase in temperature favors dehydration of the adsorbate molecules, which makes them more planar and gives them a larger dipolar moment. The increase in planarity provides the adsorbate molecules greater access to the pores of the GAC, while increase in dipolar moment leads to enhanced adsorbent–adsorbate interactions. As a result of this process, the adsorption is apparently endothermic due to the endothermicity of the dehydration of adsorbates molecules.

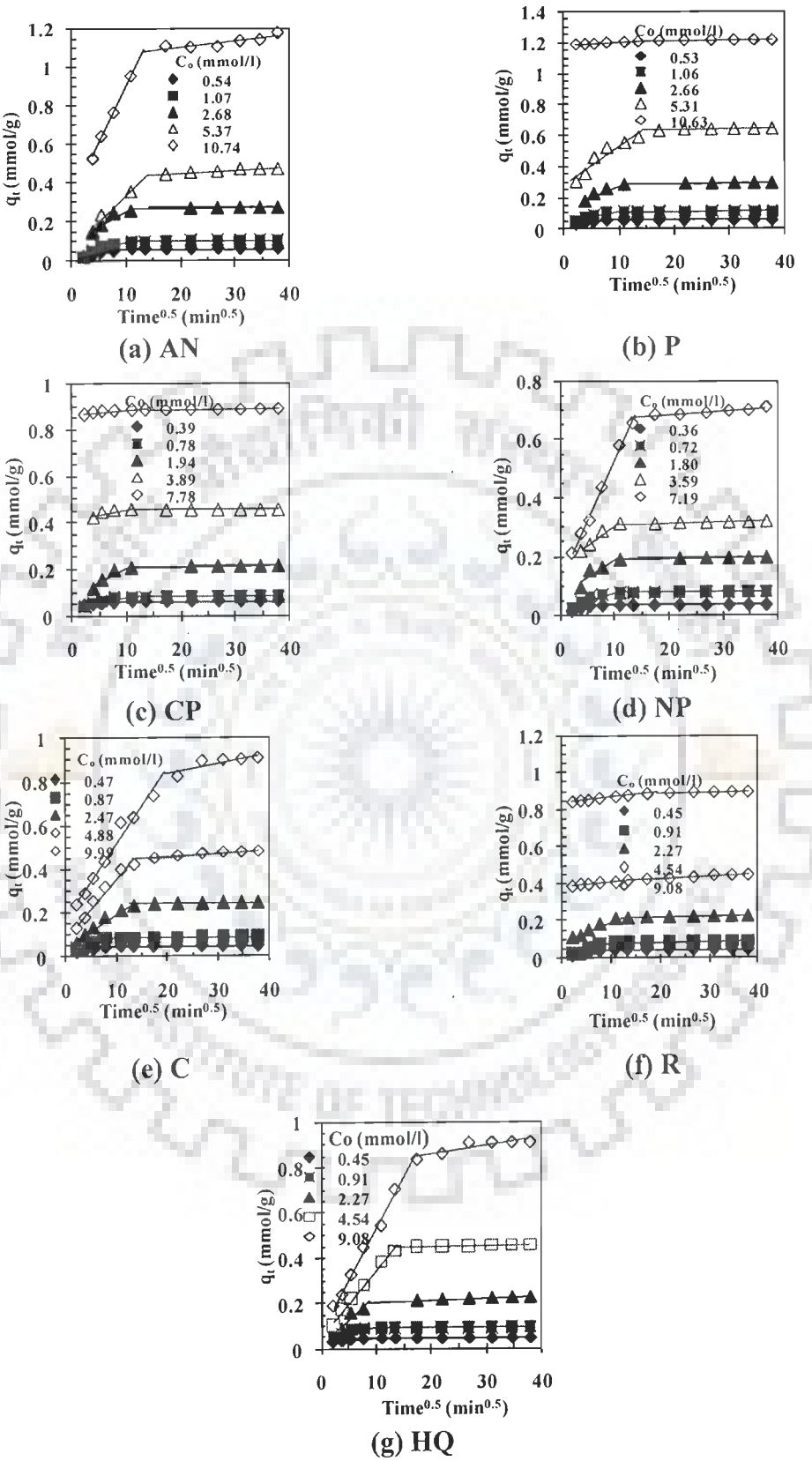

Figure 4.3.6. Weber and Morris intra-particle diffusion plot for the removal of AN, P, CP, NP, C, R and HQ by GAC. T =303 K, m =10 g/l.

4.3.7 Adsorption isotherm modeling

The experimental equilibrium adsorption data of AN, P, CP, NP, C, R and HQ adsorption onto GAC have been tested by using the two-parameter Freundlich [Freundlich, 1906], Langmuir [Langmuir, 1918], Tempkin [Tempkin and Pyzhev, 1940] and the three parameter Redlich-Peterson (R-P) [Redlich, and Peterson, 1959] equation. The following equations represent these isotherms:

Freundlich $$q_e = K_F C_e^{1/n} \quad (4.3.14)$$

Langmuir $$q_e = \frac{q_m K_L C_e}{1 + K_L C_e} \quad (4.3.15)$$

Tempkin $$q_e = B_T \ln K_T + B_T \ln C_e \quad (4.3.16)$$

Redlich-Peterson $$q_e = \frac{K_R C_e}{1 + a_R C_e^{\beta}} \quad (4.3.17)$$

where, K_F is the Freundlich constant (l/mg), $(1/n)$ is the heterogeneity factor, K_L is the Langmuir adsorption constant (l/mg) related to the energy of adsorption, q_m signifies the adsorption capacity (mg/g), B_T is Tempkin constant related to the heat of adsorption, K_T is the equilibrium binding constant (l/mol) corresponding to the maximum binding energy.K_R is R–P isotherm constant (l/g), a_R is R–P isotherm constant (l/mg) and β is the exponent which lies between 0 and 1.

The Freundlich isotherm is valid for a heterogeneous adsorbent surface with a non-uniform distribution of heat of adsorption over the surface. The Langmuir isotherm, however, assumes that the sorption takes place at specific homogeneous sites within the adsorbent. The R-P isotherm can, however, be applied in homogenous as well as heterogeneous systems.

The Langmuir, Freundlich, Tempkin and R-P isotherm parameters along with coefficient of determination (R^2) and SSE values for the fit of the equilibrium adsorption data of various adsorbates onto GAC at various temperatures are given in Tables 4.3.5 through 4.3.8. The R^2 values alone are not sufficient in determining the best isotherm model to represent the experimental data because they are generally found to be > 0.9 for all the models. The SSE values are smaller for R-P for AN-, NP- and R-GAC system, while Tempkin model gives smaller values for P-, CP-, R- and HQ-GAC systems as

comparison to other models. Therefore, it can be concluded that Tempkin model is the best among the four models for representing the adsorption isotherm data of the P, CP, R and HQ on GAC, while R-P model is the best among the five models for representing the adsorption isotherm data of the AN-, NP- and R-GAC systems.

In general, $1/n$ and K_F values of the Freundlich model are measures the surface heterogeneity and adsorption capacity of the adsorbate. When the value of $1/n$ is less than 1, then the adsorption process is favorable. The values of $1/n$ obtained are all less than 1 indicating favourable adsorption.

The q_{max} value of the Langmuir model is the most important parameter because this measures the solute adsorption capacity of GAC. These values are given in Tables 4.3.5 through 4.3.8. By comparing the results for adsorption of capacity of GAC for C or R or HQ (Table 4.3.7), it is seen that q_{max} value is clearly greater for C at higher temperature (318 K) whereas, it is greater for R at lower temperature (288 and 303 K). The q_{max} value of HQ is lowest at all temperatures. Thus, it is difficult to establish a relation between the chemical structure of C and R which are similar types of compound and their adsorption behaviour onto GAC. The amount of C and R adsorbed onto GAC depends on many factors including the size of the substrate molecule. In this regard, C tends be larger than the R thus leading to a higher adsorption capacity of R at lower temperature. Similar trend was reported by Garcia-Araya et al. [2003] for the adsorption of gallic, syringic and p-hydroxy benzoic acids onto an active charcoal. They argued that at higher temperature, the discrepancy observed between the expected order and the one observed for adsorption of compound of similar size may be due to differences in solubility rather than to differences in chemical structure. The q_{max} value of C is higher than R at higher temperature (318 K). It may be related to planarity of C and R molecules. Reasons have been explained in the previous section. Huang et al. [2009] found that the adsorption capacity of C is a little larger than R at the same temperature and equilibrium concentration. This different absorbability was explained in terms of the solubility and the polarity of two adsorbates [Sun et al., 2005]. The solubility of R in water is larger than that of R (110 and 43 g/100 ml H_2O at 298 K for C and R, respectively), thus it shows stronger affinity towards water. This may be one of the reasons for its smaller adsorption capacity.

That is, hydrophobic interaction may be one of the driving forces. In addition, the matching of the polarity between the adsorbent and the adsorbate is also an important factor affecting the adsorption. The formation of hydrogen bonds between solute and solvent, favored at low temperatures, can modify the shape and size of solute molecules such that they cannot access the micropores of the adsorbent. In addition, temperature variations may possibly affect the equilibrium among different conformers when a solute has various molecular conformations, which could affect solute uptake on the adsorbent [Sun et al., 2005].

A comparison of isotherm parameters and isotherm plots shows that the adsorption of P is greater than that of AN at 288 and 303 K while AN adsorption gets enhanced gets more adsorbed at 318 K. Higher adsorption of P at lower temperature may be due the lower intrinsic molar volume (V_l) of P (5.36 cm^3/mol) than that of AN (5.67 cm^3 /mol). The solubility of AN (34 g/l) is lower than that of P (83 g/l). At lower temperature, adsorption behavior seem not to be affected by solubility factor, however, at higher temperature higher adsorption of AN may be due to its lower solubility.

The main contributions to adsorption of organics onto GAC are π- π dispersion [Coughlin and Ezra, 1968], hydrogen-boding interactions [Franz et al., 2000] and donor-acceptor interactions [Mattson et al., 1969]. Isothermal experiments were conducted at pH values of 7, 6, 5.75 and 6 for AN, P, CP and NP, respectively. At any solution pH, organic acids and organic bases will be either in their non-dissociated or in dissociated forms. This depends on their dissociated constant (pK_a). For pH< pK_a, organic bases (like AN) for cationic (dissociation) species by protonation whereas organic acids (like P) are in non-dissociated form. For pH > pK_a, organic bases are predominately in non-dissociated neutral form whereas organic acids form anionic (dissociated) species [Yang et al., 2008]. The pK_a value of AN, P, CP and NP are 4.63, 9.95, 9.38 and 7.15, respectively. Considering the dissociation reactions of all the solutes as given in section 4.3.1.1, it is found that all the adsorbates are in neutral form at any temperature and that the electrostatic attraction/repulsion between adsorbates and the adsorbent is ruled out. The GAC surface is considered to be highly prolarizable and amphoteric in nature. It attracts π-acceptors to the electron rich graphene surface area near edges and π-donors to the

electron-deficient central regions [Zhu and Pignatello, 2005]. Generally, π- π interactions depend on the size and shape of the aromatic system and the substitution unit [Cockroft et al., 2007; Hunter et al., 1992]. A number of studies have shown that both electron withdrawing (e.g., $-NO_2$ and –Cl) and electron-donating (e.g., $-NH_2$ and –OH) substituents on benzene can increase aromatic organic compounds onto GAC. The electronic effects of substituents on benzene type adsorbates are usually examined with substituent constants developed by Hammett from reaction studies [Hammett, 1937]. The values of Hammett constant (σ) for –Cl and $-NO_2$ groups for substitution phenolic compounds are 0.23 and 1.25, respectively. Thus, it seems that the substitution of P by more electron-withdrawing $-NO_2$ group results in an increase in its adsorption onto GAC.

Comparison of q_{max} values (mmol/g) shows the q_{max} values in the following order: P>CP>NP. This trend may be attributed to the lower values of V_l for P (5.36 cm^3 /mol) than that of CP (6.25 cm^3 /mol) and NP (6.85 cm^3 /mol) and to the size exclusion (steric) effect. Larger molecular size of NP and CP cause them to occupy more area on the GAC surface resulting in lower q_{max} values in mmol/g units [Furuya et al., 1997; Pan et al., 2005]. However, the q_{max} values in mg/g follow the trend NP>CP>P. This trend is similar to that of K_D (adsorption coefficient). Table 4.3.9 shows the values of K_D as determined by procedure adopted by Srivastava et al. [2007] for all adsorbate-GAC systems. K_D represents the partition coefficient of adsorbate between the solution and the adsorbed phases at infinite dilution [Kamlet et al., 1988]. A close look at the K_D values shows that its values follows the trend NP>CP>P>AN at all temperatures. Variation of dipole moment (D) for P, CP and NP are given in Table 1.2.1. A high correlation between K_D values (for P, CP and NP) and σ and D is observed. It may, thus, be inferred that the substitution of more electron-withdrawing group onto P increases its K_D values. Also, the adsorbate having higher D value gets easily adsorbed onto GAC.

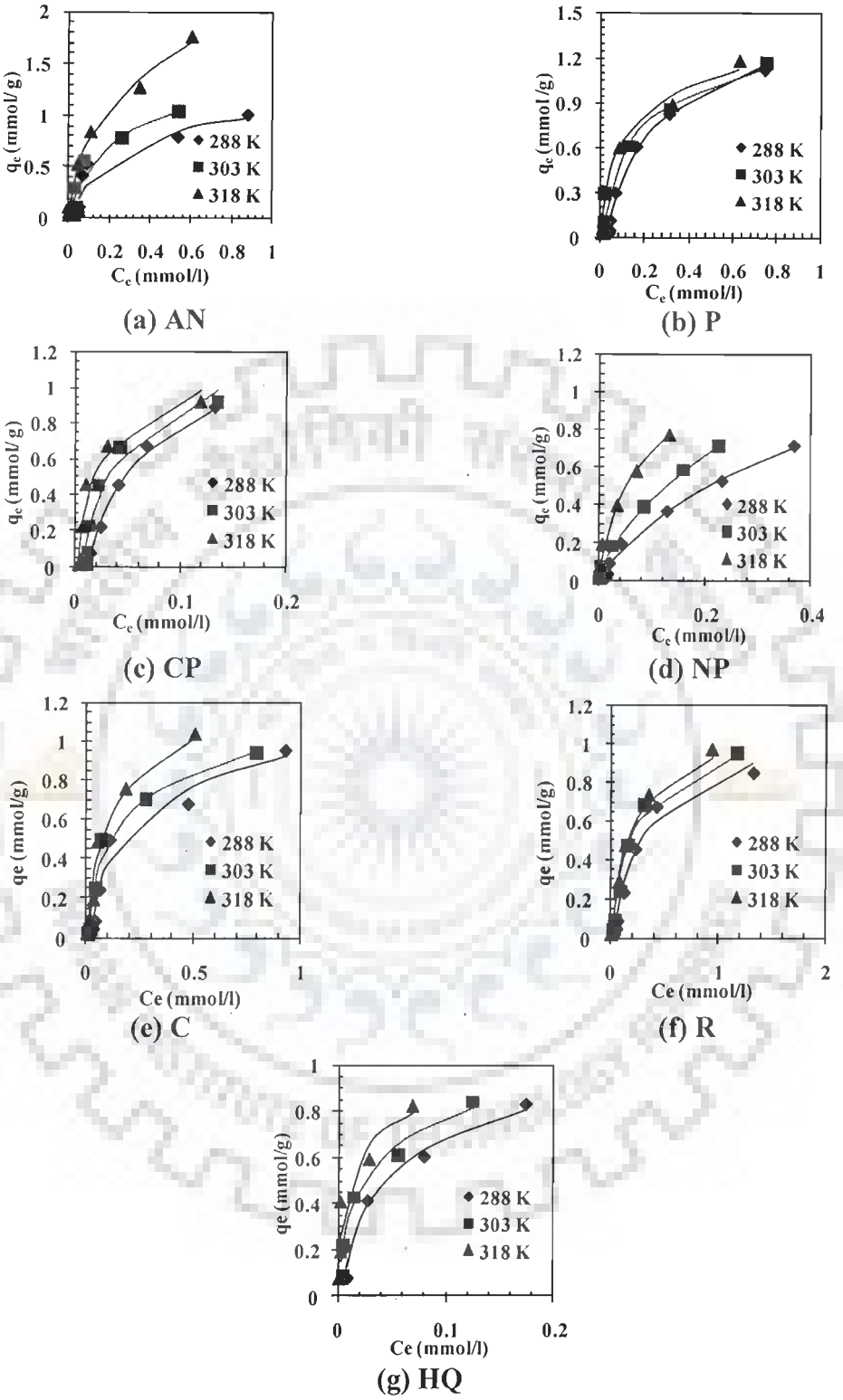

Figure 4.3.7. Equilibrium adsorption isotherms at different temperature. (a) AN-GAC system, lines fitted by R-P model; (b) P-GAC system, lines fitted by Tempkin model; (c) CP-GAC system, lines fitted by Tempkin model; and; (d) NP-GAC system, lines fitted by R-P model; (e) C-GAC system, lines fitted by Tempkin model; (f) R-GAC system, lines fitted by R-P model; and (g) HQ-GAC system lines predicted by Tempkin equation.

Table 4.3.5. Isotherm parameters for the adsorption of AN and P onto GAC at different temperature (t = 24 h, m = 10 g/l).

	AN-GAC					P-GAC				
Freundlich										
Temp. (K)	K_F [(mmol/g)/(mmol/l)$^{1/n}$]	$1/n$		R^2	SSE	K_F [(mmol/ g)/(mmol/ l)$^{1/n}$]]	$1/n$		R^2	SSE
288	1.11	0.569		0.829	0.1540	1.350	0.617		0.914	0.1211
303	1.58	0.603		0.868	0.1272	1.436	0.537		0.933	0.0838
318	2.22	0.4821		0.992	0.0280	1.499	0.467		0.961	0.0539
Langmuir										
Temp. (K)	q_m (mmol/g)	K_L (l/mmol)		R^2	SSE	q_m (mmol/ g)	K_L (l/ mmol)		R^2	SSE
288	1.29	3.51		0.854	0.1338	1.49	3.2757		0.974	0.0757
303	1.48	4.44		0.901	0.0965	1.50	4.5539		0.964	0.0425
318	2.15	5.58		0.984	0.0479	1.51	5.9323		0.966	0.0457
Tempkin										
Temp. (K)	K_T (l/mmol)	B_T (mmol/g)		R^2	SSE	K_T (l/mmol)	B_T		R^2	SSE
288	32.31	0.300		0.889	0.0986	26.35	0.3892		0.994	0.0073
303	49.15	0.318		0.923	0.0720	63.05	0.2939		0.971	0.0362
313	400.17	0.262		0.890	0.3012	120.27	0.2605		0.986	0.0165
R-P										
Temp. (K)	K_R (l/g)	a_R (l/mmol)	β	R^2	SSE	K_R (l/g)	a_R (l/mmol)	β	R^2	SSE
288	4.53	3.51	0.999	0.854	0.1338	4.17	2.261	0.999	0.958	0.0616
303	6.55	4.43	0.999	0.901	0.0965	6.94	4.660	0.999	0.965	0.0425
318	29.29	12.92	0.649	0.991	0.0245	13.38	9.478	0.869	0.974	0.0336

Table 4.3.6. Isotherm parameters for the adsorption of CP and NP onto GAC at different temperature (t = 24 h, m = 10 g/l).

	CP-GAC					NP-GAC				
Freundlich										
Temp.(K)	K_F [(mmol/g)/(mmol/l)$^{1/n}$]	$1/n$		R^2	SSE	K_F [(mmol/g)/(mmol/l)$^{1/n}$]	$1/n$		R^2	SSE
288	4.96	0.817		0.931	0.0459	1.51	0.73		0.983	0.0082
303	3.39	0.620		0.828	0.1101	1.83	0.62		0.999	0.0004
318	2.49	0.443		0.868	0.089	2.36	0.54		0.980	0.0142
Langmuir										
Temp. (K)	q_m (mmol/g)	K_L (l/mmol)		R^2	SSE	q_m (mmol/g)	K_L (l/mmol)		R^2	SSE
288	1.15	14.46		0.994	0.0747	1.21	3.48		0.986	0.0067
303	1.35	15.97		0.893	0.0768	1.24	5.73		0.996	0.0032
318	1.38	25.84		0.876	0.0742	1.35	11.17		0.986	0.0114
Tempkin										
Temp. (K)	K_T (l/ mmol)	B_T (mmol/g)		R^2	SSE	K_T (l/ mmol)	B_T (mmol/g)		R^2	SSE
288	81.94	0.3721		0.9912	0.0052	67.07	0.20		0.974	0.0120
303	124.44	0.3498		0.9407	0.0368	493.66	0.12		0.894	0.0495
318	313.84	0.2725		0.9412	0.0388	579.60	0.16		0.960	0.0205
R-P										
Temp. (K)	K_R (l/g)	a_R (l/mmol)	β	R^2	SSE	K_R (l/g)	a_R (l/mmol)	β	R^2	SSE
288	11.37	4.75	0.999	0.9604	0.0325	4.13	2.63	0.829	0.986	0.0056
303	20.40	13.90	0.999	0.8930	0.0754	65.33	35.76	0.405	0.998	0.0004
318	42.46	36.10	0.999	0.9177	0.0626	34.45	20.04	0.696	0.992	0.0036

Table 4.3.7. Isotherm parameters for the removal of C and R by GAC at different temperature (t = 24 h, m = 10 g/l).

	C-GAC				R-GAC			
Temp.(K)	K_F (mmol/g)(mmol/l)$^{1/r}$	$1/n$	R^2	SSE	K_F (mmol/g)(mmol/l)$^{1/r}$	$1/n$	R^2	SSE
288	1.02	0.57	0.912	0.072	0.79	0.57	0.876	0.088
303	1.12	0.48	0.900	0.081	0.93	0.52	0.912	0.075
318	0.59	0.55	0.915	0.089	0.49	0.99	0.948	0.045
Temp(K)	q_m (mmol/g)	K_L (l/mmol)	R^2	SSE	q_m (mmol/g)	K_L (l/mmol)	R^2	SSE
288	1.09	4.48	0.947	0.053	1.21	2.09	0.960	0.037
303	1.11	6.81	0.966	0.031	1.24	3.14	0.984	0.019
318	1.41	5.83	0.962	0.042	1.27	3.56	0.990	0.009
Temp.(K)	K_T (l/mmol)	B_1	R^2	SSE	K_T (l/mmol)	B_1	R^2	SSE
288	41.68	0.25	0.968	0.025	21.75	0.27	0.978	0.014
303	76.60	0.23	0.980	0.015	42.81	0.24	0.970	0.023
318	78.00	0.27	0.966	0.032	56.96	0.23	0.950	0.035

R-P

Temp.(K)	K_R (l/g)	a_R (l/mmol)	β	R^2	SSE	K_R (l/g)	a_R (l/mmol)	β	R^2	SSE
288	4.45	3.75	0.975	0.942	0.0495	2.55	2.10	0.999	0.960	0.037
303	7.58	6.82	0.999	0.966	0.0311	3.92	3.15	0.999	0.982	0.019
318	5.83	8.22	0.999	0.962	0.0424	4.55	3.56	0.999	0.990	0.009

Table 4.3.8. Isotherm parameters for the removal of HQ by GAC at different temperatures (t = 24.0 h, C_0 = 0.18-9.08 mmol/l, m = 10 g/l, T = 303 K).

Freundlich				
Temp. (K)	K_F [(mmol/g)/(mmol/l)$^{1/n}$]	$1/n$	R^2	SSE
288	2.0645	0.5063	0.9421	0.0216
303	2.1061	0.4313	0.9396	0.0226
318	1.888	0.3131	0.9330	0.0254
Langmuir				
Temp. (K)	q_m (mmol/g)	K_L (l/mmol)	R^2	SSE
288	1.063	18.77	0.9588	0.0151
303	1.098	30.89	0.9495	0.0254
318	1.104	60.21	0.8784	0.0816
Tempkin				
Temp. (K)	K_T (l/mmol)	B_1	R^2	SSE
288	212.023	0.2235	0.9600	0.0147
303	507.87	0.1975	0.9648	0.0129
318	1902.31	0.1634	0.9155	0.0311
R-P				
Temp. (K)	K_R (L/g)	a_R (l/mmol)	β	R^2	SSE
288	22.64	18.12	0.8942	0.9600	0.0147
303	59.02	45.40	0.8391	0.9587	0.0153
318	249.95	168.76	0.7895	0.9066	0.0346

4.3.8 Adsorption thermodynamics

The Gibbs free energy change of the adsorption process is related to the equilibrium constant by the classic Van't Hoff equation

$$\Delta G^0 = -RT \ln K \tag{4.3.18}$$

According to thermodynamics, the Gibbs free energy change is also related to the entropy change and heat of adsorption at constant temperature by the following equation:

$$\Delta G^0 = \Delta H^0 - T\Delta S^0 \tag{4.3.19}$$

Combining above two equations, we get

$$\ln K = \frac{-\Delta G^0}{RT} = \frac{\Delta S^0}{R} - \frac{\Delta H^0}{R}\frac{1}{T} \tag{4.3.20}$$

where ΔG^0 is the free energy change (kJ/mol), ΔH^0 is the change in enthalpy (kJ/mol), ΔS^0 is the entropy change (kJ/mol K), T is the absolute temperature (K) and R is the universal gas constant (8.314 J/mol K). Thus ΔH^0 can be determined by the slope of the linear Van't Hoff plot i.e. as $\ln K$ versus $(1/T)$, using equation:

$$\Delta H^0 = \left[R\frac{d \ln K}{d(1/T)} \right] \tag{4.3.21}$$

ΔH^0 obtained here corresponds to isosteric heat of adsorption ($\Delta H_{st,0}$) with zero surface coverage (i.e. q_e = 0). Fig. 4.3.8 shows the Van't Hoff's plot for AN, P, CP, NP, C, R and HQ adsorption onto GAC from which ΔH_0 and ΔS_0 values have been estimated (Table 4.3.9).

ΔG_0 values were negative indicating that the adsorption process led to a decrease in ΔG_0 and that the adsorption process is feasible and spontaneous [Sabah et al., 2007]. Generally, the change of ΔG_0 for physisorption is between −20 and 0 kJ/ mol and for chemisorption in the range of −80 to −400 kJ/ mol [Faust and Aly, 1987; Sabah et al., 2007]. Most of the ΔG_0 values obtained at 288 and 303 K for all the adsorbates lie between -20 and 0 kJ/ mol whereas ΔG_0 values obtained at 318 K are in the range of -20 to -25 kJ/mol. It may, thus, be inferred that the adsorption of AN, P, CP, NP, C, R and HQ is physical in nature, although, chemisorption plays an important role at higher temperatures. The absolute ΔG_0 values for all the adsorbates increase with an increase in

temperature, which elucidates the increasing tendency of adsorption spontaneity and further confirms the chemical character of the adsorption at higher temperatures.

The positive values of ΔH_0 indicate the endothermic nature of the adsorption process. In physiosorption, the bond between adsorbent and adsorbate is Van-der walls interaction and ΔH_0 is typically in the range of 5-10 kJ/mol for liquid phase adsorption. In case of chemisorption, a chemical bond is formed between adsorbate molecules and the surface; and the chemisorption energy is, generally, in the range of 30-70 kJ/mol [Murzin and Salami, 2005]. The adsorption for AN, P, CP, NP, C, R and HQ onto GAC, thus seems to be a coexisting process of physical adsorption and chemical transition [Jianguo et al., 2005]. The values of ΔH_0 for the present study show that the adsorption of C and R onto GAC is neither fully physical nor fully chemical and some complex mechanism dictates the adsorption process. Some researchers have suggested that adsorption of some organic compounds from aqueous solution onto AC is by a different adsorption mechanism, which may not be described as either physical adsorption or chemisorption [Mattson and Mark, 1971]. The enthalpy of adsorption of organic molecules from aqueous solution onto AC is usually within the range 8–65 kJ/mol [Mattson and Mark, 1971]. The values obtained in the present study are in the same range.

The positive value of ΔS_0 suggests an increase in the randomness at the solid/solution interface with some structural changes in the adsorbates and the GAC. It also indicates an affinity of the GAC towards the adsorbates [Srivastava et al., 2006]. The positive ΔS_0 value also corresponds to an increase in the degree of freedom of the adsorbed species [Raymon, 1998].

4.3.8.1 Isosteric heat of adsorption: Apparent isosteric heat of adsorption ($\Delta H_{st,a}$) at constant surface coverage (q_e= 0.3-1.5 mmol/g) is calculated using the Clausius–Clapeyron equation [Young and Crowell, 1962]:

$$\frac{d\ln Ce}{dT} = \frac{-\Delta H_{st,a}}{RT^2} \tag{4.3.22}$$

$$\Delta H_{st,a} = R\left.\frac{d\ln Ce}{d(1/T)}\right|_{q_e} \tag{4.3.23}$$

The equilibrium concentration (C_e) at a constant adsorbate uptake, q_e was obtained from the adsorption isotherm data at different temperatures. $\Delta H_{st,a}$ was calculated from the slope of the $\ln C_e$ versus ($1/T$) plot for varying q_e. The isosteres corresponding to different equilibrium adsorption uptake of AN, P, CP, NP, C, R and HQ by GAC are shown in Fig. 4.3.9. The linear regression correlation coefficients of the isosteres and the corresponding isosteric enthalpies for all the adsorbates are presented in Table 4.3.10. The variation of $\Delta H_{st,a}$ of the six adsorbate–adsorbent systems with the surface loading is presented in Fig. 4.3.10. The $\Delta H_{st,a}$ is high at very low coverage but decreases steadily with an increase in q_e. This indicates that the GAC has energetically heterogeneous surface. The dependence of heat of adsorption with surface coverage is usually observed to display the adsorbent–adsorbate interaction followed by the adsorbate–adsorbate interaction. The adsorbent–adsorbate interaction takes place initially at lower q_e values resulting in high heats of adsorption. On the other hand, adsorbate–adsorbate interaction occurs with an increase in the surface coverage. The variation in $\Delta H_{st,a}$ with surface loading can also be attributed to the possibility of having lateral interactions between adsorbed AN, P, CP, NP, C, R and HQ. Li et al. [2001] reported negative values of $\Delta H_{st,a}$ for adsorption of four phenolic (P, *p*-cresol, CP and NP) compounds onto Amberlite XAD-4. However, Srivastava et al. [2006] reported that the $\Delta H_{st,a}$ values for P adsorption onto bagasse fly ash and laboratory- and commercial-grade ACs were endothermic in nature. This trend matches with the trend reported in the present study.

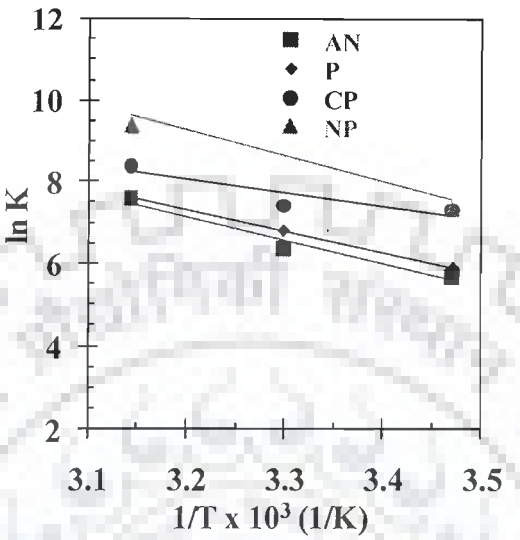

(a) AN, P, CP and NP

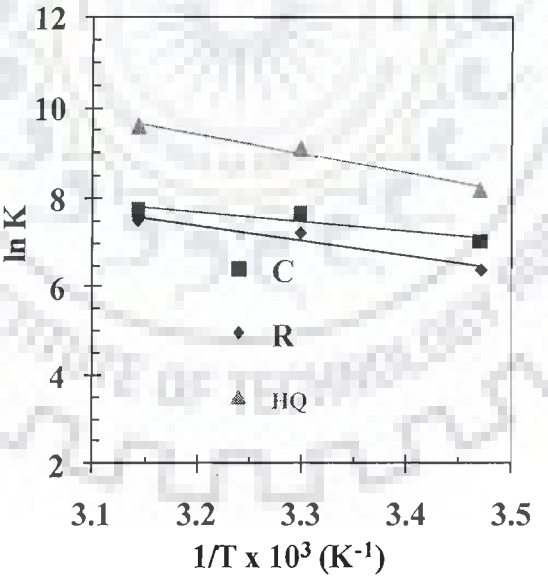

(b) C, R and HQ

Figure 4.3.8. Van't Hoff Plot of adsorption equilibrium constant K for AN, P, CP and NP, C, R and HQ

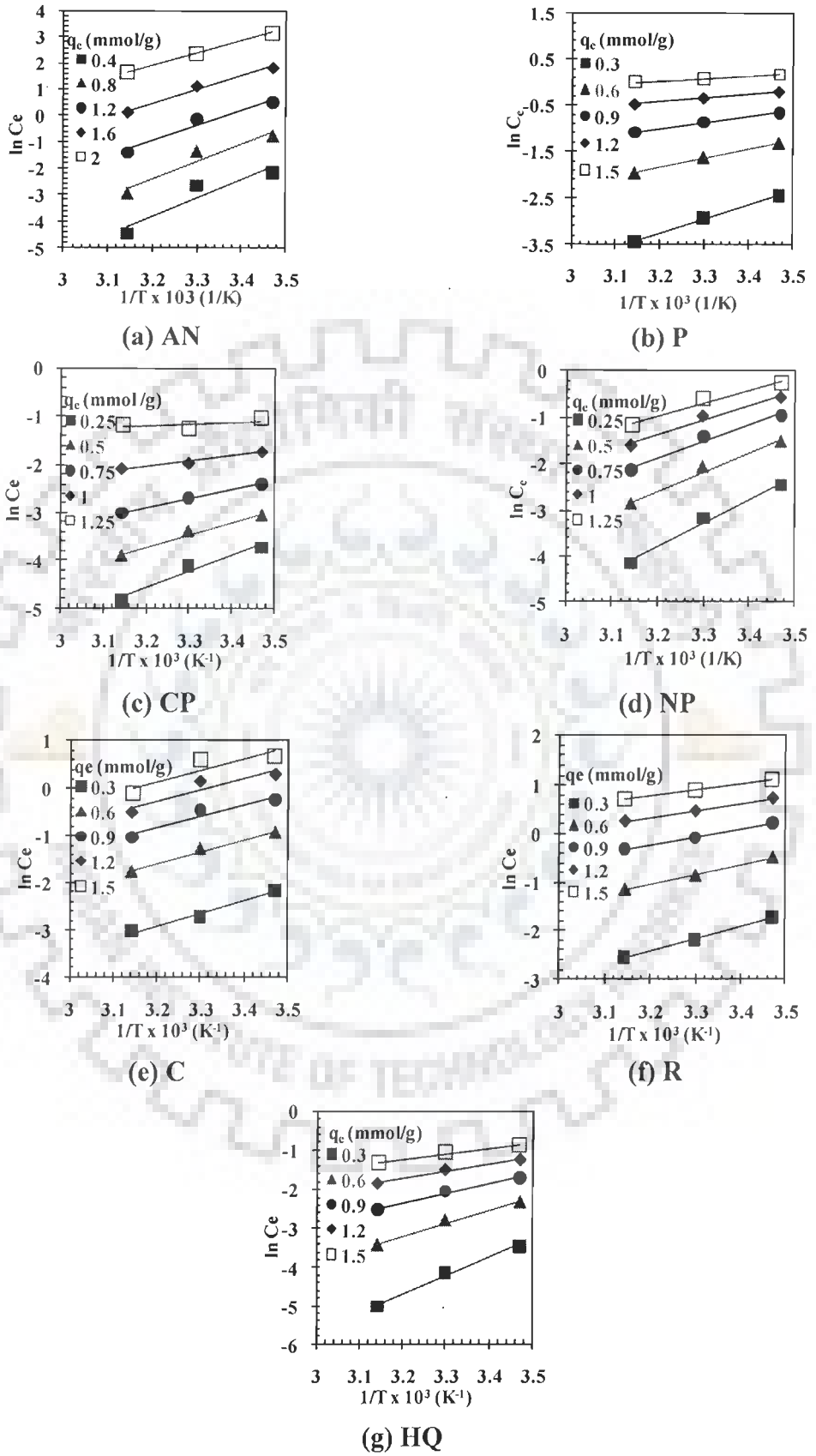

Figure 4.3.9. Adsorption isosters for determining isosteric heat of adsorption for AN, P, CP, NP, C, R and HQ adsorption onto GAC.

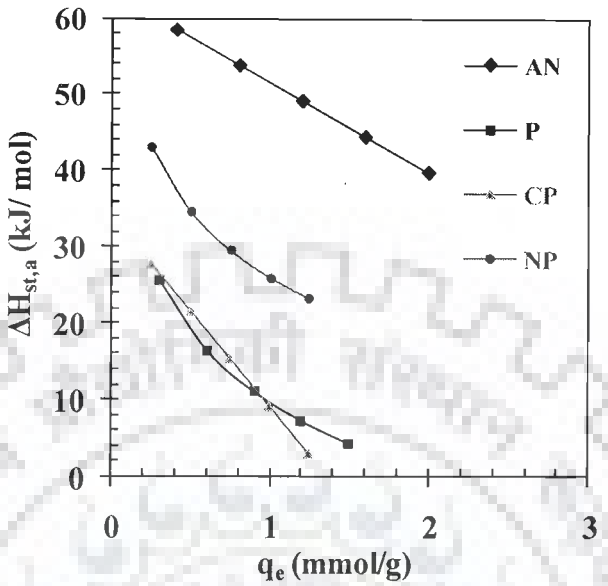

(a) AN, P, CP and NP

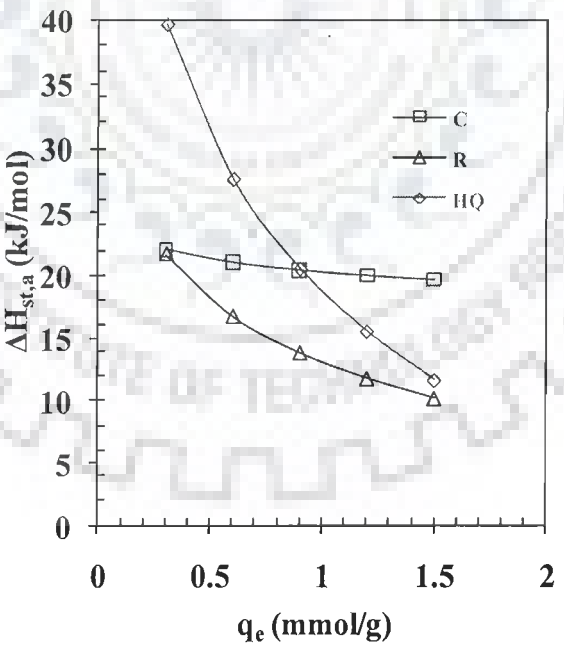

(b) C, R and HQ

Figure 4.3.10. Variation of $\Delta H_{st,a}$ with respect to surface loading for AN, P, CP, NP, C, R and HQ adsorption onto GAC.

Table 4.3.9. Thermodynamic parameters for the adsorption of AN, P, CP, NP, C, R and HQ onto GAC.

Temp. (K)	K_d (l/g)	ΔG_0 (kJ/mol)	ΔH_0 (kJ/mol)	ΔS_0 (kJ/mol.K)
	AN-GAC			
288	0.295	-13.62	48.48	214.69
303	0.585	-16.05		
318	2.010	-20.11		
	P-GAC			
288	0.365	-14.13	43.50	200.02
303	0.894	-17.12		
318	2.023	-20.13		
	CP-GAC			
288	1.513	-17.56	26.73	152.52
303	1.680	-18.71		
318	4.400	-22.22		
	NP-GAC			
288	1.543	-17.55	52.13	243.98
303	9.917	-23.19		
318	11.54	-24.74		
	C-GAC			
288	1.13	-16.84	17.99	121.63
303	2.13	-19.32		
318	2.28	-20.45		
	R-GAC			
288	0.59	-15.29	28.32	152.04
303	1.35	-18.18		
318	1.79	-19.81		
	HQ-GAC			
288	1.13	-19.69	35.28	191.25
303	2.13	-23.01		
318	2.28	-25.39		

Table 4.3.10. Isosteric enthalpy of the adsorption of AN, P, CP, NP, C, R and HQ onto GAC.

q_e (mmol/g)	$\Delta H_{st,a}$ (kJ/mol)	R^2	q_e (mmol/g)	$\Delta H_{st,a}$ (kJ/mol)	R^2
	AN-GAC			**P-GAC**	
0.4	58.45	0.8835	0.3	25.47	0.9969
0.8	53.73	0.9181	0.6	16.36	0.9976
1.2	48.99	0.9532	0.9	11.02	0.9984
1.6	44.27	0.9839	1.2	7.24	0.9994
2	39.53	0.9998	1.5	4.30	1.0000
	CP-GAC			**NP-GAC**	
0.25	27.71	0.9568	0.25	42.98	0.9854
0.5	21.55	0.9762	0.5	34.47	0.9819
0.75	15.38	0.9970	0.75	29.49	0.9787
1	9.21	0.9679	1	25.97	0.9755
1.25	3.04	0.3443	1.25	23.22	0.9721
	C-GAC			**R-GAC**	
0.3	22.03	0.9916	0.3	21.69	0.9984
0.6	21.02	0.9926	0.6	16.71	0.9987
0.9	20.42	0.9625	0.9	13.80	0.9989
1.2	20.00	0.9282	1.2	11.73	0.9992
1.5	19.68	0.8957	1.5	10.13	0.9994
	HQ-GAC				
0.3	39.65	0.9934			
0.6	27.58	0.9929			
0.9	20.52	0.9924			
1.2	15.51	0.9918			
1.5	11.62	0.9908			

4.4 MULTI-COMPONENT BATCH ADSORPTION STUDY USING TAGUCHI'S METHOD

Much of the work on the adsorption of P_s and its derivatives and associated compounds by various kinds of adsorbents has focused on the uptake of single adsorbate. Since industrial effluents contain several compounds, it is necessary to study the simultaneous sorption of two or more adsorbates and also to quantify the interference of one on the sorption of the other. Therefore, the following multi-component systems have been studied for AN, P, CP, NP, C, R and HQ adsorption onto GAC.

1. Binary systems: NP-P, NP-CP, NP-C, NP-R and NP-HQ, AN-NP, AN-P, AN-CP, AN-C, AN-R and AN-HQ
2. Ternary systems: P-CP-NP and C-R-HQ.

4.4.1 Optimization of Parameters for Binary Systems

The AN, P, CP, NP, C, R and HQ removal from the NP-P, NP-CP, NP-C, NP-R and NP-HQ, AN-NP, AN-P, AN-CP, AN-C, AN-R and AN-HQ binary systems were investigated at different initial concentrations, $C_{o,NP}/C_{o,AN}$ (parameter A), $C_{o,P}$ or $C_{o,CP}$ or $C_{o,C}$ or $C_{o,R}$ or $C_{o,HQ}$ (parameter B) and temperature T (parameter C) and the dosage, m (parameter E), and shaking time t (parameter F). According to the parametric values set by L_{27} OA matrix (Table 3.4.4), the adsorption experiments were carried out in duplicate and the mean values of q_{tot} and S/N ratio for each parameter at level 1, 2, and 3 were calculated. Tables 4.4.1 through 4.4.5 show these results for various binary systems.

In order to determine the effective parameters and their confidence levels on the AN, P, CP, NP, C, R and HQ adsorption onto GAC, a statistical analysis of variance (ANOVA) was performed to determine statistically significant process parameters. F-test was used as a tool to understand the process parameters having significant effect on the removal of AN, P, CP, NP, C, R and HQ.

4.4.1.1 NP-P and AN-P binary systems: Each experiment was repeated two times for each trial condition. The average or mean values of q_{tot} and S/N ratio for each parameter at level 1, 2, and 3 were calculated from Table 4.4.1. It is observed that adsorption of P, NP and AN were strongly dependent on the parametric values for NP-P and AN-P binary systems.

Table 4.4.6 shows the raw data for the average value of q_{tot} and S/N ratio for each parameter at the three levels along with the interactions of the initial components concentration at the assigned levels for NP-P and AN-P binary systems. It is seen that the effect of various parameters- viz. $C_{0,i}$,T , m and t on q_{tot} is significant. The interaction effect also has a significant influence on q_{tot}. However, it is found that m (parameter D) has the highest influence at level 1, and $C_{0,P}$ (parameter C) has highest influence at level 2 on q_{tot}. The difference in the values of each factor between level 2 and level 1 (L_2–L_1) indicates the relative influence of the effect of the given factor. The magnitude of difference indicates its degree of influence, i.e. the smaller the difference, the weaker is the influence. Table 4.4.6 shows that all the parameters have influence over others for the removal of P, NP and AN from aqueous solution by GAC for NP-P and AN-P binary systems. $C_{0,i}$ has maximum influence on q_{tot} in comparison to other parameters. The q_{tot} increased with an increase in $C_{0,i}$ since the resistance to the solute uptake by GAC decreased with an increase in the mass transfer driving force.

Figs. 4.4.1 and 4.4.2 show the response curves for the individual effects of sorption parameters on q_{tot} and the respective S/N ratio for the binary systems of NP-P and AN-P, respectively. An increase in the levels of parameters such as $C_{0,i}$ and t from 1 to 2 and from 2 to 3 induced an increase in q_{tot}.

Since the adsorption process is exothermic, q_{tot} should decrease with an increase in T, provided the adsorption phenomena is predominant in the over all process. However, if the diffusion process, which is endothermic in nature, controls the overall sorption process, then q_{tot} should increase with an increase in T. The temperature increase accelerates the mobility of the solute molecules and impedes the retarding forces acting on the diffusing molecules, resulting in the enhancement in the sorptive capacity of the adsorbents. However, the diffusion of the adsorbates into the pores of the adsorbent is not the only rate-controlling step [Srivastava et al., 2007; Lataye et al., 2009] and that the diffusion effect can be neglected with sufficient by large contact time. Thus, an increase in the sorptive uptake of the solutes with an increase in temperature can be ascribed to chemisorption.

An increasing in contact time from level 1 to 2 has an effect on q_{tot}; From level 2 to 3, no effect is seen. The removal of P, NP and AN increases with an increase in t until equilibrium is attained between the solute molecules in the solution and the solid phases. During the initial period of contact, a large number of vacant surface sites on the adsorbent are available for adsorption. However, with the passage of time, more and more vacant sites get occupied and the concentration of vacant sites decreases. Therefore, the sorption rate decreases. Besides, the mesopores get almost saturated with the solutes molecules during the period of contact and therefore, the solute molecule will have to traverse farther and deeper into the pores, encountering much larger transport resistance. This results in the slowing of the sorptive uptake during the later period of contact.

The interactions between initial concentrations of NP, AN and P [(A × B)] significantly affect q_{tot} (See Table 4.4.6). Figs. 4.4.12 and 4.4.13 shows that the interaction plots are not parallel to each other. This indicates that the interactive effects are significant. The larger the difference between the slopes of the interaction lines in the range tested, the greater is the interaction [Srivastava et al., 2007; Roy, 1990].

It is found that the difference in the slopes of the lines is more at level 1 and 2 for all the parameters. This indicates stronger influence of C_{oi} on q_{tot} is more significant when C_{oi} is increased from level 1 to the level 2, than that of its increase from level 2 to level 3.

Table 4.4.11 shows ANOVA results for raw and S/N ratio data with desired response characteristic (q_{tot}). The calculated ratios (F) suggest that all the parameters and interactions considered in the experimental design with q_{tot} as the desired response characteristic are statistically significant at the 95% confidence level.

Figs. 4.4.23 and 4.4.24 show the relative contribution of each parameter for q_{tot} as the desired response characteristic for the binary systems of NP-P and AN-P, respectively. Table 4.4.11 shows that the most significant parameters is D (m) with 39.76% and 54.34% contribution to the raw data for NP-P and AN-P, respectively. It can also be observed from Table 4.4.11, Figs. 4.4.23 and 4.4.24 that the interactions between the parameters A, B, and C contribute significantly to both raw and S/N ratio data for simultaneous removal of NP and P, and An and P from their binary solutions by GAC.

Because q_{tot} is an HB (higher is better) type quality characteristic, the larger q_{tot} value is considered optimal. Table 4.4.16 summarizes the optimal level of various parameters as determined obtained from the response curves shown in Figs. 4.4.1 and 4.4.2. It is found that at the first level of parameter D (m), the second level of parameter E (t), and the third level of parameter A (C_{oi}/C_{oj}), B ($C_{0,i}$) and C (temperature) q_{tot} and S/N ratio. Values are higher than those found at other levels. Since the aim of the study was to have the maximum removal of solutes from the aqueous solutions with the highest possible concentrations of An-P and NP-P binaries, the third level of parameters A and B ($C_{0,AN}$, $C_{0,P}$, $C_{0,NP}$) are recommended for estimating the optimal q_{tot}.

The mean of the response (μ) at the optimum condition was estimated using the following relation:

$$\mu = \overline{T} + (\overline{A}_3 - \overline{T}) + (\overline{B}_3 - \overline{T}) + (\overline{C}_3 - \overline{T}) + (\overline{D}_1 - \overline{T}) + (\overline{E}_2 - \overline{T})$$

$$= \overline{A}_3 + \overline{B}_3 + \overline{C}_3 + \overline{D}_1 + \overline{E}_2 - 4\overline{T} \qquad (4.4.1)$$

It is customary to represent μ is generally represented within a confidence interval (CI) which is the range between a maximum and a minimum value at same stated level of confidence. The confidence interval is defined for the entire population (CI_{pop}) i.e., all the experimental runs under the specified conditions, and for a sample group of experiments under specified condition (CI_{CE}) [Roy, 1990; Oguz et al., 2006; Srivastava et al., 2007].

Three confirmation experiments have been conducted for the simultaneous removal of NP-P and AN-P from binary solution by GAC at selected optimal levels of the process parameters, as indicated above. The above estimated value of q_{tot} are compared with the predicted values of q_{tot} as given in Table 4.4.16. The values of q_{tot} obtained through the confirmation experiments are within 95% of CI_{CE}. However, it is to be noted that these optimal values are valid within the specified range of process parameters and that any extrapolation/ interpolation should be confirmed through additional experiments.

4.4.1.2 NP-C and NP-R binary systems: Each experiment was repeated two times for each level of parametric values. The average or mean values of q_{tot} and S/N ratio for each parameter at level 1, 2, and 3 were calculated from Table 4.4.2. It is observed that the adsorption of NP, C and R from NP-C and NP-R binary systems is strongly dependent on the parametric conditions.

Table 4.4.7 shows the raw data for the average value of q_{tot} and S/N ratio for each parameter at the three levels along with the interactions of the initial components concentration at the assigned levels. It is seen that the effect of various parameters-viz. $C_{0,i}$, T, m and t on q_{tot} is significant. The interaction effect also has a significant influence on q_{tot}. However, it is found that m (parameter D) has the highest influence at level 1, and $C_{0,P}$ (parameter C) has the highest influence at level 2, on q_{tot}. The difference in the values of each factor between level 2 and level 1 (L_2–L_1) indicates the relative influence of the effect of the given factor. Table 4.4.7 shows that all the parameters have influence over others for the removal of a solute from aqueous solution from NP-C and NP-R binary systems by GAC. $C_{0,i}$ has strong influence on q_{tot} than that of other parameters. The q_{tot} increased with an increase in $C_{0,i}$ since the resistance to the solute uptake by GAC decreased with an increase in the mass transfer driving force.

Figs. 4.4.3 and 4.4.4 show the response curves for the individual effects of sorption parameters on q_{tot} and the respective S/N ratio for the binary systems of NP-C and NP-R. An increase in the levels of parameters such as $C_{0,i}$, T and t from level 1 to level 2 and from level 2 to level 3 resulted in an increase in q_{tot}. As discussed in sub-section 4.4.1.1 for NP-P and AN-P binaries, the temperature effect on the adsorption of NP-C and NP-R system on to GAC leads to the conclusion that the process of uptake is chemisorption. Contact time t increase from level 1 to 2 shows an effect on q_{tot}. The explanations are similar as that for N-P and An-P system.

The interactions between initial concentrations of NP, C and R [(A × B)] have significant effect on q_{tot} (See Table 4.4.7 and Figs. 4.4.23 and Figure 4.4.24). Figs. 4.4.14 and Figure 4.4.15 show that the interaction plots are not parallel to each other. As discussed earlier for NP-P and AN-P systems, the nature of the plots indicate significant effect of interactions.

ANOVA results for raw and S/N ratio data with q_{tot} are given in Table 4.4.12. The calculated ratios (F) suggest that all the parameters and interactions considered in the experimental design with q_{tot} are statistically significant at the 95% confidence limit. Table 4.4.13 shows that the most significant parameters is D (m) with 26.68% and

22.59% contribution to the raw data for NP-P and An-P systems, respectively, within the assigned levels for each parameters.

With q_{tot} is an HB type quality characteristic, the optimal level of various parameters is shown in Figs. 4.4.14 and Fig. 4.4.15 for NP-P and AN-P systems, respectively. It is found that the first level of parameter D (m), the second level of parameters E(t), and the third level of parameter A, B, ($C_{0,i}$), and C (T) result in higher values of q_{tot} and S/N ratio. However the third level of parameters A and B ($C_{0,NP}$, $C_{0,C}$, $C_{0,R}$) are recommended for estimating the optimal q_{tot}, because the maximum removal of solute is desired.

Table 4.4.16 shows that the parameters A, B ($C_{o,i}$), C (T) and E (t) at level 3, and parameter D (m) at level 2 result in higher average value of q_{tot} for adsorption on GAC. Since the objective is to maximize the adsorbates removal with the highest possible initial concentrations of adsorbates in the wastewater, parameters A, B, and C ($C_{0,NP}$, $C_{0,C}$ and $C_{0,R}$) level 3 are used.

The mean of the response (μ) at the optimum condition was estimated using the following relation:

$$\mu = \overline{T} + (\overline{A}_3 - \overline{T}) + (\overline{B}_3 - \overline{T}) + (\overline{C}_3 - \overline{T}) + (\overline{D}_2 - \overline{T}) + (\overline{E}_3 - \overline{T})$$

$$= \overline{A}_3 + \overline{B}_3 + \overline{C}_3 + \overline{D}_2 + \overline{E}_3 - 4\overline{T} \qquad (4.4.2)$$

The range of CI_{CE} is 0.64-1.30 mmol/g for NP-C system and 0.48-1.21 mmol/g for NP-R system (Table 4.4.16). Three confirmation experiments have been conducted for the simultaneous removal of NP-C and NP-R from binary solutions by GAC at selected optimal levels of the process parameters. Average values of q_{tot} for confirmation experiments were found to be 0.95 and 0.87 mmol/g, respectively, for NP-C and NP-R binary systems. The values of q_{tot} obtained through the confirmation experiments are within 95% of CI_{CE}.

4.4.1.3 AN-C and AN-R binary systems: Figs. 4.4.5 and 4.4.6 show the response curves for the individual effects of initial concentration of AN and C or AN and R from AN-C and AN-R binary systems on the average value of q_{tot} and S/N ratio. An increase in the

level from 1 to 2 and from level 2 to 3 of $C_{0,i}$, resulted in an increase in the q_{tot} values. This increase is due to the decreased resistance for uptake at higher concentration.

Figs. 4.4.5 and 4.4.6 show the effect of T on q_{tot} and S/N ratio for AN-C and AN-R systems. It may be seen that q_{tot} and S/N ratio values increase with an increase in T indicating endothermic nature of the adsorption process.

An increase in m from level 1 to level 2 and subsequently to level 3 led to a decrease in the value of q_{tot} for both the binary systems (Figs. 4.4.5 and 4.4.6). However, when the data were analyzed in terms of average removal of the solutes, an increase in m from level 1 to level 2 significant increase in average percent removal, and thereafter, it became almost constant. An increase in the removal with m was because of the availability of larger number of adsorption sites and greater surface area.

Figs. 4.4.5 and 4.4.6 shows the effect of t on q_{tot} values for both AN-C and AN-R systems, respectively. An increase in t from level 1 to 2 and subsequently from level 2 to 3 resulted in an increase in q_{tot}. The sorption of adsorbates increased with t until equilibrium condition is reached.

Figs. 4.4.25 and 4.4.26 show the interactions between $C_{o,AN}$ with $C_{o,C}$ and $C_{o,R}$ which affect the average value of q_{tot}. It can be seen from Figs. 4.4.5 and 4.4.6 that the difference in the slopes of the lines is greater when the level of the parameters is lower. Thus, the effect of initial concentration of adsorbates on q_{tot} is more pronounced when $C_{0,i}$ is increased from the lowest level to the middle level than an increase from the middle level to the highest level. The adsorption of AN and C, and AN and R from AN-C and AN-R binary systems, respectively, seems to be antagonistic in nature. It appears that the adsorbate components share the binding sites on the surface, and therefore, the sorption of one species reduces the number of binding sites available for the sorption of other species. The screening effect may also be having a role in the antagonistic behaviour during sorption. The antagonistic behaviour seemed to be more pronounced when the initial concentration is increased from level 1 to 2 than from level 2 to 3.

ANOVA was tested on the output raw data and S/N ratio associated with every test run to identify the distinct characteristic between the control or signal factors. The contribution of individual parameters is weighted to enforce control on sorptive uptake of

various compounds. ANOVA results for raw and S/N ratio data with q_{tot} are given in Table 4.4.13 for the simultaneous sorption of the adsorbate components onto GAC for both the binary mixtures. ANOVA can also be used to identify which factors would significantly affect the quality characteristic of the output responses or which factors that can be relaxed. The F-value and the contribution for factor D (m) was found to be the highest, with value of 174.41 and 37.04%; 33.66 and 35.14% for AN-C and AN-R binary systems, respectively, corresponding to the raw q_{tot} and S/N ratio values. This indicated that any changes in the m will lead to the most significant influence on the removal of adsorbates. The F-values for other factors of $C_{o,AN}$, $C_{o,C}$ or $C_{o,R}$, T and t were also estimated. It was found that the F-values for $C_{o,AN}$, $C_{o,C}$ or $C_{o,R}$, T and t were quite significant, corresponding to contributions of 33.22%, 11.21%, 8.23%, 5.46%; and 24.63%, 12.12%, 4.10% and 2.93%, respectively for both AN-C and AN-R binary mixtures.

Table 4.4.13 and Figs. 4.4.27 and 4.4.28 also revealed that the interactions between $C_{0,i}$ also contributed significantly to both raw and S/N ratio data for simultaneous removal of the two components by the GAC for two binaries mixture.

Table 4.4.8 show that the parameters A, B ($C_{o,i}$), C (T) and E (t) at level 3, and parameter D (m) at level 2 lead to result in higher average value of q_{tot} for adsorption on to GAC. Since the objective is to maximize the solute removal with the highest possible initial concentrations of solutes in the wastewater, parameters A, B, and C ($C_{o,AN}$, $C_{o,C}$ and $C_{o,R}$) at level 3 are used. Thus, it can be concluded that the optimal operating conditions for maximum adsorption in both binary systems are: $C_{o,AN}$ = 5.37 mmol/l (A3), $C_{o,C}$ or $C_{o,R}$ = 4.54 mmol/l (B3), T =318 K (C3), m = 10 g/l (D2) and t = 660 min (E3).

The mean of the response (μ) at the optimum condition was estimated using the following relation:

$$\mu = \overline{T} + (\overline{A}_3 - \overline{T}) + (\overline{B}_3 - \overline{T}) + (\overline{C}_3 - \overline{T}) + (\overline{D}_2 - \overline{T}) + (\overline{E}_3 - \overline{T})$$

$$= \overline{A}_3 + \overline{B}_3 + \overline{C}_3 + \overline{D}_2 + \overline{E}_3 - 4\overline{T} \qquad (4.4.3)$$

where, $\overline{T}$ is the overall mean of the response and $\overline{A}_3$, $\overline{B}_3$, $\overline{C}_3$ and $\overline{E}_3$ are the average values of the response at the third levels of parameters A, B, C and E, respectively and

$\overline{D}_2$ is the average value of the response at the first level of parameter D. The range of CI_{CE} is 0.65-0.85 mmol/g for AN-C system and 0.62-1.18 mmol/g for AN-R system. Average values of q_{tot} for there confirmation experiments were found to be 0.73 and 0.95 mmol/g, respectively, for AN-C and AN-R binary systems. The values of q_{tot} obtained through the confirmation experiments are within 95% of CI_{CE}.

Similar trends were found for other binary systems too (NP-CP, NP-HQ, AN-NP, AN-CP, AN-HQ) (see Tables 4.4.4-4.4.5, 4.4.9-4.4.10, 4.4.14-4.4.16; and Figs. 4.4.7-4.4.11, 4.4.18-4.4.22, 4.4.29-4.4.33).

Table 4.4.1. Experimental q_{tot} and S/N ratio values for Taguchi's L_{27} (3^{13}) orthogonal array for NP-P and AN-P adsorption onto GAC.

	NP-P			AN-P		
Exp. no.	R1	R2	S/N	R1	R2	S/N
1	0.00	0.00	0.00	0.00	0.00	S/N
2	0.00	0.00	0.00	0.00	0.00	0.00
3	0.00	0.00	0.00	0.00	0.00	0.00
4	0.18	0.19	-14.79	0.98	0.98	0.00
5	0.17	0.17	-15.52	0.28	0.29	-0.20
6	0.09	0.09	-20.59	0.13	0.13	-10.86
7	0.18	0.19	-14.57	0.95	0.97	-17.49
8	0.30	0.30	-10.40	0.55	0.57	-0.36
9	0.17	0.17	-15.30	0.29	0.29	-5.08
10	0.57	0.54	-5.11	0.31	0.32	-10.72
11	0.17	0.17	-15.60	0.02	0.03	-10.03
12	1.20	1.21	1.64	1.12	1.12	-31.67
13	0.72	0.69	-3.04	0.55	0.55	0.99
14	0.23	0.22	-12.99	0.29	0.30	-5.23
15	1.31	1.33	2.42	1.44	1.20	-10.64
16	0.83	0.80	-1.74	0.80	0.81	2.32
17	0.27	0.47	-9.55	0.43	0.44	-1.92
18	1.09	1.09	0.76	1.28	1.41	-7.21
19	0.12	0.14	-17.68	0.31	0.32	2.57
20	1.30	1.32	2.36	1.74	1.73	-10.05
21	0.51	0.51	-5.84	0.46	0.45	4.78
22	0.20	0.22	-13.50	0.45	0.45	-6.86
23	1.48	1.50	3.46	0.84	0.84	-6.90
24	0.64	0.64	-3.92	0.56	0.20	-1.54
25	0.29	0.30	-10.61	0.55	0.56	-11.68
26	1.81	0.81	0.37	1.17	1.12	-5.11
27	0.67	0.66	-3.50	0.63	0.53	1.18
Total	14.51	13.74		16.139	15.601	-4.85
Mean		0.52			0.59	

[1]S/N: S/N Ratio (dB)

Table 4.4.2. Experimental q_{tot} and S/N ratio values for Taguchi's L_{27} (3^{13}) orthogonal array for NP-C and NP-R adsorption onto GAC.

	NP-C			NP-R		
Exp. no.	R1	R2	S/N	R1	R2	S/N
1	0.00	0.00	0.00	0.00	0.00	0.00
2	0.00	0.00	0.00	0.00	0.00	0.00
3	0.00	0.00	0.00	0.00	0.00	0.00
4	0.15	0.13	-17.14	0.37	0.26	-10.39
5	0.27	0.27	-11.27	0.20	0.20	-14.00
6	0.87	0.85	-1.31	0.98	0.93	-0.43
7	0.89	0.86	-1.15	1.42	1.41	3.02
8	0.17	0.11	-17.62	0.40	0.39	-8.09
9	0.17	0.12	-17.21	0.21	0.21	-13.58
10	0.18	0.11	-17.71	0.24	0.24	-12.47
11	0.30	0.30	-10.57	0.79	0.79	-2.08
12	1.48	1.50	3.48	0.76	0.81	-2.12
13	0.53	0.53	-5.55	0.48	0.47	-6.48
14	0.26	0.26	-11.74	0.22	0.22	-13.05
15	0.66	0.68	-3.51	1.19	0.99	0.64
16	0.67	0.67	-3.43	0.70	0.71	-3.03
17	0.31	0.31	-10.16	0.33	0.33	-9.54
18	1.34	1.34	2.53	1.17	1.17	1.38
19	0.48	0.48	-6.32	1.01	0.38	-5.94
20	1.38	1.25	2.35	1.35	1.35	2.61
21	0.49	0.48	-6.21	0.40	0.49	-7.11
22	0.35	0.35	-9.04	0.39	0.39	-8.10
23	1.12	1.12	0.98	0.47	0.47	-6.55
24	0.52	0.51	-5.77	0.92	0.92	-0.73
25	0.46	0.46	-6.71	0.24	0.25	-12.27
26	0.21	0.51	-11.25	0.90	0.83	-1.31
27	0.59	0.59	-4.60	0.49	0.55	-5.73
Total	13.85	13.811		15.64	14.76	
Mean		0.51			0.56	

Table 4.4.3. Experimental q_{tot} and S/N ratio values for Taguchi's L_{27} (3^{13}) orthogonal array for AN-C, AN-R and AN-HQ adsorption onto GAC.

	AN-C			AN-R		
Exp. no.	R1	R2	S/N	R1	R2	S/N
1	0.00	0.00	0.00	0.00	0.00	0.00
2	0.00	0.00	0.00	0.00	0.00	0.00
3	0.00	0.00	0.00	0.00	0.00	0.00
4	0.10	0.37	-17.14	0.37	0.26	-10.39
5	0.11	0.11	-19.07	0.20	0.20	-14.00
6	0.07	0.07	-23.28	0.10	0.09	-20.43
7	0.17	0.23	-14.25	0.45	0.74	-5.25
8	0.23	0.22	-13.01	0.40	0.39	-8.09
9	0.14	0.14	-17.18	0.21	0.21	-13.58
10	0.18	0.15	-15.60	0.24	0.24	-12.47
11	0.10	0.09	-20.27	0.09	0.09	-21.17
12	0.51	0.40	-7.03	0.76	0.81	-2.12
13	0.28	0.27	-11.22	0.48	0.47	-6.48
14	0.15	0.15	-16.37	0.22	0.22	-13.05
15	0.73	0.78	-2.45	0.99	0.99	-0.08
16	0.43	0.43	-7.40	0.70	0.71	-3.03
17	0.21	0.21	-13.50	0.33	0.33	-9.54
18	0.94	0.94	-0.51	0.97	0.97	-0.24
19	0.20	0.15	-15.37	0.24	0.24	-12.24
20	0.92	0.42	-5.31	0.97	0.97	-0.24
21	0.32	0.21	-12.20	0.37	0.37	-8.65
22	0.27	0.27	-11.25	0.39	0.39	-8.10
23	0.91	0.98	-0.48	0.47	0.47	-6.55
24	0.60	0.60	-4.45	0.92	0.92	-0.73
25	0.22	0.23	-13.03	0.24	0.25	-12.27
26	1.08	1.22	1.16	1.59	1.61	4.09
27	0.52	0.50	-5.85	0.49	0.55	-5.73
Total	9.41	9.15		12.21	12.49	
Mean		0.34			0.46	

Table 4.4.4. Experimental q_{tot} and S/N ratio values for Taguchi's L_{27} (3^{13}) orthogonal array for NP-AN, NP-CP and NP-HQ systems.

	NP-AN			NP-CP			NP-HQ		
Exp. no.	R1	R2	S/N	R1	R2	S/N	R1	R2	S/N
1	0.00	0.00	0.00	0.00	0.00	0.00	0.00	0.00	0.00
2	0.00	0.00	0.00	0.00	0.00	0.00	0.00	0.00	0.00
3	0.00	0.00	0.00	0.00	0.00	0.00	0.00	0.00	0.00
4	1.25	1.26	1.98	0.20	0.20	-14.00	0.75	0.42	-5.78
5	1.67	1.85	4.88	0.16	0.16	-15.82	0.46	0.42	-7.10
6	0.72	0.73	-2.80	0.09	0.09	-21.33	0.27	0.25	-11.8
7	1.86	1.87	5.40	0.25	0.25	-12.11	1.57	1.59	3.98
8	1.23	1.26	1.89	0.30	0.30	-10.41	0.91	0.73	-1.90
9	1.29	1.29	2.23	0.17	0.17	-15.57	0.54	0.44	-6.32
10	1.70	1.70	4.61	0.22	0.22	-13.05	0.16	0.24	-14.7
11	0.38	0.38	-8.45	0.12	0.12	-18.49	0.11	0.14	-18.0
12	2.90	2.94	9.32	1.05	1.05	0.46	0.82	0.60	-3.25
13	1.83	1.83	5.24	0.58	0.58	-4.79	0.38	0.62	-6.74
14	0.95	0.95	-0.44	0.19	0.19	-14.38	0.23	0.33	-11.6
15	1.02	1.99	2.16	0.96	0.96	-0.33	0.89	0.83	-1.29
16	1.77	1.76	4.94	0.34	0.34	-9.32	0.32	0.90	-7.36
17	1.44	1.44	3.15	0.30	0.30	-10.34	0.34	0.54	-7.77
18	1.73	1.68	4.63	1.20	1.20	1.55	1.38	1.27	2.44
19	0.69	0.76	-2.82	0.25	0.25	-12.18	0.65	0.60	-4.11
20	1.92	1.94	5.72	1.36	1.36	2.67	0.98	0.82	-1.05
21	0.95	1.04	-0.06	0.42	0.42	-7.49	0.26	0.20	-12.8
22	1.35	1.37	2.70	0.25	0.25	-12.02	0.33	0.29	-10.3
23	2.38	2.35	7.47	1.32	1.32	2.40	0.58	1.35	-2.48
24	1.77	1.77	4.96	0.52	0.52	-5.64	0.68	0.58	-4.10
25	1.47	1.06	1.68	0.40	0.40	-7.91	0.33	0.25	-11.0
26	1.74	1.74	4.82	0.99	0.99	-0.09	0.92	2.01	1.45
27	2.14	2.13	6.60	0.62	0.62	-4.14	1.14	0.92	0.10
Total	36.15	37.11		12.27	12.26		15.01	16.33	
Mean		1.36			0.45			0.58	

Table 4.4.5. Experimental q_{tot} and S/N ratio values for Taguchi's L_{27} (3^{13}) orthogonal array for AN-CP and AN-HQ systems.

	AN-CP			AN-HQ			
Exp. no.	R1	R2	S/N	S/N	R1	R2	S/N
1	0.00	0.00	0.00	0.00	0.00	0.00	0.00
2	0.00	0.00	0.00	0.00	0.00	0.00	0.00
3	0.00	0.00	0.00	0.00	0.00	0.00	0.00
4	0.31	0.31	-10.29	-0.20	0.46	0.45	-6.80
5	0.20	0.20	-13.95	-10.86	0.32	0.33	-9.78
6	0.10	0.09	-20.52	-17.49	0.18	0.18	-15.09
7	0.48	0.47	-6.40	-0.36	0.69	0.85	-2.43
8	0.38	0.37	-8.53	-5.08	0.63	0.64	-3.99
9	0.21	0.21	-13.59	-10.72	0.36	0.37	-8.81
10	0.22	0.22	-13.30	-10.03	0.85	0.61	-3.06
11	0.13	0.12	-18.23	-31.67	0.15	0.25	-14.60
12	0.56	0.60	-4.77	0.99	0.30	0.20	-12.43
13	0.40	0.37	-8.41	-5.23	0.34	0.33	-9.45
14	0.20	0.20	-13.93	-10.64	0.19	0.19	-14.53
15	0.88	0.87	-1.14	2.32	0.97	1.11	0.28
16	0.56	0.56	-5:03	-1.92	0.69	0.69	-3.21
17	0.28	0.28	-11.03	-7.21	0.35	0.35	-9.14
18	1.14	0.87	-0.22	2.57	1.16	1.32	1.82
19	0.24	0.24	-12.39	-10.05	0.71	0.53	-4.46
20	1.17	1.17	1.35	4.78	0.26	0.26	-11.69
21	0.32	0.31	-10.11	-6.86	0.32	0.36	-9.50
22	0.35	0.34	-9.29	-6.90	0.24	0.24	-12.31
23	0.41	0.45	-7.36	-1.54	1.08	1.07	0.62
24	0.45	0.45	-6.92	-11.68	0.73	0.74	-2.69
25	0.46	0.46	-6.74	-5.11	0.13	0.15	-17.02
26	1.10	1.13	0.91	1.18	1.19	1.57	2.56
27	0.51	0.52	-5.80	-4.85	0.53	0.53	-5.50
Total	11.04	10.79			12.85	13.30	
Mean		0.40				0.48	

Table 4.4.6. Average and main effects of q_{tot} values for raw and S/N data for NP-P and AN-P systems.

	Raw data, Average value			Main effects (Raw data)		S/N data, Average value			Main effects (S/N data)	
	L1	L2	L3	L2-L1	L3-L2	L1	L2	L3	L2-L1	L3-L2
	NP-P									
A	0.12	0.72	0.73	0.60	0.01	-10.13	-4.80	-5.43	5.33	-0.63
B	0.43	0.56	0.58	0.13	0.02	-4.47	-8.72	-7.17	-4.25	1.55
C	0.34	0.59	0.63	0.25	0.04	-9.01	-6.43	-4.93	2.58	1.50
D	0.90	0.49	0.19	-0.41	-0.30	-2.04	-5.45	-12.87	-3.41	-7.42
E	0.33	0.53	0.72	0.20	0.19	-8.97	-6.99	-4.40	1.98	2.59
AxB	0.51	0.52	0.54	0.01	0.03	-2.88	-9.24	-8.24	-6.36	1.00
	AN-P									
A	0.36	0.69	0.72	0.33	0.03	-4.97	-6.76	-4.56	-1.79	2.20
B	0.44	0.58	0.74	0.14	0.16	-5.87	-6.91	-3.50	-1.04	3.41
C	0.55	0.59	0.63	0.04	0.03	-4.42	-6.78	-5.08	-2.36	1.70
D	1.05	0.44	0.28	-0.61	-0.16	1.08	-6.28	-11.09	-7.36	-4.81
E	0.46	0.66	0.65	0.21	-0.02	-8.16	-3.57	-4.55	4.60	-0.98
AxB	0.48	0.65	0.63	0.16	-0.01	-2.72	-6.96	-6.60	-4.24	0.36

Table 4.4.7. Average and main effects of q_{tot} values for raw and S/N data for NP-C and NP-R systems.

	Raw data, Average value			Main effects (Raw data)		S/N data, Average value			Main effects (S/N data)	
	L1	L2	L3	L2-L1	L3-L2	L1	L2	L3	L2-L1	L3-L2
	NP-C									
A	0.27	0.63	0.63	0.36	0.00	-7.30	-6.29	-5.17	1.00	1.12
B	0.47	0.52	0.54	0.06	0.02	-3.89	-7.15	-7.73	-3.26	-0.58
C	0.41	0.45	0.68	0.05	0.22	-7.45	-7.70	-3.62	-0.25	4.08
D	0.81	0.37	0.35	-0.44	-0.02	-2.63	-8.02	-8.12	-5.38	-0.10
E	0.39	0.58	0.57	0.19	-0.01	-7.48	-5.38	-5.90	2.10	-0.52
AxB	0.40	0.58	0.55	0.18	-0.03	-3.79	-7.11	-7.86	-3.32	-0.75
	NP-R									
A	0.39	0.65	0.66	0.26	0.01	-4.83	-5.19	-5.02	-0.36	0.18
B	0.48	0.56	0.65	0.08	0.09	-3.01	-6.57	-5.46	-3.55	1.10
C	0.50	0.51	0.68	0.02	0.16	-6.19	-5.78	-3.08	0.41	2.70
D	0.83	0.43	0.43	-0.40	-0.01	-1.41	-6.41	-7.22	-4.99	-0.82
E	0.55	0.55	0.58	0.00	0.03	-5.07	-5.39	-4.58	-0.32	0.81
AxB	0.41	0.62	0.66	0.20	0.05	-3.60	-5.96	-5.48	-2.36	0.48

Table 4.4.8. Average and main effects of q_{tot} values for raw and S/N data for AN-C and AN-R systems.

	Raw data, Average value			Main effects (Raw data)		S/N data, Average value			Main effects (S/N data)	
	L1	L2	L3	L2-L1	L3-L2	L1	L2	L3	L2-L1	L3-L2
	AN-C									
A	0.11	0.39	0.54	0.28	0.15	-11.55	-10.48	-7.42	1.07	3.06
B	0.20	0.38	0.45	0.18	0.07	-8.42	-11.75	-9.29	-3.32	2.46
C	0.22	0.40	0.42	0.18	0.02	-11.70	-9.65	-8.10	2.04	1.55
D	0.60	0.29	0.15	-0.31	-0.14	-5.11	-9.87	-14.47	-4.75	-4.61
E	0.25	0.35	0.43	0.10	0.08	-11.56	-9.08	-8.81	2.48	0.27
AxB	0.36	0.34	0.33	-0.02	-0.01	-4.74	-13.00	-11.72	-8.25	1.28
	AN-R									
A	0.20	0.53	0.64	0.33	0.10	-7.97	-7.58	-5.60	0.40	1.97
B	0.30	0.45	0.62	0.15	0.17	-6.32	-8.87	-5.96	-2.55	2.91
C	0.36	0.48	0.54	0.12	0.06	-7.80	-7.62	-5.73	0.19	1.89
D	0.74	0.42	0.20	-0.32	-0.22	-2.31	-6.58	-12.26	-4.27	-5.69
E	0.37	0.47	0.53	0.10	0.06	-8.28	-6.35	-6.52	1.93	-0.17
AxB	0.44	0.46	0.48	0.02	0.01	-3.43	-9.63	-8.10	-6.20	1.53

Table 4.4.9. Average and main effects of q_{tot} values for raw and S/N data for NP-AN, NP-CP and NP-HQ systems.

	Raw data, Average value			Main effects (Raw data)		S/N data, Average value			Main effects (S/N data)	
	L1	L2	L3	L2-L1	L3-L2	L1	L2	L3	L2-L1	L3-L2
	NP-AN									
A	0.90	1.58	1.59	0.67	0.01	1.51	2.79	3.45	1.28	0.66
B	0.96	1.50	1.61	0.54	0.10	0.92	2.91	3.93	1.98	1.02
C	1.31	1.31	1.45	0.00	0.14	2.64	2.12	3.00	-0.52	0.89
D	1.70	1.47	0.90	-0.23	-0.56	4.61	3.67	-0.53	-0.94	-4.20
E	1.20	1.39	1.48	0.19	0.10	1.46	2.72	3.58	1.26	0.87
AxB	1.10	1.46	1.51	0.35	0.06	2.66	2.35	2.75	-0.31	0.40
	NP-CP									
A	0.13	0.55	0.68	0.42	0.13	-9.91	-7.63	-4.93	2.28	2.70
B	0.38	0.47	0.51	0.09	0.03	-5.34	-9.54	-7.59	-4.20	1.95
C	0.28	0.53	0.56	0.25	0.03	-9.48	-7.16	-5.83	2.32	1.33
D	0.81	0.35	0.20	-0.46	-0.16	-2.16	-7.85	-12.47	-5.69	-4.62
E	0.29	0.51	0.56	0.22	0.05	-9.62	-6.29	-6.56	3.33	-0.27
AxB	0.43	0.45	0.48	0.03	0.03	-3.61	-10.03	-8.83	-6.42	1.20
	NP-HQ									
A	0.46	0.56	0.72	0.10	0.15	-3.21	-7.58	-4.92	-4.38	2.66
B	0.31	0.54	0.89	0.23	0.36	-5.99	-6.79	-2.93	-0.80	3.86
C	0.52	0.60	0.62	0.08	0.01	-6.22	-5.39	-4.11	0.83	1.28
D	0.93	0.50	0.31	-0.44	-0.18	-0.66	-6.06	-8.99	-5.40	-2.92
E	0.54	0.60	0.60	0.05	0.00	-6.23	-4.06	-5.43	2.17	-1.37
AxB	0.48	0.58	0.67	0.10	0.09	-3.26	-6.96	-5.49	-3.71	1.47

Table 4.4.10. Average and main effects of q_{tot} values for raw and S/N data for AN-CP and AN-HQ systems.

	Raw data, Average value			Main effects (Raw data)		S/N data, Average value			Main effects (S/N data)	
	L1	L2	L3	L2-L1	L3-L2	L1	L2	L3	L2-L1	L3-L2
	AN-CP									
A	0.18	0.47	0.56	0.28	0.09	-8.14	-8.45	-6.26	-0.31	2.19
B	0.29	0.36	0.55	0.07	0.19	-6.38	-10.20	-6.27	-3.82	3.93
C	0.33	0.43	0.45	0.10	0.02	-7.98	-7.86	-7.01	0.12	0.86
D	0.66	0.33	0.22	-0.33	-0.12	-3.10	-8.01	-11.75	-4.90	-3.74
E	0.30	0.45	0.46	0.16	0.01	-9.19	-6.34	-7.33	2.85	-0.99
AxB	0.37	0.43	0.41	0.06	-0.02	-4.16	-9.72	-8.97	-5.55	0.74
	AN-HQ									
A	0.30	0.56	0.59	0.26	0.03	-5.21	-7.15	-6.67	-1.94	0.48
B	0.27	0.51	0.68	0.24	0.17	-6.19	-7.75	-5.08	-1.56	2.67
C	0.44	0.49	0.52	0.05	0.03	-6.53	-6.73	-5.77	-0.20	0.96
D	0.72	0.48	0.25	-0.24	-0.23	-3.12	-5.24	-10.66	-2.12	-5.42
E	0.40	0.50	0.56	0.10	0.06	-7.24	-6.43	-5.35	0.81	1.09
AxB	0.44	0.48	0.53	0.04	0.05	-3.81	-8.31	-6.90	-4.50	1.40

Table 4.4.11. ANOVA of q_{tot} and S/N ratio data for NP-P and AN-P systems.

	Sum of squares	DOF	Mean square	% contribution	F - value		Sum of squares	DOF	Mean square	% contribution	F - value
NP-P											
	Raw data						**S/N data**				
A	2.17	2	1.08	37.18	485.48	A	152.69	2	76.34	10.66	57.93
B	0.12	2	0.06	1.98	25.87	B	83.23	2	41.61	5.81	31.58
C	0.45	2	0.22	7.64	99.79	C	76.62	2	38.31	5.35	29.07
D	2.32	2	1.16	39.76	519.16	D	552.03	2	276.02	38.54	209.44
E	0.68	2	0.34	11.72	153.04	E	94.69	2	47.35	6.61	35.93
AxB	0.01	4	0.00	0.23	1.51	AxB	421.84	4	105.46	29.45	80.02
Residual	0.09	39	0.00	1.49		Residual	51.40	39	1.32	3.59	
Model	5.74	14	2.87	98.51	1284.85	Model	1381.09	14	585.09	96.41	443.96
Cor. Total	5.83	53	2.87	100.00		Cor. Total	1432.49	53	586.40	100.00	
AN-P											
A	0.73	2	0.36	13.21	24.24	A	24.65	2	12.32	1.65	1.71
B	0.41	2	0.20	7.44	13.65	B	55.07	2	27.54	3.69	3.82
C	0.03	2	0.01	0.50	0.92	C	26.72	2	13.36	1.79	1.85
D	2.99	2	1.50	54.34	99.71	D	676.31	2	338.16	45.37	46.91
E	0.24	2	0.12	4.27	7.84	E	105.41	2	52.70	7.07	7.31
AxB	0.53	4	0.13	9.61	8.82	AxB	321.20	4	80.30	21.55	11.14
Residual	0.58	39	0.01	10.63		Residual	281.14	39	7.21	18.86	
Model	4.92	14	2.33	89.37	155.18	Model	1209.37	14	524.38	81.14	72.74
Cor. Total	5.50	53	2.34	100.00		Cor. Total	1490.51	53	531.59	100.00	

Table 4.4.12. ANOVA of q_{tot} and S/N ratio data for NP-C and NP-R systems.

	Sum of squares	DOF	Mean square	% contribution	F - value		Sum of squares	DOF	Mean square	% contribution	F - value
NP-C											
	Raw data						**S/N data**				
A	0.79	2	0.39	17.27	11.18	A	20.32	2	10.16	1.84	0.81
B	0.03	2	0.01	0.60	0.39	B	77.37	2	38.69	6.99	3.10
C	0.38	2	0.19	8.28	5.36	C	94.04	2	47.02	8.50	3.77
D	1.22	2	0.61	26.68	17.26	D	177.16	2	88.58	16.01	7.10
E	0.22	2	0.11	4.71	3.05	E	21.49	2	10.75	1.94	0.86
AxB	0.56	4	0.14	12.32	3.99	AxB	229.22	4	57.31	20.72	4.59
Residual	1.38	39	0.04	30.14		Residual	486.68	39	12.48	43.99	
Model	3.19	14	1.45	69.86	41.22	Model	619.60	14	252.49	56.01	20.23
Cor. Total	4.57	53	1.49	100.00		Cor. Total	1106.28	53	264.97	100.00	
NP-R											
A	0.42	2	0.21	9.82	4.58	A	0.59	2	0.30	0.08	0.03
B	0.13	2	0.07	3.15	1.47	B	59.55	2	29.77	7.93	3.03
C	0.18	2	0.09	4.20	1.96	C	51.42	2	25.71	6.85	2.62
D	0.96	2	0.48	22.59	10.53	D	177.90	2	88.95	23.70	9.07
E	0.01	2	0.00	0.15	0.07	E	2.98	2	1.49	0.40	0.15
AxB	0.77	4	0.19	18.28	4.26	AxB	75.48	4	18.87	10.06	1.92
Residual	1.77	39	0.05	41.82		Residual	382.66	39	9.81	50.98	
Model	2.46	14	1.04	58.18	22.87	Model	367.92	14	165.09	49.02	16.83
Cor. Total	4.24	53	1.08	100.00		Cor. Total	750.58	53	174.90	100.00	

Table 4.4.13. ANOVA of q_{tot} and S/N ratio data for AN-C and AN-R systems.

	Sum of squares	DOF	Mean square	% contribution	F - value		Sum of squares	DOF	Mean square	% contribution	F - value
AN-C											
	Raw data						**S/N data**				
A	0.84	2	0.42	33.22	156.43	A	82.72	2	41.36	6.03	74.62
B	0.28	2	0.14	11.21	52.78	B	53.56	2	26.78	3.91	48.32
C	0.21	2	0.10	8.23	38.74	C	58.40	2	29.20	4.26	52.68
D	0.94	2	0.47	37.04	174.41	D	394.30	2	197.15	28.76	355.72
E	0.14	2	0.07	5.46	25.71	E	41.28	2	20.64	3.01	37.24
AxB	0.02	4	0.00	0.69	1.64	AxB	719.26	4	179.82	52.46	324.44
Residual	0.11	39	0.00	4.14		Residual	21.61	39	0.55	1.58	
Model	2.44	14	1.21	95.86	449.71	Model	1349.52	14	494.94	98.42	893.03
Cor. Total	2.54	53	1.22	100.00		Cor. Total	1371.13	53	495.50	100.00	
AN-R											
A	0.94	2	0.47	24.63	23.60	A	28.99	2	14.49	2.61	3.83
B	0.46	2	0.23	12.12	11.61	B	45.21	2	22.60	4.07	5.98
C	0.16	2	0.08	4.10	3.93	C	23.68	2	11.84	2.13	3.13
D	1.33	2	0.67	35.14	33.66	D	448.81	2	224.40	40.39	59.35
E	0.11	2	0.06	2.93	2.81	E	20.54	2	10.27	1.85	2.72
AxB	0.03	4	0.01	0.72	0.34	AxB	396.47	4	99.12	35.68	26.21
Residual	0.77	39	0.02	20.36		Residual	147.47	39	3.78	13.27	
Model	3.02	14	1.50	79.64	75.94	Model	963.69	14	382.73	86.73	101.22
Cor. Total	3.80	53	1.52	100.00		Cor. Total	1111.16	53	386.51	100.00	

Table 4.4.14. ANOVA of q_{tot} and S/N ratio data for NP-AN, NP-CP and NP-HQ systems.

NP-AN											
	Raw data						S/N data				
A	2.76	2	1.38	20.57	20.26	A	17.58	2	8.79	4.91	2.68
B	2.15	2	1.08	16.06	15.82	B	41.95	2	20.97	11.70	6.39
C	0.12	2	0.06	0.88	0.87	C	3.57	2	1.78	1.00	0.54
D	3.01	2	1.50	22.42	22.08	D	134.82	2	67.41	37.62	20.54
E	0.38	2	0.19	2.82	2.77	E	20.50	2	10.25	5.72	3.12
AxB	2.34	4	0.59	17.45	8.59	AxB	11.98	4	3.00	3.34	0.91
Residual	2.66	39	0.07	19.80		Residual	127.98	39	3.28	35.71	
Model	10.76	14	4.79	80.20	70.39	Model	230.39	14	112.20	64.29	34.19
Cor. Total	13.41	53	4.86	100.00		Cor. Total	358.38	53	115.48	100.00	
NP-CP											
A	1.50	2	0.75	33.48	148.60	A	111.96	2	55.98	8.65	30.89
B	0.08	2	0.04	1.75	7.77	B	79.64	2	39.82	6.15	21.98
C	0.43	2	0.22	9.63	42.73	C	61.55	2	30.78	4.76	16.98
D	1.86	2	0.93	41.50	184.21	D	480.07	2	240.03	37.09	132.47
E	0.37	2	0.18	8.23	36.51	E	61.42	2	30.71	4.75	16.95
AxB	0.05	4	0.01	1.02	2.27	AxB	428.93	4	107.23	33.14	59.18
Residual	0.20	39	0.01	4.39		Residual	70.67	39	1.81	5.46	
Model	4.29	14	2.13	95.61	422.09	Model	1223.57	14	504.55	94.54	278.45
Cor. Total	4.48	53	2.14	100.00		Cor. Total	1294.24	53	506.37	100.00	
NP-HQ											
A	0.29	2	0.14	5.98	7.46	A	87.54	2	43.77	10.57	11.18
B	1.56	2	0.78	32.25	40.20	B	74.57	2	37.29	9.01	9.52
C	0.05	2	0.02	0.98	1.22	C	20.30	2	10.15	2.45	2.59
D	1.82	2	0.91	37.71	47.00	D	321.07	2	160.54	38.78	41.00
E	0.02	2	0.01	0.36	0.45	E	21.70	2	10.85	2.62	2.77
AxB	0.34	4	0.09	7.08	4.41	AxB	150.11	4	37.53	18.13	9.58
Residual	0.76	39	0.02	15.64		Residual	152.70	39	3.92	18.44	
Model	4.08	14	1.96	84.36	100.74	Model	675.31	14	300.13	81.56	76.65
Cor. Total	4.84	53	1.97	100.00		Cor. Total	828.01	53	304.04	100.00	

Table 4.4.15. ANOVA of q_{tot} and S/N ratio data for AN-CP and AN-HQ systems.

	Sum of squares	DOF	Mean square	% contribution	F - value		Sum of squares	DOF	Mean square	% contribution	F - value
AN-CP											
A	0.69	2	0.34	26.09	44.38	A	25.31	2	12.66	2.74	6.17
B	0.33	2	0.16	12.47	21.21	B	90.11	2	45.05	9.75	21.96
C	0.07	2	0.04	2.74	4.66	C	5.13	2	2.56	0.56	1.25
D	0.95	2	0.48	36.29	61.71	D	338.14	2	169.07	36.60	82.42
E	0.16	2	0.08	6.00	10.21	E	37.77	2	18.89	4.09	9.21
AxB	0.13	4	0.03	4.93	4.20	AxB	347.33	4	86.83	37.60	42.33
Residual	0.30	39	0.01	11.47		Residual	80.01	39	2.05	8.66	
Model	2.33	14	1.13	88.53	146.37	Model	843.78	14	335.06	91.34	163.33
Cor. Total	2.63	53	1.14	100.00		Cor. Total	923.79	53	337.11	100.00	
AN-CP											
AN-HQ											
A	0.45	2	0.23	12.29	7.24	A	18.32	2	9.16	2.06	1.10
B	0.76	2	0.38	20.85	12.28	B	32.38	2	16.19	3.64	1.95
C	0.03	2	0.01	0.72	0.42	C	4.59	2	2.30	0.52	0.28
D	0.98	2	0.49	26.65	15.70	D	272.32	2	136.16	30.58	16.37
E	0.12	2	0.06	3.25	1.92	E	16.27	2	8.13	1.83	0.98
AxB	0.12	4	0.03	3.14	0.92	AxB	222.29	4	55.57	24.96	6.68
Residual	1.21	39	0.03	33.10		Residual	324.38	39	8.32	36.42	
Model	2.45	14	1.20	66.90	38.49	Model	566.17	14	227.51	63.58	27.35
Cor. Total	3.67	53	1.23	100.00		Cor. Total	890.54	53	235.83	100.00	

Table 4.4.16. Comparison of predicted optimal q_{tot} values, confidence intervals and results of confirmation experiments for binary systems.

System	Optimal levels of process parameters	Predicted optimal values (mmol/g)	Confidence intervals (95%)	Average of Confirmation experiments (mmol/g)
NP-P	A3, B3, C3, D2, E3	1.06	$CI_{POP}: 0.99 < \mu_{GAC} < 1.13$ $CI_{CE}: 0.96 < \mu_{GAC} < 1.16$	1.02
AN-P	A3, B3, C3, D2, E2	1.14	$CI_{POP}: 0.97 < \mu_{GAC} < 1.31$ $CI_{CE}: 0.89 < \mu_{GAC} < 1.39$	1.10
NP-C	A3, B3, C3, D2, E3	0.97	$CI_{POP}: 0.74 < \mu_{GAC} < 1.20$ $CI_{CE}: 0.64 < \mu_{GAC} < 1.30$	0.95
NP-R	A3, B3, C3, D2, E3	0.85	$CI_{POP}: 0.59 < \mu_{GAC} < 1.10$ $CI_{CE}: 0.48 < \mu_{GAC} < 1.21$	0.87
AN-C	A3, B3, C3, D2, E3	0.75	$CI_{POP}: 0.68 < \mu_{GAC} < 0.82$ $CI_{CE}: 0.65 < \mu_{GAC} < 0.85$	0.73
AN-R	A3, B3, C3, D2, E3	0.92	$CI_{POP}: 0.69 < \mu_{GAC} < 1.10$ $CI_{CE}: 0.62 < \mu_{GAC} < 1.18$	0.95
NP-CP	A3, B3, C3, D2, E2	0.86	$CI_{POP}: 0.76 < \mu_{GAC} < 0.96$ $CI_{CE}: 0.72 < \mu_{GAC} < 1.01$	0.89
NP-AN	A3, B3, C3, D2, E3	2.15	$CI_{POP}: 1.78 < \mu_{GAC} < 2.53$ $CI_{CE}: 1.63 < \mu_{GAC} < 2.68$	2.18
NP-HQ	A3, B3, C3, D2, E3	1.00	$CI_{POP}: 0.80 < \mu_{GAC} < 1.20$ $CI_{CE}: 0.72 < \mu_{GAC} < 1.30$	0.96
AN-CP	A3, B3, C3, D2, E3	0.76	$CI_{POP}: 0.63 < \mu_{GAC} < 0.88$ $CI_{CE}: 0.58 < \mu_{GAC} < 0.94$	0.79
AN-HQ	A3, B3, C3, D2, E3	0.90	$CI_{POP}: 0.65 < \mu_{GAC} < 1.16$ $CI_{CE}: 0.55 < \mu_{GAC} < 1.26$	0.93

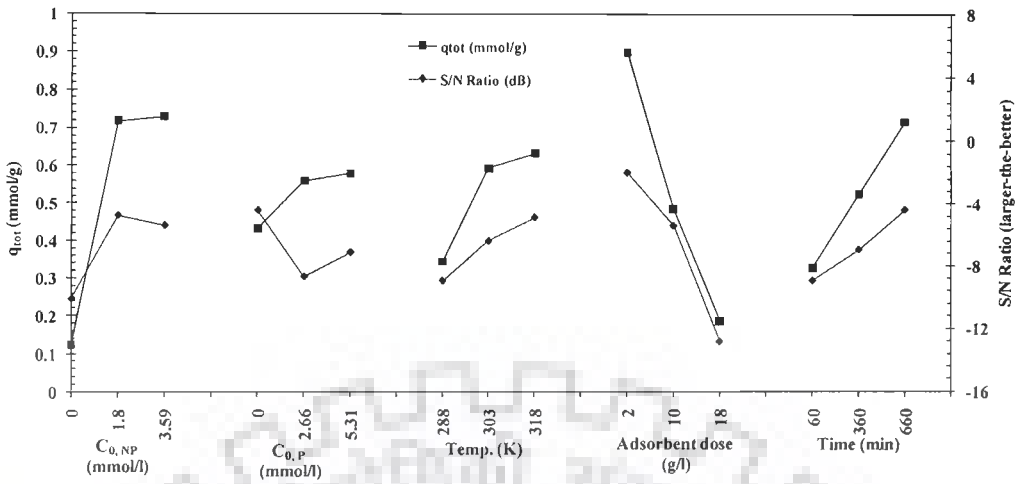

Figure 4.4.1. Effect of process parameters on q_{tot} and S/N ratio for binary adsorption of NP and P onto GAC.

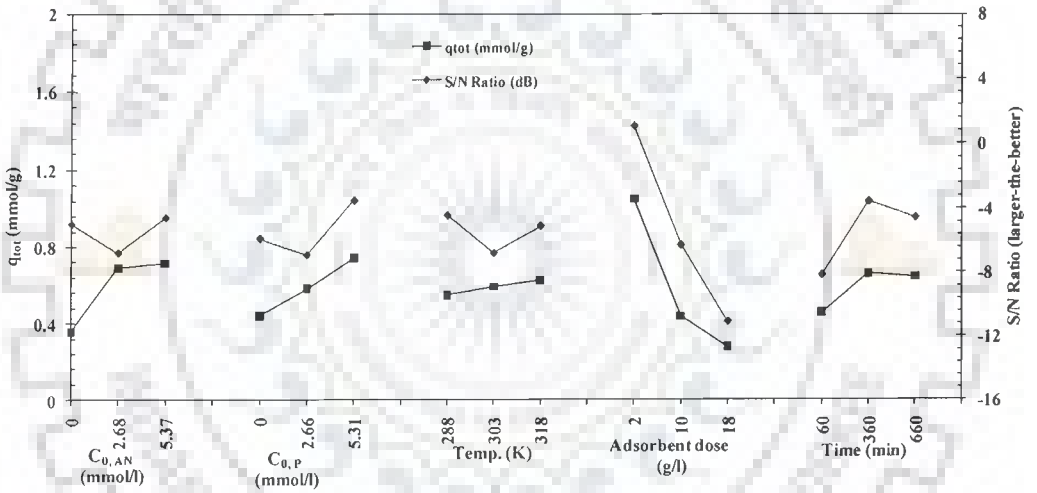

Figure 4.4.2. Effect of process parameters on q_{tot} and S/N ratio for binary adsorption of AN and P onto GAC.

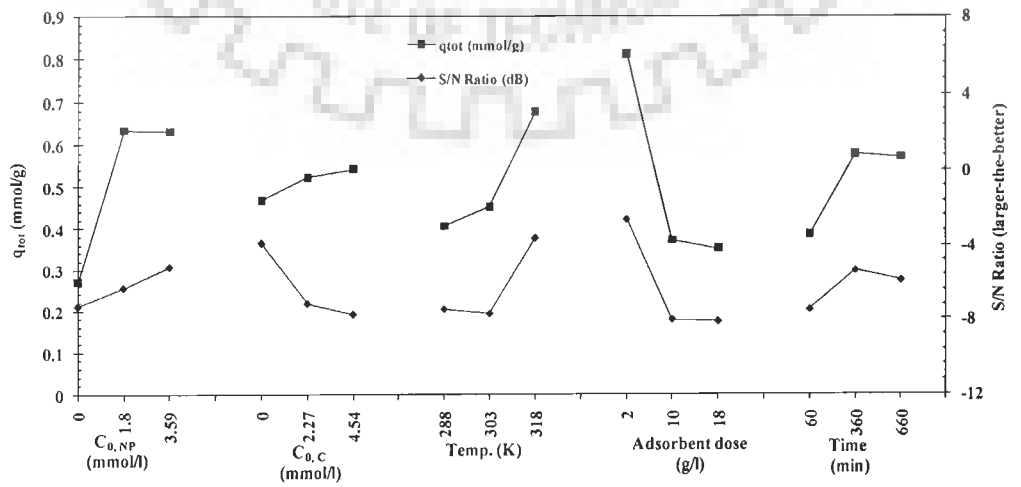

Figure 4.4.3. Effect of process parameters on q_{tot} and S/N ratio for binary adsorption of NP and C onto GAC.

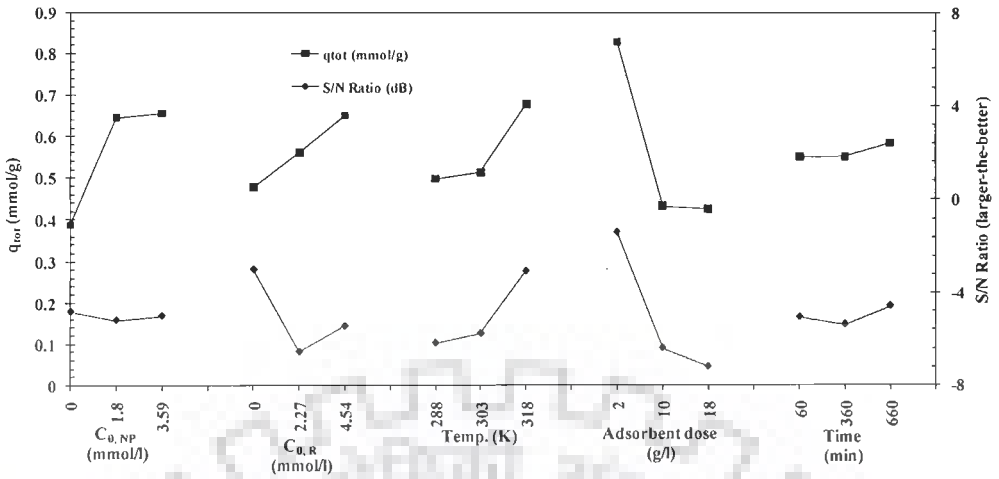

Figure 4.4.4. Effect of process parameters on q_{tot} and S/N ratio for binary adsorption of NP and R onto GAC.

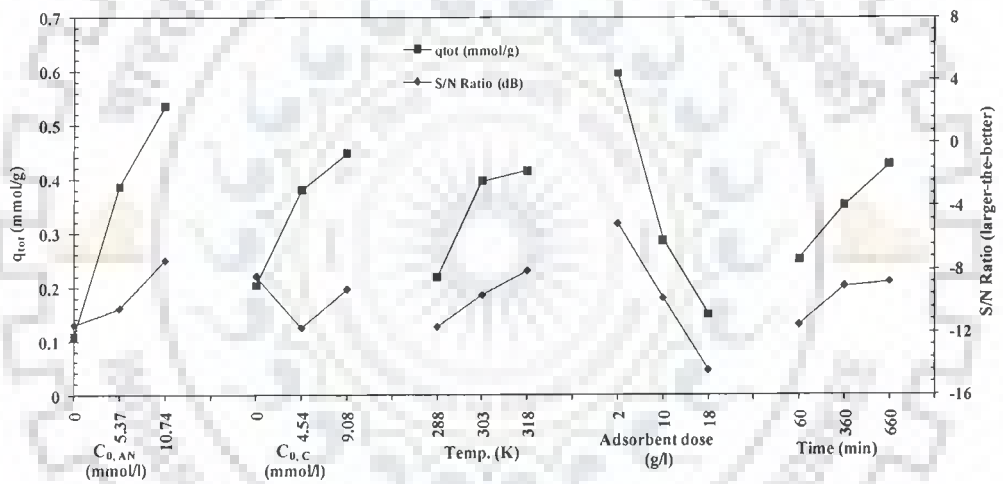

Figure 4.4.5. Effect of process parameters on q_{tot} and S/N ratio for binary adsorption of AN and C onto GAC.

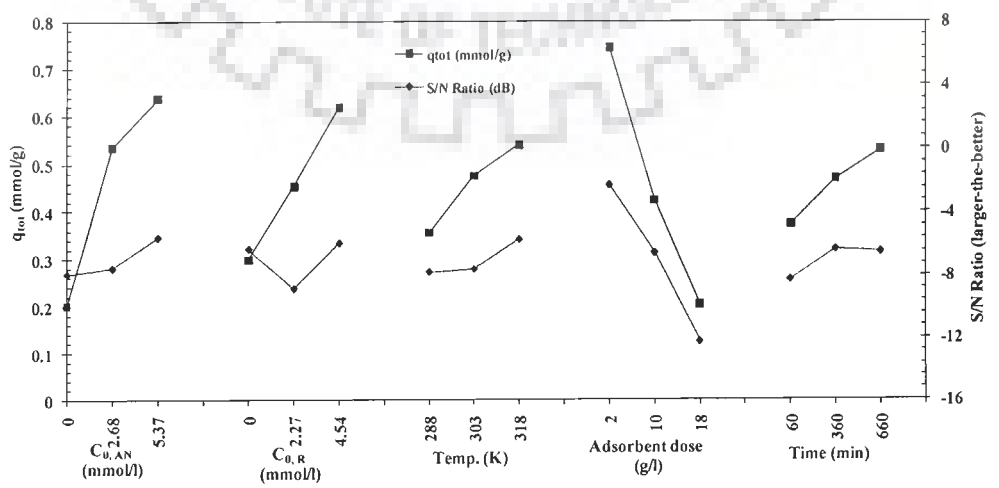

Figure 4.4.6. Effect of process parameters on q_{tot} and S/N ratio for binary adsorption of AN and R onto GAC.

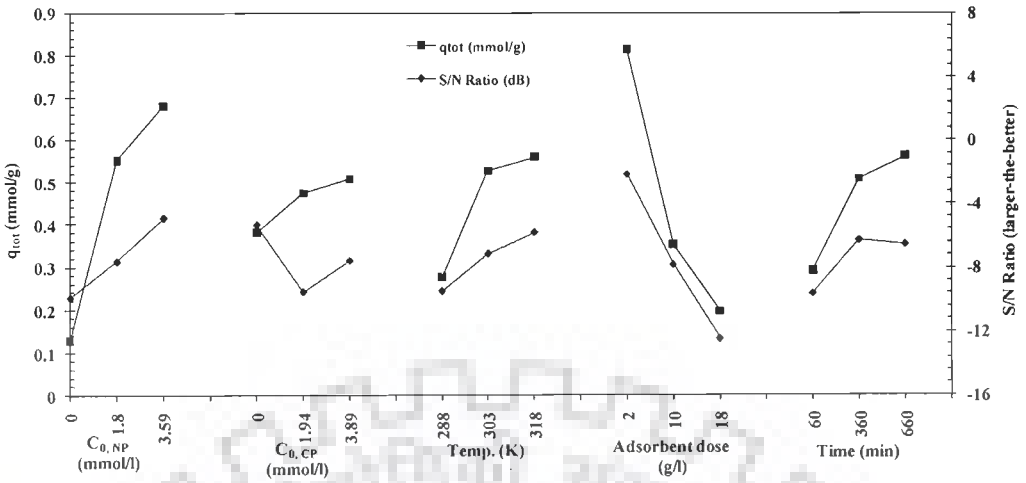

Figure 4.4.7. Effect of process parameters on q_{tot} and S/N ratio for binary adsorption of NP and CP onto GAC.

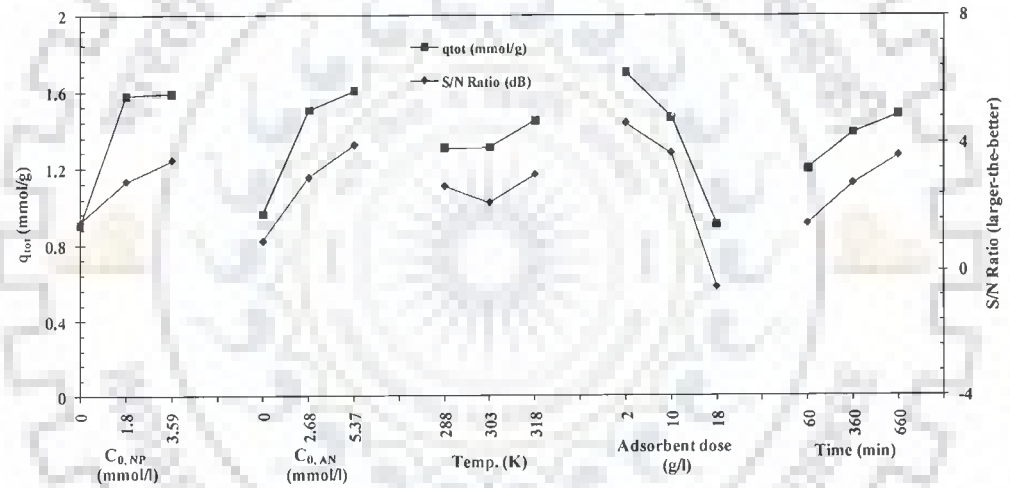

Figure 4.4.8. Effect of process parameters on q_{tot} and S/N ratio for binary adsorption of NP and AN onto GAC.

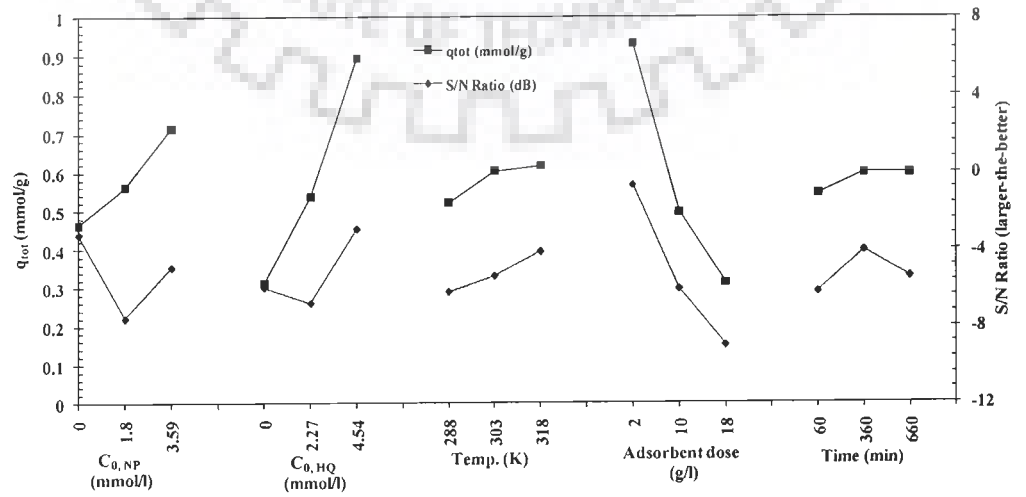

Figure 4.4.9. Effect of process parameters on q_{tot} and S/N ratio for binary adsorption of NP and HQ onto GAC.

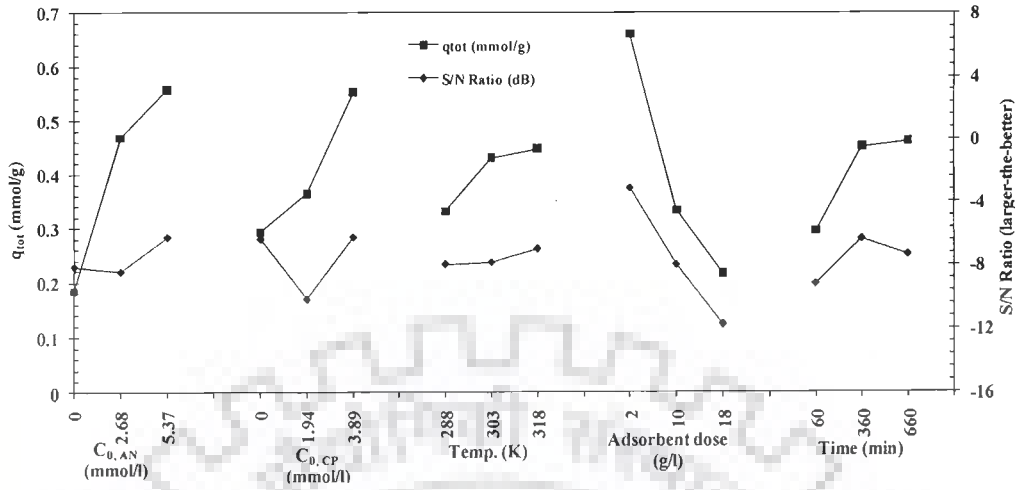

Figure 4.4.10. Effect of process parameters on q_{tot} and S/N ratio for binary adsorption of AN and CP onto GAC.

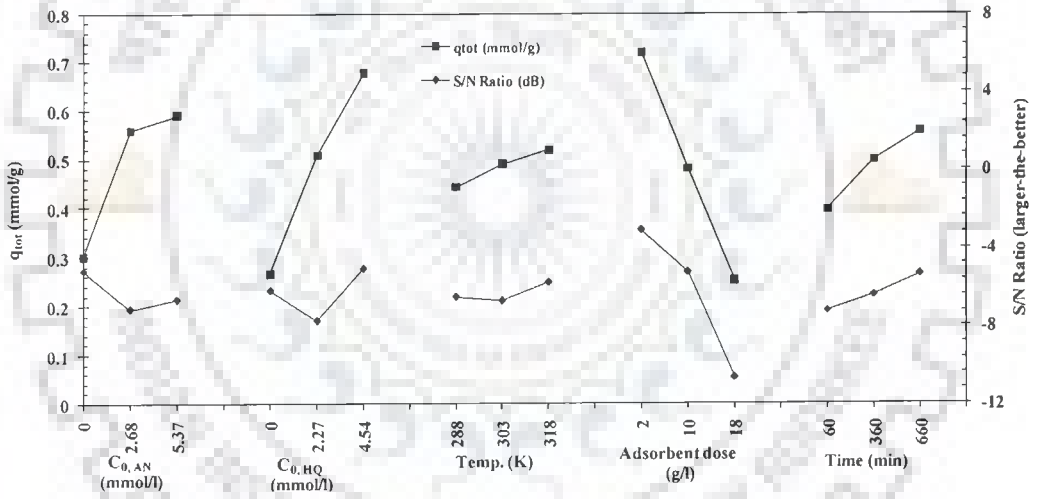

Figure 4.4.11. Effect of process parameters on q_{tot} and S/N ratio for binary adsorption of AN and HQ onto GAC.

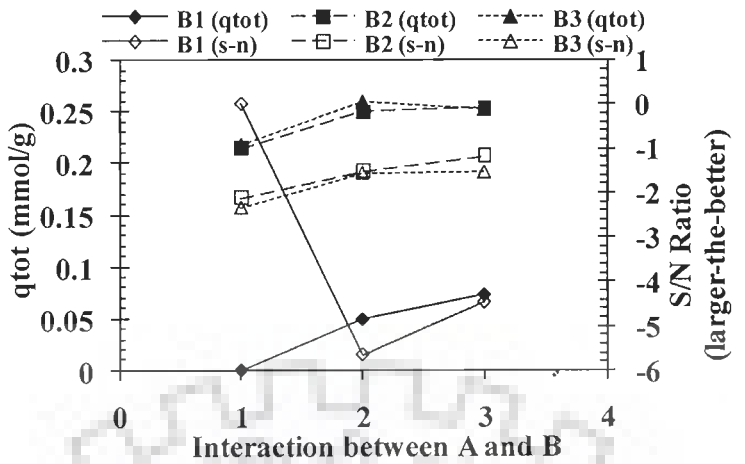

Figure 4.4.12. The interaction between A and B parameters at 3 levels on q_{tot} and S/N ratio for binary adsorption of NP and P onto GAC.

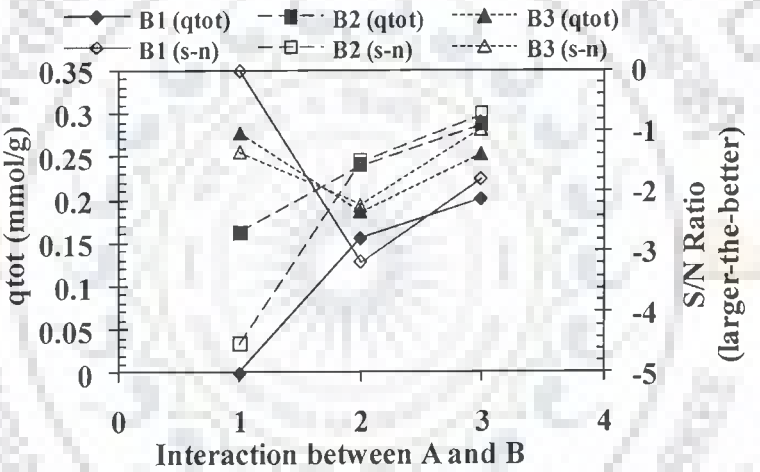

Figure 4.4.13. The interaction between A and B parameters at 3 levels on q_{tot} and S/N ratio for binary adsorption of AN and P onto GAC.

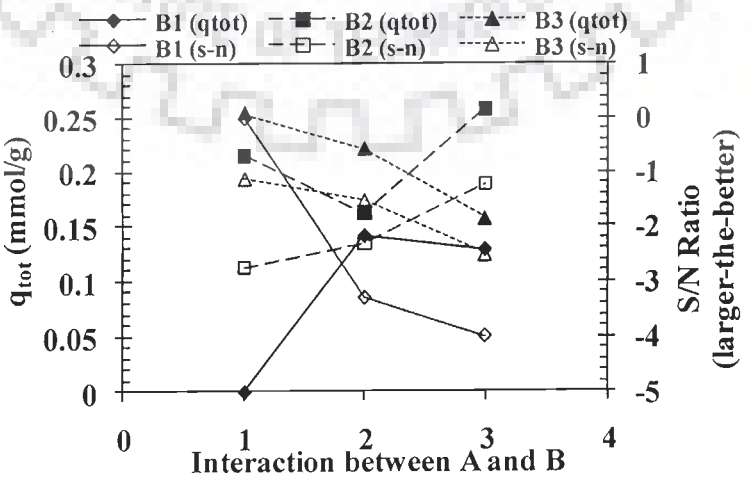

Figure 4.4.14. The interaction between A and B parameters at 3 levels on q_{tot} and S/N ratio for binary adsorption of NP and C onto GAC.

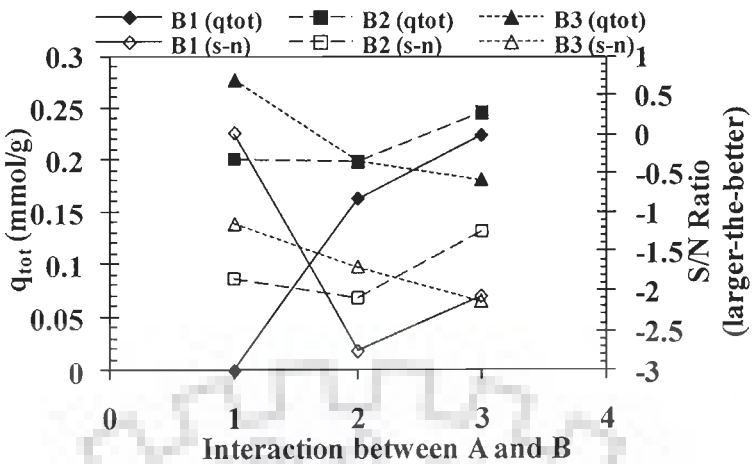

Figure 4.4.15. The interaction between A and B parameters at 3 levels on q_{tot} and S/N ratio for binary adsorption of NP and R onto GAC.

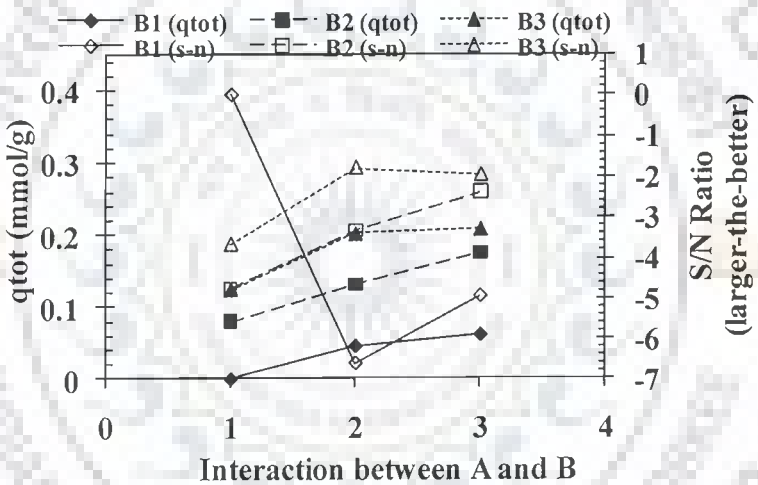

Figure 4.4.16. The interaction between A and B parameters at 3 levels on q_{tot} and S/N ratio for binary adsorption of AN and C onto GAC.

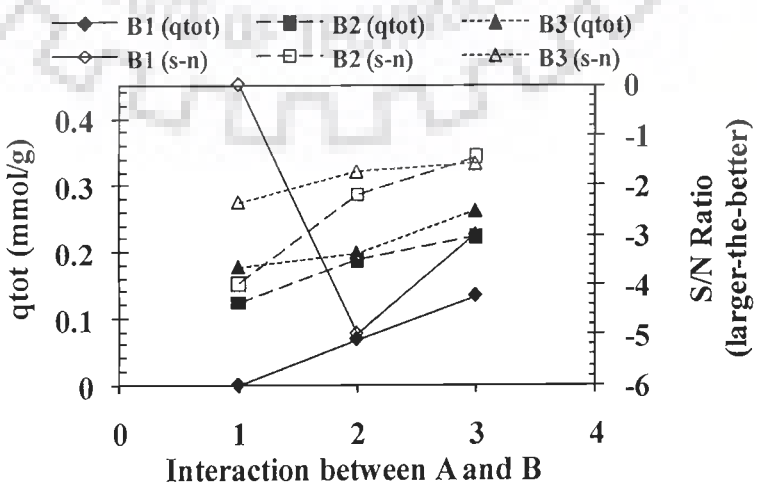

Figure 4.4.17. The interaction between A and B parameters at 3 levels on q_{tot} and S/N ratio for binary adsorption of AN and R onto GAC.

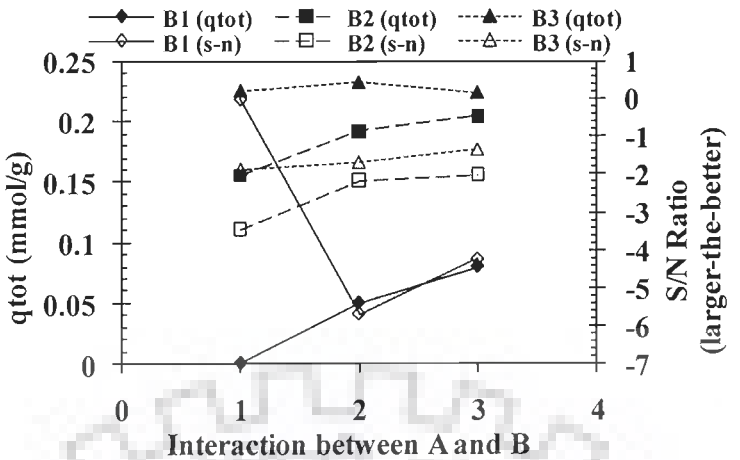

Figure 4.4.18. The interaction between A and B parameters at 3 levels on q_{tot} and S/N ratio for binary adsorption of NP and CP onto GAC.

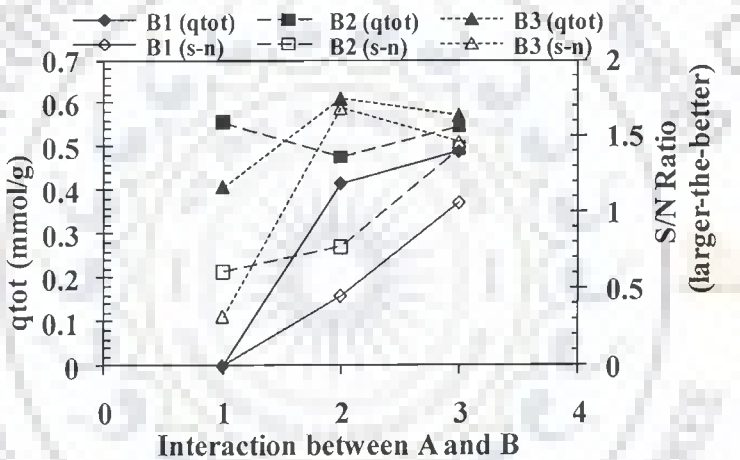

Figure 4.4.19. The interaction between A and B parameters at 3 levels on q_{tot} and S/N ratio for binary adsorption of NP and AN onto GAC.

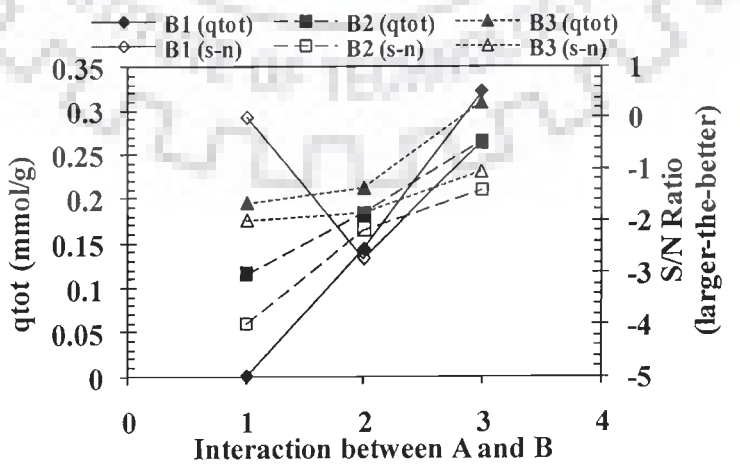

Figure 4.4.20. The interaction between A and B parameters at 3 levels on q_{tot} and S/N ratio for binary adsorption of NP and HQ onto GAC.

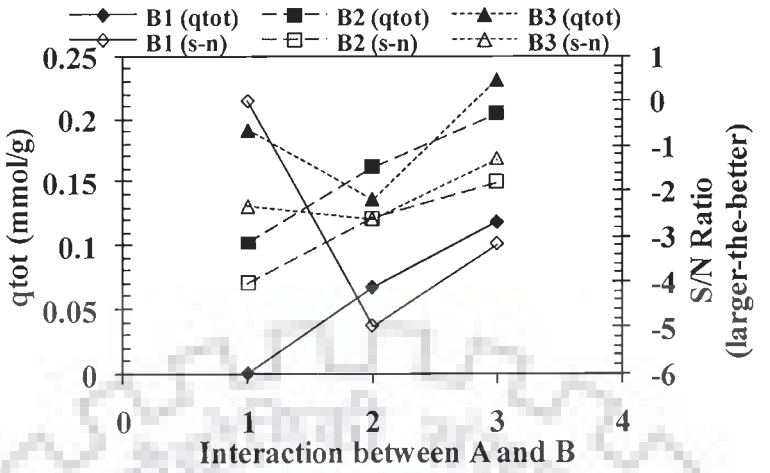

Figure 4.4.21. The interaction between A and B parameters at 3 levels on q_{tot} and S/N ratio for binary adsorption of AN and CP onto GAC.

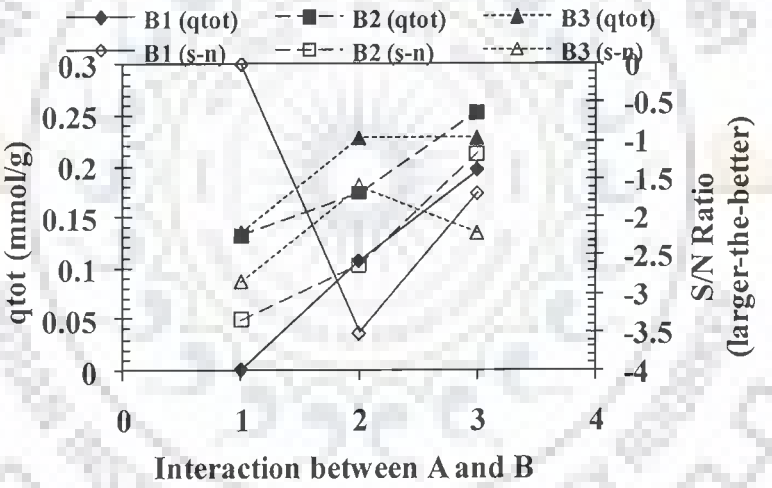

Figure 4.4.22. The interaction between A and B parameters at 3 levels on q_{tot} and S/N ratio for binary adsorption of AN and HQ onto GAC.

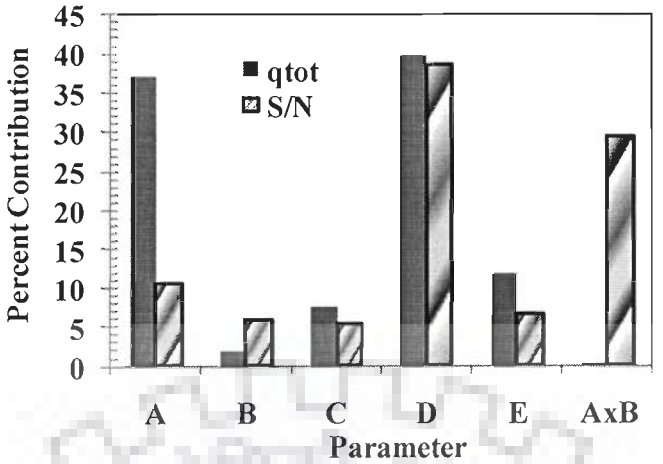

Figure 4.4.23. Percent contribution of various parameters for q_{tot} for binary adsorption of NP and P onto GAC.

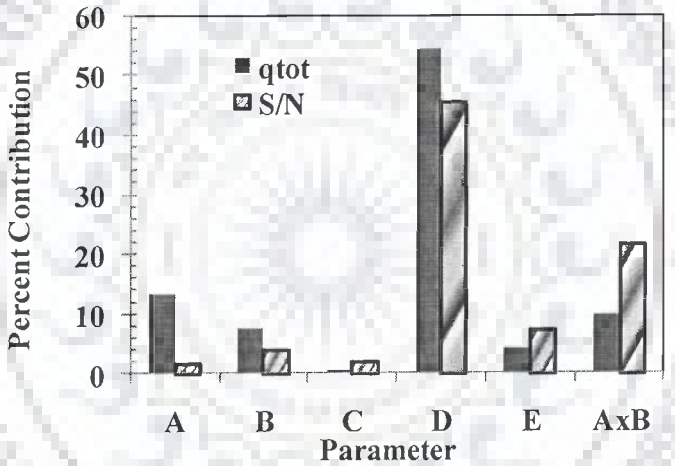

Figure 4.4.24. Percent contribution of various parameters for q_{tot} for binary adsorption of AN and P onto GAC.

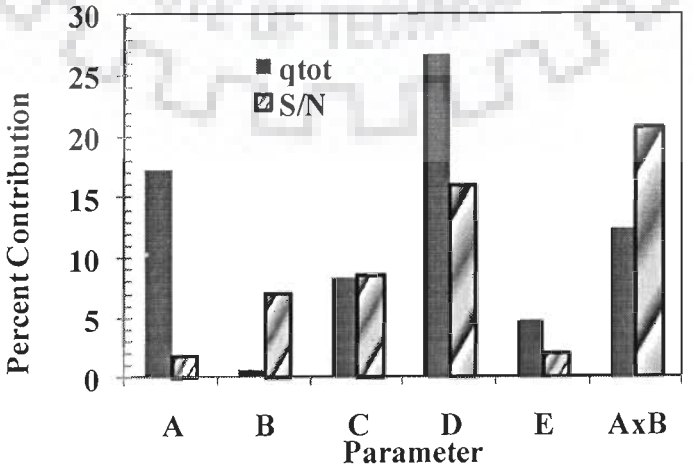

Figure 4.4.25. Percent contribution of various parameters for q_{tot} for binary adsorption of NP and C onto GAC.

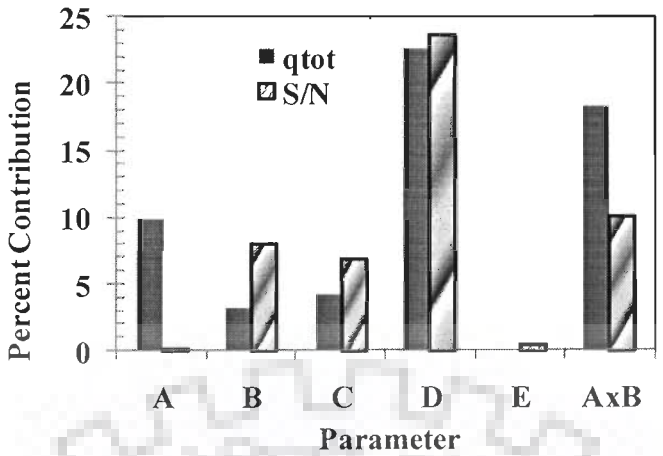

Figure 4.4.26. Percent contribution of various parameters for q_{tot} for binary adsorption of NP and R onto GAC.

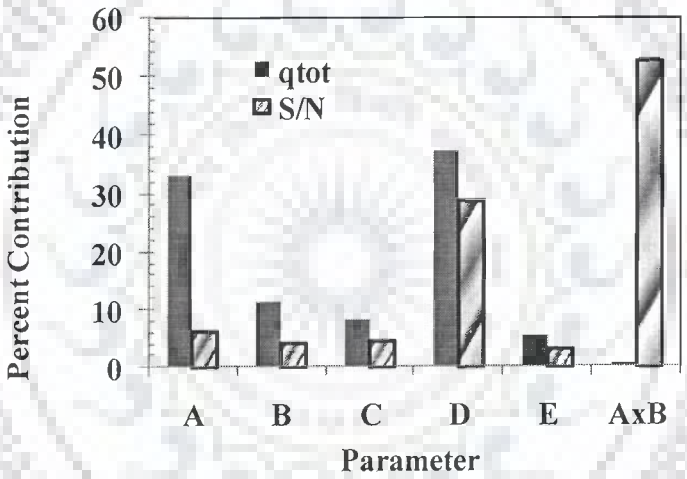

Figure 4.4.27. Percent contribution of various parameters for q_{tot} for binary adsorption of AN and C onto GAC.

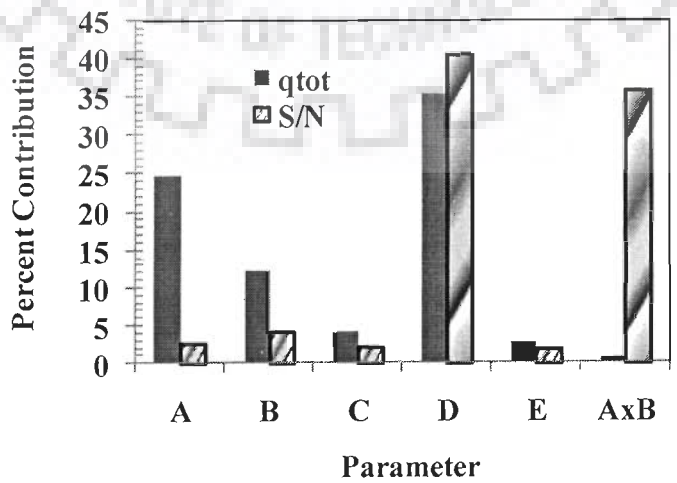

Figure 4.4.28. Percent contribution of various parameters for q_{tot} for binary adsorption of AN and R onto GAC.

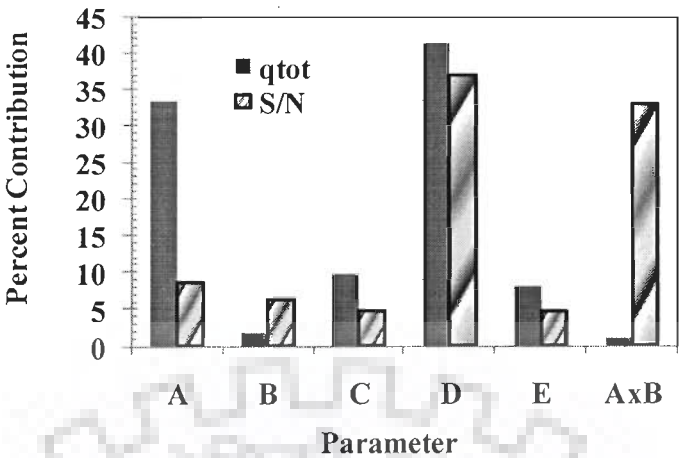

Figure 4.4.29. Percent contribution of various parameters for q_{tot} for binary adsorption of NP and CP onto GAC.

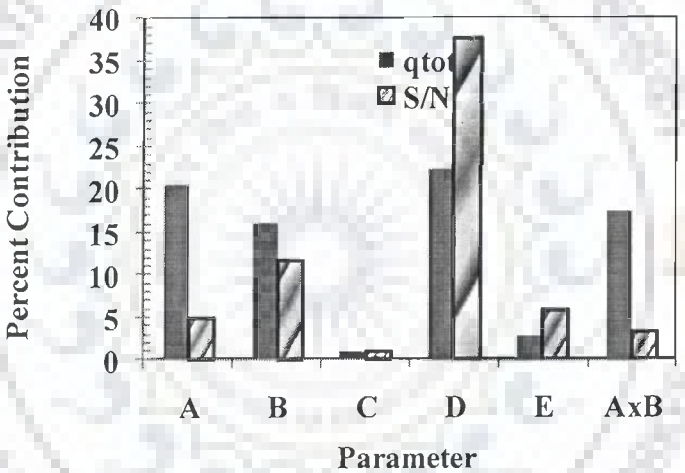

Figure 4.4.30. Percent contribution of various parameters for q_{tot} for binary adsorption of NP and AN onto GAC.

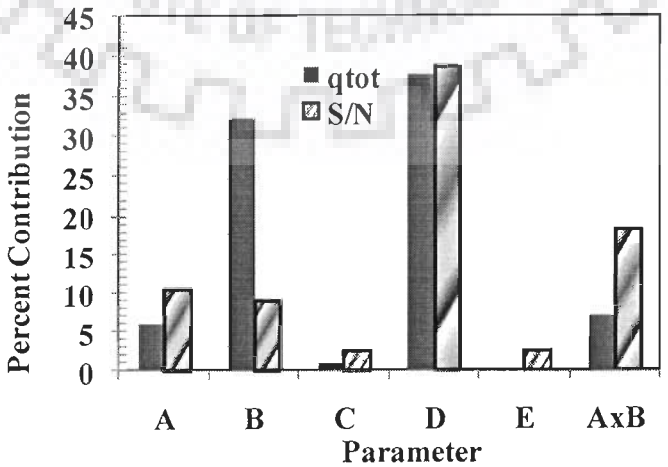

Figure 4.4.31. Percent contribution of various parameters for q_{tot} for binary adsorption of NP and HQ onto GAC.

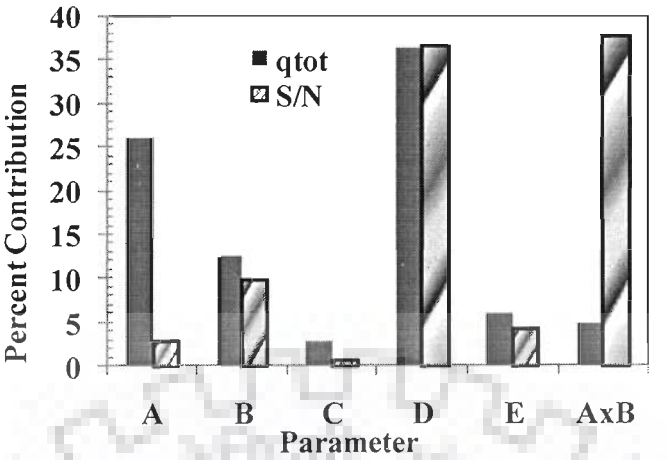

Figure 4.4.32. Percent contribution of various parameters for q_{tot} for binary adsorption of AN and CP onto GAC.

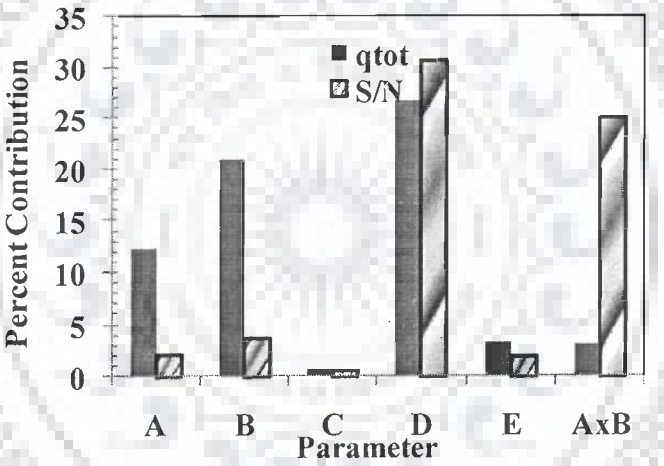

Figure 4.4.33. Percent contribution of various parameters for q_{tot} for binary adsorption of AN and HQ onto GAC.

4.4.2 Optimization of Parameters for Ternary Systems

The effect of individual parameters ($C_{0,i}$, T, m and t) on the selected response characteristics (q_{tot}) for the simultaneous removal of adsorbates from P-CP-NP and C-R-HQ ternary systems are being reported in this section. The interaction effect of concentration of one adsorbate with respect to (w.r.t) other adsorbate will also be discussed. The average or mean values of response characteristics and S/N ratio for each parameter at level 1, 2, and 3 are calculated from Table 4.4.17.

Individually at level stage with q_{tot} as the desired response characteristic, $C_{0,i}$ (parameter A) has highest influence at level 1, $C_{0,i}$ (parameter B) has highest influence at level 2. and $C_{0,i}$ or $C_{0,Zn}$ (parameters A or C) have highest influence at level 3. An increase in adsorption with m can be attributed to the availability of greater surface area and more adsorption sites.

It can be seen from Table 4.4.18 that no single parameter has overriding influence for the removal of P, CP and NP from aqueous solution by GAC. The difference between level 2 and level 1 (L2−L1) of each factor indicates the relative influence of the effect. The larger the difference, the stronger is the influence. $C_{0,i}$ show strong influence on q_{tot} as compared to other parameters. The q_{tot} removal increased with the increase in the adsorbate concentration as the resistance to the uptake of adsorbates from the solution decreases with the increase in $C_{0,i}$.

The response curves for the individual effects of adsorption parameters on the average value of q_{tot} and respective S/N ratio for P-CP-NP and C-R-HQ ternary systems are given in Fig. 4.4.34 and 4.4.35, respectively.

An increase in the levels of factors such as T from 1 to 2 and from 2 to 3 has resulted in an increase in the q_{tot} values for all adsorbents. It has been shown in earlier sections that the adsorption of P, CP, NP, C, R and HQ from aqueous solution onto GAC is endothermic in nature due to the endothermicity of the pore-diffusion of adsorbate into meso- and micro-pores of the adsorbents and the chemisorptive nature of the adsorption process. This endothermicity manifests itself in the enhancement of the sorptive capacity of the GAC with an increase in T.

It can be noted from Table 4.4.18 that the interactions between initial

concentrations of adsorbates [(A x B), (A x C) or (B x C)] is significant in affecting the average value of q_{tot}. These interaction graphs for P-CP-NP and C-R-HQ ternary systems are shown in Figs. 4.4.36 and 4.4.37, respectively, for q_{tot} values along-with the S/N ratios. From these graphs, it can be seen that the effect of initial concentration of one adsorbate on q_{tot} values is more pronounced at the lower concentration of other adsorbate for all possible interactions. It has been shown earlier that the mutual effect of one adsorbate ion for the adsorption of other adsorbate ion is antagonistic in nature. At lower initial adsorbate concentrations, the antagonistic nature is least observed. Therefore, when the initial concentration is increased from lowest level to next higher level, q_{tot} values show highest increment rate. When initial concentration is further increased, this rate of increment of q_{tot} values decreases for both P-CP-NP and C-R-HQ ternary systems.

In Taguchi approach, ANOVA is used to analyze the results of the OA experiment and to determine how much variation each factor has contributed. ANOVA results for raw and S/N ratio data with desired response characteristics (q_{tot}) are given in Table 4.4.19 for both P-CP-NP and C-R-HQ ternary systems. From the calculated ratios (F), it can be referred that all factors and interactions considered in the experimental design with q_{tot} as desired response characteristic are statically significant effects at 95% confidence limit. The percentage contribution of each parameter for q_{tot} as desired response characteristic for P-CP-NP and C-R-HQ ternary systems is shown in Figs. 4.4.38 and 4.4.39, respectively. It can also be observed from these figures that the interaction between the parameters A, B and C contribute significantly to both raw and S/N ratio data for simultaneous adsorbate removal onto GAC for both P-CP-NP and C-R-HQ ternary systems.

Table 4.4.20 summarizes the optimal level of various parameters obtained after examining the response curves (Fig. 4.4.34 and 4.4.35) of the average value of q_{tot} and S/N ratios for both P-CP-NP and C-R-HQ ternary systems. Table 4.4.20 indicates that 3rd levels of parameters A, B and C ($C_{0,i}$) and D (Temperature) and 1st level of parameter F (m) give higher average value of q_{tot} and S/N ratio. Since the aim of the work is to removal maximum amount of adsorbates with highest possible concentration of present together, therefore, 3rd levels of parameters A, B and C are suggested for further

calculations.

The Taguchi approach for predicting the mean of response characteristics and the determination of confidence intervals for the predicted means have been presented in Chapter III. By adopting a similar procedure, predicted optimal q_{tot} values and confidence intervals (CI_{POP} and CI_{CE}) have been calculated and presented in Table 4.4.20 for simultaneous adsorption of P, CP, NP, and C, R, HQ from aqueous solution onto GAC for both P-CP-NP and C-R-HQ ternary systems.

Three confirmation experiments have been conducted at selected optimal levels of the process parameters. The average values of the characteristics are obtained and compared with the predicted values. The results are given in Table 4.4.20. The values of q_{tot} obtained through confirmation experiments are within 95% of CI_{CE} for respective ternary systems.

4.4.3 Summary

Taguchi's method is applied in adsorption studies of AN, P, CP, NP, C, R and HQ from aqueous solutions by GAC. The following conclusions can be drawn from the results: (i) The most important parameter affecting the adsorption of AN, P, CP, NP, C, R and HQ from aqueous solutions by GAC is the adsorbent dose (m), and (ii) All the factors and the interactions considered in the experimental design with q_{tot} as the desired response characteristic are statistically significant at 95% confidence level.

Table 4.4.17. Experimental q_{tot} and S/N ratio values for Taguchi's L_{27} (3^{13}) orthogonal array for P-CP-NP and C-R-HQ ternary systems.

	P-CP-NP				C-R-HQ			
Exp. no.	R1	R2	R3	S/N	R1	R2	R3	S/N
1	0.000	0.000	0.000	0	0.000	0.000	0.000	0
2	1.164	1.167	1.166	1.33	1.183	0.998	0.990	0.40
3	1.336	1.335	1.336	2.51	1.372	1.225	1.298	2.24
4	1.079	1.076	1.078	0.65	1.920	1.966	1.929	5.75
5	1.111	1.136	1.123	1.01	1.989	2.046	2.017	6.09
6	0.803	1.438	1.120	0.25	2.559	2.555	2.557	8.16
7	1.376	1.376	1.376	2.77	3.949	3.136	3.593	10.91
8	3.695	3.526	3.610	11.15	3.345	3.268	3.306	10.39
9	3.143	3.109	3.126	9.90	1.059	1.087	1.073	0.61
10	0.675	0.665	0.671	-3.48	0.685	0.684	0.684	-3.29
11	3.163	7.618	3.391	11.67	2.848	3.830	2.839	9.78
12	1.759	1.802	1.780	5.01	1.659	1.699	1.679	4.50
13	4.205	3.605	3.905	11.78	1.685	1.310	1.875	3.91
14	2.500	2.502	2.501	7.96	1.989	2.046	2.017	6.09
15	2.110	2.049	2.080	6.36	2.559	2.555	2.557	8.16
16	3.102	3.085	3.093	9.81	3.949	3.136	3.593	10.91
17	1.611	1.512	1.561	3.86	2.282	2.212	2.285	7.08
18	7.818	7.994	11.406	18.78	5.345	5.268	5.306	14.50
19	2.348	2.335	2.342	7.39	2.059	2.087	2.073	6.33
20	1.432	1.384	1.408	2.97	1.750	1.766	1.758	4.90
21	2.797	3.283	3.040	9.60	5.984	5.900	5.493	15.24
22	1.922	1.921	1.922	5.67	1.580	1.614	1.597	4.07
23	8.144	3.490	3.317	12.03	4.680	4.917	4.999	13.73
24	2.659	2.631	2.645	8.45	4.210	4.131	4.170	12.40
25	8.309	8.681	8.995	18.74	5.807	5.177	4.442	14.07
26	3.622	3.544	3.583	11.08	4.340	3.809	3.575	11.76
27	3.612	3.583	3.598	11.12	3.272	2.286	3.279	9.00
Total	75.50	75.85	75.17		74.06	70.71	70.99	
Mean			6.97				7.991	

Table 4.4.18. Average and main effects of q_{tot} values for raw and S/N data for P-CP-NP and C-R-HQ ternary systems.

	Raw data, Average value			Main effects (Raw data)		S/N data, Average value			Main effects (S/N data)	
	L1	**L2**	**L3**	**L2-L1**	**L3-L2**	**L1**	**L2**	**L3**	**L2-L1**	**L3-L2**
	P-CP-NP									
A	1.55	3.27	3.58	1.72	0.31	3.29	7.97	9.67	4.69	1.70
B	1.83	2.37	4.19	0.54	1.81	4.11	6.02	10.80	1.91	4.78
C	2.56	2.74	3.09	0.18	0.35	5.93	7.01	8.00	1.08	0.99
D	2.11	2.93	3.35	0.81	0.42	5.99	6.55	8.38	0.56	1.83
E	2.69	2.72	2.98	0.03	0.27	6.86	6.00	8.08	-0.86	2.08
F	2.52	2.43	3.44	-0.10	1.02	7.23	6.17	7.53	-1.06	1.36
AxB	2.92	2.79	2.68	-0.14	-0.11	7.41	6.13	7.39	-1.28	1.26
AxC	2.55	3.03	2.81	0.48	-0.23	6.43	7.57	6.93	1.14	-0.63
BxC	2.50	3.13	2.76	0.62	-0.36	6.10	7.57	7.26	1.47	-0.30
	C-R-HQ									
A	1.87	2.54	3.58	0.67	1.04	4.95	6.85	10.17	1.90	3.32
B	1.95	2.59	3.45	0.65	0.86	4.45	7.60	9.91	3.14	2.32
C	2.24	2.71	3.04	0.46	0.34	5.85	7.80	8.31	1.95	0.51
D	2.16	2.82	3.01	0.66	0.20	6.45	6.86	8.66	0.41	1.80
E	2.19	2.94	2.86	0.75	-0.08	5.95	7.54	8.48	1.58	0.94
F	2.63	2.51	2.85	-0.12	0.33	7.40	7.11	7.45	-0.29	0.34
AxB	2.48	2.85	2.66	0.37	-0.19	6.72	8.04	7.20	1.32	-0.84
AxC	2.86	2.77	2.36	-0.09	-0.41	8.36	7.42	6.19	-0.94	-1.23
BxC	2.36	2.67	2.96	0.31	0.30	6.34	7.37	8.26	1.03	0.90

Table 4.4.19. ANOVA of q_{tot} and S/N ratio data for P-CP-NP and C-R-HQ ternary systems.

	Sum of squares	DOF	Mean square	% contribution	F - value		Sum of squares	DOF	Mean square	% contribution	F - value
P-CP-NP											
Raw data						**S/N data**					
A	64.40	2	32.20	16.30	12.85	A	196.99	2	98.49	24.42	0.95
B	82.29	2	41.14	20.83	16.42	B	213.77	2	106.89	26.50	1.03
C	3.89	2	1.94	0.98	0.78	C	19.32	2	9.66	2.40	0.09
D	21.15	2	10.58	5.35	4.22	D	28.12	2	14.06	3.49	0.14
E	1.41	2	0.71	0.36	0.28	E	19.64	2	9.82	2.43	0.09
F	17.03	2	8.51	4.31	3.40	F	9.15	2	4.58	1.13	0.04
AxB	3.18	4	0.80	0.81	0.32	AxB	25.91	4	6.48	3.21	0.06
AxC	26.23	4	6.56	6.64	2.62	AxC	31.19	4	7.80	3.87	0.07
BxC	35.13	4	8.78	8.89	3.51	BxC	54.18	4	13.55	6.72	0.13
Residual	140.31	56	2.51	35.52		Residual	208.30	2	104.15	25.82	
Model	254.72	24	111.22	64.48	43.39	Model	598.28	24	167.17	48.35	1.61
Cor. Total	395.03	80	113.73	100		Cor. Total	806.58	26	375.47	100	
C-R-HQ											
A	40.38	2	20.19	22.80	32.04	A	125.49	2	62.74	20.26	1.25
B	30.78	2	15.39	17.38	24.42	B	135.03	2	67.51	21.80	1.35
C	8.72	2	4.36	4.92	6.92	C	30.37	2	15.19	4.90	0.30
D	10.88	2	5.44	6.14	8.63	D	24.90	2	12.45	4.02	0.25
E	9.13	2	4.57	5.16	7.24	E	29.31	2	14.66	4.73	0.29
F	1.55	2	0.77	0.87	1.23	F	0.60	2	0.30	0.10	0.01
AxB	7.54	4	1.89	4.26	2.99	AxB	31.64	4	7.91	5.11	0.16
AxC	7.61	4	1.90	4.30	3.02	AxC	45.33	4	11.33	7.32	0.23
BxC	25.25	4	6.31	14.26	10.02	BxC	96.53	4	24.13	15.59	0.48
Residual	35.29	56	0.63	19.92		Residual	100.14	2	50.07	16.17	
Model	141.83	24	60.82	80.08	95.51	Model	519.20	24	166.15	83.83	3.32
Cor. Total	177.12	80	61.45	100		Cor. Total	619.33	26	266.29	100.00	

Table 4.4.20. Comparison of predicted optimal q_{tot} values, confidence intervals and results of confirmation experiments for P-CP-NP and C-R-HQ ternary systems.

System	Optimal levels of process parameters	Predicted optimal values (mmol/g)	Confidence intervals (95%)	Average of Confirmation experiments (mmol/g)
P-CP-NP	A3, B3, C3, D3, E1,F3	6.95	$CI_{POP}: 6.55 < \mu_{GAC} < 7.38$ $CI_{CE}: 6.38 < \mu_{GAC} < 7.55$	6.97
C-R-HQ	A3, B3, C3, D3, E1,F3	7.95	$CI_{POP}: 7.57 < \mu_{GAC} < 8.40$ $CI_{CE}: 7.41 < \mu_{GAC} < 8.58$	7.98

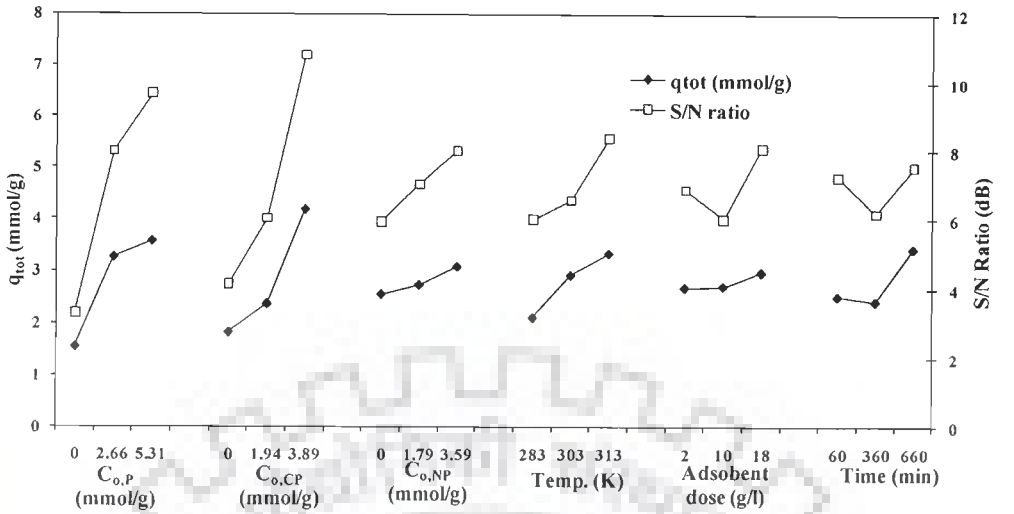

Figure 4.4.34. Effect of process parameters on q_{tot} and S/N ratio for ternary adsorption of P, CP and NP onto GAC.

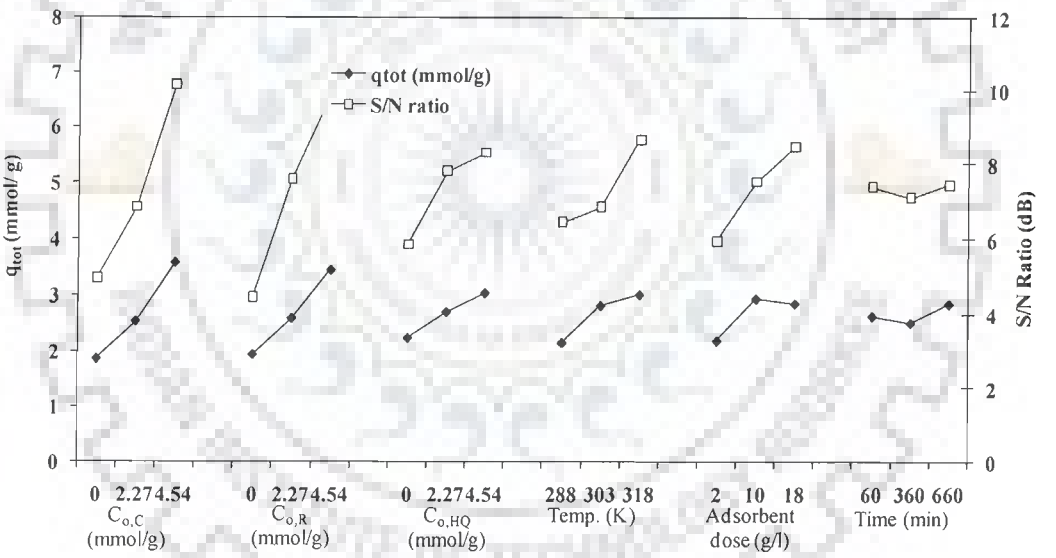

Figure 4.4.35. Effect of process parameters on q_{tot} and S/N ratio for ternary adsorption of C, R and HQ onto GAC.

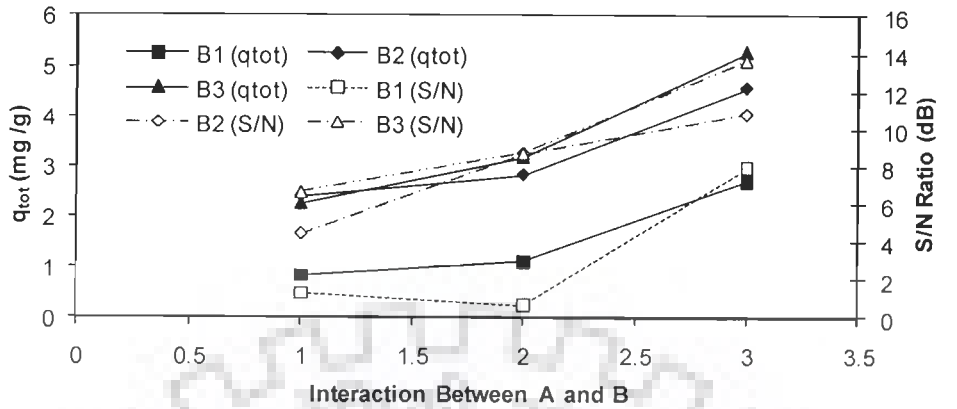

(A) A x B

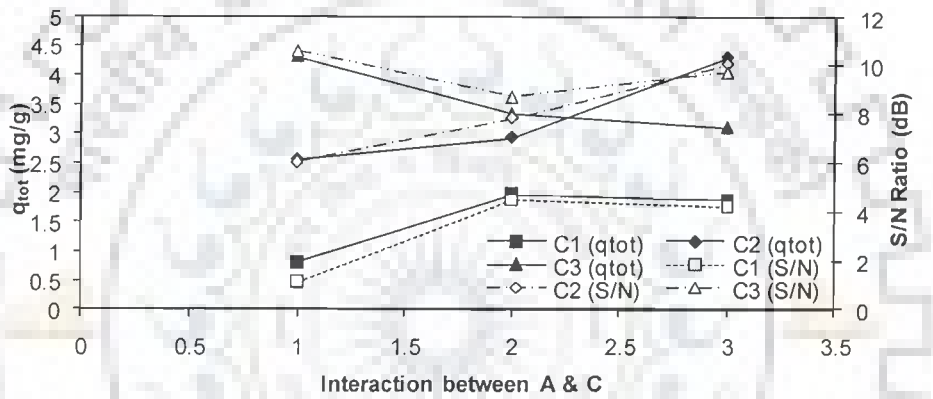

(B) A x C

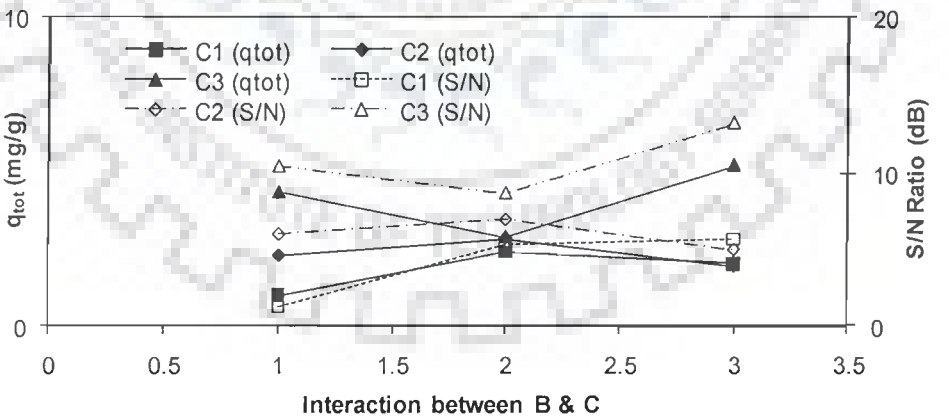

(C) B x C

Figure 4.4.36. The interaction between A, B and C parameters at 3 levels on q_{tot} and S/N ratio for ternary adsorption of P, CP and NP onto GAC.

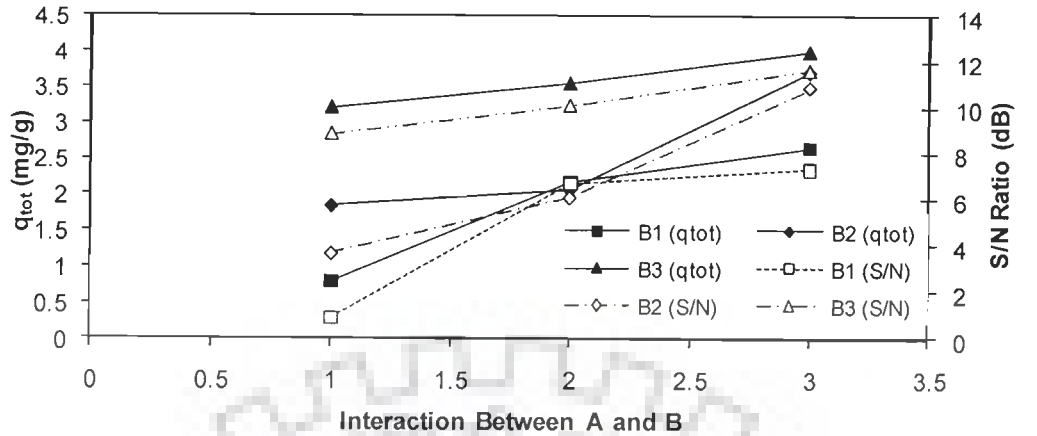

(A) A x B

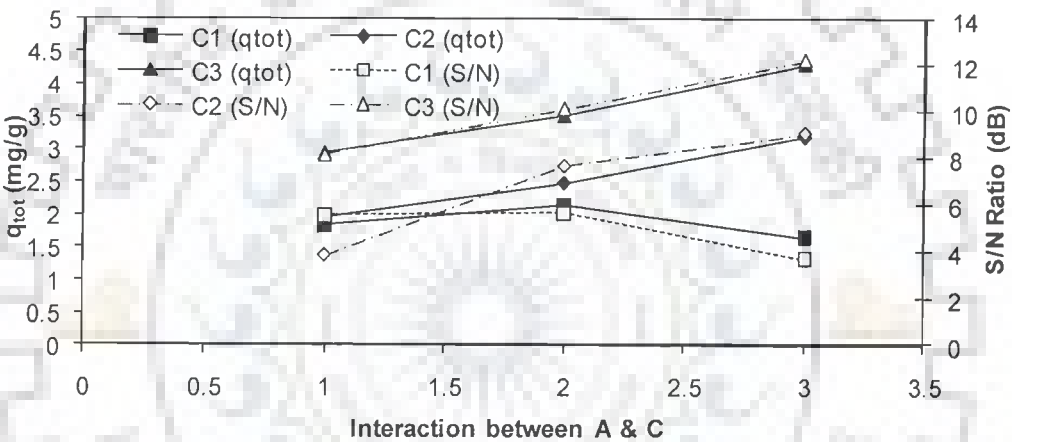

(B) A x C

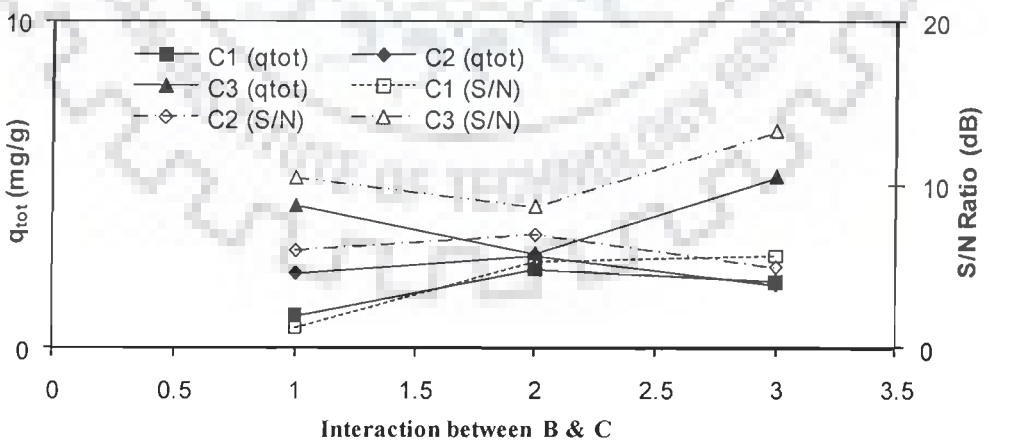

(C) B x C

Figure 4.4.37. The interaction between A, B and C parameters at 3 levels on q_{tot} and S/N ratio for ternary adsorption of C, R and HQ onto GAC.

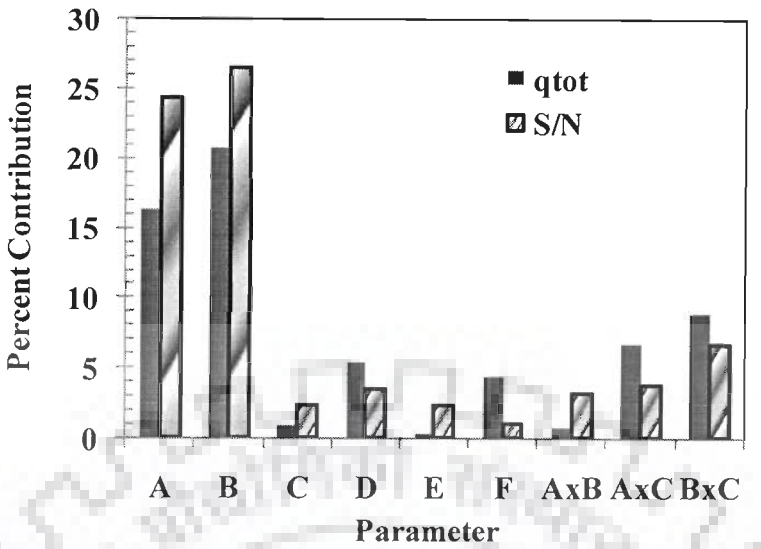

Figure 4.4.38. Percent contribution of various parameters for q_{tot} for ternary adsorption of P, CP and NP onto GAC.

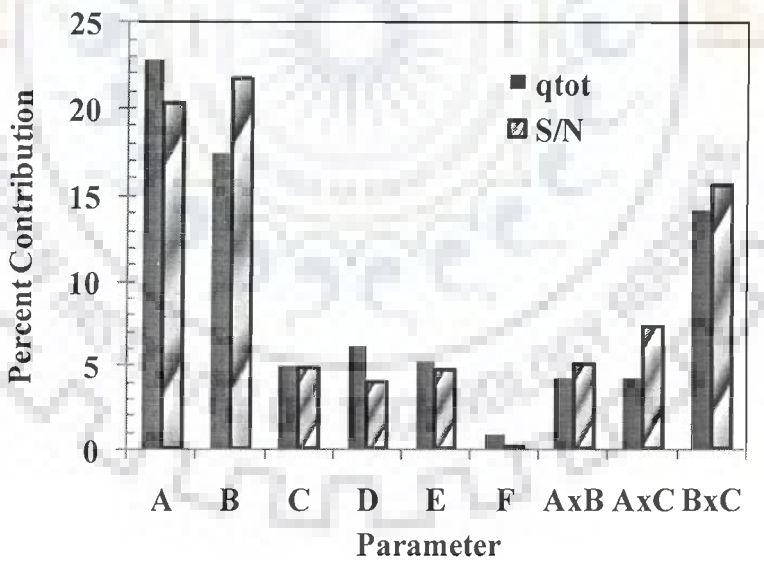

Figure 4.4.39. Percent contribution of various parameters for q_{tot} for ternary adsorption of C, R and HQ onto GAC.

4.5 MULTI-COMPONENT BATCH ADSORPTION ISOTHERM STUDY

The prediction of adsorption equilibria in multi-component systems is of prime importance. Therefore, the equilibrium adsorption data for the following multi-component systems have been studied for AN, P, CP, NP, C, R and HQ adsorption onto GAC.

1. Binary systems: NP-P, NP-CP, NP-C, NP-R and NP-HQ, AN-NP, AN-P, AN-CP, AN-C, AN-R and AN-HQ
2. Ternary systems: P-CP-NP and C-R-HQ.

Various multi-component isotherm equations have been developed by various researchers. The following multi-component isotherm equations were tested for their applicability to represent the experimental isotherm data:

Non-modified competitive Langmuir Model isotherm

$$q_{e,i} = \frac{q_{m,i} K_{L,i} C_{e,i}}{1 + \sum_{j=1}^{N} K_{L,j} C_{e,j}} \tag{4.5.1}$$

Modified competitive Langmuir isotherm [Bellot and Condoret, 1993]

$$q_{e,i} = \frac{q_{m,i} K_{L,i} \left(C_{e,i} / \eta_{L,i}\right)}{1 + \sum_{j=1}^{N} K_{L,j} \left(C_{e,j} / \eta_{L,j}\right)} \tag{4.5.2}$$

Extended Langmuir isotherm [Yang, 1987]

$$q_{e,i} = \frac{q_{\max} K_{EL,i} C_{e,i}}{1 + \sum_{j=1}^{N} K_{EL,j} C_{e,j}} \tag{4.5.3}$$

Extended Freundlich isotherm [Fritz and Schluender, 1974]

$$q_{e,1} = \frac{K_{F,1} C_{e,1}^{(1/n_1)+x_1}}{C_{e,1}^{x_1} + y_1 C_{e,2}^{z_1}} \tag{4.5.4}$$

$$q_{e,2} = \frac{K_{F,2} C_{e,2}^{(1/n_2)+x_2}}{C_{e,2}^{x_2} + y_2 C_{e,1}^{z_2}} \tag{4.5.5}$$

Sheindorf–Rebuhn–Sheintuch (SRS) Model [Sheindorf et al., 1981]

$$q_{e,i} = K_{F,i} C_{e,i} \left(\sum_{j=1}^{N} a_{ij} C_{e,j} \right)^{(1/n_i)-1} \tag{4.5.6}$$

Modified competitive Redlich-Peterson Model

$$q_{e,i} = \frac{K_{R,i} C_{e,i}}{1 + \sum_{j=1}^{N} a_{R,j} C_{e,j}^{\beta,j}} \tag{4.5.7}$$

Non-modified competitive Redlich-Peterson Model

$$q_{e,i} = \frac{K_{R,i} \left(C_{e,i} / \eta_{R,i}\right)}{1 + \sum_{j=1}^{N} a_{R,j} \left(C_{e,j} / \eta_{R,j}\right)^{\beta,j}} \tag{4.5.8}$$

Non-modified competitive Langmuir model is the extension of the basic Langmuir model. Individual adsorption constants may not define exactly the multi-component adsorption behaviour of metal ion mixtures. For that reason, better accuracy may be achieved by using modified isotherms related to the individual isotherm parameters and the correction factors. An interaction term, $\eta_{L,i}$, which is a characteristic of each species and depends on the concentrations of the other components, has been added in the competitive Langmuir model by Bellot and Condoret [1993] to formulate the modified competitive Langmuir isotherm. Similarly, the competitive non-modified R-P model is modified, using an interaction term $\eta_{R,i}$, to the obtain modified competitive R-P Model. Assuming that the surface sites are uniform, and that all the adsorbate molecules (ions) in the solution compete for the same surface sites, Yang [1987] extended the mono-component Langmuir equation to give extended Langmuir isotherm for multi-component systems. Similarly, Fritz and Schluender [1974] extended the mono-component Freundlich equation to give extended Freundlich isotherm for binary systems. Sheindorf et al. [1981] derived a Freundlich-type multi-component adsorption isotherm known as the Sheindorf–Rebuhn–Sheintuch (SRS) equation, to represent the experimental data. The competition coefficients a_{ij} in the SRS model describe the inhibition to the adsorption of component i by component j, and can be determined from the thermodynamic data, or more likely, from the experimental sorption data of multicomponent systems. The SRS equation assumes that (i) each component individually obeys the Freundlich isotherm; (ii) that for each component in a multi-component adsorption system, there exists an exponential distribution of site adsorption energies, i.e.

$$N_i(Q) = \alpha_i \exp(-\beta_i Q/RT) \tag{4.5.9}$$

where, α_i and β_i are constants;

and (iii) the coverage by each adsorbate molecule (or ion) at each energy level Q is given by the multicomponent Langmuir isotherm equation:

$$\theta_i(Q) = \frac{K_i C_{e,i}}{1 + \sum_{j=1}^{N} K_j C_{e,j}} \tag{4.5.10}$$

where, $K_j = K_{0_j} \exp(Q/RT)$ (4.5.11)

Integration of $N_i(Q)\theta_i(Q)$ over energy level in the range of $-\infty$ to $+\infty$ yields Eq. (4.5.10) and the competition coefficients are defined as $a_{ij} = K_{0j}/K_{0i}$ and thus $a_{ji} = 1/a_{ij}$.

The parameters of all the multi-component models were found by fitting them to the equilibrium adsorption data by using the MS Excel 2002 for Windows by minimizing Marquardt's percent standard deviation (MPSD) [Marquardt, 1963]. MPSD has been used by a few researchers in the field [Wong et al., 2004; Mall et al., 2005a,b] to test the adequacy and accuracy of various isotherm models to fit with the experimental data. It has somewhat similarity to the geometric mean error distribution, but modified by incorporating the number of degrees of freedom. This error function is given as:

$$MPSD = 100\sqrt{\frac{1}{n_m - n_p}\sum_{i=1}^{n}\left(\frac{\left(\sum_{i=1}^{N} q_{e,i,\exp}\right) - \left(\sum_{i=1}^{N} q_{e,i,cal}\right)}{\sum_{i=1}^{N} q_{e,i,\exp}}\right)_i^2} \qquad (4.5.12)$$

In the above equation, the subscripts 'exp' and 'calc' mean the experimental and 'calculated' values, respectively, n_m the number of measurements and n_p the number of parameters in the model.

4.5.1 Binary Batch Isotherm Study

Binary adsorption modelling

To optimize the design of an adsorption system, it is important to establish the most appropriate correlation for the equilibrium sorption curves. Therefore, the equilibrium adsorption data for NP-C and NP-R from binary systems onto GAC have been used to test the applicability of various multi-component isotherm equations. These isotherm equations are given in Table 4.5.25. Srivastava et al. [2006] have discussed the theory associated with these models.

The simultaneous adsorption of NP, C and R from their binary mixtures was also investigated at solution pH. In the first stage of adsorption studies, the initial NP concentration was varied from 0.36 to 7.12 mmol/l, at each initial C concentration of 0.45, 0.91, 2.27, 4.54 and 9.08 mmol/l. The non-linear adsorption isotherms of NP in the absence and presence of C are shown in Figure. 4.5.23. It is seen that the equilibrium NP uptake increases with an increase in the initial NP concentration up to 7.12 mmol/l at all C concentrations. The equilibrium uptake of NP decreases continuously with increasing C

concentration. The individual and total adsorption equilibrium uptakes and yields of NP and C on GAC as obtained at different initial NP concentrations in the absence of C or the presence of C with increasing concentrations.

Figure. 4.5.24 depicts the variations in the equilibrium uptake of C with increasing initial C concentrations (from 0.45-9.08 mmol/l) at a constant initial NP concentration (0.36-7.12 mmol/l). Similar adsorption patterns were observed in the binary NP-R system (shown in the figure); R equilibrium uptake increases with an increase in the initial R concentration up to 9.08 mmol/l. Increase in NP concentration decreases the equilibrium uptake of R.

In general, multi-component adsorbates–adsorbents exhibit three possible types of behaviour mainly antagonism (the effect of the mixture is less than that of each of the components in the mixture) synergism (the effect of the mixture is more than that each of the component in the mixture),and anachronism (the effect of the mixture is the same as that of each of the components) [Srivastava et al., 2006]. The experimental equilibrium sorption data obtained for the binary systems indicate that the adsorption capacity of GAC for NP is, in general, lower than that of C and R. There are possible interaction effects between different species in the solution and, in particular, potential interactions on the surface depending on the adsorption mechanism. The combined effect of the both binary mixture of NP-C and C, and NP - R seems to be antagonistic in nature.

The factors that affect the sorption preference of an adsorbent for different kinds of adsorbates may be related to the characteristics of the binding sites (e.g. functional groups, structure, surface properties, etc.), the properties of the adsorbates (e.g., concentration, ionic size, ionic weight, ionic charge, molecular structure, ionic nature or standard redox potential, etc.) and the solution chemistry (e.g. pH, ionic strength, etc.). However, it is difficult to identify a common denominator from the physical and chemical properties of NP and C, and R which may explain the interactive mechanism and the increase in the selectivity for sorption of an adsorbate from the both binary mixtures.

Multi-component adsorption isotherm models

The simultaneous equilibrium adsorption data of NP-C and NP-R by GAC have been fitted to the multi-component isotherm models, viz., non-modified, modified and extended Langmuir models; the extended Freundlich and the SRS models and the non-

modified and modified R–P models. The parametric values of all the multi-component adsorption models are given in Table 6. The MPSD values for the model fit of the experimental data set of NP, C and R were also given in Table 4.5. The comparisons of the experimental and calculated q_e values of NP, C, and R in their binary mixtures are also presented in the parity plots (Figs. 6a, b and 7a, b). Since most of the data points are distributed around the 45^0 line, this indicates that all the multicomponent isotherm models could represent the experimental adsorption data for the binary systems with varying degree of fit.

The multi-component non-modified Langmuir model shows a poor fit to the experimental data (MPSD = 90.15). All the modified Langmuir coefficients ($\eta_{L,i}$) estimated were much greater than 1.0 indicating that non-modified multi-component Langmuir model related to the individual isotherm parameters could not be used to predict the binary-system adsorption. However, the use of the interaction term, $\eta_{L,i}$, in the modified Langmuir model (MPSD = 80.6) clearly increased the fit of non-modified Langmuir model. The use of interaction term, $\eta_{R,i}$, for modified R–P model (MPSD = 91.1), similarly, improved the fit of the non-modified R–P model (MPSD = 102.7).

The use of the extended Langmuir model (MPSD = 57.1 for NP-C and MPSD = 66.70 for NP-R) also does not improve the fit to the binary adsorption data of both binary mixtures onto GAC. The K_i values, reflecting the affinity between GAC and the in the binary systems were: 53.71 l/mmol for NP and 16.64 l/mmol for C and 32.22 l/mmol for NP and 9.982 l/mmol for R. The overall total metal ions uptake (q_{max}) by GAC was 1.561 mmol/g and 2.601 mmol/g for NP-C and NP-R binary mixtures. This value is considerably lower than the sum of the maximum total capacities of NP and C and R resulting from the single component adsorption. For that reason, the adsorption sites of NP-C and NP-R in the binary system onto GAC may likely be partially overlapped. It may also imply that there may be a variety of binding sites on GAC showing partial specificity to the individual NP, C and R. The information obtained from the maximum capacities seems to violate the basic assumptions of the Langmuir model, i.e. the entire adsorbent surface is homogeneous and that there is no lateral interaction between the adsorbate molecules, and thus the affinity of each binding site for the adsorbate molecules should be uniform.

The SRS model fitted to the both binary adsorption data of NP-C and NP-R onto GAC reasonably well (MPSD = 66.51, 116.9). The competition coefficients a_{ij} and a_{ji}

were estimated from the competitive adsorption data of NP-C and NP-R. A comparison of the competition coefficients shows that the uptake of the more favourably adsorbed C and R were strongly affected by the presence of NP (a_{21} = 3.83 and 30. 23), while the inhibition exerted in the reverse situation was less (a_{12} = 0.19 and 0.07). The competition coefficients seem to prove that the sorption of NP, C and R onto GAC were inhibited by the presence of either one. For the SRS model, GAC shows different capacities, $K_{F,i}$, for NP-C and NP-R and competition coefficients during their coexistence. This suggests that the surface sites of the GAC are heterogeneous, and some of the sites may be specific to certain metals [Sag et al., 2003; Srivastava et al., 2007].

A comparison of MPSD values for different isotherm models shows that the extended Freundlich model best-fits the experimental adsorption data of NP-C and NP-R from binary systems onto GAC. This is expected as GAC has a heterogeneous surface. It is evident that the modification of the Freundlich equation as given by extended Freundlich model takes into account the interactive effects of individual NP, C and R between and among themselves and also the adsorbent GAC reasonably well. Therefore, the binary adsorption of both NP-C and NP-R onto GAC can be represented satisfactorily and adequately by the extended Freundlich model. The SRS model, which is also based on Freundlich model, also fitted the equilibrium binary metal adsorption data reasonably well.

Three-dimensional (3D) adsorption isotherm surfaces are used to evaluate the performance of the binary mixture adsorption systems [de Carvalho et al., 1995; Chong et al., 1996; Srivastava et al., 2007]. A 3D graphical representation of the sorption isotherm plot for the both binary systems is given in Figs. 4.5.26 and 4.5.27. In these plots, the experimental data points are shown along with the predicted isotherms using the extended Freundlich isotherm equations for both NP-C and NP-R binary mixtures. As can be seen, the predictions are found to be satisfactory.

Summary

Based on MPSD error function, the extended-Freundlich adsorption isotherm model showed the best fit to the binary equilibrium adsorption data. It may be concluded that the GAC may be used for the simultaneous removal of AN, P, CP, NP, C R, HQ from phenolic containing effluents.

Table 4.5.1. Binary isotherm parameter values for NP-CP and NP-AN systems.

NP-CP				NP-AN			
Non-modified Langmuir Model							
MPSD	237.54			MPSD	48.823		
Modified Langmuir Model							
Adsorbate	$\eta_{L,i}$			Adsorbate	$\eta_{L,i}$		
NP	2.272			NP	1.258		
CP	7.325			AN	1.228		
MPSD	55.135			MPSD	47.596		
Extended Langmuir Model							
Adsorbate	$K_{EL,i}$	$q_{\max}$		Adsorbate	$K_{EL,i}$	$q_{\max}$	
NP	8.248	0.557		NP	6.897	1.179	
CP	7.069			AN	6.105		
MPSD	42.869			MPSD	46.583		
Extended Freundlich Model							
Adsorbate	x_i	y_i	z_i	Adsorbate	x_i	y_i	z_i
NP	0	3.258	0.523	NP	0.599	1.584	1.833
CP	0.1620	7.068	0.449	AN	0.559	1.552	1.064
MPSD	40.760			MPSD	33.903		
SRS Model							
Adsorbate	a_{ij}	a_{ij}		Adsorbate	a_{ij}	a_{ij}	
NP	12.530	1		NP	3.129	1	
CP	1	106.2		AN	1	3.675	
MPSD	61.258			MPSD	48.220		
Non-modified R-P Model							
MPSD	119.61			MPSD	182.92		
Modified R-P Model							
Adsorbate	$\eta_{R,i}$			Adsorbate	$\eta_{R,i}$		
NP	3.940			NP	8.360		
CP	0.497			AN	17.434		
MPSD	52.034			MPSD	119.238		

Table 4.5.2. Binary isotherm parameter values for AN-P and AN-C systems.

AN-P				AN-C			
Non-modified Langmuir Model							
MPSD	148.33			MPSD	347.89		
Modified Langmuir Model							
Adsorbate	$\eta_{L,i}$			Adsorbate	$\eta_{L,i}$		
AN	4.556			AN	9.635		
P	1.712			C	11.815		
MPSD	43.268			MPSD	98.342		
Extended Langmuir Model							
Adsorbate	$K_{EL,i}$	q_{max}		Adsorbate	$K_{EL,i}$	q_{max}	
AN	1.438	1.224		AN	88099	0.187	
P	3.840			C	70202		
MPSD	41.190			MPSD	80.532		
Extended Freundlich Model							
Adsorbate	x_i	y_i	z_i	Adsorbate	x_i	y_i	z_i
AN	0.212	6.071	0.644	AN	0.221	7.503	0.9220
P	0.228	1.116	0.419	C	1.971	518.24	3.604
MPSD	38.741			MPSD	64.068		
SRS Model							
Adsorbate	a_{ij}	a_{ij}		Adsorbate	a_{ij}	a_{ij}	
AN	78.876	1		AN	29.972	1	
P		1.224		C		36.451	
MPSD	57.496			MPSD	15.415		
Non-modified R-P Model							
MPSD	145.86			MPSD	248.06		
Modified R-P Model							
Adsorbate	$\eta_{R,i}$			Adsorbate	$\eta_{R,i}$		
AN	1.541			AN	6.959		
P	2.371			C	12.940		
MPSD	122.52			MPSD	96.418		

Table 4.5.3. Binary isotherm parameter values for NP-C, NP-R and NP-HQ systems.

NP-C				NP-R				NP-HQ			
Non-modified Langmuir Model											
MPSD	90.148			MPSD	98.727			MPSD	120.928		
Modified Langmuir Model											
Adsorbate	$\eta_{L,i}$			Adsorbate	$\eta_{L,i}$			Adsorbate	$\eta_{L,i}$		
NP	0.894			NP	1.725			NP	4.025		
C	2.347			R	2.139			HQ	40.424		
MPSD	80.626			MPSD	104.1			MPSD	100.92		
Extended Langmuir Model											
Adsorbate	$K_{EL,i}$	q_{max}		Adsorbate	$K_{EL,i}$	q_{max}		Adsorbate	$K_{EL,i}$	q_{max}	
NP	53.711	1.561		NP	32.22	2.601		NP	69.054	1.214	
C	16.637			R	9.982			HQ	21.390		
MPSD	57.076			MPSD	66.70			MPSD	51.460		
Extended Freundlich Model											
Adsorbate	x_i	y_i	z_i	Adsorbate	x_i	y_i	z_i	Adsorbate	x_i	y_i	z_i
NP	1.0426	0.0164	3.784	NP	1.938	0.00003	6.888	NP	0.808	0.081	3.066
C	1.065	7.116	2.253	R	5.315	46.476	6.477	HQ	0.253	9.354	0.994
MPSD	48.903			MPSD	48.90			MPSD	48.903		
SRS Model											
Adsorbate	a_{ij}	a_{ij}		Adsorbate	a_{ij}	a_{ij}		Adsorbate	a_{ij}	a_{ij}	
NP	0.187	1		NP	0.071	1		NP	0.278	1	
C	1	3.830		R	1	30231		HQ	1	23.100	
MPSD	66.507			MPSD	116.9			MPSD	64.308		
Non-modified R-P Model											
MPSD	102.66			MPSD	132.6			MPSD	126.66		
Modified R-P Model											
Adsorbate	$\eta_{R,i}$			Adsorbate	$\eta_{R,i}$			Adsorbate	$\eta_{R,i}$		
NP	1.541			NP	6.252			NP	1.550		
C	2.371			R	3344			HQ	1502.0		
MPSD	91.220			MPSD	105.4			MPSD	86.586		

Table 4.5.4. Binary isotherm parameter values for AN-CP and NP-P systems.

AN-CP				NP-P			
Non-modified Langmuir Model							
MPSD	423.121			MPSD	220.317		
Modified Langmuir Model							
Adsorbate	$\eta_{L,i}$			Adsorbate	$\eta_{L,i}$		
AN	14.103			NP	1.675		
CP	33.416			P	10.089		
MPSD	101.399			MPSD	88.684		
Extended Langmuir Model							
Adsorbate	$K_{EL,i}$	q_{max}		Adsorbate	$K_{EL,i}$	q_{max}	
AN	14.395	0.357		NP	57.067	0.557	
CP	20.954			P	18.646		
MPSD	69.308			MPSD	65.283		
Extended Freundlich Model							
Adsorbate	x_i	y_i	z_i	Adsorbate	x_i	y_i	z_i
AN	0.335	10.808	0.847	NP	0.746	0.434	0.785
CP	0.626	5.685	0.864	P	0	12.972	0.834
MPSD	59.162			MPSD	56.403		
SRS Model							
Adsorbate	a_{ij}	a_{ij}		Adsorbate	a_{ij}	a_{ij}	
AN	130.75	1		NP	1.623	1	
CP	1	212.84		P	1	312.50	
MPSD	82.0657			MPSD	90.603		
Non-modified R-P Model							
MPSD	121.086			MPSD	98.561		
Modified R-P Model							
Adsorbate	$\eta_{R,i}$			Adsorbate	$\eta_{R,i}$		
AN	9.00			NP	2.063		
CP	43.435			P	5.033		
MPSD	100.137			MPSD	96.702		

Table 4.5.5. Binary isotherm parameter values for AN-R and AN-HQ systems.

AN-R				AN-HQ			
Non-modified Langmuir Model							
MPSD	264.227			MPSD	587.04		
Modified Langmuir Model							
Adsorbate	$\eta_{L,i}$			Adsorbate	$\eta_{L,i}$		
AN	9.092			AN	1.725		
R	5.879			HQ	2.139		
MPSD	97.865			MPSD	473.51		
Extended Langmuir Model							
Adsorbate	$K_{EL,i}$	$q_{\max}$		Adsorbate	$K_{EL,i}$	$q_{\max}$	
AN	42428	0.236		AN	43748	0.168	
R	23106			HQ	3796		
MPSD	74.5823			MPSD	91.537		
Extended Freundlich Model							
Adsorbate	x_i	y_i	z_i	Adsorbate	x_i	y_i	z_i
AN	0.258	5.689	0.976	AN	0	11.466	0.490
R	2.367	609.28	4.358	HQ	1.082	125.07	2.069
MPSD	64.959			MPSD	81.244		
SRS Model							
Adsorbate	a_{ij}	a_{ij}		Adsorbate	a_{ij}	a_{ij}	
AN	24.542	1		AN	67.741	1	
R	1	22.479		HQ	1	84.368	
MPSD	85.547			MPSD	92.128		
Non-modified R-P Model							
MPSD	264.035			MPSD	490.16		
Modified R-P Model							
Adsorbate	$\eta_{R,i}$			Adsorbate			
AN	10.073			AN	1.541		
R	6.207			HQ	2.371		
MPSD	99.515			MPSD	453.813		

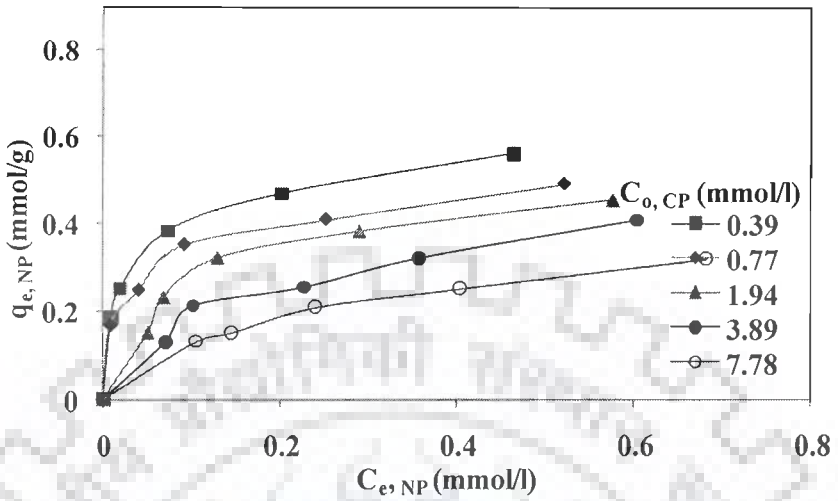

(a)

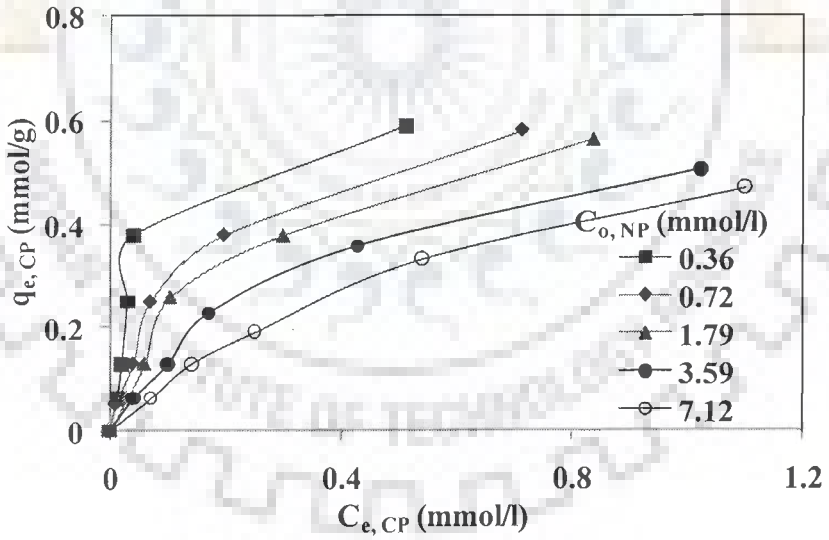

(b)

Figure 4.5.1. Comparison of non-linearized adsorption isotherms of NP-CP binary system. [a] NP in the presence of increasing concentration of CP, [b] CP with increasing concentration of NP. T = 30^{0}C, t =12 h, GAC dosage = 10 g/l.

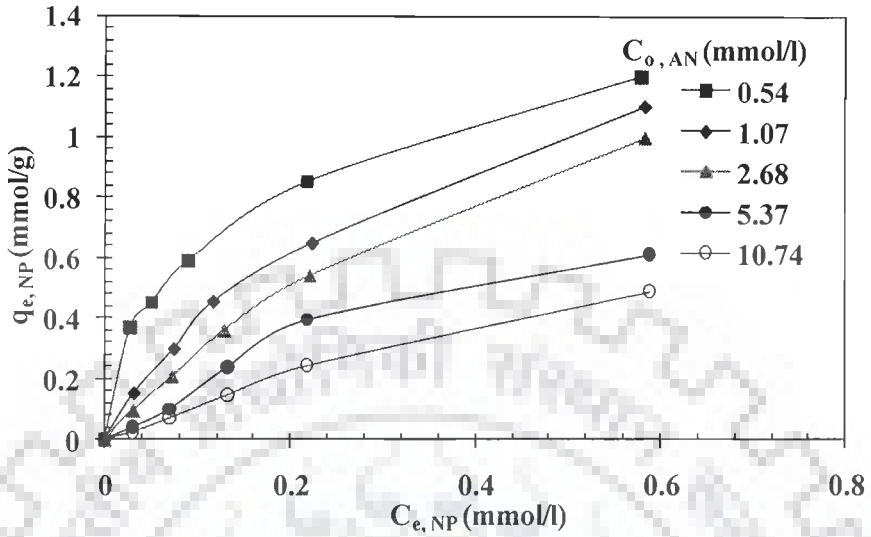

(a)

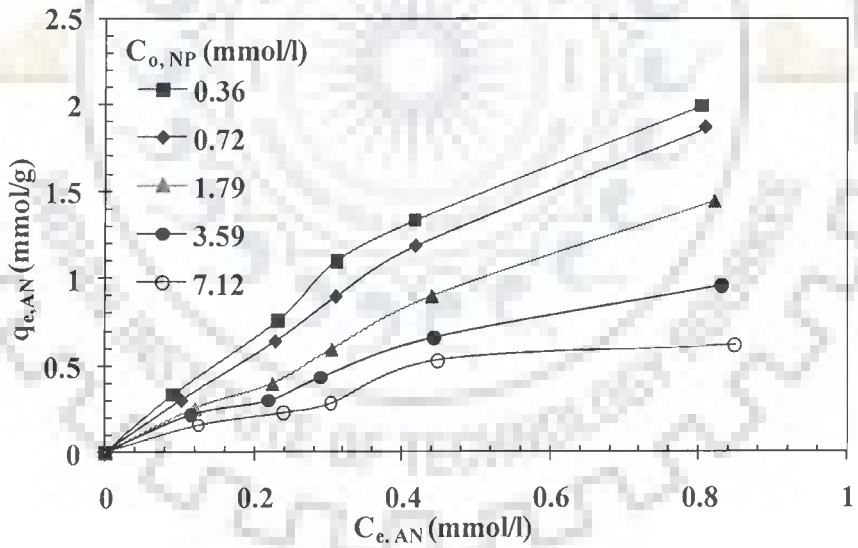

(b)

Figure 4.5.2. Comparison of non-linearized adsorption isotherms of NP-AN binary system. [a] NP in the presence of increasing concentration of AN, [b] AN with increasing concentration of NP. T = 30^{0}C, t =12 h, GAC dosage = 10 g/l.

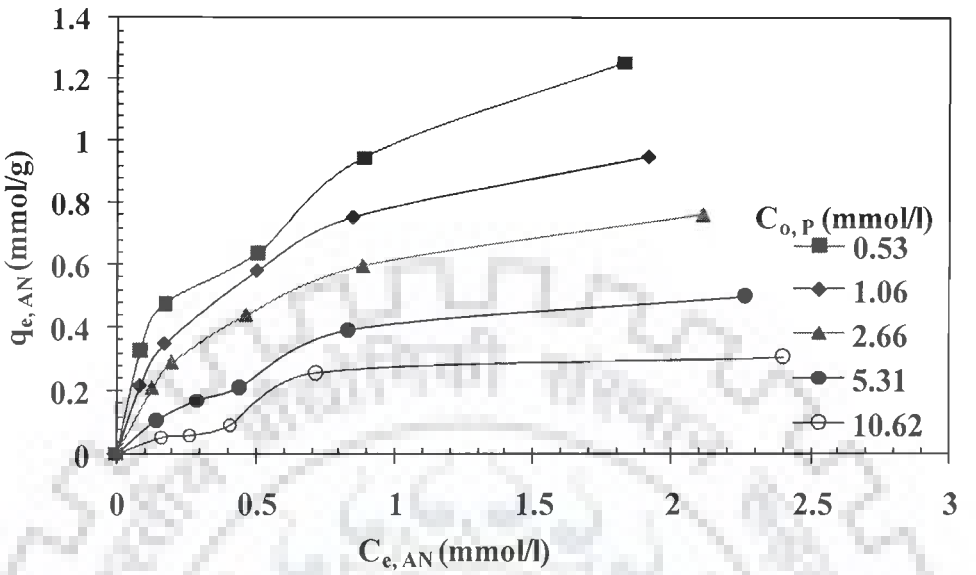

(a)

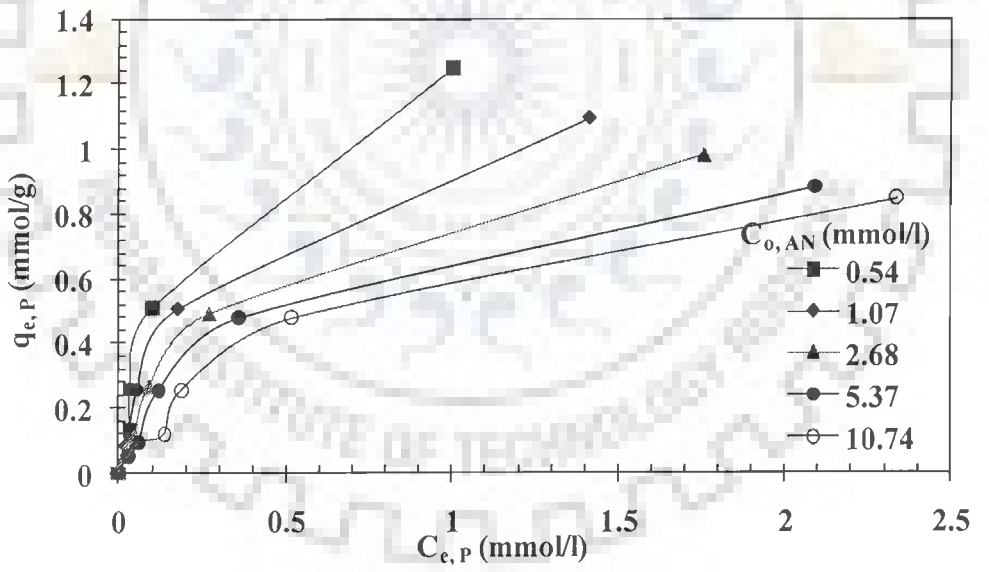

(b)

Figure 4.5.3. Comparison of non-linearized adsorption isotherms of AN-P binary system. [a] AN in the presence of increasing concentration of P, [b] P with increasing concentration of AN. T = 30^{0}C, t =12 h, GAC dosage = 10 g/l.

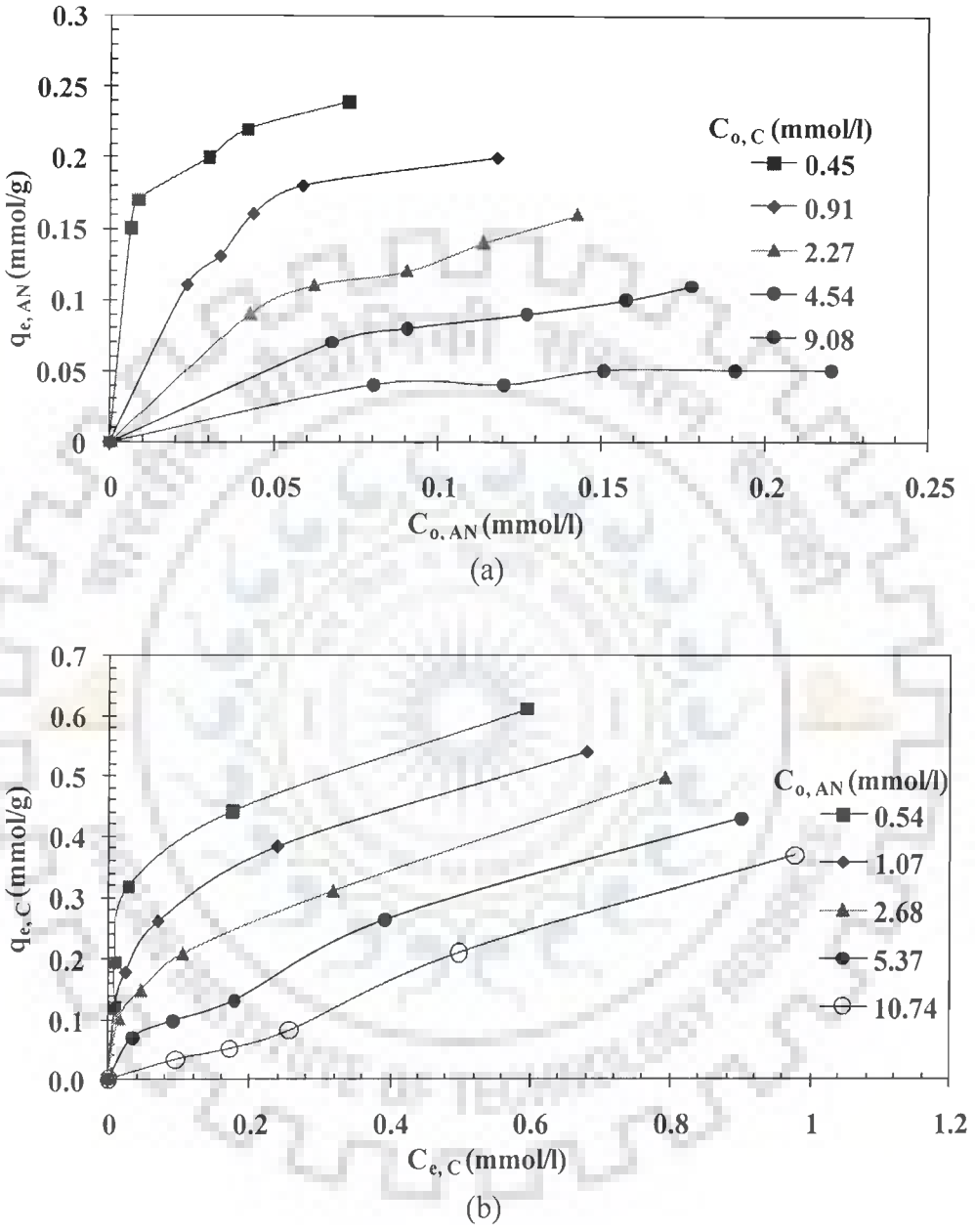

Figure 4.5.4. Comparison of non-linearized adsorption isotherms of AN-C binary system. [a] AN in the presence of increasing concentration of C, [b] C with increasing concentration of AN. T = 30^{0}C, t =12 h, GAC dosage = 10 g/l.

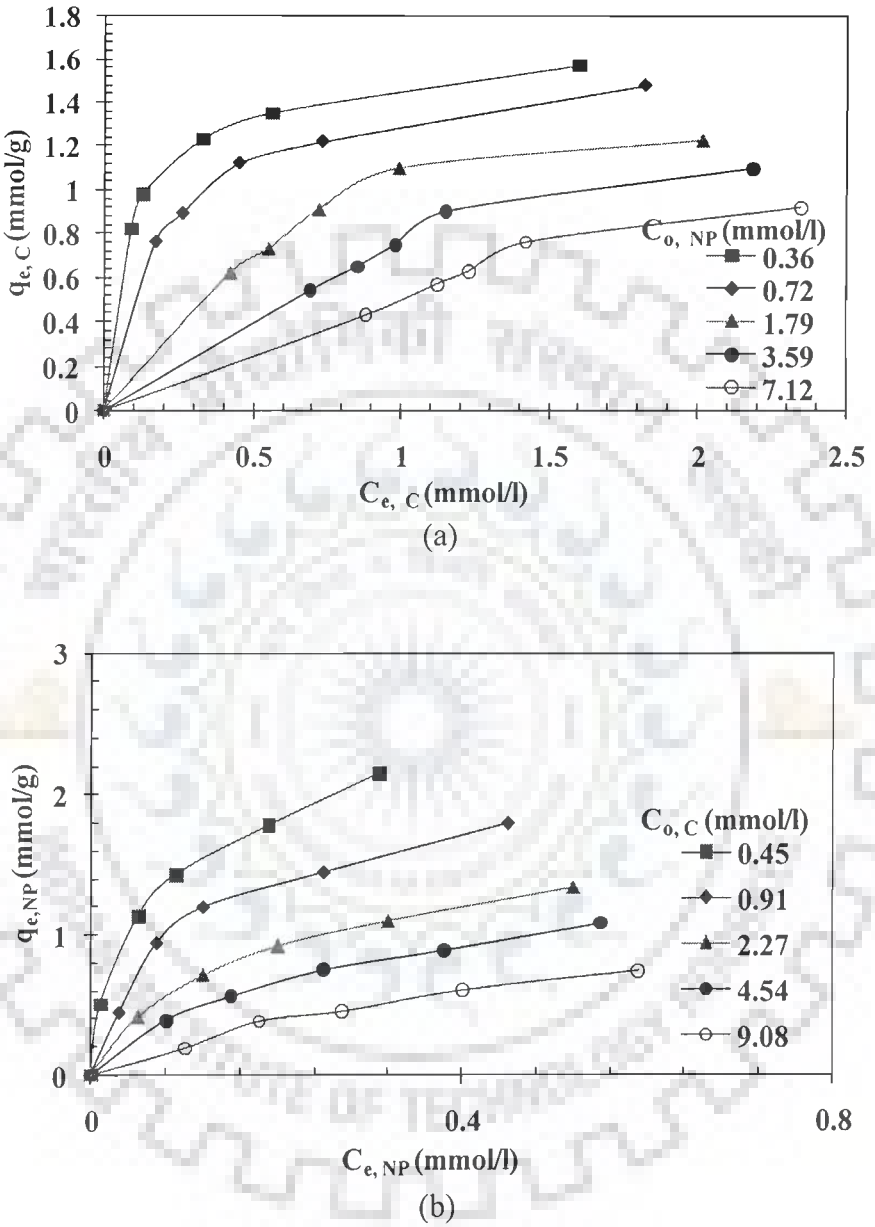

Figure 4.5.5. Comparison of non-linearized adsorption isotherms of NP-C binary system. [a] C in the presence of increasing concentration of NP, [b] NP with increasing concentration of C. $T = 30^0$C, t =12 h, GAC dosage = 10 g/l.

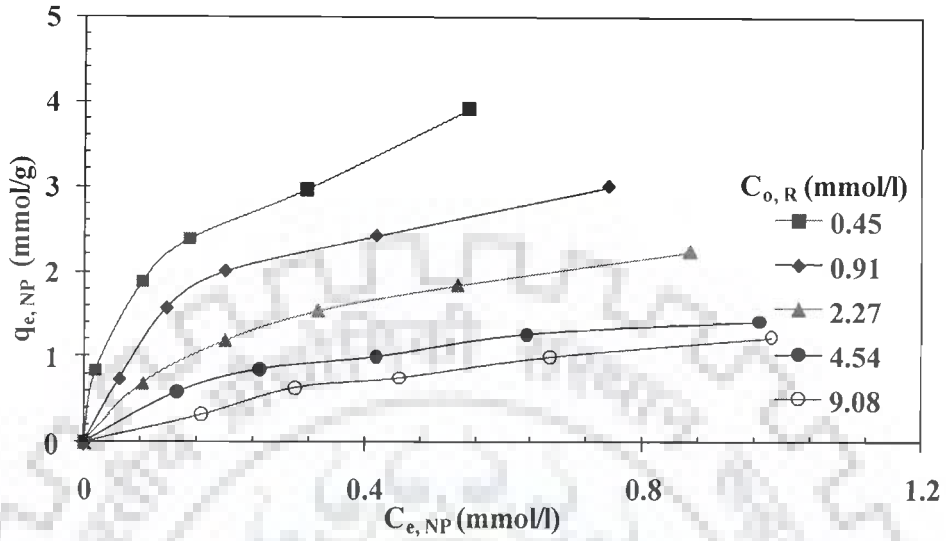

(a)

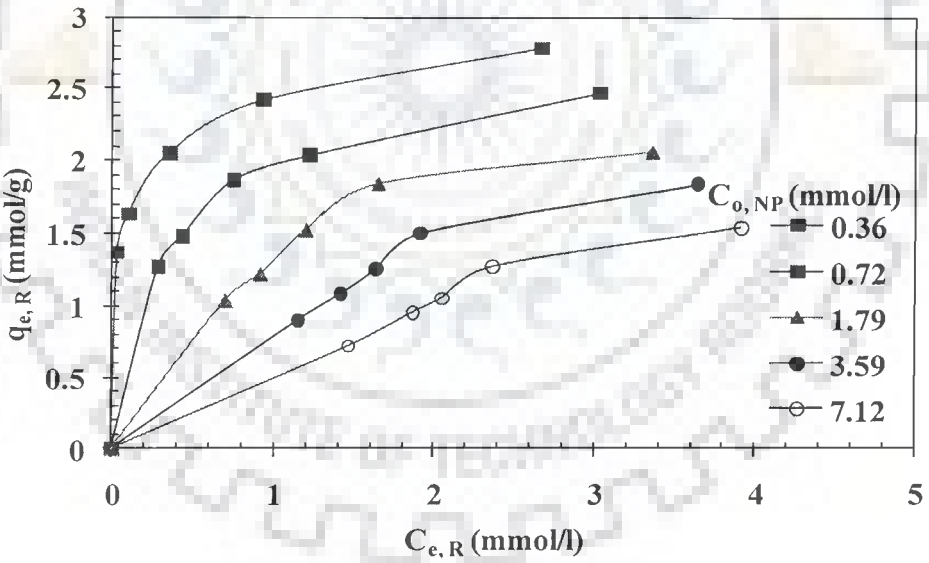

(b)

Figure 4.5.6. Comparison of non-linearized adsorption isotherms of NP-R binary system. [a] NP in the presence of increasing concentration of R, [b] R with increasing concentration of NP. T = 30^{0}C, t =12 h, GAC dosage = 10 g/l.

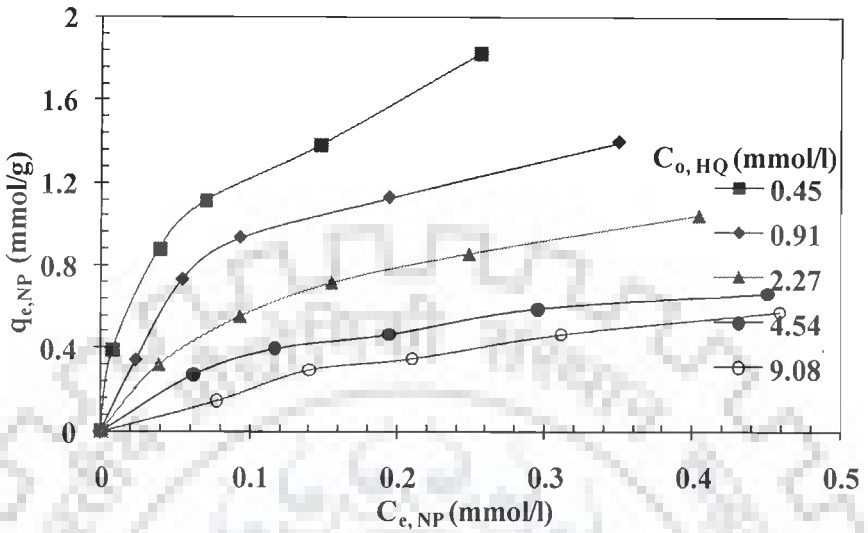

(a)

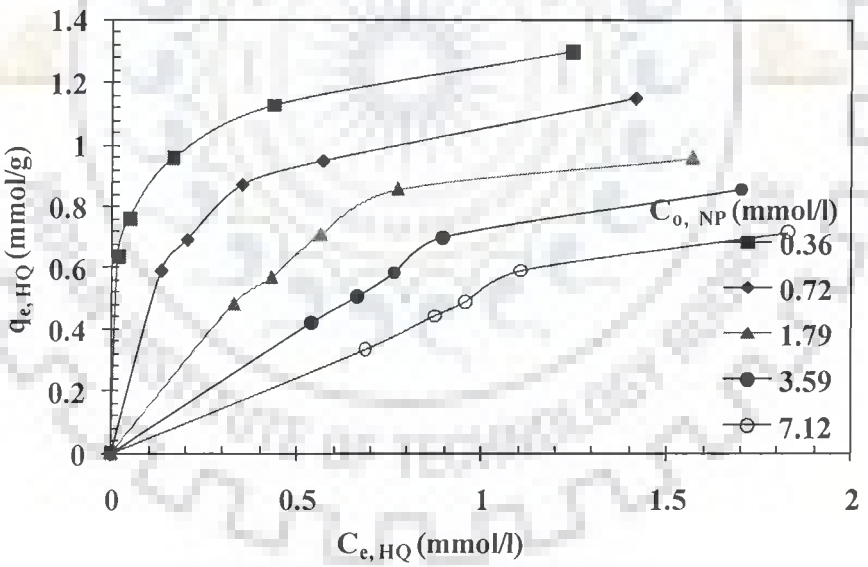

(b)

Figure 4.5.7. Comparison of non-linearized adsorption isotherms of NP-HQ binary system. [a] NP in the presence of increasing concentration of HQ, [b] HQ with increasing concentration of NP. T = 30^{0}C, t =12 h, GAC dosage = 10 g/l.

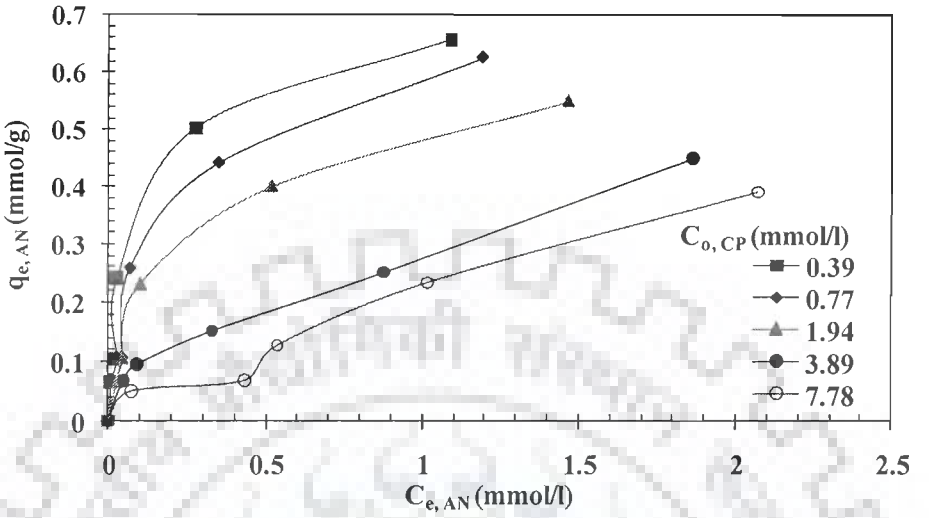

(a)

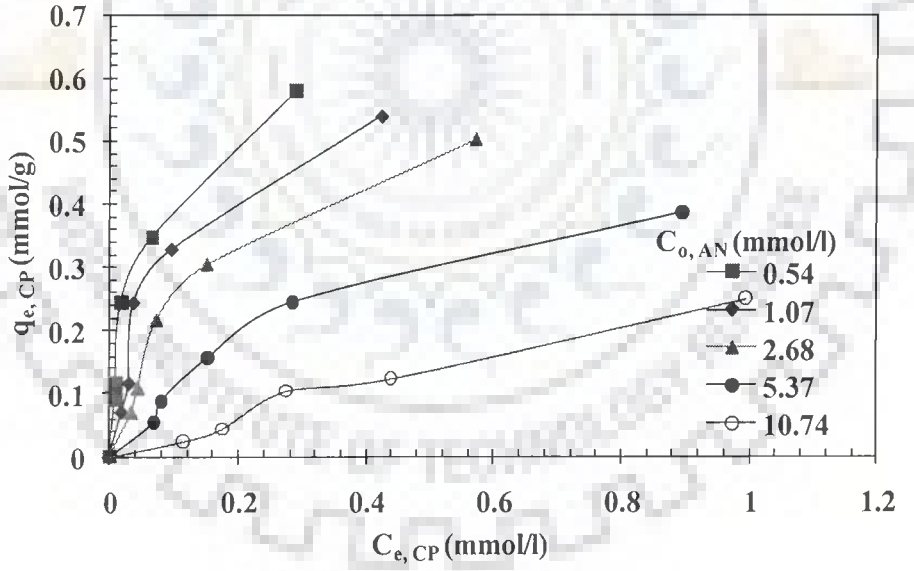

(b)

Figure 4.5.8. Comparison of non-linearized adsorption isotherms of AN-CP binary system. [a] AN in the presence of increasing concentration of CP, [b] CP with increasing concentration of AN. T = 30^{0}C, t =12 h, GAC dosage = 10 g/l.

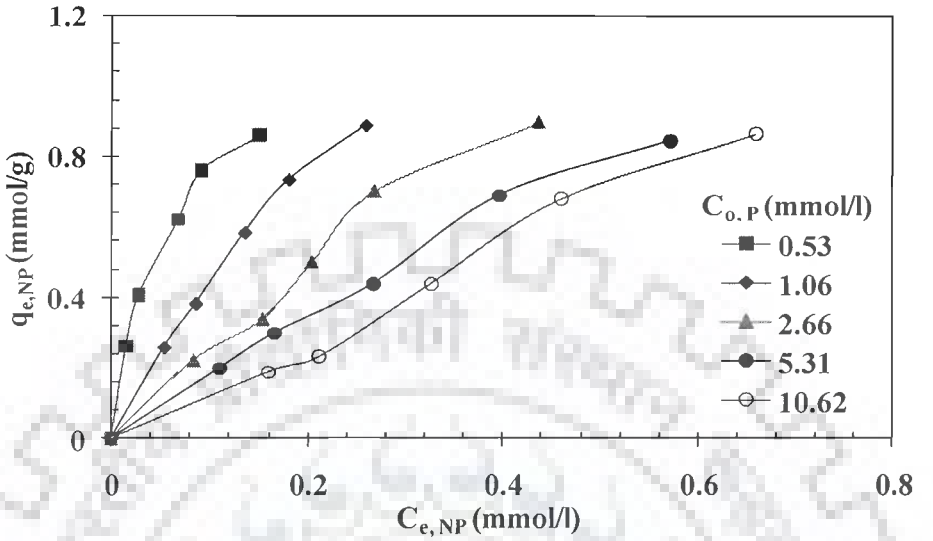

(a)

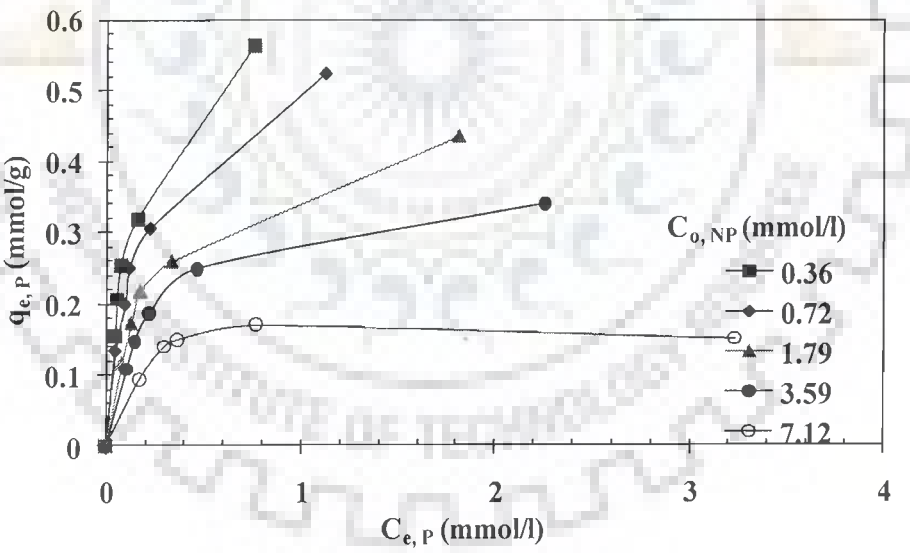

(b)

Figure 4.5.9. Comparison of non-linearized adsorption isotherms of NP-P binary system. [a] NP in the presence of increasing concentration of P, [b] P with increasing concentration of NP. T = 30^{0}C, t =12 h, GAC dosage = 10 g/l.

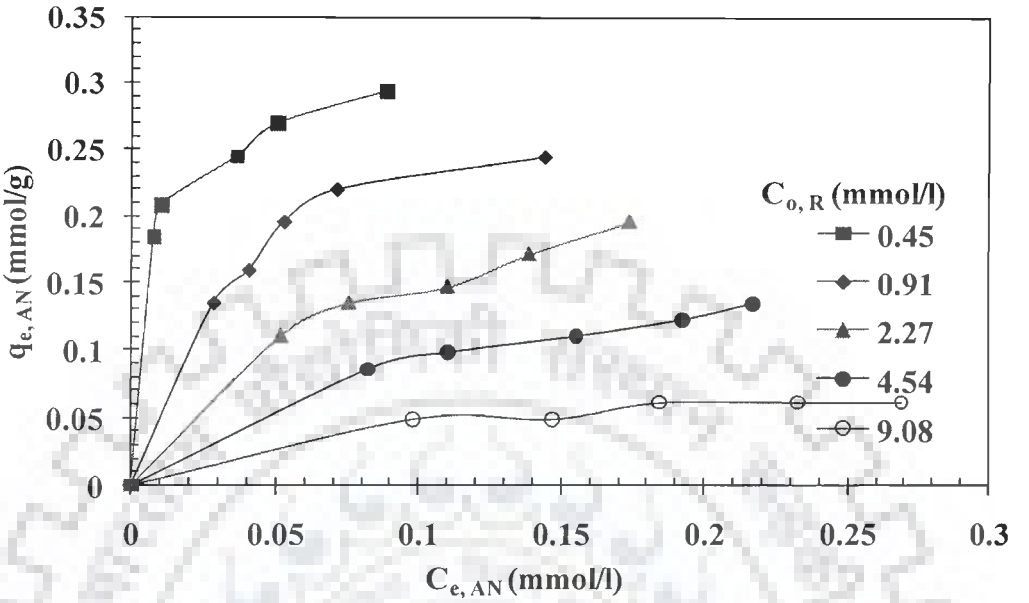

(a)

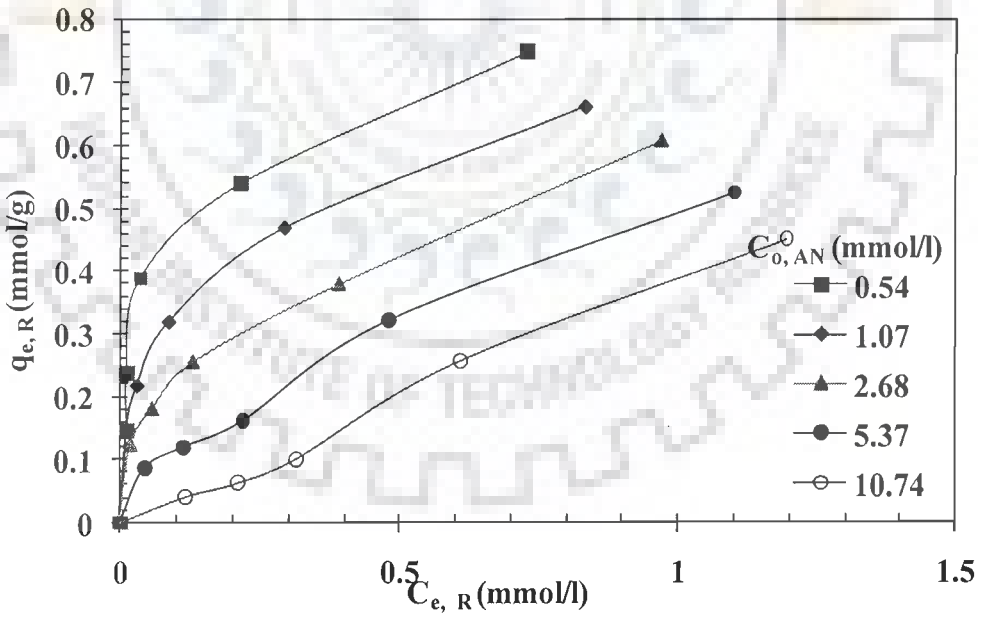

(b)

Figure 4.5.10. Comparison of non-linearized adsorption isotherms of AN-R binary system. [a] AN in the presence of increasing concentration of R, [b] R with increasing concentration of AN. T = 30^{0}C, t =12 h, GAC dosage = 10 g/l.

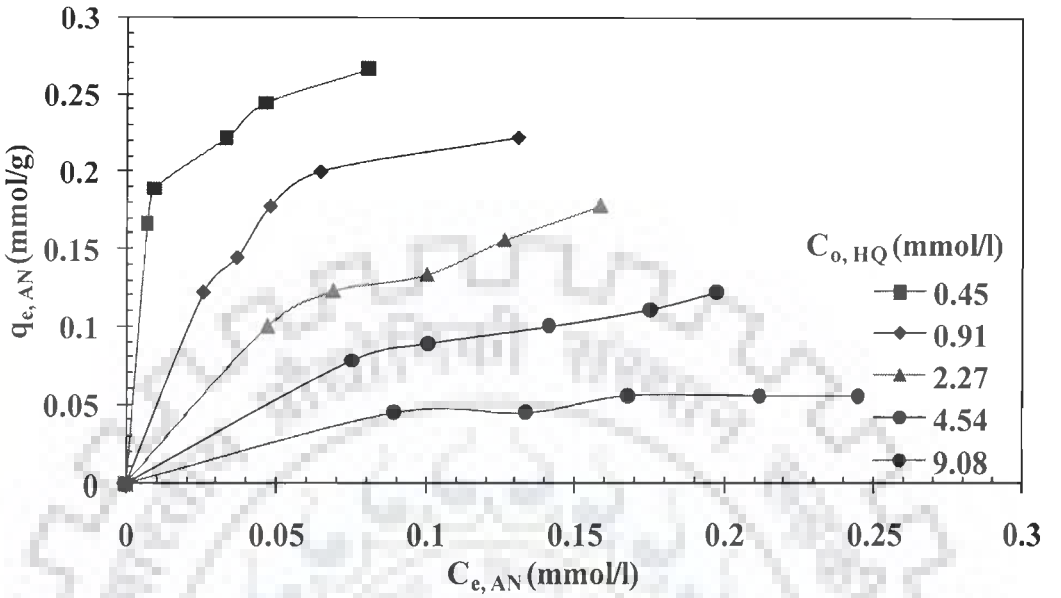

(a)

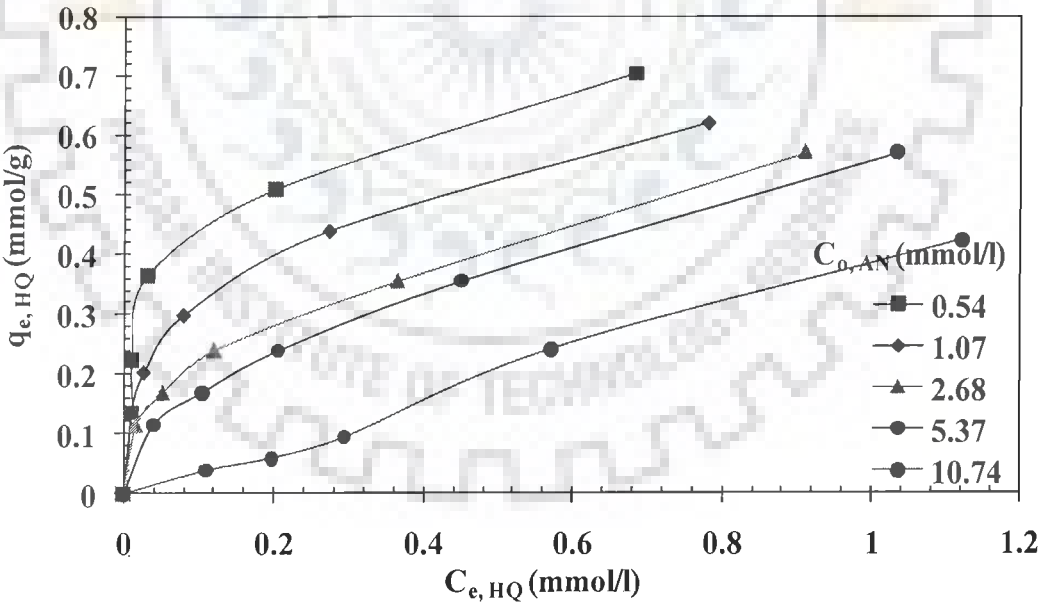

(b)

Figure 4.5.11. Comparison of non-linearized adsorption isotherms of AN-HQ binary system. [a] AN in the presence of increasing concentration of HQ, [b] HQ with increasing concentration of AN. T = 30^{0}C, t =12 h, GAC dosage = 10 g/l.

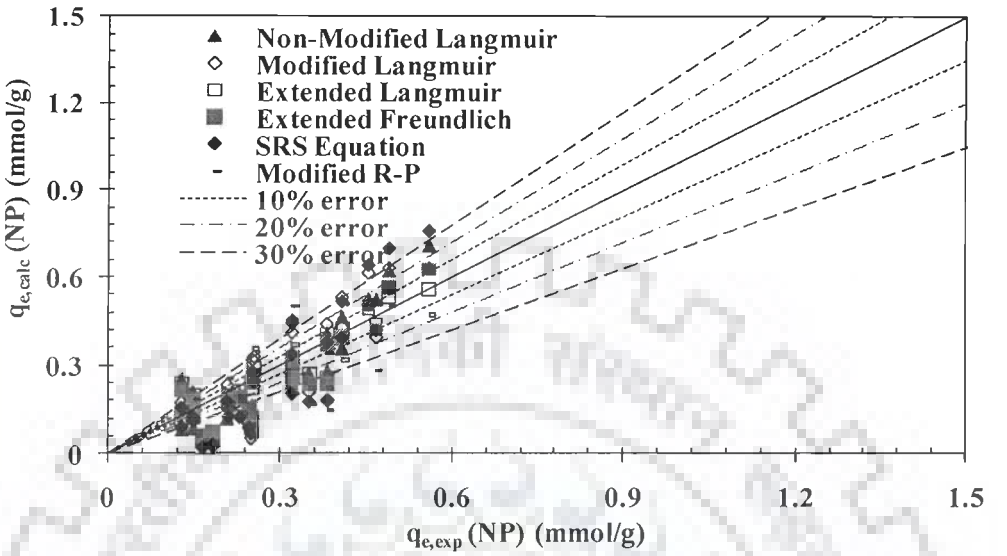

(a)

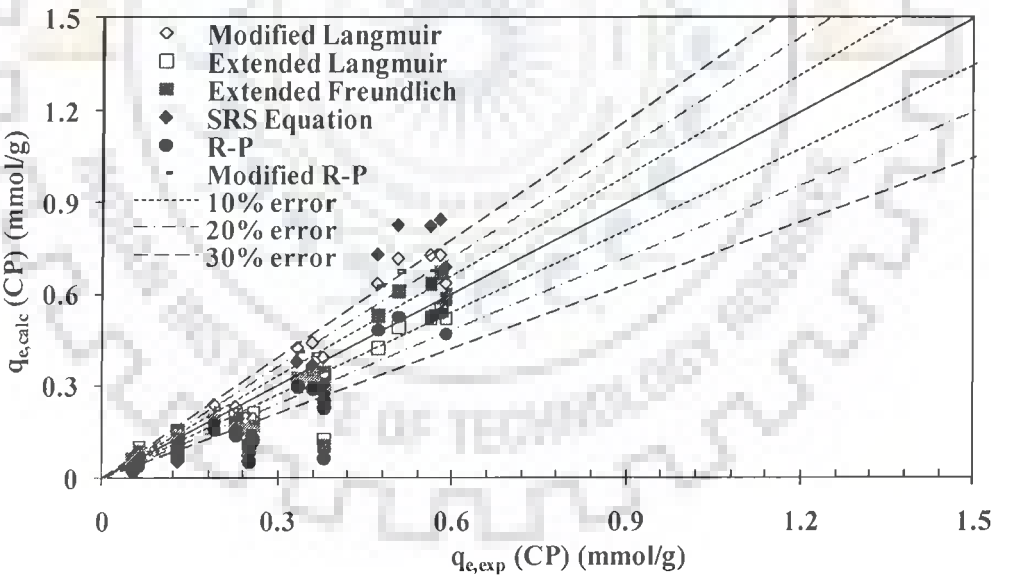

(b)

Figure 4.5.12. Comparison of the experimental and calculated q_e values for NP-CP binary system. [a] NP, [b] CP.

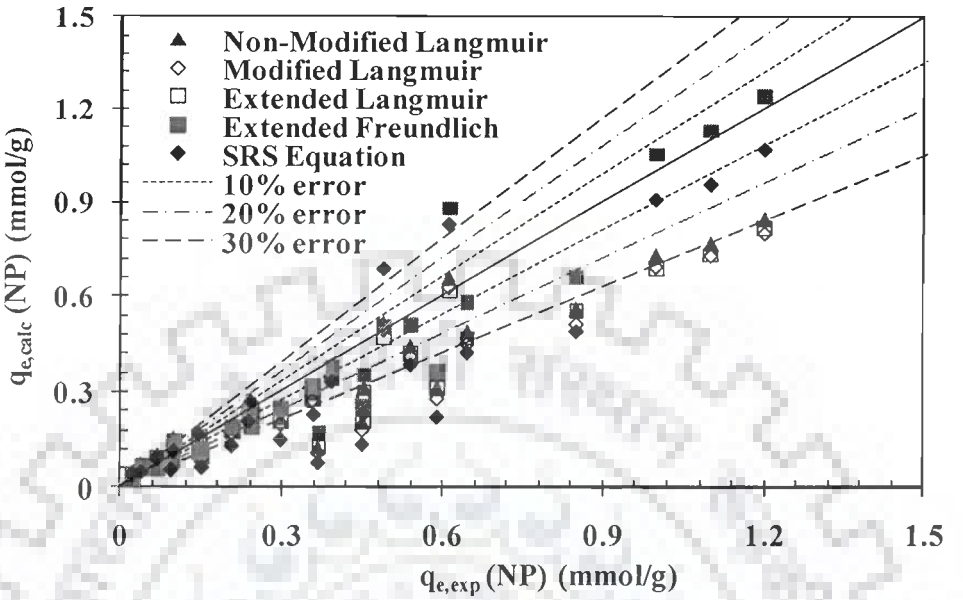

(a)

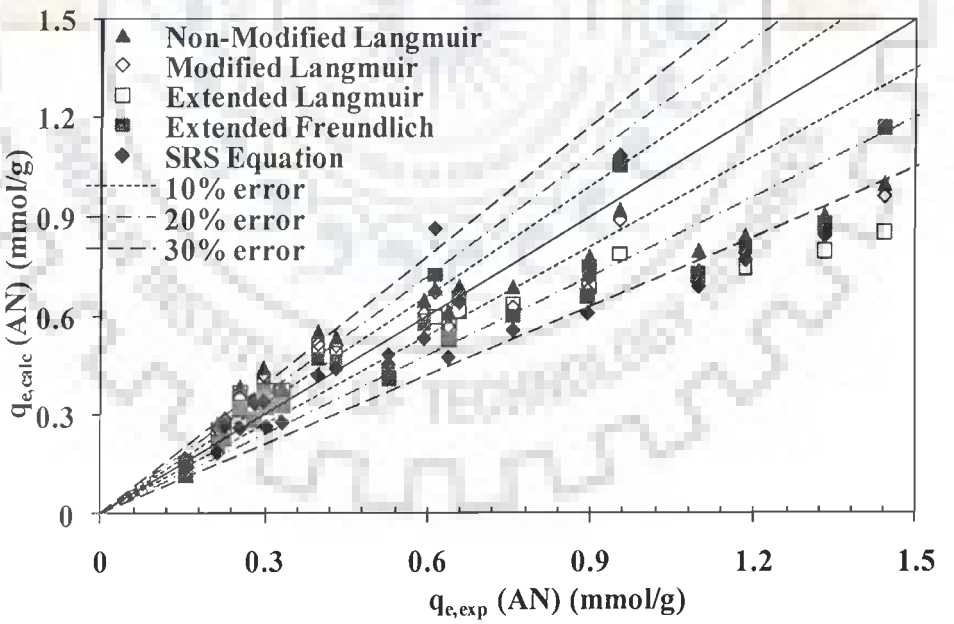

(b)

Figure 4.5.13. Comparison of the experimental and calculated q_e values for NP-AN binary system. [a] NP, [b] AN.

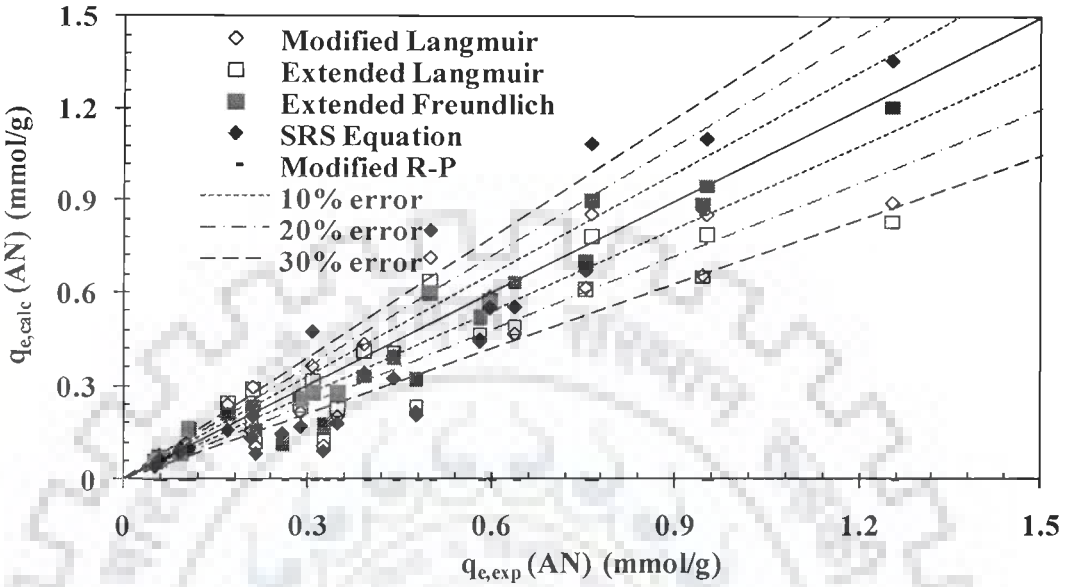

(a)

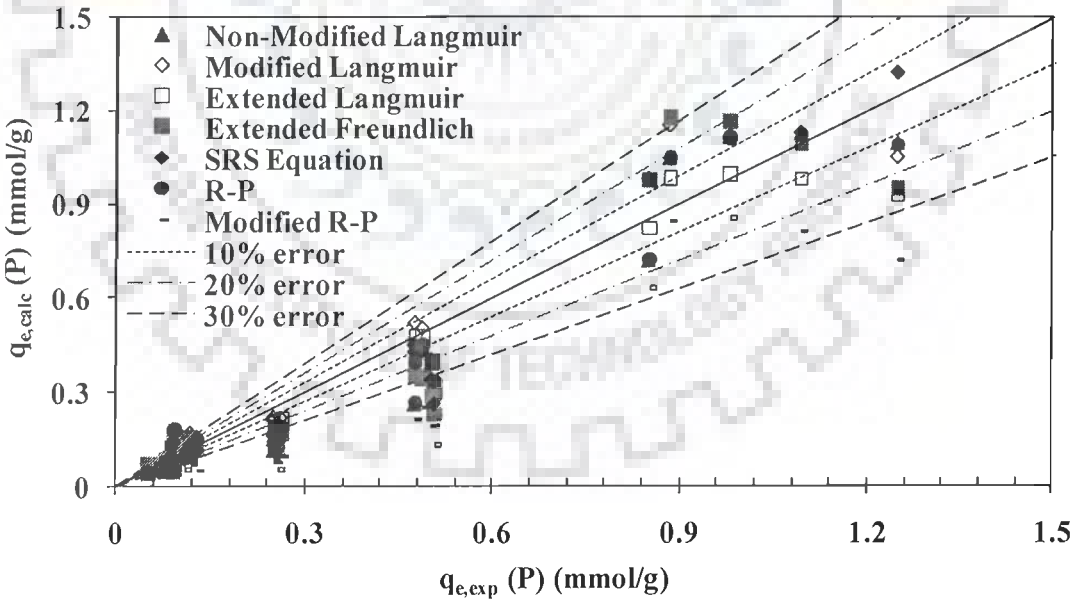

(b)

Figure 4.5.14. Comparison of the experimental and calculated q_e values for AN-P binary system. [a] AN, [b] P.

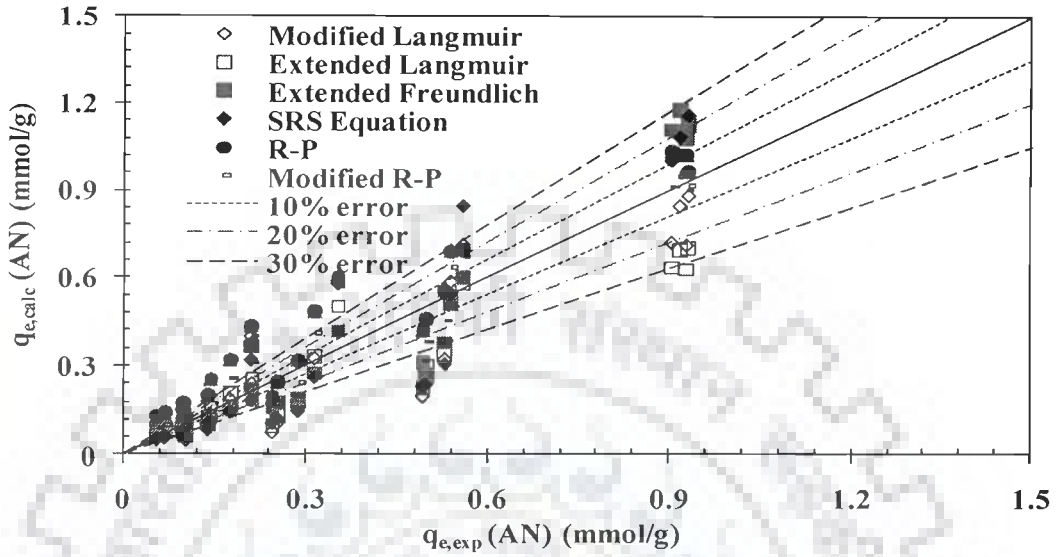

(a)

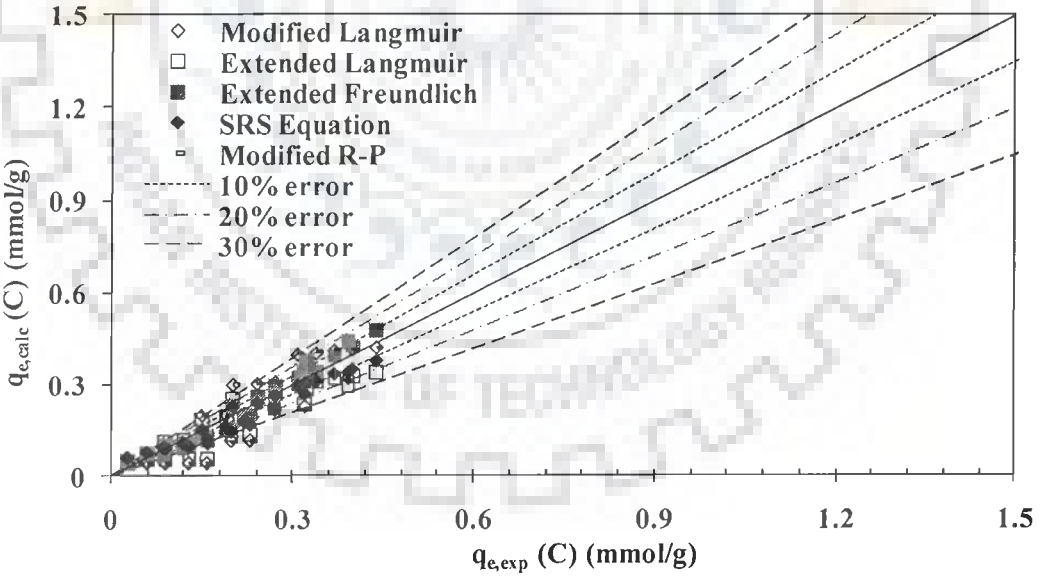

(b)

Figure 4.5.15. Comparison of the experimental and calculated q_e values for AN-C binary system. [a] AN, [b] C.

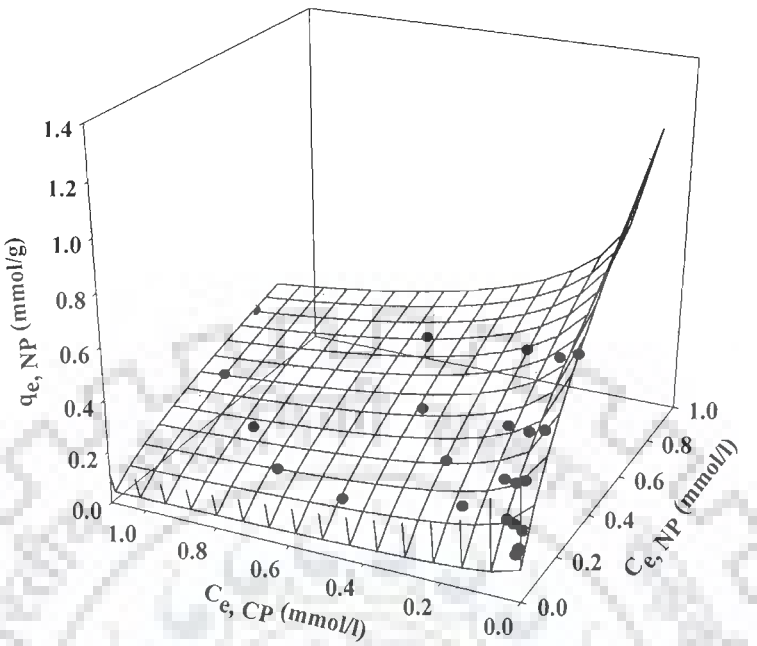

(a)

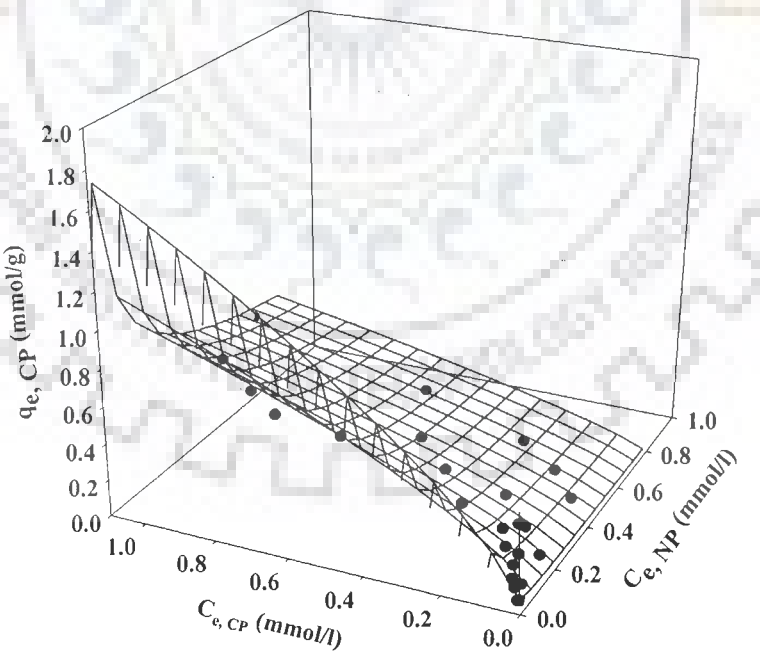

(b)

Figure 4.5.16. Binary adsorption isotherms for NP-CP binary system. [a] NP, [b] CP. The surfaces are predicted by the extended Freundlich model and the symbols are experimental data.

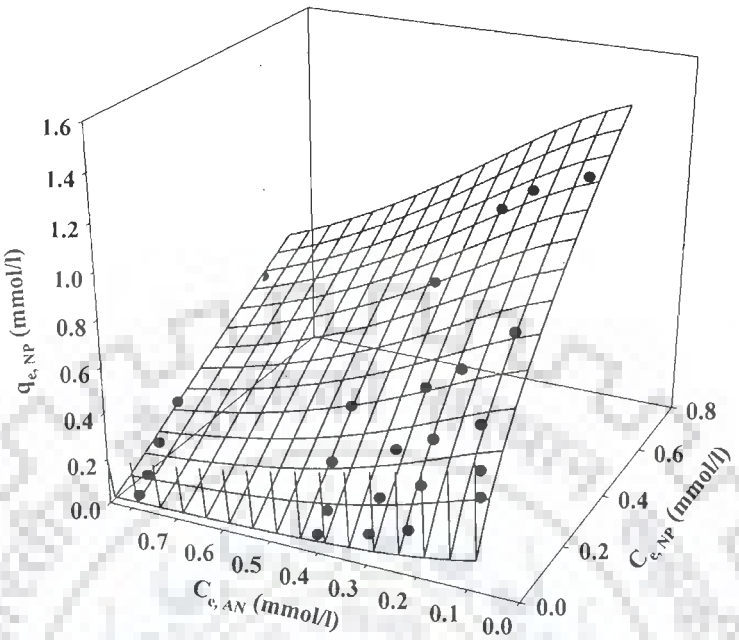

(a)

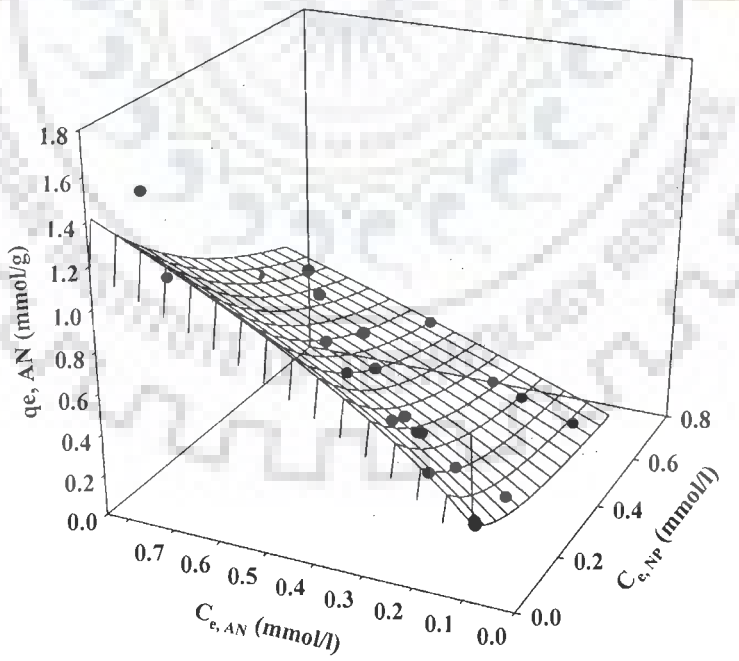

(b)

Figure 4.5.17. Binary adsorption isotherms for NP-AN binary system. [a] NP, [b] AN. The surfaces are predicted by the extended Freundlich model and the symbols are experimental data.

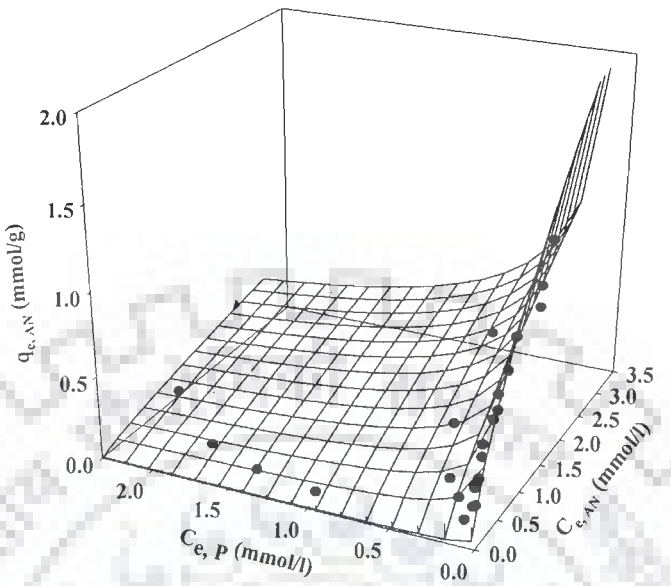

(a)

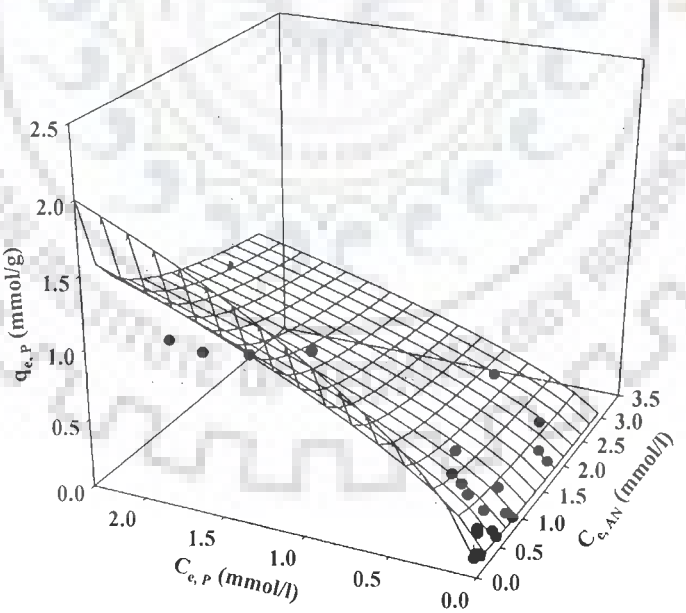

(b)

Figure 4.5.18. Binary adsorption isotherms for AN-P binary system. [a] AN, [b] P. The surfaces are predicted by the extended Freundlich model and the symbols are experimental data.

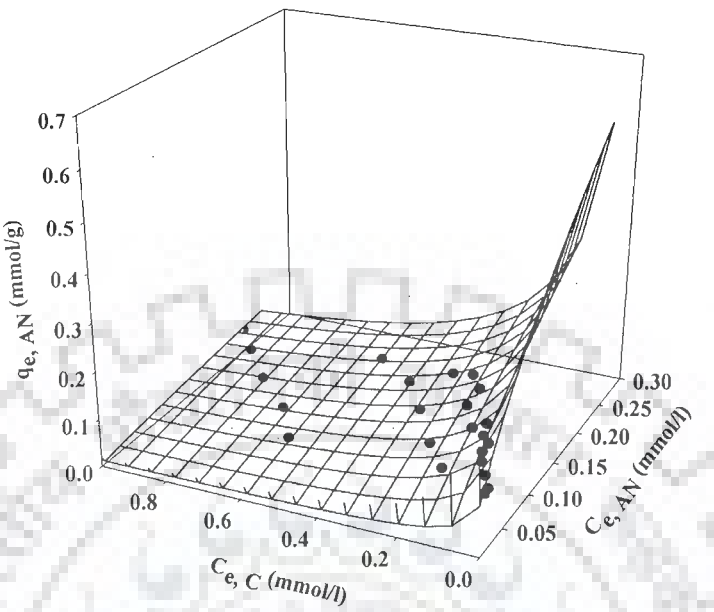

(a)

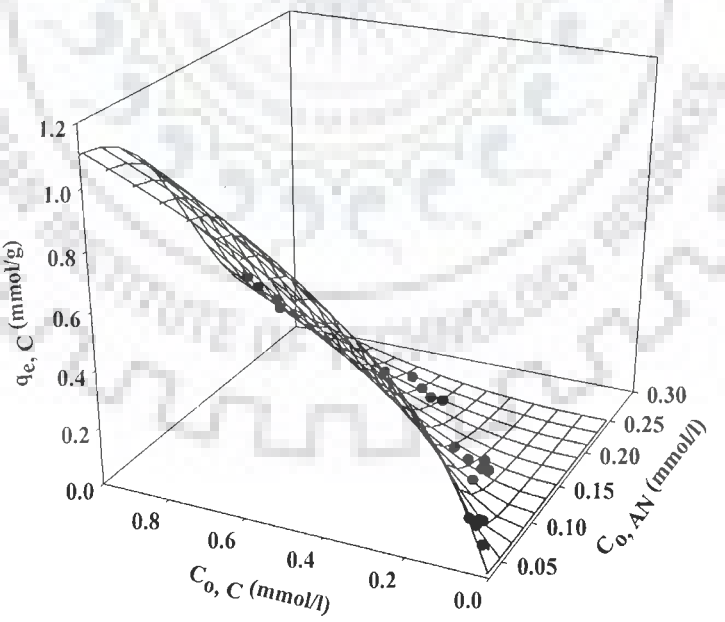

(b)

Figure 4.5.19. Binary adsorption isotherms for AN-C binary system. [a] AN, [b] C. The surfaces are predicted by the extended Freundlich model and the symbols are experimental data.

4.5.2. Ternary Batch Isotherm Study

Equilibrium isotherms for the ternary adsorption have been analyzed by using non-modified Langmuir, modified Langmuir, extended-Langmuir, SRS, non-modified and modified R-P models. The parametric and MPSD values of all the multi-component adsorption models for the adsorption of P, CP, NP, C, R and HQ by GAC from ternary systems of P-CP-NP and C-R-HQ are given in Table 4.5.6. A comparison of MPSD values for different isotherm models shows that modified-Langmuir, extended-Langmuir, SRS and modified R-P models show comparable fit to the adsorption equilibrium data. However, SRS model best-fitted the experimental adsorption data.

The multi-component non-modified Langmuir model shows a poor fit to the experimental data with MPSD values of 101.01 and 104.44 for P-CP-NP and C-R-HQ systems, respectively. The values of the modified Langmuir coefficient ($\eta_{L,i}$) deviate from one for both the systems indicating that non-modified multi-component Langmuir model related to the individual isotherm parameters could not be used to predict the binary-system adsorption. However, the use of the interaction term, $\eta_{L,i}$, improved the fit of the modified-Langmuir model as shown by lowering of MPSD values (72.67 for P-CP-NP and 74.34 for C-R-HQ) of modified-Langmuir model in comparison to non-modified Langmuir model.

The multi-component extended-Langmuir model has been found to adequately describe the adsorption equilibria of the ternary system of Cr(VI), Cu(II) and Cd(II) for a biosorbent *R. arrhizus* [Sag et al., 2002]. This model also shows good fitting of the data for present ternary adsorption systems also. The overall total adsorbate uptakes ($q_{\max}$) for P-CP-NP and C-R-HQ systems are 0.597 and 1.12 mmol/g, respectively. These values are considerably lower than the sum of the maximum total capacities of P, CP and NP or C, R and HQ resulting from the single component adsorption systems. For that reason, the adsorption sites of adsorbates in ternary systems of P-CP-NP and C-R-HQ may likely be partially overlapped. It may also imply that there may be a variety of binding sites on the GAC showing partially specific to the individual adsorbate. The information obtained from the maximum capacities seems to violate the basic assumptions of the Langmuir model [Sag et al., 2003]. Non-modified Redlich-Peterson (R-P) model gave high MPSD

values, however, modified R-P model improved the fit considerably. The fits of the modified R-P model (MPSD=75.67 for P-CP-NP and 89.54 for C-R-HQ) are comparably better than the single component based modified Langmuir models.

The multi-component SRS model applies to those systems where each component individually obeys the single-component Freundlich isotherm. The isotherm coefficients can be determined from the mono-component isotherm except for the adsorption competition coefficients, a_{ij}, which have to be determined experimentally. The competition coefficients, a_{ij}, describe the inhibition to the adsorption of component i by component j. The three components individually were found to obey the single-component Freundlich model. The main assumptions incorporated in the derivation are that for each component in a multi-component adsorption, adsorption energies of sites are exponentially distributed.

A comparison of the competition coefficients in the adsorption isotherm equation for NP-CP-P shows that the uptake of the CP was strongly affected by the presence of NP or P (a_{21} and a_{23} values are very high), while the inhibition exerted in the reverse situation is not that strong strong (a_{12} or a_{32} are not that high). Also, NP significantly inhibited the adsorption of P onto GAC (a_{31}= 80.92). Similar behavior is observed for the simultaneous adsorption of C, R and HQ onto GAC.

4.5.2.1 Three-dimensional (3-D) adsorption isotherm surfaces: For plotting 3-D adsorption isotherm surfaces for ternary systems, the residual concentration of one of the adsorbate has been taken as a parameter in these plots. A 3-D diagram is plotted on the basis of the randomly generated data, and the experimental data are fitted to a smooth surface according to the appropriate input equation. The multi-component SRS model can be used to simulate the equilibrium sorption behavior of the ternary system through 3-D plots.

The adsorption isotherm surfaces for P-CP-NP and C-R-HQ systems, as shown in Figs. 4.5.20-4.5.21 and Figs. 4.5.22-4.5.23, respectively, were created by using the multi-component SRS model and smoothed and fitted to the experimental adsorption data. When

both P and CP were present in the solution together and the effect of NP was ignored, some reduction of the P uptake was observed with increasing CP concentrations (Fig. 4.5.20b). The uptake of CP, however, decreased marginally with increasing equilibrium P concentrations (Fig. 4.5.20a). Thus inhibition effect of CP was more pronounced than P. Fig. 4.5.21 shows the plots of unadsorbed P and NP concentrations in solution at equilibrium against the P, NP, and total (P+NP) uptakes by GAC. The initial concentration of CP was taken as a parameter. It is found that the P uptake by the GAC was more strongly affected by the presence of NP (Fig. 4.5.21b) whereas uptake of NP by the GAC is less affected by the presence of P (Fig. 4.5.21a). Fig. 4.5.22 shows the plots of unadsorbed R and HQ concentrations in solution at equilibrium against the R, HQ, and total (R+HQ) uptakes by GAC with initial concentration of C as c constant parameter. It seems that the R uptake by the GAC was more strongly affected by the presence of HQ as compared to vice-versa. Similarly uptake of C is also strongly affected by HQ concentration (Fig. 4.5.23).

Table 4.5.6. Ternary isotherm parameter values for P-CP-NP and C-R-HQ systems.

P-CP-NP				**C-R-HQ**			
Non-modified Langmuir Model							
MPSD	101.01			MPSD	104.44		
Modified Langmuir Model							
Adsorbate	$\eta_{L,i}$			Adsorbate	$\eta_{L,i}$		
NP	3.91			C	4.65		
CP	44.88			R	8.56		
P	7.18			HQ	114.81		
MPSD	72.67			MPSD	74.34		
Extended-Langmuir Model							
Adsorbate	$K_{EL,i}$	q_{max}		Adsorbate	$K_{EL,i}$	q_{max}	
NP	3.20	0.597		C	2.55	1.12	
CP	1.43			R	1.41		
P	0.23			HQ	5.89		
MPSD	73.49			MPSD	75.64		
SRS Model							
Adsorbate	a_{ij}	a_{ij}	a_{ij}	Adsorbate	a_{ij}	a_{ij}	a_{ij}
NP	1	65.38	5.50	C	1	17.91	0.0028
CP	5062.1	1	13675.7	R	94.55	1	0.071
P	80.92	3.44	1	HQ	285.62	0.202	1
MPSD	71.85			MPSD	73.11		
Non-modified R-P Model							
MPSD	91.84			MPSD	117.05		
Modified R-P Model							
Adsorbate	$\eta_{R,i}$			Adsorbate	$\eta_{R,i}$		
NP	16.49			C	0.019		
CP	15.21			R	0.001		
P	0.21			HQ	26.54		
MPSD	75.67			MPSD	89.54		

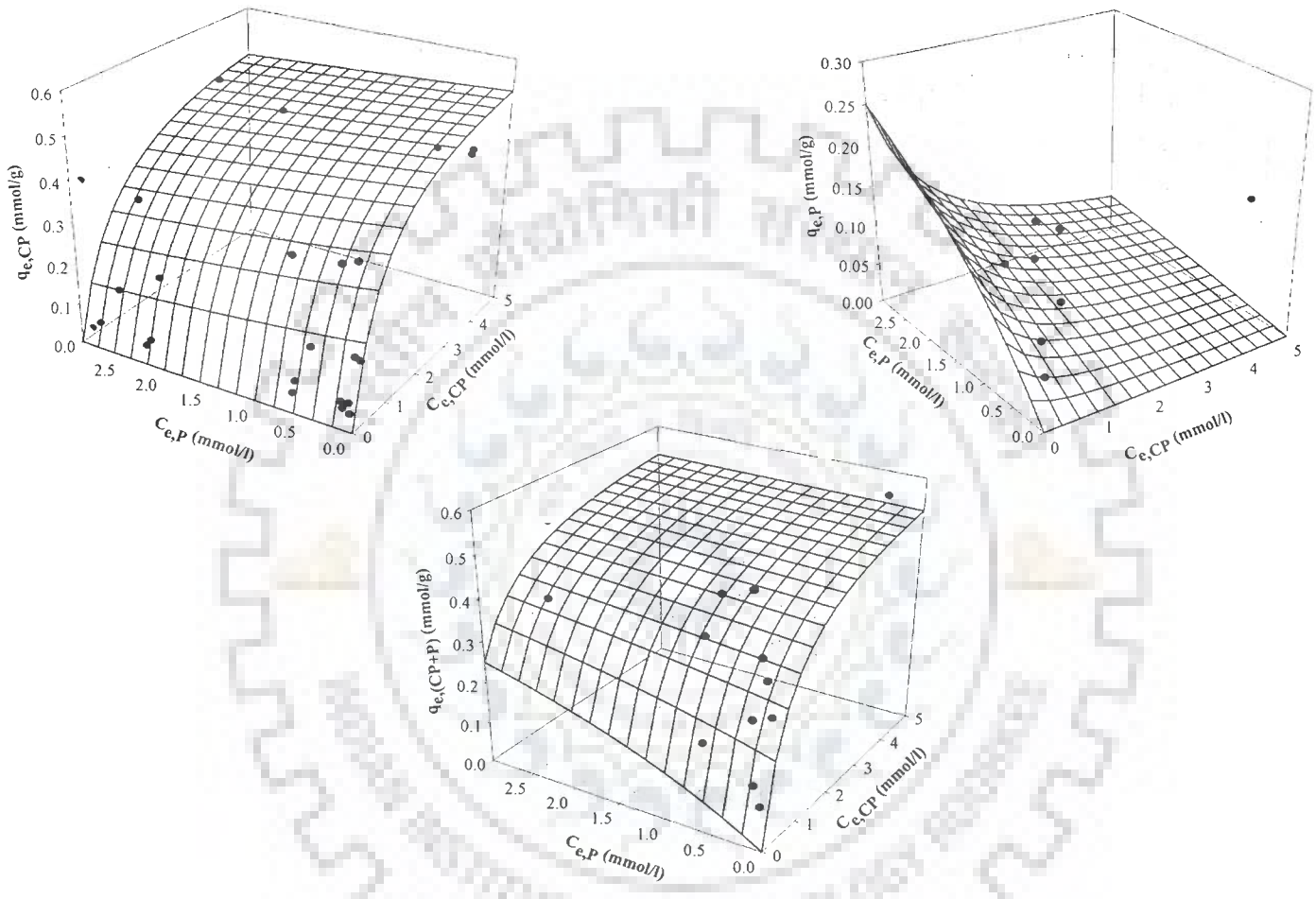

Figure 4.5.20. Three-dimensional adsorption isotherm surfaces created using multicomponent SRS model for the P-CP-NP systems with $C_{e,NP}$, as a parameter. (a) The effect of P concentration on the equilibrium uptake of CP; (b) the effect of CP concentration on the equilibrium uptake of P (c) the effect of P and CP concentration on the equilibrium total uptake of P+CP onto GAC.

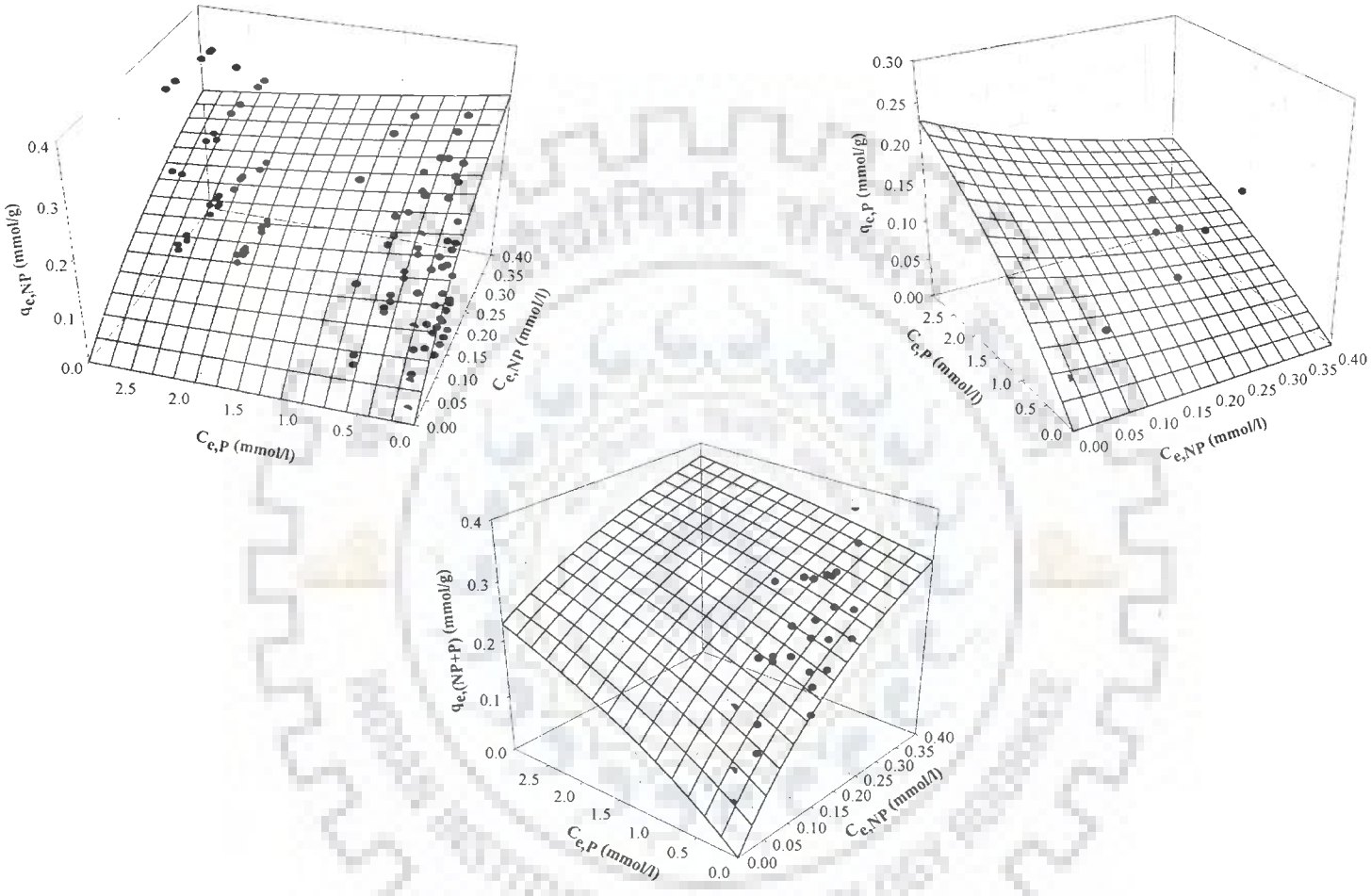

Figure 4.5.21. Three-dimensional adsorption isotherm surfaces created using multicomponent SRS model for the P-CP-NP systems with $C_{e,CP}$, as a parameter. (a) The effect of P concentration on the equilibrium uptake of NP; (b) the effect of NP concentration on the equilibrium uptake of P (c) the effect of P and NP concentration on the equilibrium total uptake of P+NP onto GAC.

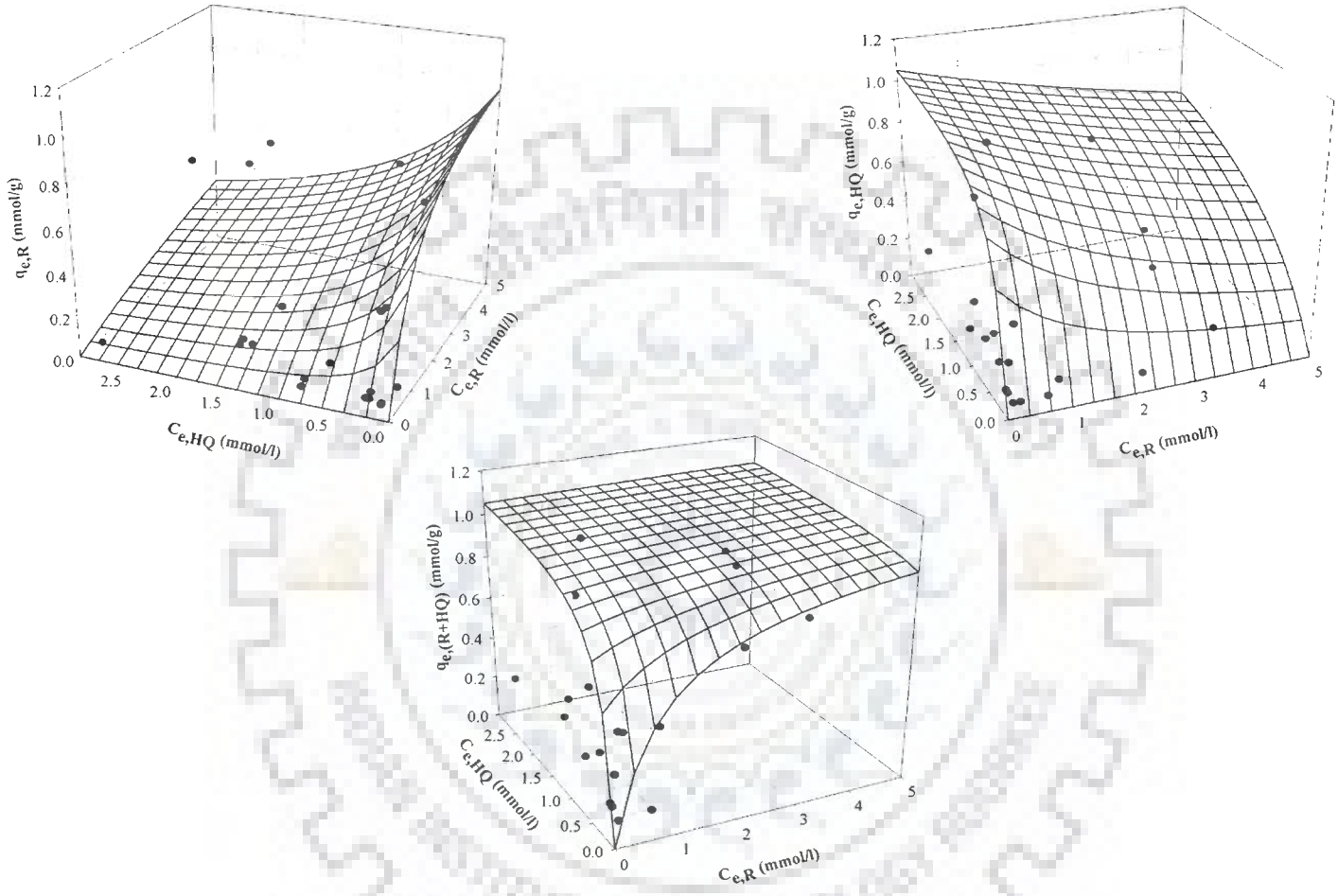

Figure 4.5.22. Three-dimensional adsorption isotherm surfaces created using multicomponent SRS model for the C-R-HQ systems with $C_{e,C}$, as a parameter. (a) The effect of HQ concentration on the equilibrium uptake of R; (b) the effect of R concentration on the equilibrium uptake of HQ (c) the effect of R and HQ concentration on the equilibrium total uptake of R+HQ onto GAC.

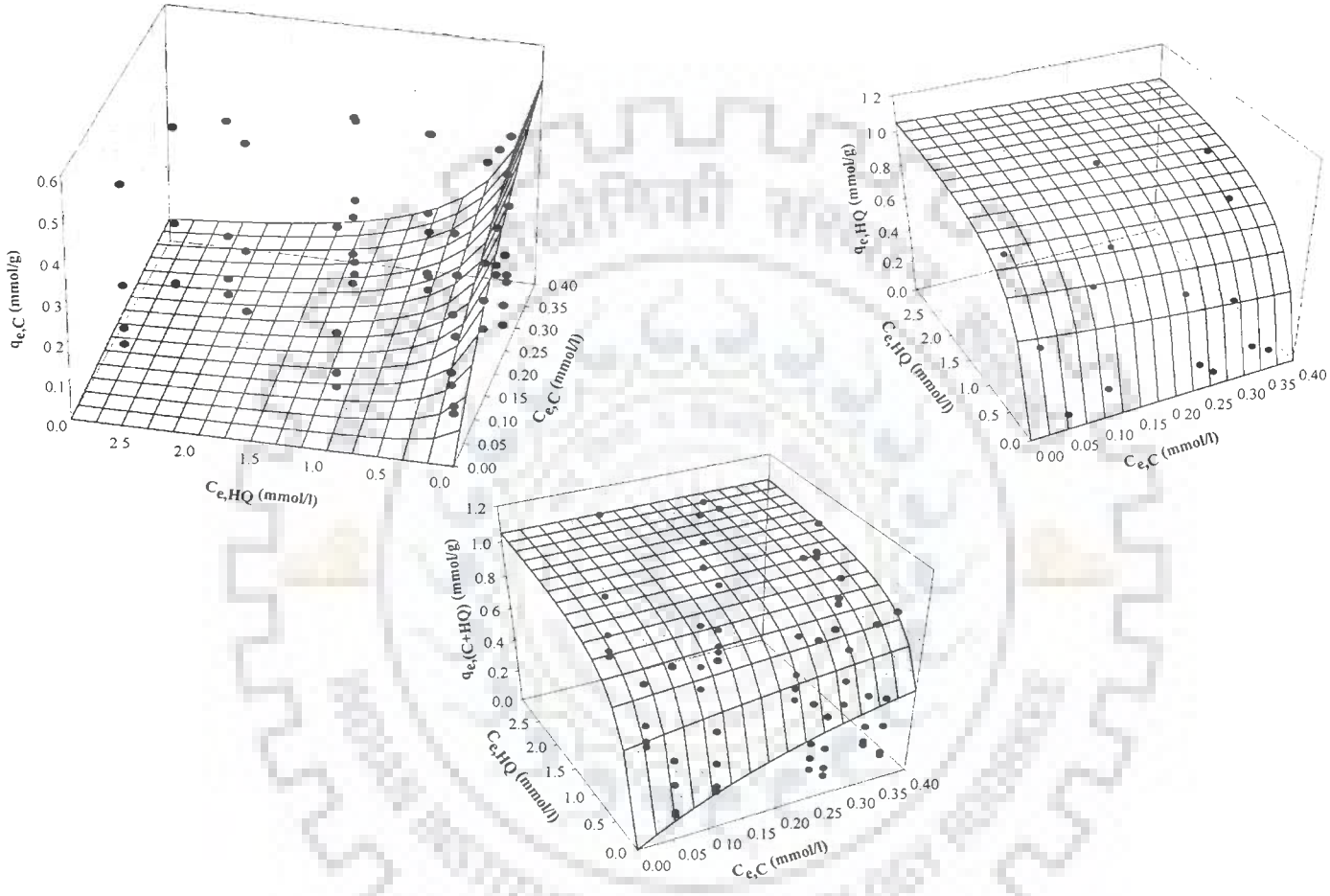

Figure 4.5.23. Three-dimensional adsorption isotherm surfaces created using multicomponent SRS model for the C-R-HQ systems with $C_{e,R}$, as a parameter. (a) The effect of HQ concentration on the equilibrium uptake of C; (b) the effect of C concentration on the equilibrium uptake of HQ (c) the effect of C and HQ concentration on the equilibrium total uptake of C+HQ onto GAC.

4.6 MULTI-COMPONENT COLUMN ADSORPTION STUDY USING TAGUCHI'S METHOD

In the present study, results of column studies conducted for the removal of P, CP, NP, C, R and HQ from P-CP-NP and C-R-HQ ternary systems have been presented. Taguchi's L_9 OA matrix (Table 3.4.5) was applied to investigate the effect of process parameters namely flow rate (Q), bed height (Z) and column diameter (D) on breakthrough point and total quantity of adsorbates adsorbed at breakthrough (q_{tot}). The q_{tot}, (mg/g) in column study was calculated using Eq. (3.4.2):

$$q_{tot} = \frac{\sum_{N=1}^{3}\left[QC_0\int_0^{t_b}\left(1-\frac{C_t}{C_0}\right)dt\right]_N}{\frac{\pi}{4}D^2 Z\rho_{BD,ads}} \tag{3.4.2}$$

where, C_0 is the initial adsorbate concentration (mg/l), C_t is the residual adsorbate concentration at time t (mg/l), t_b is the breakthrough time (min), Q is the flow rate (l/min), D is the diameter of the column (cm) and Z is the bed height (cm), $\rho_{BD,ads}$ is the bulk density of the GAC, and N is the number of adsorbates.

Empty bed contact time (EBCT) is an important parameter in the design of adsorption columns. It affects the shape of the breakthrough curve and breakthrough volume (V_b). This is determined by the following equation:

$$EBCT = \frac{V_C}{Q} = \frac{A_C Z}{Q} \tag{4.6.1}$$

where, V_C is the volume of the adsorbent in the bed (l). The performance of a fixed-bed can be further evaluated in terms of the adsorbent usage rate (U_r) defined as the weight of adsorbent saturated per litre of solution treated [Srivastava et al., 2008c]:

$$U_r = \frac{m_C}{V_b} = \frac{V_C\rho}{V_C N_b} = \frac{\rho}{N_b} \tag{4.6.2}$$

Choosing 10% breakthrough point as the treatment objective, the values of EBCT and U_r were determined using the data from the breakthrough curves obtained at various Q, Z and D.

Breakthrough curves of 9 runs performed in column study as per Taguchi's L_9 OA matrix (Table 3.4.5) for the removal of P, CP, NP, C, R and HQ from P-CP-NP and C-R-HQ ternary systems have been presented in Figs. 4.6.1-4.6.3 and 4.6.4-4.6.6, respectively. Values of EBCT, t_b, V_b, number of reactor volume treated at breakthrough (N_b), U_r and q_i (uptake till breakthrough point for individual adsorbates) as calculated from breakthrough curves for P-CP-NP and C-R-HQ ternary systems are given in Tables 4.6.1 and 4.6.2, respectively. From these tables, it can be seen that the value of U_r generally tends to decrease with an increase in EBCT.

It is seen from the breakthrough curves (Figs. 4.6.1-4.6.6) that the breakthrough generally occurred faster with higher Q value. Time required for reaching saturation increased significantly with decrease in the value of Q. Obviously, the GAC particles get saturated early at higher value of Q. This is because the time required to reach an equilibrium between GAC particles and adsorbate solutions is much longer (about 24 h). Therefore, an increase in the Q causes a shorter retention time, which causes a negative effect on the mass transfer efficiency of the adsorbates. At higher value of Q, the rate of mass transfer tends to increase. The amount of adsorbate adsorbed onto the unit bed height (mass transfer zone) increased with an increase in Q leading to faster saturation at a higher value of Q [Ko et. al., 2000].

Also it may be seen that higher q_i values are observed at higher Z (Tables 4.6.1 and 4.6.2). This was due to the increase in the number of binding sites owing to an increase in adsorption surface area of the GAC [Vijayaraghavan et al., 2004]. As the value of Z increased, adsorbates had sufficient time to diffuse into the whole mass of the GAC that resulted in an increase in t_b.

Sharper profiles are obtained with thin packed beds having a D value of 2 and 2.54 cm (Figs. 4.6.1-4.6.6). For a lower value of D, the bed is better packed so that the control of flow distribution is easier. A shallower breakthrough curve and a longer t_b is obtained with wider bed (D=4 cm) may be due the channeling of the adsorbates [Srivastava et al., 2008c].

4.6.1 Optimization of Parameters for Ternary Column Adsorption Study

The effect of individual parameters (Q, Z and D) on q_{tot} for the simultaneous removal of adsorbates from P-CP-NP and C-R-HQ ternary systems are being reported in this section. The average or mean values of q_{tot} for each parameter at level 1, 2, and 3, as calculated from Table 4.6.3, are given in Table 4.6.4. Individually at level stage with q_{tot} as the desired response characteristic, Q (parameter A) has highest influence at level 1 and D (parameter C) has highest influence at level 3. Q or Z (parameters A or B) have highest influence at level 2. The difference between level 2 and level 1 (L2−L1) of each factor indicates the relative influence of the effect. The larger the difference, the stronger is the influence. It can be seen from Table 4.6.4 that no single parameter has overriding influence for the removal of P, CP, NP, C, R and HQ from P-CP-NP and C-R-HQ ternary systems. D shows strong influence on q_{tot} as compared to other parameters. The reasons for increase in q_{tot} with an increase in the D are described earlier.

The response curves for the individual effects of adsorption parameters on the average value of q_{tot} for P-CP-NP and C-R-HQ ternary systems are given in Figs. 4.6.7 and 4.6.8, respectively. An increase in the levels of factors such as Z and D from 1 to 2 and from 2 to 3 has resulted in an increase in the q_{tot} values for all adsorbents. It can also be noted that an increase in Q led to decrease q_{tot} values for both the systems. The reasons for these have already been described in this section itself.

ANOVA was used to analyze the results of the OA experiment and to determine how much variation each factor has contributed. ANOVA results for q_{tot} values for both the systems are given in Table 4.6.5 for both P-CP-NP and C-R-HQ ternary systems. From the calculated ratios (F), it can be referred that all factors and interactions considered in the experimental design with q_{tot} as desired response characteristic are statistically significant at 95% confidence limit. The percentage contribution of each parameter in q_{tot} values for P-CP-NP and C-R-HQ ternary systems is shown in Table 4.6.5. It can be observed from this table that the parameter C (D) contributes significantly for

simultaneous adsorbate removal onto GAC for both P-CP-NP and C-R-HQ ternary systems.

Table 4.6.7 summarizes the optimal level of various parameters obtained after examining the response curves (Figs. 4.6.7 and 4.6.8) of the average value of q_{tot} for both P-CP-NP and C-R-HQ ternary systems. It indicates that 3rd levels of parameters B and C, and 1st level of parameter A give higher average value of q_{tot}. Optimal q_{tot} values and confidence intervals (CI_{POP} and CI_{CE}) at these levels have been calculated and are presented in Table 4.6.7 for simultaneous adsorption of P, CP, NP, and C, R, HQ from aqueous solution onto GAC packed column for P-CP-NP and C-R-HQ ternary systems. The q_{tot} values obtained through confirmation experiments are within 95% of CI_{CE} for respective ternary systems.

Table 4.6.1 Ternary column adsorption study using Taguchi's method for P-CP-NP system.

Expt. No.	Q (l/min)	Z (cm)	D (cm)	EBCT (min)	t_b (min)	V_b (l)	N_b	U_r (g/l)	q_i (mg/g)
P									
1	0.02	30	2	4712.4	19.16	0.38	0.0041	178.36	1.66
2	0.02	45	2.54	11400.9	24.42	0.49	0.0021	338.51	2.76
3	0.02	60	4	37699.2	776.05	15.52	0.0206	35.22	86.43
4	0.04	30	2.54	3800.3	20.82	0.83	0.0055	132.36	3.18
5	0.04	45	4	14137.2	708.03	28.32	0.0501	14.48	35.36
6	0.04	60	2	4712.4	24.70	0.99	0.0052	138.29	2.60
7	0.06	30	4	6283.2	594.55	35.67	0.0946	7.66	10.88
8	0.06	45	2	2356.2	17.54	1.05	0.0074	97.38	5.31
9	0.06	60	2.54	5067.1	29.75	1.78	0.0059	123.49	2.37
CP									
1	0.02	30	2	4712.4	21.35	0.43	0.0045	160.03	2.07
2	0.02	45	2.54	11400.9	34.90	0.70	0.0031	236.82	3.48
3	0.02	60	4	37699.2	787.31	15.75	0.0209	34.72	86.29
4	0.04	30	2.54	3800.3	21.77	0.87	0.0057	126.55	3.88
5	0.04	45	4	14137.2	738.76	29.55	0.0523	13.87	35.50
6	0.04	60	2	4712.4	24.26	0.97	0.0051	140.85	3.05
7	0.06	30	4	6283.2	654.84	39.29	0.1042	6.96	11.98
8	0.06	45	2	2356.2	22.23	1.33	0.0094	76.85	2.76
9	0.06	60	2.54	5067.1	40.66	2.44	0.0080	90.34	5.81
NP									
1	0.02	30	2	4712.4	48.60	0.97	0.0103	70.30	3.91
2	0.02	45	2.54	11400.9	60.55	1.21	0.0053	136.51	6.74
3	0.02	60	4	37699.2	795.27	15.91	0.0211	34.37	86.17
4	0.04	30	2.54	3800.3	52.40	2.10	0.0138	52.58	10.72
5	0.04	45	4	14137.2	777.56	31.10	0.0550	13.18	37.72
6	0.04	60	2	4712.4	54.61	2.18	0.0116	62.56	7.71
7	0.06	30	4	6283.2	716.89	43.01	0.1141	6.35	13.11
8	0.06	45	2	2356.2	49.83	2.99	0.0212	34.28	7.10
9	0.06	60	2.54	5067.1	70.98	4.26	0.0140	51.76	14.62

Table 4.6.2 Ternary column adsorption study using Taguchi's method for C-R-HQ system.

Expt. No.	Q (l/min)	Z (cm)	D (cm)	EBCT (min)	t_b (min)	V_b (l)	N_b	U_r (g/l)	q_t (mg/g)
C									
1	0.02	30	2	4712.4	17.74	0.35	0.0038	192.54	2.672
2	0.02	45	2.54	11400.9	151.67	3.03	0.0133	54.50	15.868
3	0.02	60	4	37699.2	795.57	15.91	0.0211	34.36	107.347
4	0.04	30	2.54	3800.3	92.61	3.70	0.0244	29.75	8.93
5	0.04	45	4	14137.2	786.57	31.46	0.0556	13.03	99.417
6	0.04	60	2	4712.4	35.44	1.42	0.0075	96.40	6.136
7	0.06	30	4	6283.2	751.04	45.06	0.1195	6.07	80.738
8	0.06	45	2	2356.2	20.54	1.23	0.0087	83.16	4.981
9	0.06	60	2.54	5067.1	166.15	9.97	0.0328	22.11	22.096
R									
1	0.02	30	2	4712.4	20.94	0.42	0.0044	163.14	3.047
2	0.02	45	2.54	11400.94	109.49	2.19	0.0096	75.49	7.997
3	0.02	60	4	37699.2	723.21	14.46	0.0192	37.79	13.143
4	0.04	30	2.54	3800.3	64.05	2.56	0.0168	43.02	4.010
5	0.04	45	4	14137.2	705.23	28.21	0.0498	14.53	10.045
6	0.04	60	2	4712.4	23.26	0.93	0.0049	146.91	5.1371
7	0.06	30	4	6283.2	679.56	40.77	0.1081	6.70	8.79
8	0.06	45	2	2356.2	21.66	1.30	0.0092	78.87	3.215
9	0.06	60	2.54	5067.1	120.66	7.24	0.0238	30.45	10.702
HQ									
1	0.02	30	2	4712.4	23.26	0.47	0.0049	146.91	6.124
2	0.02	45	2.54	11400.9	26.18	0.52	0.0022	315.76	9.017
3	0.02	60	4	37699.2	583.46	11.67	0.0154	46.84	25.561
4	0.04	30	2.54	3800.3	29.58	1.18	0.0077	93.16	7.564
5	0.04	45	4	14137.2	579.40	23.18	0.0409	17.69	21.419
6	0.04	60	2	4712.4	33.90	1.36	0.0072	100.79	5.587
7	0.06	30	4	6283.2	567.34	34.04	0.0902	8.03	17.452
8	0.06	45	2	2356.2	25.89	1.55	0.0109	65.98	5.245
9	0.06	60	2.54	5067.1	36.52	2.19	0.0072	100.60	11.16

Table 4.6.3 q_{tot} values in column study for P-CP-NP and C-R-HQ ternary systems.

Expt. No.	Q (l/min)	Z (cm)	D (cm)	EBCT (min)	q_{tot} (mg/g)	
					P-CP-NP	C-R-HQ
1	0.02	30	2	4712.4	7.65	11.84
2	0.02	45	2.54	11400.9	12.98	32.88
3	0.02	60	4	37699.2	258.89	146.05
4	0.04	30	2.54	3800.3	17.78	20.50
5	0.04	45	4	14137.2	108.58	130.88
6	0.04	60	2	4712.4	13.36	16.85
7	0.06	30	4	6283.2	35.97	106.98
8	0.06	45	2	2356.2	15.17	13.44
9	0.06	60	2.54	5067.1	22.81	43.95

Table 4.6.4 Average and main effects of q_{tot} values in column study for P-CP-NP and C-R-HQ ternary systems.

Parameter	L1	L2	L3	L2-L1	L3-L2
	P-CP-NP				
A: Q	93.17	46.57	24.65	-46.60	-21.92
B: Z	20.47	45.58	98.35	25.11	52.77
C: D	12.06	17.85	134.48	5.80	116.62
	C-R-HQ				
A: Q	63.59	56.08	54.79	-7.51	-1.29
B: Z	46.44	59.07	68.96	12.63	9.89
C: D	14.05	32.45	127.97	18.40	95.52

Table 4.6.5 ANOVA of q_{tot} values in column study for P-CP-NP and C-R-HQ ternary systems.

Factors	Sum of square	DOF	Mean Square	F - value	% contribution
	P-CP-NP				
A	7347.91	2	3673.96	0.807	13.47
B	9481.33	2	4740.67	1.042	17.38
C	28621.8	2	14310.9	3.145	52.47
Error	9101.42	2	4550.71	1.00	16.68
Total	54552.4	8	6819.05		100
	C-R-HQ				
A	135.50	2	67.75	0.822	0.58
B	764.03	2	382.01	4.633	3.25
C	22441.55	2	11220.78	136.082	95.47
Error	164.91	2	82.46	1.00	0.70
Total	23506	8	2938.25		100

Table 4.6.6 Comparison of predicted optimal q_{tot} values, confidence intervals and results of confirmation experiments for P-CP-NP and C-R-HQ ternary systems in column study.

System	Optimal levels of process parameters	Predicted optimal values (mmol/g)	Confidence intervals (95%)	Average of Confirmation experiments (mmol/g)
P-CP-NP	A1, B3, C3	216.40	$CI_{POP}: 175.08 < \mu_{GAC} < 257.72$	210.22
			$CI_{CE}: 170.73 < \mu_{GAC} < 262.07$	
C-R-HQ	A1, B3, C3	144.20	$CI_{POP}: 112.31 < \mu_{GAC} < 176.08$	151.82
			$CI_{CE}: 99.10 < \mu_{GAC} < 189.29$	

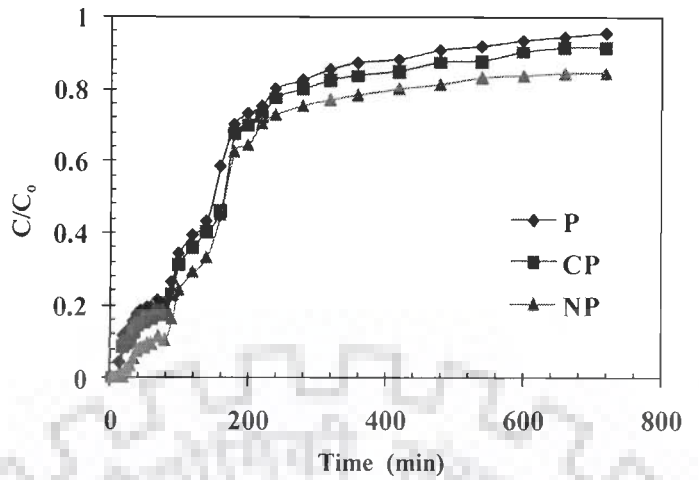

(A)

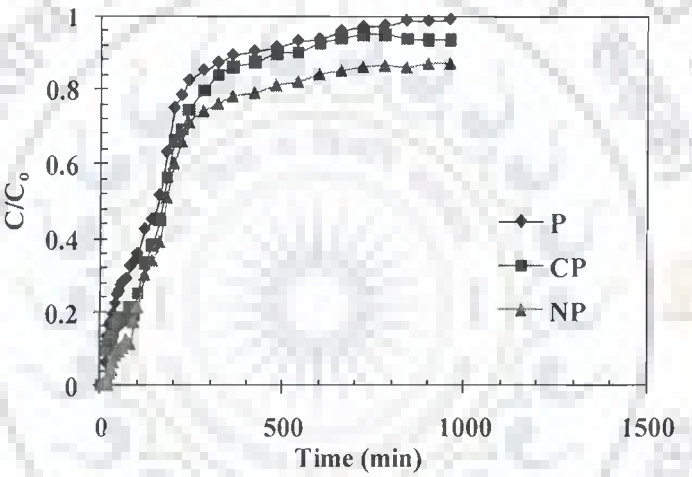

(B)

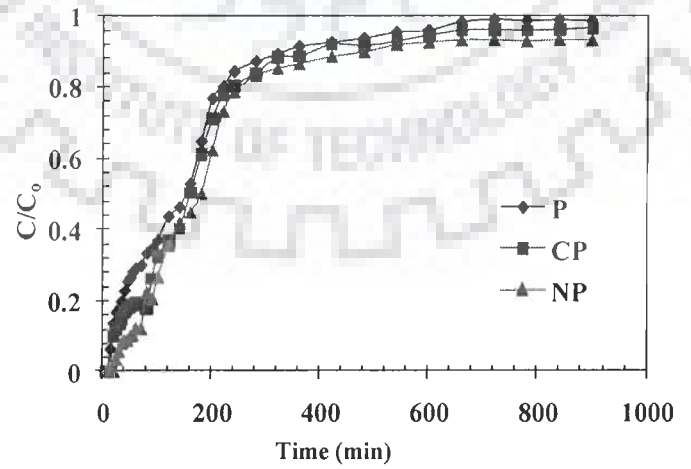

(C)

Figure 4.6.1. Breakthrough curves for simultaneous adsorption of P, CP and NP onto GAC for D=2 cm. (A) Expt. No. 1: Q=0.02 l/min, Z=30 cm; (B) Expt. No. 6: Q=0.04 l/min, Z=60 cm; (C) Expt. No. 8: Q=0.06 l/min, Z=45 cm.

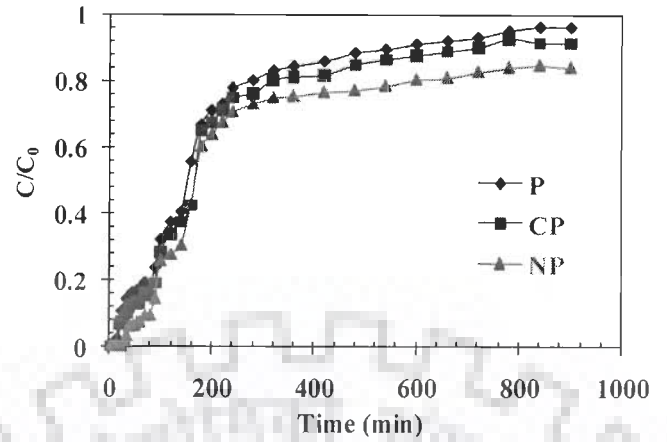

(A)

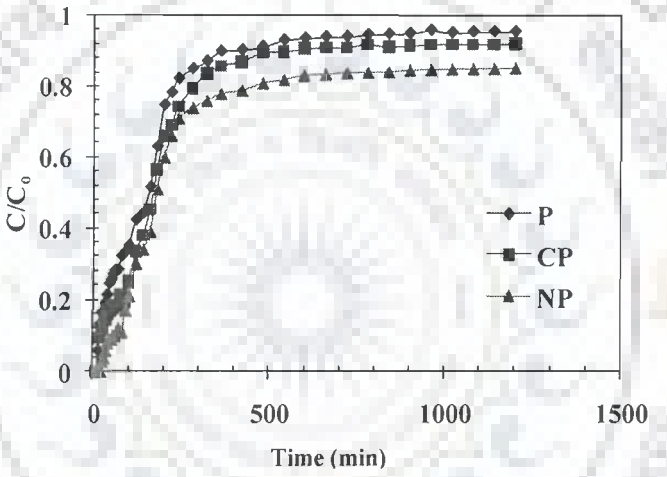

(B)

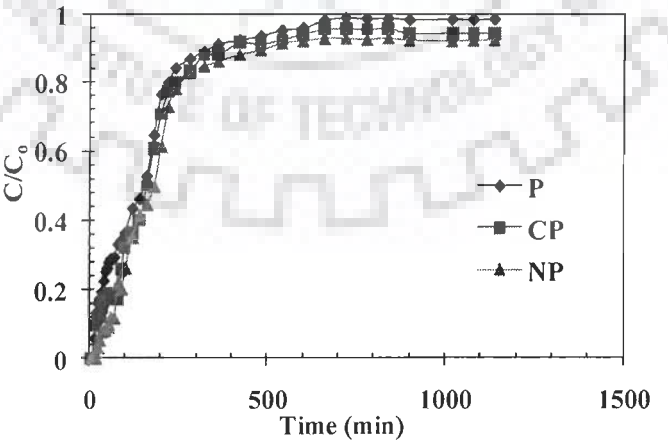

(C)

Figure 4.6.2. Breakthrough curves for simultaneous adsorption of P, CP and NP onto GAC for D=2.54 cm. (A) Expt. No. 2: Q=0.02 l/min, Z=45 cm; (B) Expt. No. 4: Q=0.04 l/min, Z=30 cm; (C) Expt. No. 9: Q=0.06 l/min, Z=60 cm.

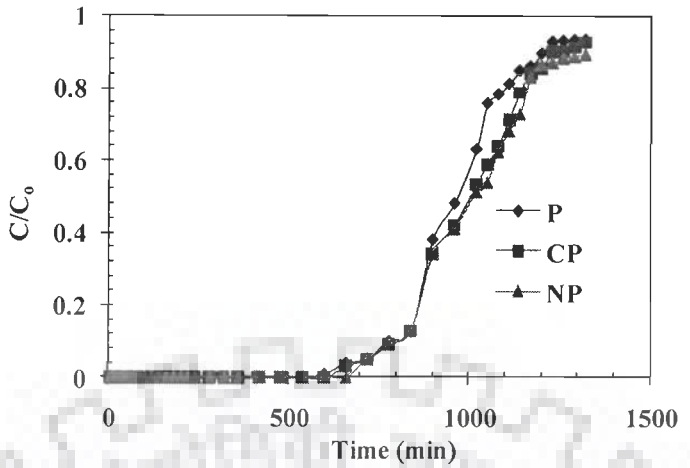

(A)

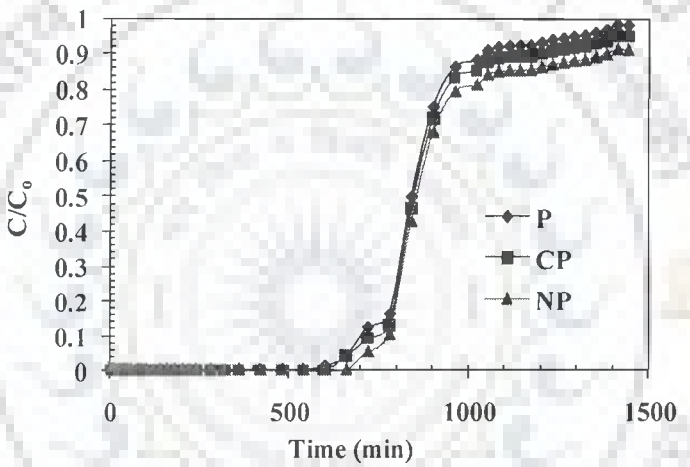

(B)

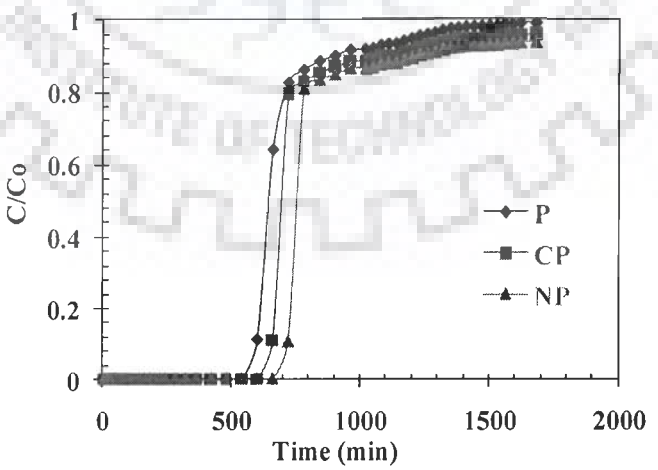

(C)

Figure 4.6.3. Breakthrough curves for simultaneous adsorption of P, CP and NP onto GAC for D=4 cm. (A) Expt. No. 7: Q=0.06 l/min, Z=30 cm; (B) Expt. No. 5: Q=0.04 l/min, Z=45 cm; (C) Expt. No. 3: Q=0.02 l/min, Z=60 cm.

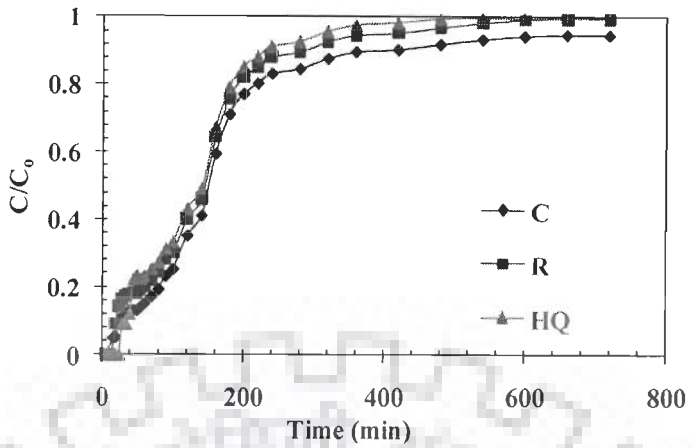

(A)

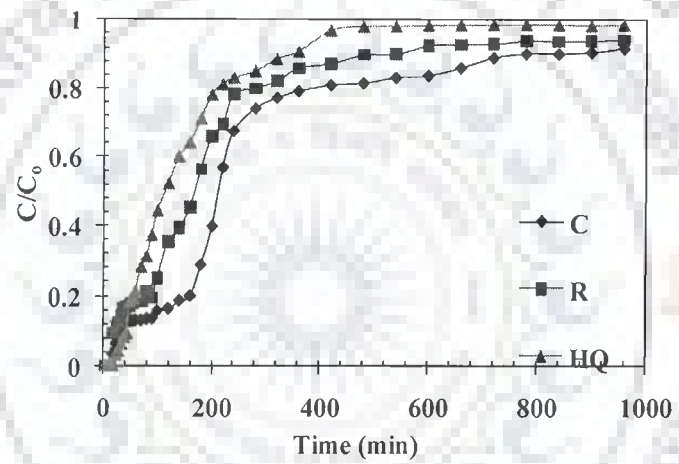

(B)

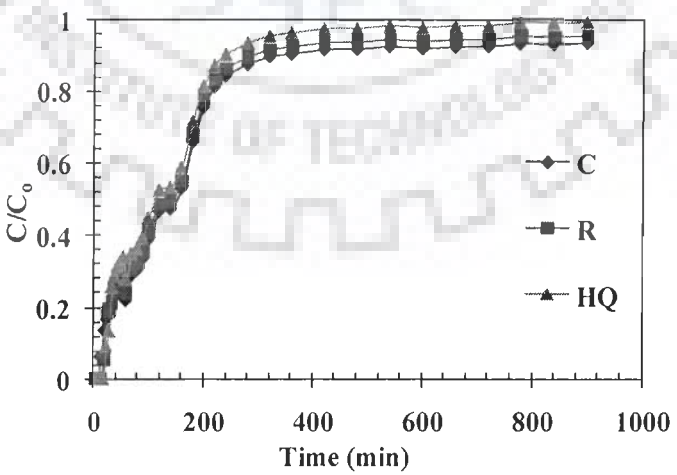

(C)

Figure 4.6.4. Breakthrough curves for simultaneous adsorption of C, R and HQ onto GAC for D=2 cm. (A) Expt. No. 1: Q=0.02 l/min, Z=30 cm; (B) Expt. No. 6: Q=0.04 l/min, Z=60 cm; (C) Expt. No. 8: Q=0.06 l/min, Z=45 cm.

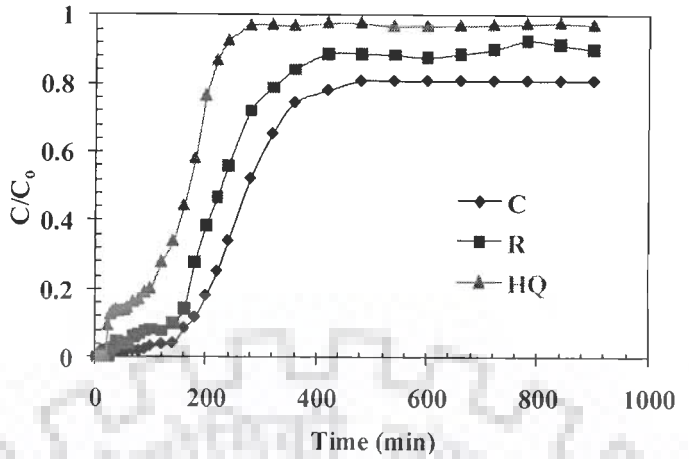

(A)

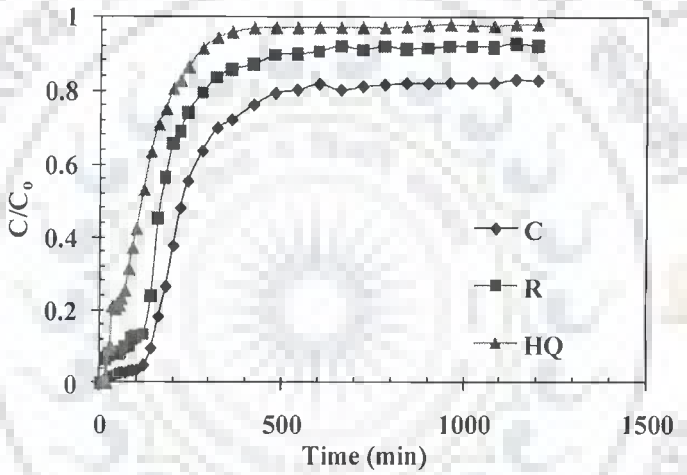

(B)

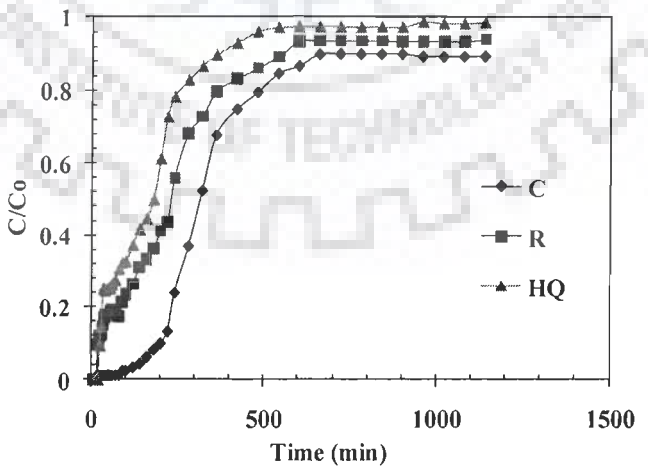

(C)

Figure 4.6.5. Breakthrough curves for simultaneous adsorption of C, R and HQ onto GAC for D=2.54 cm. (A) Expt. No. 2: Q=0.02 l/min, Z=45 cm; (B) Expt. No. 4: Q=0.04 l/min, Z=30 cm; (C) Expt. No. 9: Q=0.06 l/min, Z=60 cm.

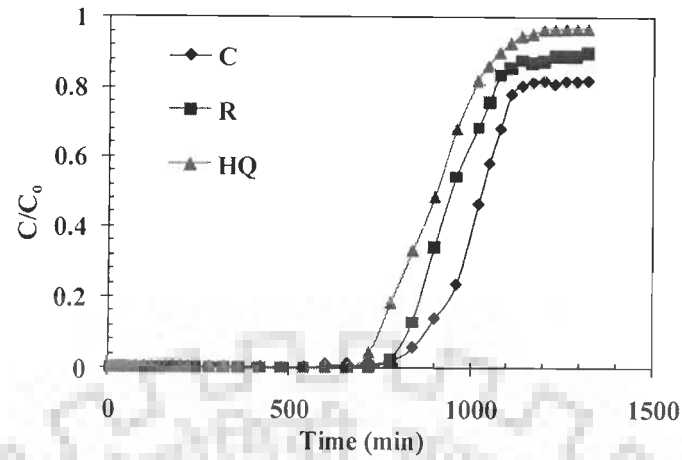

(A)

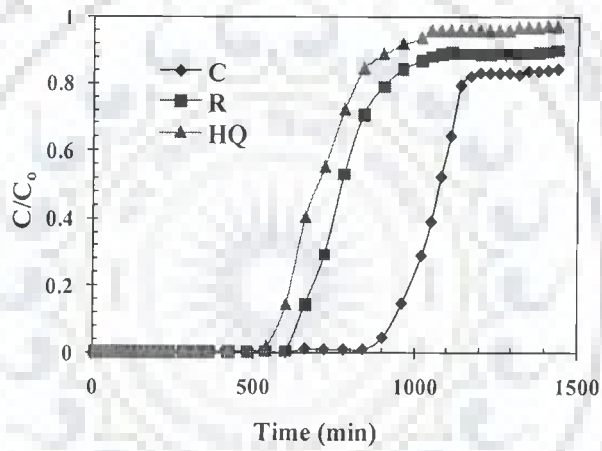

(B)

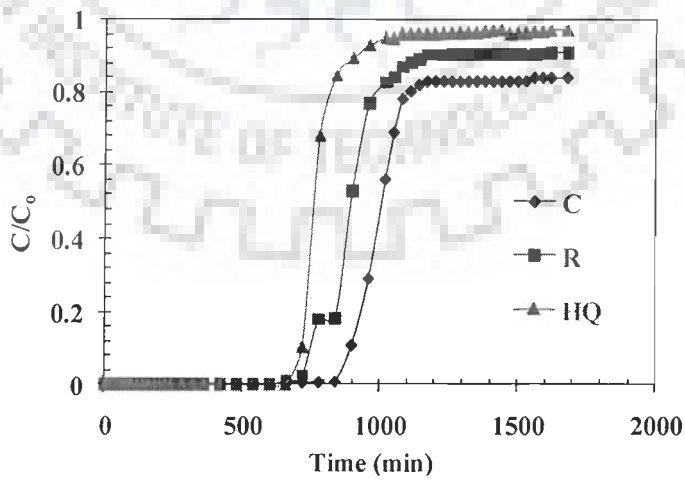

(C)

Figure 4.6.6. Breakthrough curves for simultaneous adsorption of C, R and HQ onto GAC for D=4 cm. (A) Expt. No. 7: Q=0.06 l/min, Z=30 cm; (B) Expt. No. 5: Q=0.04 l/min, Z=45 cm; (C) Expt. No. 3: Q=0.02 l/min, Z=60 cm.

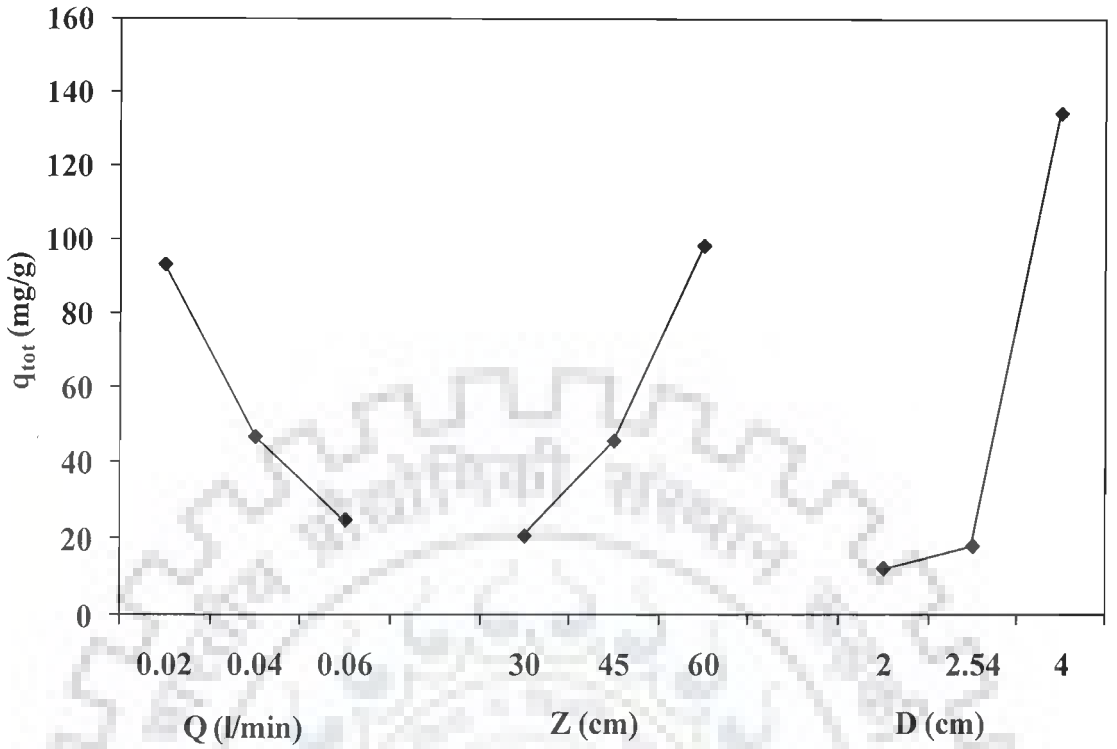

Figure 4.6.7. Effect of process parameters on q_{tot} for ternary adsorption of P, CP and NP in GAC packed-bed.

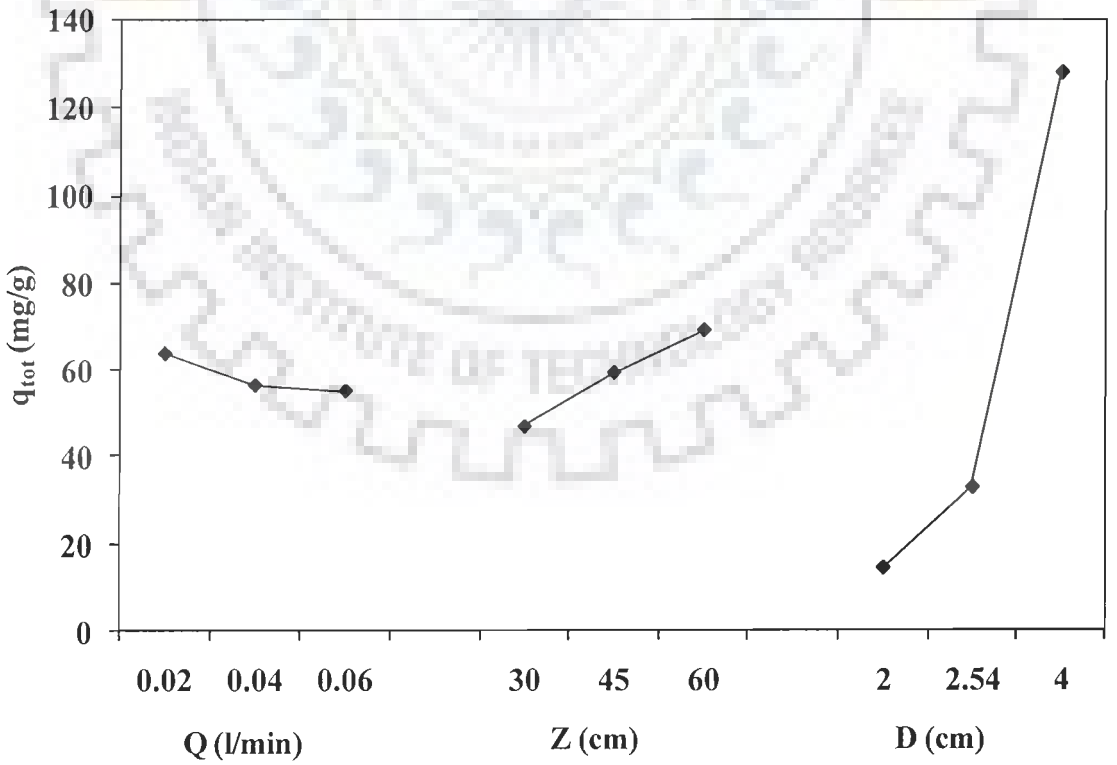

Figure 4.6.8. Effect of process parameters on q_{tot} for ternary adsorption of C, R and HQ in GAC packed-bed.

4.7 DESORPTION STUDY

4.7.1 Solvent desorption

Solvent desorption studies help in finding the mechanism of an adsorption process. If the adsorbates adsorbed onto the adsorbent can be desorbed by water, it can be said that the attachment of the adsorbate onto the adsorbent is by weak bonds. If the strong acid, such as HNO_3 and HCl, or strong bases, such as NaOH can substantially desorb the adsorbent, it can be said that the attachment of the adsorbate onto the adsorbent is by ion exchange. If organic acids, for example, such as CH_3COOH, can desorb the adsorbent, it can be said that the adsorption of the adsorbate onto the adsorbent is by chemisorption. Various solvents, viz. ethanol, HNO_3, HCl, NaOH, CH_3COOH, acetone and water were used in the present study for the elution of AN or P or CP or NP from the GAC [Mall et al., 2006; Suresh et al., 2010].

AN or P or CP or NP or C or R or HQ-loaded GAC was stirred with 50 ml of various eluents and the results are shown in Fig. 4.7.1. Among the various solvents, only NaOH was found to be better elutant for the desorption of P, CP, NP, C, R and HQ with a maximum desorption efficiency of 5.43%, 6.6%, 9.98%, 10.1%, 11.4% and 7.18%, respectively. HNO_3 was found to be better elutant for the desorption of AN with a maximum desorption efficiency of 9.63%. Other solvents didn't show any desorption efficiency. Negligible desorption efficiency by all solvents could be attributed to the chemical attachment between GAC and adsorbed AN, P, CP, NP, C, R and HQ which prevented the adsorbed adsorbates from being effectively desorbed by any solvent. This reinforces the earlier inference that the sorption of AN, P, 4CP, 4NP, C, R and HQ onto activated carbon is through strong chemical bond, i.e. by chemisorption.

4.7.2 Thermal desorption

Spent-GAC was thermal desorbed by process described in material and method section. Thermally desorbed GAC was again used for adsorption. This cycle of adsorption-desorption was repeated five times. Percent removal of AN, P, CP, NP, C, R and HQ in those cycles is shown in Fig.4.7.2. It is seen that the spent-GAC can be reused for a number of adsorption-desorption cycles. Percent removal of adsorbates, however, decreased after each adsorption-desorption cycle.

4.8 THERMAL OXIDATION OF SPENT-GAC

It is necessary to properly dispose the spent-GAC and/or utilize it for some beneficial purpose if possible. The dried spent-GAC can be used directly or by making fire-briquettes in the furnace combustors/incinerators to recover its energy value. AN-, P-, CP-, NP-, C-, R- and HQ-loaded adsorbents were studied for their thermal degradation characteristics by thermo gravimetric instrument. The differential thermal analysis (DTA), differential thermal gravimetery (DTG) and thermo gravimetric (TG) curves of the blank, and AN-, P-, CP-and NP-loaded GAC under oxidizing atmosphere at the heating rate of 10 K/min are shown in Fig. 4.8.1. The TG traces show the loss of moisture and the evolution of some light weight molecules including water upto 500 °C. The weight loss was 18% for blank-GAC, 10.2% for AN-GAC, 13.7% for P-GAC, 14% for CP-GAC and 22.9% for NP-GAC. Higher temperature drying (>100 °C) occurs due to loss of the surface tension bound water of the particles. Blank, AN, P, CP-and NP-GAC do not show any endothermic transition between room temperature and 400 °C, indicating the lack of any crystalline or other phase change during the heating process [Ng et al., 2002]. The rate of weight loss was found to increase between ~500 °C to ~601 °C (81% weight loss), ~501 °C to ~701 °C (67.2%),~499 °C to ~601 °C (79.3%),~500 °C to ~599 °C (78.5%) and ~500 °C to ~600 °C(49.4%) for blank, An, P, CP and NP-GAC, respectively. In these temperature ranges, the AN, P, 4CP and 4NP-loaded GAC oxidize and completely lose their weight. The strong exothermic peak centered between ~500-660 °C is due to the oxidative degradation of the samples. This broad peak as that observed from the first derivative loss curve (DTG) may be due to the combustion of carbon species. Fig. 4.8.2 shows similar DTA, DTG and TG graphs for C-, R- and HQ-loaded GAC. TGA and DTA curves could be used to deduce drying and thermal degradation characteristics.

Blank GAC has a heating value of about 8.26 MJ/kg. Thus, the GAC along-with the adsorbed AN, P, CP, NP, C, R and HQ can be dried and used as a fuel in the boilers/incinerators, or can be used for the production of fuel-briquettes. The bottom ash may be blended with clay to make fire bricks, or with cement-concrete mixture to make colored building blocks thus disposing of AN, P, CP, NP, C, R and HQ through chemical and physical fixation. Thus, spent GAC could not only be safely disposed but also its energy value can be recovered.

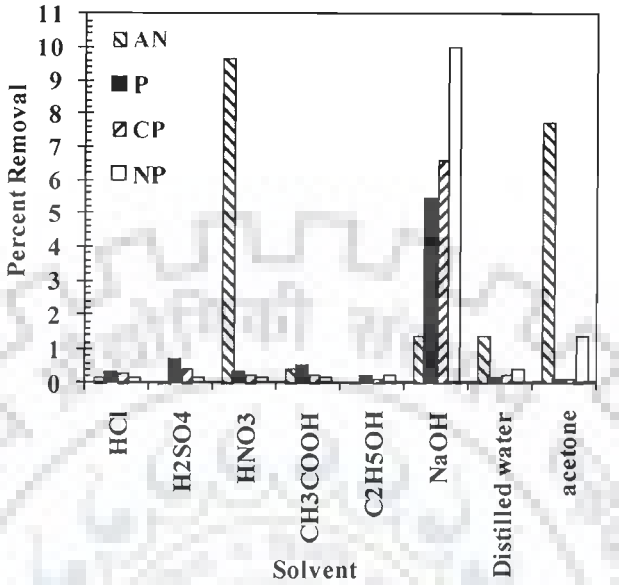

(a) AN, P, CP and NP

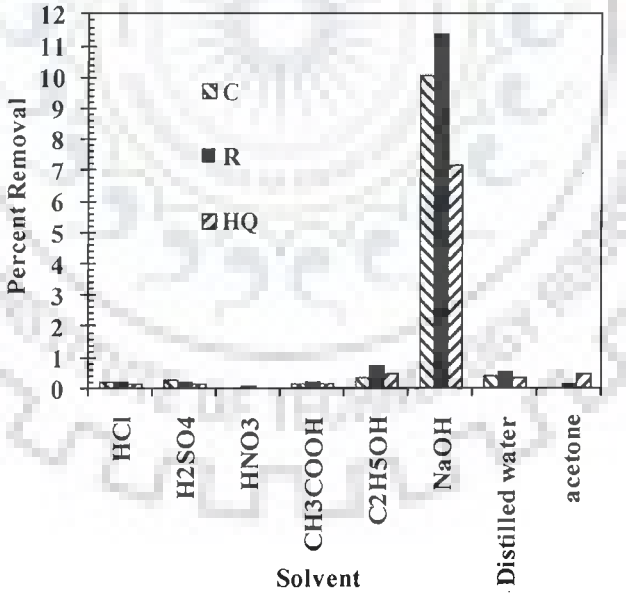

(b) C, R and HQ

Figure 4.7.1. Desorption efficiencies of AN, P, CP, NP, C, R and HQ by various desorbing agents. T=303 K t=24 h, C_0 (desorbing agents)=0.1 N, m=1 g/1.

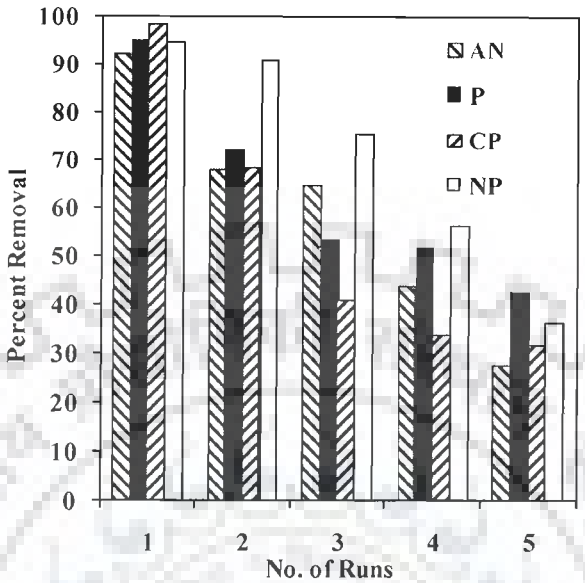

(a) AN, P, CP and NP

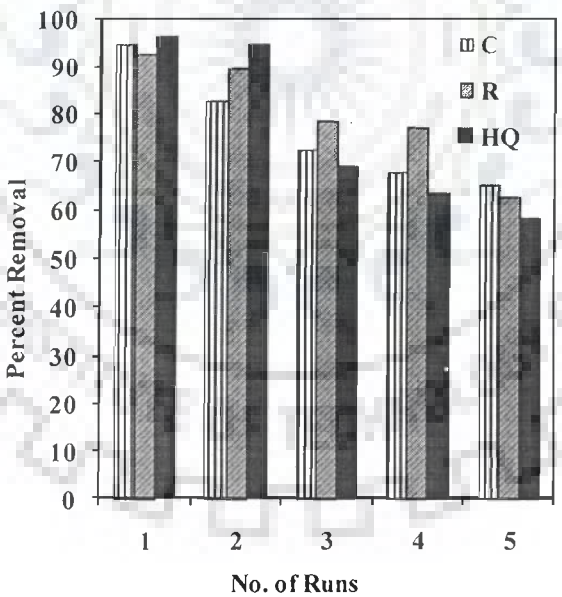

(b) C, R and HQ

Figure 4.7.2. Thermal desorption efficiencies of AN, P, CP, NP, C, R and HQ in a sequence of adsorption/desorption cycle.

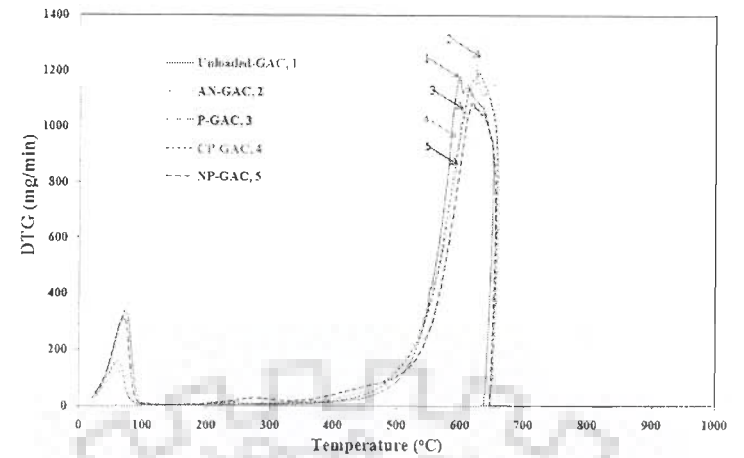

(a) DGA

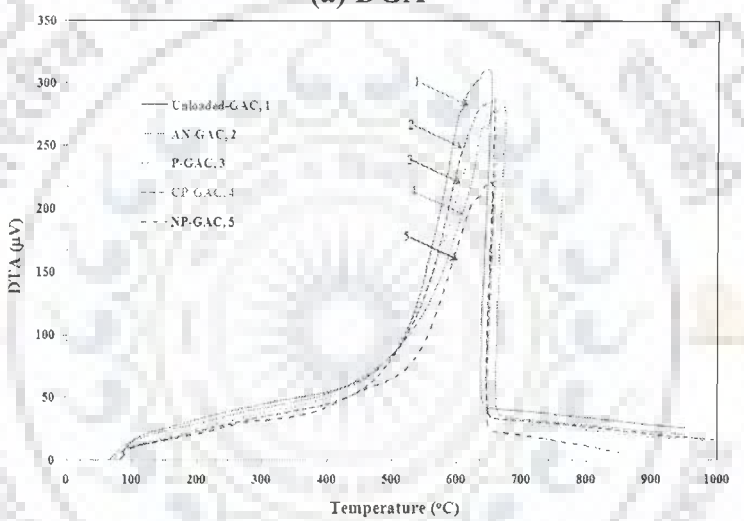

(b) DTA

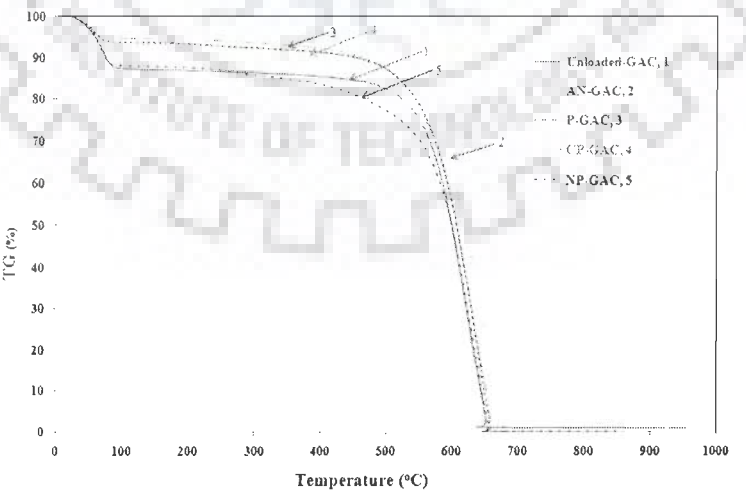

(c) TG

Figure 4.8.1. DTA, DTG and %TG graphs of blank and AN-, P-, CP- and NP-loaded GAC under oxidizing atmosphere.

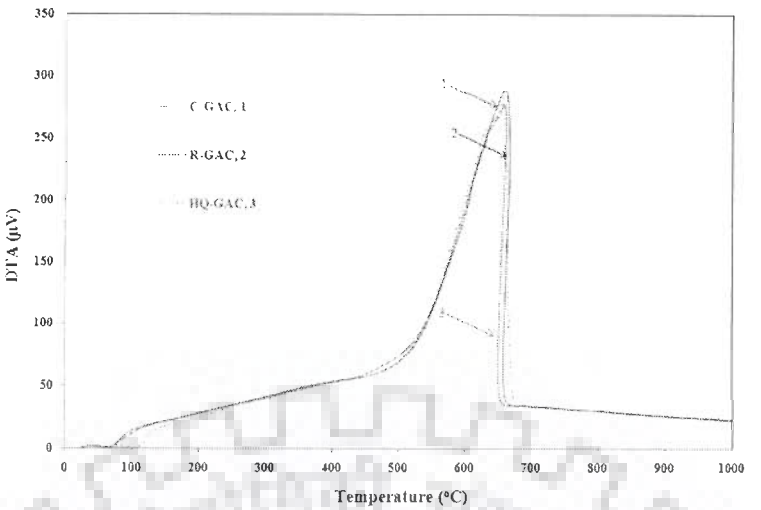

(a) DGA

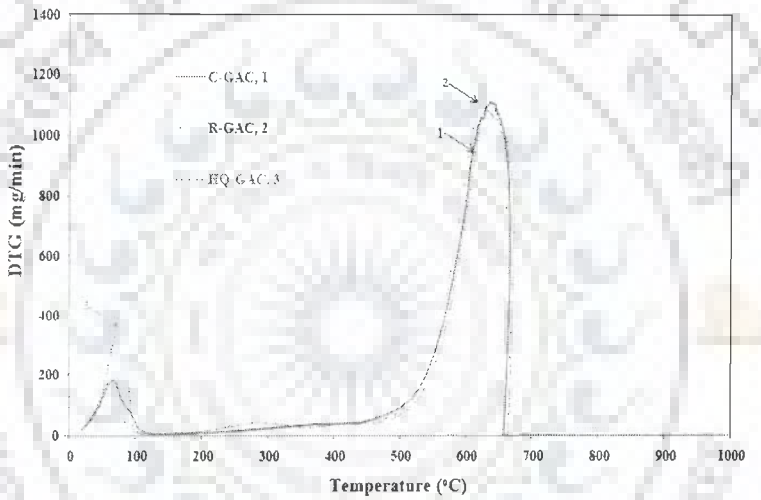

(b) DTA

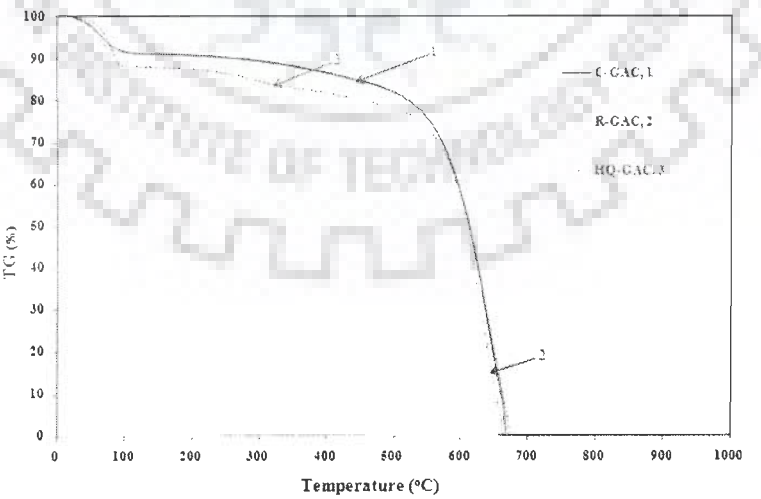

(c) TG

Figure 4.8.2. DTA, DTG and %TG graphs of C-, R- and HQ-loaded GAC under oxidizing atmosphere.

Chapter – V

CONCLUSIONS AND RECOMMENDATIONS

5.1 CONCLUSIONS

On the basis of various studies and the results and discussion presented heretofore, the following conclusions can be drawn:

1 Pore size distribution analysis indicated mesoporous nature of the GAC. EDX analysis showed that the distribution of elements in various adsorbate loaded GAC depended on the elemental distribution in original adsorbate.

2 Bohem titration and FTIR spectra indicated the presence of various types of functional groups e.g. free and hydrogen bonded OH group, the silanol groups (Si-OH), CO group stretching on the surface of GAC.

3 The point of zero charge (pH_{PZC}) of the GAC is 10.3. The natural solution pH is found to be the optimum for the individual removal of P and its derivatives and associated compounds from the aqueous solution by adsorption using GAC.

4 Optimum GAC dosage is found to be 10 g/l for C_0=500 mg/l of AN, P, CP, NP, C, R and HQ. Percent removal increases with the increase in GAC concentration, while removal per unit weight of GAC increases with the decrease in GAC concentration.

5 The sorption kinetics of P and its derivatives and associated compounds onto GAC could be represented by the pseudo-second-order kinetic model. The adsorption processes could be well described by a two-stage diffusion model.

6 A decrease in temperature induces a positive effect on the sorption process. Tempkin and Redlich-Peterson isotherms generally well-represent the equilibrium adsorption of AN, P, CP, NP, C, R and HQ onto GAC.

7 The heat of adsorption (ΔH^0) and change in entropy (ΔS^0) for adsorption on GAC were found to be in the range of 18-52 kJ/mol and 121-243 kJ/mol K. The

negative value of change in Gibbs free energy (ΔG^0) indicated the feasibility and spontaneity of adsorption by GAC. The isosteric heat of adsorption calculated from the equilibrium adsorption data using the Clausius-Clapeyron equation was quantitatively correlated with the fractional loading of compounds onto GAC.

8 All the factors and the interactions considered in the experimental design with q_{tot} as the desired response characteristic are statistically significant at 95% confidence limit.

9 The adsorption of AN, P, CP, NP, C, R and HQ from the binary and ternary solutions onto GAC is generally is found to be antagonistic in nature.

10 The competitive extended-Freundlich and SRS models fit the equilibrium data satisfactorily and adequately for binary and ternary adsorption of AN, P, CP, NP, C, R and HQ onto GAC.

11 Column study indicated that the breakthrough generally occurred faster with higher flow rate, and lower bed height and diameter. It was observed that the column diameter contributes most significantly for simultaneous adsorbate removal from ternary systems.

12 For the desorption experiments, several solvents (acids and alcohol, water) have been used. Among the various solvents, only NaOH was found to be better solvent for the desorption of P, CP, NP, C, R, HQ; while HNO_3 was found to be better solvent for the desorption of AN. Thermal desorption at 623 K was found to better as compared to solvent desorption. GAC worked well for at least five adsorption-desorption cycle, with continuous decrease in adsorption efficiency after each thermal desorption.

5.2 RECOMMENDATIONS

On the basis of the present studies, the following recommendations may be made for future studies:

1. GAC may be modified so as to increase its suitability as adsorbent for the removal of P and its derivatives and associated compounds from wastewater.
2. More batch experiments may be conducted for studying the relationship between adsorption behavior and various solvate-chromic parameters in multi-component systems.
3. Taguchi's design of experimental methodology should be applied more in column study so as to evaluate its application in effluent treatment experiments using adsorption process.

REFERENCES

Abburi, K. Adsorption of phenol and p-chlorophenol from their single and bisolute aqueous solutions on amberlite XAD-16 resin. *J. Hazard. Mater.* B105, 143, (2003).

Abdelwahaba, O.; Amin, N.K.; El-Ashtoukhy, E-S.Z. Electrochemical removal of phenol from oil refinery wastewater. *J. Hazard. Mater.* 163, 711–716, (2009).

Abram, F.S.H.; Sims, I.R. The toxicity of aniline to rainbow trout. *Water Res.* 16, 1309–1312, (1982).

Achaerandio, J.; Guell, C.; Lopez, F. Continuous vinegar decolorization with exchange resins. *J. Food Eng.* 51, 311–317, (2002).

Ahmaruzzaman, M.; Sharma, D.K. Adsorption of phenols from wastewater. *J. Colloid Interface Sci.* 287, 14–24, (2005).

Ahmaruzzaman, Md.; Gayatri, S. L. Adsorptive Removal of p-Nitrophenol (p-NP) On Charred Jute Stick. *Int. J. Chem. Reactor Eng.* A98, 1-8, (2010).

Ahn, M.Y.; Martinez, C.E.; Archibald, D.D.; Zimmerman, A.R.; Bollag, J-M.; Dec, J. Transformation of resorcinol in the presence of a laccase and birnessite. *Soil Biol. Biochem.* 38, 1015-1020, (2006).

Akaya, G.; Erhan, E.; Keskinler, B.; Algur, O.F. Removal of phenol from wastewater using membrane-immobilized enzymes Part II. Cross-flow filtration. *J. Membrane Sci.* 206, 61–68, (2002).

Akbal, F. Sorption of phenol and 4-chlorophenol onto pumice treated with cationic surfactant. *J. Environ. Manage.* 74 (3), 239-244, (2005).

Aksu, Z.; Kabasakal, E. Batch adsorption of 2, 4-dichlorophenoxy-acetic acid (2, 4-D) from aqueous solution by granular activated carbon. *Sep. Purif. Technol.* 35 (3), 223-240, (2004).

Akyurtlua, J.F.; Akyurtlua, A.; Kovenklioglu, S. Catalytic oxidation of phenol in aqueous solutions. *Catal. Today.* 40, 343-352, (1998).

Almeida, T.O.; Talens-Alesson, F.I. Removal of phenylamine and catechol by adsorptive micellar flocculation. *Colloids and Surfaces A: Physicochem. Eng. Aspects.* 279, 28–33, (2006).

Alzaydien, A.S.; Manasreh, W. Equilibrium, kinetic and thermodynamic studies on the adsorption of phenol onto activated phosphate rock. *Int. J. Physical Sci.* 4 (4), 172-181, (2009).

An, F.; Feng, X.; Gao, B. Adsorption of aniline from aqueous solution using novel adsorbent PAM/SiO_2. *Chem. Eng. J.* 151, 183–187, (2009).

Ania, C.O.; Cabal, B.; Pevida, C.; Arenillas, A.; Parra, J.B.; Rubiera, F.; Pis, J.J. Removal of naphthalene from aqueous solution on chemically modified activated carbons. *Water Res.* 41 (2), 333–340, (2007).

Arana, J.; Lopez, V.M.R.; Rodriguez, J.M.D.; Melian, J.A.H.; Pena, J.P. Grupo de Fotocata´lisis y Electroqui´mica Aplicada al Medio-Ambiente (FEAM). The effect of aliphatic carboxylic acids on the photocatalytic degradation of p-nitrophenol. *Catal. Today.* 129, 185–193, (2007).

Arana, J.; Rodriguez, C.F.; Diaz, O.G.; Melian, J.A.H.; Pena, J.P. Role of Cu in the Cu–TiO_2 photocatalytic degradation of dihydroxybenzenes. *Catal. Today.* 101, 261-266, (2005).

Aravindhan, R.; Rao, J.R.; Nair, B.U. Removal of basic yellow dye from aqueous solution by sorption on green alga *Caulerpa scalpelliformis*. *J. Hazard. Mater.* 142, 68–76, (2007).

Aribike, D.S.; Olafadehan, O.A. Modeling of fixed bed adsorption of phenols on granular activated carbon. *Theor. Foundations Chem. Eng.* 42, 257-263, (2008).

ATSDR, Agency for Toxic Substances and Disease Registry (ATSDR). Toxicological Profile for phenol. Atlanta, GA: Department of Health and Human Service; Public health service; Centers for Disease Control, (1998).

Ayranci, E.; Duman, O. Adsorption behaviors of some phenolic compounds onto high specific area activated carbon cloth. *J. Hazard. Mater.* B124, 125, (2005).

Babel, S.; Kurniawan, T.A.; Babel. Low-cost adsorbents for heavy metals uptake from contaminated water: a reiview. *J. Hazard. Mater.* B97, 219-243, (2003).

Balistrieri, L.S.; Murray, J.W. The surface chemistry of goethite (α-FeOOH) in major ion seawater. *J. Am. Sci.* 281(6), 788-806, (1981).

Banat, F.A.; Al-Bashir, B.; Al-Asheh, S.; Hayajneh, O. Adsorption of phenol by bentonite. *Environ. Pollut.* 107, 391-398, (2000).

Barbier, J.J.; Oliviero, L.; Renard, B.; Duprez, D. Catalytic wet air oxidation of ammonia over M/CeO_2 catalysts in the treatment of nitrogen-containing pollutants. *Catal. Today.* 75, 29, (2002).

Bardakci, B. FTIR-ATR Spectroscopic Characterization of Monochlorophenols and Effects of Symmetry on Vibrational Frequencies. *J. Arts Sci.* 7, 13-19, (2007).

Barker, T. B.; Engineering Quality by Design. Marcel Dekker, New York, (1990).

Barrado, E.; Vega, M.; Pardo, R.; Grande, P.; del Valle, J.L. optimisation of purification method for metal-containing wastewater. *Water Res.* 30, 2309-2314, (1996).

Barret, E.P.; Joyner, L.G.; Hanlenda, P.P. The determination of pore volume and area distributions in porous substances: 1. Computations from nitrogen isotherms. *J. Am. Chem. Soc.* 73, 373-380, (1951).

Bayram, E.; Hoda, N.; Ayranci, E. Adsorption/electrosorption of catechol and resorcinol onto high area activated carbon cloth. *J. Hazard. Mater.* 168, 1459-1466, (2009).

Beezer, A.E.; Hunter, W.H.; Storey, D.E. Quantitative structure relationships: the Van't Hoff heat of transfer of resorcinol monoethers from water to n-octanol. *J. Pharm. Pharmacol.* 32, 815-819, (1980).

Beg, Q.K.; Sahai, V.; Gupta, R. Statistical media optimization and alkaline protease production from *Bacillus mojavensis* in a bioreactor. *Process. Biochem.* 39(2), 203-209 (2003).

Beker, U.; Ganbold. B.; H. Dertlic.; Gülbayir, D.D. *Energy Conversion Manage.* 51, 235-240, (2010).

Belhachemi, M.; Belala, Z.; Lahcene, D.; Addoun, F. Adsorption of phenol and dye from aqueous solution using chemically modified date pits activated carbons. *Desalination Water Treatment,* 7, 182–190, (2009).

Bellot, J.C.; Condoret, J.S. Modelling of liquid chromatography equilibria. *Process Biochem.* 28, 365-376, (1993).

Bhandari, A.; Cho, I. Peroxidase mediated binding of phenols to soils, proceedings of the 14th annual conference on hazardous waste Research. 27-40, (1999).

Bilgili, M.S. Adsorption of 4-chlorophenol from aqueous solutions by xad- 4 resin: isotherm, kinetic, and thermodynamic analysis. *J. Hazard. Mater.* 137, 157–164, (2006).

Blanco, S.E.; Almandoz, M.C.; Ferretti, F.H. Determination of the overlapping pKa values of R using UV-visible spectroscopy and DFT methods. *Spectrochim. Acta A.* 61, 93-102, (2005).

Blanco-Martinez, D.A.; Giraldo, L.; Moreno-Pirajan, J.C. Effect of the pH in the adsorption and in the immersion enthalpy of monohydroxylated phenols from aqueous solutions on activated carbons. *J. Hazard. Mater.169*, 291-296, (2009).

Boyd, G.E.; Adamson, A.W.; Meyers, L.S. The exchange adsorption of ions from aqueous solution by organic zeolites. II Kinetics. *J. Am. Chem. Soc.* 69, 2836-2848, (1947).

Brillas, E.; Casado, J. Aniline degradation by Electro-Fenton and peroxi-coagulation processes using a flow reactor for wastewater treatment. *Chemosphere.* 47(3), 241-248, (2002).

Bruce, A.; Schink, B. Phloroglucinol pathway in the strictly anaerobic Pelobacter acidigallici: fermentation of trihydroxy-benzene to acetate via triacetic acid. *Arch. Microbiol.* 157, 417-424, (1992).

Brunauer, S.; Emmet, P.H.; Teller, F. Adsorption of Gases in Multimolecular Layers. *J. Am. Chem. Soc.* 60, 309-319, (1938).

Burdock,T. Safety Assessment of Castoreum Extract as a Food Ingredient. *Int. J. Toxicol.* 26, 51-55, (2007).

Busca, G.; Berardinelli, S.; Resini, C.; Arrighi, L. Technologies for the removal of phenol from fluid streams: A short review of recent developments. *J. Hazard. Mater.* 160, 265–288, (2008).

Byrne, D.M.; Taguchi, S. The taguchi approach to parameter design. Quality Progress, December, 19-26, (1987).

Capasso, R.; Evidente, A.; Schivo, L.; Orru, G.; Marcialis, M. A.; Cristinzio, G. Antibacterial polyphenols from olive oil mill waste waters. *J. Appl. Bacteriol.* 79, 393-398, (1995).

Carmona, M.; Lucas, A.D.; Valverde, J.L.; Velasco, B.; Rodríguez, J.F. Combined adsorption and ion exchange equilibrium of phenol on Amberlite IRA-420. *Chem. Eng. J.* 117, 155-160, (2006).

Casero I.; D. Sicilia.; S. Rubio.; Pérez-Bendito, D. Chemical degradation of aromatic amines by Fenton's reagent. *Water Res.* 31, 985-1995, (1997).

Castroa, I.U.; Stubera, F.; Fabregat, A.; Font, J.; Fortuny, A.; Bengoa, C. Supported Cu(II) polymer catalysts for aqueous phenol oxidation. *J. Hazard. Mater.* 163, 809–815, (2009).

Chakraborty, S.; Basu, J. K.; De, S.; Das Gupta, S. Adsorption of reactive dyes from a textile effluent using sawdust as the adsorbent. *Ind. Eng. Chem. Res.* 45, 4732 - 4741 (2006).

Chaliha, S.; Bhattacharyya, K.G.; Paul, P. Oxidation of 4-nitrophenol in water over Fe(III), Co(II), and Ni(II) impregnated MCM41 catalysts. *J. Chem. Technol. Biotechnol.* 83, 1353–1363, (2008).

Chang, Y-C.; Chen, D-H. Catalytic reduction of 4-nitrophenol by magnetically recoverable Au nanocatalyst. *J. Hazard. Mater.* 165, 664-669, (2009).

Chaturvedi, A.K.; Pathak, K.C.; Singh, V.N. Fluoride removal from water by adsorption on china clay. *Appl. Clay Sci.* 3, 337-346, (1988).

Chen, B-Y. Toxicity assessment of aromatic amines to Pseudomonas Luteola: chemostat pulse technique and dose–response analysis. *Process Biochem.* 41(7), 1529–1538, (2006).

Chen, S.; Xu, Z.P.; Zhang, Q.; Lu, G.Q.M.; Haod, Z.P.; Liu, S. Studies on adsorption of phenol and 4-nitrophenol on MgAl-mixed oxide derived from MgAl-layered double hydroxide. *Sep. Purif. Technol.* 67, 194-200, (2009).

Chen, W.; Duan, L.; Zhu, D.Q. Adsorption of polar and nonpolar organic chemicals to carbon nanotubes. *Environ. Sci. Technol.* 41, 8295-8300, (2007).

Chern, J.M.; Chien, Y.W. Competitive adsorption of benzoic acid and p-nitrophenol onto activated carbon: isotherm and breakthrough curves. *Water Res.* 37, 2347-2356, (2003).

Chiang, H.L.; Huang, C.P.; Chiang, P.C. The adsorption of benzene and methylethylketone onto activated carbon: thermodynamic aspects. *Chemosphere.* 46, (1),143–152, (2002).

Chien, S.W.C.; Chen, H.L.; Wang, M.C.; Seshaiah, K. Oxidative degradation and associated mineralization of hydroquinone and resorcinol catalyzed by birnessite. *Chemosphere.* 74, 1125–1133, (2009).

Chiou, C-H.; Juang, R-S. Photocatalytic degradation of phenol in aqueous solutions by Pr-doped TiO_2 nanoparticles. *J. Hazard. Mater.*149, 1–7, (2007).

Chong K.H.; Volesky. Metal biosorption equilibria in a ternary system. *Biotechnol. Bioeng.* 49, 629-638, (1996).

Cobb, B.D.; Clarkson, J.M. A simple procedure for optimizing the polymerase chain reaction (PCR) using modified Taguchi methods. *Nucleic Acids Res.* 22, 3801–3805, (1994).

Cockroft, S. L.; Perkins, J.; Zonta, C.; Adams, H.; Spey, S. E.; Low, C.M.R.; Vinter, J. G.; Lawson, K.R.; Urch, C.J.; Hunter, C. A. Substituent effects on aromatic stacking interactions. *Org. Biomol. Chem.* 5, 1062–1080, (2007).

Conway, B.E. The solvation factor in specificity of ion adsorption at electrodes. *Electrochim. Acta.* 40, 1501–1512, (1995).

Costa, E.; Calleja, G.; Marijuan, L. Comparative adsorption of phenol, p-nitrophenol and p-hydroxybenzoic acid on activated carbon. *Adsorpt. Sci. Technol.* 5, 213–228, (1988).

Cotoruelo, L.M.; Marques, M.D.; Rodriguez-Mirasol, J.; Cordero, T.; Rodriguez, J.J.; Adsorption of aromatic compounds on activated carbons from lignin: kinetic study. *Ind. Eng. Chem. Res.* 46, 2853-2860, (2007).

Coughlin, R.W.; Ezra, F.S. Role of surface acidity in the adsorption of organic pollutants on the surface of carbon. *Environ. Sci. Technol.* 2, 291, (1968).

CPCB, Central Pollution Control Board (CPCB), Delhi, Pollution Control Acts, Rules and Notifications Issued Thereunder, Pollution Control Law Series: PCLS/02/2006, Ministry of Environment and Forests, Govt. of India, New Delhi, (2006).

Crank, J. The mathematics of diffusion, Oxford Clarendon Press, London, pp. 84, (1965).

Cypres, R.; Bettens, B. Mecanismes de fragmentation pyrolytique du phenol et des cresols. *Tetrahedron.* 30, 1253- 1260, (1974).

Daifullah, A.A.; Girgis, B.S. Removal of some substituted phenols by activated carbon obtained from agricultural waste. *Water Res.* 32, 1169–1177, (1998).

Das, C.P.; Patnaik, L.N. Removal of phenol by industrial solid waste. *Pract. Period. Hazard. Toxic, Radioactive Waste Manage.* 9, 135-140, (2005).

De Carvalho, R.P.; Chong, K.H.; Volesky, B. Evaluation of the Cd, Cu and Zn biosorption in two-metal systems using algal biosorbent. *Biotechnol. Prog.* 11, 39-44, (1995).

Dellinger, B.; Pryor, W.A.; Cueto, R.; Squadrito, G.L.; Hegde, V.; Deutsch, W.A. Role of free radicals in the toxicity of airborne fine particulate matter. *Chem. Res. Toxicol.* 14, 1371–1377, (2001).

Derbyshire, F.; Jagtoyen, M.; Andrews, R.; Rao, A.; Martin-Gullon, I.; Grulke, E. Carbon materials in environmental applications. In: Radovic LR, editor. Chemistry and physics of carbon, vol. 27. New York: Marcel Dekker; pp.1–66, (2001).

Deselms, R. H. *UV-Active Phenol Ester Compounds*; Enigen Science Publishing: Washington, DC, (2008).

Devulapalli, R.; Jones, F. Separation of aniline from aqueous solutions using emulsion liquid membranes. *J. Hazard. Mater.* B70, 157–170, (1999).

Diez, M.C.; Mora, M.L.; Videla, S. Adsorption of phenolic compounds and color from bleached kraft mill effluent using allophonic compounds. *Water. Res.* 33, 125-130, (1999).

Din, A.T.M.; Hameeda, B.H.; Ahmada, A.L. Batch adsorption of phenol onto physiochemical-activated coconut shell. *J. Hazard. Mater.* 161, 1522-1529, (2009).

Drioli, E.; Giorno, L. Biocatalytic Membrane Reactors, T.J. International Ltd., Padstow, UK, (1999).

EHC 157, International Programme on Chemical Safety (IPCS), *Environmental Health Criteria 157*, Hydroquinone, (1994).

Emtiazi, G; Satarii, M.; Mazaherion, F. The utilization of aniline, chlorinated aniline, and aniline blue as the only source of nitrogen by fungi in water. *Water Res.* 35(5), 1219-1224, (2001).

Engin, A.B.; Ozdemir, O.; Turan, M.; Turan, A.Z. Color removal from textile dyebath effluents in a zeolite fixed bed reactor: determination of optimum process conditions using Taguchi method. *J.Hazard. Mater.* 159, 348–353, (2008).

Faria, P.C.C.; Orfao, J.J.M.; Figueiredo, J.L.; Pereira, M.F.R. Adsorption of aromatic compounds from the biodegradation of azo dyes on activated carbon. *Appl. Surf. Sci.* 254, 3497–3503, (2008).

Faust, S.D.; Aly, O.M. Adsorption processes for water Treatment Butterwort Publishers, Boston. pp. 108-113, (1987).

Feng, Q.; Zhaoa, L.; Lin, J.M. Molecularly imprinted polymer as micro-solid phase extraction combined with high performance liquid chromatography to determine phenolic compounds in environmental water samples. *Anal. Chim. Acta.* 650, 70–76 (2009).

Fiore, S.; Zanetti, M.C. Sorption of Phenols: Influence of Groundwater pH and of Soil Organic Carbon Content. *Am. J. Environ. Sci.* 5 (4), 546-554, (2009).

Franz, M.; Arafat, H.A.; Pinto, N.G. Effect of chemical surface heterogeneity on the adsorption mechanism of dissolved aromatics on activated carbon. *Carbon.* 38, 1807-1819, (2000).

Freundlich, H. M. F. Over the adsorption in solution. *J. Phys. Chem.* 57, 385-471, (1906).

Frisch M.J.; Trucks, G.W.; Head-Gordon, M.; Gill, P.M.W.; Wong, M.W.; Foresman, J.B.; Johnson, B.G.; Schlegel, H.B.; Robb, M.A.; Replogle, E.S.; Gomperts, R.; Andres, J.L.; Raghavachari, K.; Binkley, J.S.; Gonzalez, C.; Martin, R.L.; Fox, D.J.; Defrees, D.J.; Baker, J.; Stewart, J.J.P.; Pople, J.A. Gaussian 92 User's Guide, Gaussian Inc., Pittsburgh, PA, (2003).

Fritz, W.; Schluender, E.U. Simultaneous adsorption equilibria of organic solutes in dilute aqueous solutions on activated carbon. *Chem. Eng. Sci.* 29, 1279-1282, (1974).

Furuya, E.G.; Chang, H.T.; Miura, Y.; Noll, K.E. A fundamental analysis of the isotherm for the adsorption of Phenolic compounds on activated carbon. *Sep. Purif. Technol.* 11, 69–78, (1997).

Galindez-Mayer, J.; Ramon-Gallegos, J.; Ruiz-Ordaz, N.; Juarez-Ramirez ,C.; Salmeron-Alcocer, A.; Poggi-Varaldo, H.M. Phenol and 4-chlorophenol biodegradation by yeast *Canidda tropicalis* in a fluidized bed reactor, *Biochem. Eng. J.* 38, 147–157, (2008).

Galinos, A.G.; Zafiropoulos, T. F. Aniline and Quinoline Compounds of Mixed Complex Haloacids of Indium(III) With Thiocyanate. *Monatshefte ftir Chemie.* 109, 1475-1479, (1978).

Garcia-Araya, J.; Beltrn de Heredia, J.; Alvarez, P.; Masa, F.J. Activated carbon adsorption of some phenolic compounds present in agroindustrial wastewater. *Adsorption.* 9, 107–115, (2003).

Garcia-Mendieta, A.; Solache-Rios, M.; Olguin, M.T. Comparison of Phenol and 4-Chlorophenol Adsorption in Activated Carbon with Different Physical Properties. Sep. Sci. Technol. 38, 2549-2564, (2003).

Garg, A.; Mishra, I. M.; Chand, S. Oxidative phenol degradation using non-noble metal based catalysts. *Clean.* 38, 27, (2010).

Gheewala, S.H.; Pole, R.K.; Annachhatre, A.P. Nitrification modelling in biofilms under inhibitory conditions. *Water Res.* 38, 3179–3188, (2004).

Gomes, H.T.; Selvam, P.; Dapurkar, S.E.; Figueiredo, J.L.; Faria, J.L. Transition metal (Cu, Cr, and V) modified MCM-41 for the catalytic wet air oxidation of aniline. *Micropor. Mesopor. Mater.* 86, 287–294, (2005).

Graham, N.; Chen, X.G.; Jayaseelan, S. The potential application of activated carbon from sewage sludge to organic dyes removal. *Water Sci. Technol.* 43 (2), 245–252, (2004).

Haggi, E.; Bertolotti, S.; Garcia, N.A. Modelling the environmental degradation of water contaminants. Kinetics and mechanism of the riboflavin-sensitised-photooxidation of phenolic compounds. Chemosphere. 55, 1501–1507, (2004).

Hamdaouia, O.; Naffrechoux, E. Modeling of adsorption isotherms of phenol and chlorophenols onto granular activated carbon Part II. Models with more than two parameters. *J. Hazard. Mater.* 147 (1-2), 381-394, (2007).

Hameed, B.H.; China, L.H.; Rengaraj, S. Adsorption of 4-chlorophenol onto activated carbon prepared from rattan sawdust. *Desalination.* 225, 185–198, (2008).

Hammett, L.P. The effect of structure upon the reactions of organic compounds. Benzene derivatives. *J. Am. Chem. Soc.* 59, 96, (1937).

Han, S.; Castelo, F.F.; Livingston, A. Membrane aromatic recovery system (MARS) — a new membrane process for the recovery of phenols from wastewaters. *J. Membrane Sci.* 188, 219-233, (2001).

Han, S.K.; Ichikawa, K.; Utsumi, H. Quantitative analysis for the enhancement of hydroxyl radical generation by phenols during ozonation of water. *Water Res.* 32, (1998).

Hanada, Y.; Imaizumi, I.; Kido, K.; Tanizaki, T.; Koga, M.; Shiraishi, H.; Soma, M. Application of a pentafluorobenzyl bromide derivatization method in gas chromatography/mass spectrometry of trace levels of halogenated phenols in air, water and sediment samples. *Anal. Sci.* 18, 655, (2002).

Hannafi, N.E.; Boumakhla, M.A.; Berrama, T.; Bendjama, Z. Elimination of phenol by adsorption on activated carbon prepared from the peach cores: modelling and optimisation. *Desalination.* 223, 264–268, (2008).

Hansch, C.; Leo, A.; Taft, R.W. A survey of Hammett substituent constants and resonance and field parameters. *Chem. Rev.* 91, 165, (1991).

Hays, M.D.; Fine, P.M.; Geron, C.D.; Kleeman, M.J.; Gullett, B.K. Open burning of agricultural biomass: physical and chemical properties of particle-phase emissions. *Atmos. Environ.* 39, 6747–6764, (2005).

Ho, Y.S.; McKay, G. Pseudo-second order model for sorption processes. *Process Biochem.* 34, 451-465, (1999).

Hou, Y.; Guo, L-P.; Wang, G. Synthesis and electrochemical performance of ordered mesoporous carbons with different pore characteristics for electrocatalytic oxidation of hydroquinone. *J. Electroanalyt. Chem.* 617, 211-217, (2008).

Hoyer, H.; Peperle, W. Dampfdrunkmessungen an organischen substanzen und ihre sublimationswarmen, *Z. Electrochem.* 62, 61-66, (1958).

Huang, J.; Huang, K.; Yan, C. Application of an easily water-compatible hypercrosslinked polymeric adsorbent for efficient removal of catechol and resorcinol in aqueous solution. *J. Hazard. Mater.* 167, 69-74, (2009).

Hunter, D.M.; Timerding, B.L.; Leonard, R.B.; McCalmont, T.H.; Schwartz, E. Effects of isopropyl alcohol, ethanol, and polyethylene glycol/industrial methylated spirits in the treatment of acute phenol burns. *Annals of Emergency Medicine.* 21, 1303–1307, (1990).

Ibrahim, M.; Koglin, E. Spectroscopic study of polyaniline emeraldine base: modelling approach. *Acta Chim. Slov.* 52, 159-163, (2005).

IPCS, International Programme on Chemical Safety (IPCS), Prepared in the context of cooperation between the International Programme on Chemical Safety and the European Commission, (2005).

Ivancev-Tumbasa, I.; Hobby, R.; Kuchle, B.; Panglisch, S.; Gimbel, R. p-Nitrophenol removal by combination of powdered activated carbon adsorption and ultrafiltration – comparison of different operational modes. *Water Res.* 42, 4117– 4124, (2008).

Jadhav, S.R.; Verma, N.; Sharma, A.; Bhattacharya, P.K. Flux and retention analysis during micellar enhanced ultrafiltration for the removal of phenol and aniline. *Sep. Purif. Technol.* 24, 541–557, (2001).

Jiang, Y.; Petrier, C.; Waite, T.D. Sonolysis of 4-chlorophenol in aqueous solution: Effects of substrate concentration, aqueous temperature and ultrasonic frequency. *Ultrason. sonochem.* 13, 415–422, (2006).

Jianguo, C.; Aimin, L.; Hongyan, S.; Zhenghao, F.; Chao, L.; Quanxing, Z. Equilibrium and kinetic studies on the adsorption of aniline compounds from aqueous phase onto bifunctional polymeric adsorbent with sulfonic groups. *Chemosphere*. 61, 502–509, (2005).

Joseph, R.; Vangani, V.; Devi, S.G.; Rakshit, A.K. Studies of adsorption of polyacrylonitrile and polyacrylates at solid-liquid interface. *Colloid. Polym. Sci.* 272, 130-140, (1994).

Juang, R-S.; Huang W-C.; Hsu, Y-H. Treatment of phenol in synthetic saline wastewater by solvent extraction and two-phase membrane biodegradation. *J. Hazard. Mater.* 164, 46–52, (2009).

Jung, M-W.; Ahn, K-H.; Lee, Y.; Kim, K-P.; Rhee, J-S.; Park, J.T.; Paeng, K-J. Adsorption characteristics of phenol and chlorophenols on granular activated carbons (GAC). *Microchem. J.* 70, 123-131, (2001).

Kalderis, D.; Koutoulakis, D.; Paraskeva, P.; Diamadopoulos, E.; Otal, E.; del Valle, J.O. Fernandez-Pereira, C. Adsorption of polluting substances on activated carbons prepared from rice husk and sugarcane bagasse. *Chem. Eng. J.* 144, 42–50, (2008).

Kamble, S. P.; Mangrulkar, P. A.; Bansiwal, A. K.; Rayalu, S. S. *Chem. Eng. J. 138* (1-3), 73–83, (2008).

Kamenev, I.; Munter, R.; Pikkov, L.; Kekisheva, L. Wastewater treatment in oil shale chemical industry. *Oil Shale*. 20, 443-457, (2003).

Kaminari, N.M.S.; Schultz, D.R.; Ponte, M.J.J.S.; Ponte, H.A.; Marino, C.E.B.; Neto, A.C. Heavy metals recovery from industrial wastewater using Taguchi method. *Chem. Eng. J.* 126 139–146, (2007).

Kamlet, M.J.; Doherty, R.M.; Abraham, M.H.; Marcus, Y.; Taft, R.W. Linear Solvation Energy Relationships. An Improved Equation for Correlation and Prediction of Octano-Water Partition Coefficients of Organic Nonelectrolytes (Including Strong Hydrogen Bond Donor Solutes). *J. Phys. Chem.* 92, 5244-5255, (1988).

Kang, N.; Lee, D.S.; Yoon, J. Kinetic modeling of Fenton oxidation of phenol and monochlorophenols, Chemosphere. 47, 915–924, (2002).

Kaul, S.N.; Nandy, T.; Deshpande, C.V.; Srivastava, A.; Shastry, S.; Szpyrkowicz, L. *Water Sci. Technol.* 38, 363, (1998).

Kaushik, G.; Thakur, I.S. Isolation and characterization of distillery spent wash color reducing bacteria and process optimization by Taguchi approach. *Int. Biodeterior. Biodegrad.* 63, 420-426, (2009).

Kennedy, J.L.; Vijaya, J.J.; Kayalvizhi, K.; Sekaran, G. Adsorption of phenol from aqueous solutions using mesoporous carbon prepared by two-stage process. *Chem. Eng. J.* 132, 279–287, (2007).

Khaleghi, F.; Khalilzadeh M.A.; Raoof, J.B.; Tajbakhsh, M.; Karimi-Maleh, H. Electrochemical oxidation of catechol in the presence of an aromatic amine in aqueous media. *J. Appl. Electrochem.* 39, 1651–1654, (2009).

Khan, A.R.; Al-Bahri, T.A.; Al-Haddad, A. Adsorption of phenol based organic pollutants on activated carbon from multi-component dilute aqueous solutions. *Water Res*, 31, 2102–2112, (1997).

Khan, M.F.; Boor, P.J.; Kaphalia, B.S.; Alcock, N.W.; Ansari, G.A.S. Hematopoietic toxicity of linoleic acid anilide: importance of aniline. *Fund. Appl. Toxicol.* 25, 224–232, (1995).

Kilduff, J.E.; King, C.J. Effect of Carbon adsorbent surface properties on the uptake and solvent regeneration of phenol. *Ind. Eng. Chem. Res.* 36, 1603, (1997).

Kim, D-G.; Jung, M-W.; Paeng, I.; Rhee, J.; Paeng, K.J. Solid-Phase Extraction of Phenol and Chlorophenols in Water with a Chemically Modified Polymer-Supported Tetrakis(p-carboxyphenyl) Porphyrin (H_2TCPP). *Microchem. J.* 63, 134–139, (1999).

Kim, K.D.; Han, D.N.; Kim, H.T. Optimization of experimental conditions based on the Taguchi robust design for the formation of nano-sized silver particles by chemical reduction method. *Chem. Eng. J.* 104, 55–61, (2004).

Kim, K-H.; Kim, J-R.; Ihm, S-K. Wet oxidation of phenol over transition metal oxide catalysts supported on Ce0.65Zr0.35O2 prepared by continuous hydrothermal synthesis in supercritical water. *J. Hazard. Mater.* 167, 1158–1162, (2009).

Ko, C.H.; Fan, C.; Chiang, P.N.; Wang, M.K.; Lin, K.C. p-Nitrophenol, phenol and aniline sorption by organo-clays., *J. Hazard. Mater.* 149, 275–282, (2007).

Ko, D.C.K.; Cheung, C. W.; Choy, K.K.H.; Porter, J. F.; McKay, G. Sorption equilibria of metal ions on bone char. *Chemosphere*, 54, 273-281, (2004).

Kojima, T.; Buseck, P.R., Wilson, J. C.; Reeves, J. M.; Mahoney, M. J. Aerosol particles from tropical convective systems: Cloud tops and cirrus anvils. *J. Geophys. Res.* 109, D12201, (2004).

Krishnakumar, V.K.; Sharma, M.M.A. Novel Method of Recovering Phenolic Substances from Alkaline Waste Streams. *Ind. Eng. Chem. Process Des. Dev.* 23, 410-413, (1984).

Kuleyin, A. Removal of phenol and 4-chlorophenol by surfactant-modified natural zeolite. *J. Hazard. Mater.* 144, 307-315, (2007).

Kumar N.S.; Boddu, V.M.; Krishnaiah, A. Biosorption of Phenolic Compounds by Trametes versicolor polyporus Fungus. *Adsorption Sci. Technol.* 27,31-46, (2009).

Kumar, A.; Kumar, S.; Kumar S. Biodegradation kinetics of phenol and resorcinol using *Pseudomonas putida MTCC 1194. Biochem. Eng. J. 22*, 151-159, (2005).

Kumar, A.; Kumar, S.; Kumar, S. Adsorption of resorcinol and catechol on activated carbon: Equilibrium and kinetics. *Carbon.* 41, 3015-3025, (2003).

Kumar, A.; Kumar, S.; Kumar, S.; Gupta, D.V. Adsorption of phenol and 4-nitrophenol on granular activated carbon in basal salt medium: Equilibrium and kinetics. *J. Hazard. Mater.* 147, 155–166, (2007).

Kumar, A.; Mathur, N. Photocatalytic degradation of aniline at the interface of TiO_2 suspensions containing carbonate ions. *J. Colloid Interf. Sci.* 300, 244-252, (2006).

Kumar, S.; Upadhyay, S.N.; Upadhyay, Y.D. Removal of phenol by adsorption on fly ash, *J. Chem. Technol. Biotechnol.* 37, 188–196, (1987).

Kumaran, P.; Paruchuri, Y.L. Kinetics of phenol biotransformation. *Water Res.* 31 (1), 11–22, (1997).

Kuo, W.S. Synergistic effects of combination of photolysis and ozonation on destruction of chlorophenols in water. *Chemosphere.* 39, 1853-1860, (1999).

Kuscu, O.S.; Sponza, D. T. Performance of p-nitrophenol (p-NP) fed sequential anaerobic migrating blanket reactor (AMBR)/aerobic completely stirred tank reactor (CSTR) system under increasing organic loading conditions. *Enzyme Microb. Technol.* 40, 1026-1034, (2007).

Lagergren, S. About the theory of so called adsorption of soluble substances. *Ksver Veterskapsakad Handl.* 24, 1-6, (1898).

Langmuir, I. The adsorption of gases on plane surfaces of glass, mica and platinum. *J. Am. Chem. Soc.* 40, 1361-1403, (1918).

Lanonette, K.H. Treatment of phenolic wastes. *Chem. Eng.* 84, 99,(1977).

Laszlo, K.; Tombacz, E.; Novak, C. pH-dependent adsorption and desorption of phenol and aniline on basic activated carbon. *Colloids and Surf A: Physicochem Eng Aspects.* 306, 95–101, (2007).

Lataye, D.H.; Mishra, I. M.; Mall, I.D. Multi-component sorptive removal of toxics-pyridine, 2-picoline and 4-picoline from aqueous solution by bagasse fly ash: optimization of process parameters. *Ind. Eng. Chem. Res.* 47, 5629–5635, (2008).

Lataye, D.H.; Mishra, I.M.; Mall, I.D. Multi-component sorption of pyridine and its derivatives from aqueous solution onto rice husk ash and granular activated carbon. *Pract. Period. Hazard. Toxic Radioactive Waste Manage.* 13, 218-227, (2009).

Latkar, M.; Swaminathan, K.; Chakrabarti, T. Kinetics of anaerobic biodegradation of R R and hydroquinone in upflow fixed film–fixed bed reactors. *Bioresour. Technol.* 88, 69-74, (2003).

Lawrence, M.A.M.; Kukkadapu, R.K.; Boyd, S.A. Adsorption of phenol and chlorinated phenols from aqueous solution by tetramethylammonium- and tetramethylphosphonium-exchanged montmorillonite. *Appl. Clay. Sci.* 13, 13-20 (1998).

Le Floch, F.; Tena, M.T.; Ríos, A.; Valcarcel, M. Supercritical fluid extraction of phenol compounds from olive leaves. *Talanta.* 46, 1123-1130, (1998).

Leon y Leon, C.A.; Solar, J.M.; Calemma, V.; Radovic, L.R. Evidence for the protonation of basal plane sites on carbon. *Carbon. 30*,797, (1992).

Li, A.M.; Zhang, Q.X.; Chen, J.L. Adsorption of phenolic compounds on Amberlite XAD-4 and its acetylated derivated MX-4. *React. Funct. Polym.* 49, 225-233, (2001).

Li, A.M.; Zhang, Q.X.; Zhang, G.C.; Chen, J.L.; Fei, Z.H.; Liu, F.Q. Adsorption of phenolic compouds from aqueous solutions by a water compatible hypercrosslinked polymeric adsorbent. Chemosphere. 47, 981, (2002).

Li, K., Zheng, Z.; Huang, X.; Zhao, G.; Feng, J.; Zhang, J. Equilibrium, kinetic and thermodynamic studies on the adsorption of 2-nitroaniline onto activated carbon prepared from cotton stalk fibre. *J. Hazard. Mater.* 166, 213-220, (2008).

Liao C-J.; Kuo, S-L. Photocatalytic degradation of 4-chlorophenol with a smectite catalyst. *J. Chinese Institute of Chem. Eng.* 38, 177–184, (2007).

Lin, D.; Xing, B. Adsorption of phenolic compounds by carbon nanotubes: role of aromaticity and substitution of hydroxyl groups. *Environ Sci Technol.* 42,7254-7259, (2008).

Lin, YL.; Chiang, P.C.; Chang, E.E. Reduction of disinfection by-products precursors by nanofiltration process. *J. Hazard. Mater.* B137, 324–331, (2006).

Liu, M.Y.; Daniel T. C. W.; Hu, J.; Kelvin, N.T.W.; Liu, T.; Irene, L.M. C. Adsorption of Methylene Blue and Phenol by Wood Waste Derived Activated Carbon. *J. Environ. Eng.*134, 338-345, (2008).

Liu, X.; Pinto, N.G. Ideal adsorbed phase model for adsorption of phenolic compounds on activated carbon. *Carbon.* 35, 1387-1397, (1997).

Lo, S.C.; Lin, C.F.; Wu, C.H. Capability of coupled $CdSe/TiO_2$ for photocatalytic degradation of 4-chlorophenol. *J. Hazard. Mater.* 114, 183-190, (2004).

Lopez-Linares, F.; Carbognani, L.; Stull, C.S.; Pereira-Almao, P. Adsorption Kinetics of Anilines on Macroporous Kaolin. *Energy Fuels.* 22 (4), 2188-2194, (2008).

Lu, C.; Chung, Y.L.; Chang, K.-F. Adsorption of trihalomethanes from water with carbon nanotubes. *Water Res.* 39, 1183– 1189, (2005).

Lua, A.C.; Jiaa, Q. Adsorption of phenol by oil–palm-shell activated carbons in a fixed bed. *Chem. Eng. J.* 150, 455-461, (2009).

Luan, J.; Plaisier, A. Study on treatment of wastewater containing nitrophenol compounds by liquid membrane process. *J. Membrane Sci.* 229, 235–239, (2004).

Lupetti K.O.; Rocha, F.R.P.; Fatibello-Filho, O. An improved flow system for phenols determination exploiting multicommutation and long path length spectrophotometry. *Talanta.* 62, 463-467, (2004).

Madaeni, S.S.; Koocheki, S. Application of Taguchi method in the optimization of wastewater treatment using spiral-wound reverse osmosis element. *Chem. Eng. J.* 119, 37–44, (2006).

Mahvi, A.H.; Maleki, A.; Eslami, A. Potential of Rice Husk and Rice Husk Ash for Phenol Removal in Aqueous Systems. *J. Appl. Sci.* 1(4), 321-326, (2004).

Maiti, A.; Sharma, H.; Basu, J.K.; De, S. Modeling of adsorption kinetics of arsenic of synthetic and contaminated groundwater on natural laterite .J. Hazard. Mater. 172, 928–934, (2009).

Majumder, P.S.; Gupta, S.K. Degradation of 4-chlorophenol in UASB reactor under methanogenic conditions. *Bioresour Technol.* 99(10), 4169-4177, (2008).

Mall, I.D.; Srivastava, V.C.; Agarwal, N.K.; Mishra, I.M. Adsorptive removal of malachite green dye from aqueous solution by bagasse fly ash and activated carbon-kinetic study and equilibrium isotherm analyses. *Colloids. Surfaces. A.* 264, 17-28, (2005).

Mall, I.D.; Srivastava, V.C.; Kumar, G.V.A.; Mishra, I.M. Characterization and utilization of mesoporous fertilizer plant waste carbon for adsorptive removal of dyes from aqueous solution. *Colloid. Surface. A.* 278, (1-3), 175-187, (2006).

Mall, I.D.; Upadhyay, S.N.; Sharma, Y.C. A review on economical treatment of wastewaters and effluents by adsorption. *Int. J. Environ. Stud.* 51, 77-124, (1996).

Mandal, A.; Ojha, K.; Deb, A.K.; Bhattacharjee, S. Removal of catechol from aqueous solution by advanced photo-oxidation process. *Chem. Eng. J.* 102, 203–208, (2004).

Marczewski, A.W. Kinetics and equilibrium of adsorption of organic solutes on mesoporous carbons. *Appl. Surf. Sci.* 253, 5818–5826, (2007).

Marquardt, D.W. An algorithm for least-squares estimation of nonlinear parameters. *J. Soc. Ind. Appl. Math.*11, 431, (1963)

Marquardt, D.W. An algorithm for least-squares estimation of nonlinear parameters. *J. Soc. Ind. Appl. Math.*11, 431, (1963)

Matheswaran, M.; Moon, S. Influence parameters in the ozonation of phenol wastewater treatment using bubble column reactor under continuous circulation. *J. Ind. Eng. Chem.* 15, 287–292, (2009).

Mattson, J.; Mark, H. Activated carbon: surface chemistry and adsorption from solution, Marcel Dekker, Inc., New York, (1971).

Mattson, J.; Mark, H.; Malbin, M.; Weber, J.; Crittenden, W.J. Surface chemistry of active carbon. Specific adsorption of phenols. *J. Colloids Interface Sci.* 31,116-130, (1969).

Mbui, D.N.; Shiundu, P.M.; Ndonye, R.M.; Kamau, G.N. Adsorption and detection of some phenolic compounds by rice husk ash of Kenyan origin. *J. Environ. Monit.* 4, 978 – 984, (2002).

McKay, G.; Allen, S.J.; McConvey, I.F.; Otterburn, M.S. Transport process in the sorption of colored ions by peat particles. *J. Colloid Interface Sci.* 80, 323, (1981).

McKay, G.; Otterburn, M. S.; Sweeney, A. G. The removal of colour from effluent using various adsorbents- III Silica: Rate processes. *Water. Res.* 14, 15-20, (1980).

Merck, *The Merck Index*, 11th ed., Rahway, N.J, Merck, (1989).

Milligan, P.W.; Haggblom, M.M. Biodegradation of resorcinol and catechol by denitrifying enrichment cultures. *Environ. Toxicol. Chem.* 17, 1456-1461, (1998).

Minero, C.; Bono, F.; Rubertelli. F.; Pavino. D.; Maurino,V.; Pelizzetti, E.; Vione, D. On the effect of pH in aromatic photonitration upon nitrate photolysis. *Chemosphere.* 66, 650–656, (2007).

Mitra, A.; Fundamentals of Quality Control and Improvement, Pearson Educational Asia, Delhi (1998).

Modirshahla, N.; Behnajadya, M.A.; Mohammadi-Aghdam, S. Investigation of the effect of different electrodes and their connections on the removal efficiency of 4-chtrophenol from aqueous solution by electrocoagulation. *J. Hazard. Mater.* 154, 778-786, (2008).

Moghaddama, J.; Sarraf-Mamoorya, R.; Abdollahy, M.; Yamini, Y. Purification of zinc ammoniacal leaching solution by cementation: Determination of optimum process conditions with experimental design by Taguchi's method. *Sep. Purif. Technol.* 51, 157-164, (2006).

Mohamed, F.S.; Khater, W.A.; Mostafa, M.R. Characterization and phenols sorptive properties of carbons activated by sulphuric acid. *Chem. Eng. J.* 116, 47-52, (2006).

Mohammadi, T.; Moheb, A.; Sadrzadeh, M.; Razmi, A. Separation of copper ions by electrodialysis using Taguchi experimental design, *Desalination.* 169, 21–31, (2004).

Molinari, R.; Borgesea, M.; Drioli, E.; Palmisano, L.; Schiavello, M. Hybrid processes coupling photocatalysis and membranes for degradation of organic pollutants in water. *Catal. Today.* 75, 77-85, (2002).

Mondal, P.; Balomajumder, C. Treatment of resorcinol and phenol bearing wastewater by simultaneous adsorption biodegradation (SAB): optimization of process parameters. *International J. Chem. React. Eng.* 5, S1, 1-16, (2007).

Moreale, A.; Van Bladel, R. Adsorption of herbicide-derived anilines in dilute aqueous montmorillonite suspensions. *Clay Miner.* 14 (1), 1–11, (1979).

Moreno-Castilla, C.; Rivera-Utrilla, J.; Joly, J.P.; Lopez-Ramon, M.V.; Ferro-Garcia, M.A.; Carrasco-Martin F. Thermal regeneration of an activated carbon exhausted with different substituted phenols. *Carbon.* 33(10), 1417–23,(1995).

Muir, G.D. Hazards in the Chemical Laboratory, The Royal Institute of Chemistry, London, (1971).

Mukherjee, S.; Kumar S., Misra, A.K.; Fan, M. Removal of phenols from water environment by activated carbon, bagasse ash and wood charcoal. *Chem. Eng.J.* 129 133–142, (2007).

Murzin, D.; Salami, T. Chemical kinetics, Elsevier, Amsterdam, (2005).

Mussatto, S.I.; Roberto, I.C. Hydrolysate detoxification with activated charcoal for xylitol product by *Candida guilliermondii. Biotechnol. Letters.* 23, 1681-1684, (2001).

Namasivayam, C.; Sumithra, S. Adsorptive removal of catechol on waste Fe(III)/Cr(III) hydroxide: equilibrium and kinetics study. *Ind. Eng. Chem. Res.* 43, 7581-7587, (2004).

Namasivayam.C and Sumithra.S, Adsorptive removal of phenols by Fe(III)/Cr(III) hydroxide, an industrial solid waste , Clean Technologies and Environmental Policy, 9 (3) 1618-9558 (2007).

Nasr, B.; Abdellatif, G.; Canizares, P.; Saez, C.; Lobato, J.; Rodrigo, M.A. Electrochemical oxidation of hydroquinone, resorcinol and catechol on boron doped diamond anodes. *Environ. Sci. Technol.* 39, 7234-7239, (2005).

Netke, S.A.; Pangarkar, V.G. Extraction of naphthenic acid kerosene using porous and nonporous polymeric membranes. *Sep. Sci. Technol. 31*, 63, (1996).

Neves, M.C.; Nogueira, J.M.F.; Trindade, T.; Mendonc, M.H.; Pereirac, M.I.; Monteiro, O.C. Photosensitization of TiO_2 by Ag_2S and its catalytic activity on phenol photodegradation. *J. Photochem. Photobiol. A: Chem.* 204, 168–173, (2009).

Nevskaia, D.M.; Castillejos-Lopez, E.; Munoz, V.; Guerrero-Ruiz, A. Adsorption of aromatic compounds fromwater by treated carbon materials. *Environ. Sci. Technol.* 38 (21), 5786–5796, (2004).

Ng, C.; Losso, J.N.; Marshall, W.E.; Rao, R.R. Physical and chemical properties of selected agricultural byproduct-based activated carbons and their ability to adsorb geosmin. *Bioresour. Technol.* 84,177–185, (2002).

NIOSH, The National Institute for Occupational Safety and Health (NIOSH), Pocket Guide to Chemical Hazards, NIOSH Publication, (2005).

Niu, J.; Conway, B.E. Development of techniques for purification of wastewaters removal of pyridine from aqueous solution by adsorption at high area AC-cloth electrodes using in situ optical spectrometry. *J. Electroanal. Chem.* 521, 16–28, (2002).

Northcott, J. Amines, aromatic-aniline and its derivatives, in: H.F. Mark, D.F. Othmer, C.G. Overberger, G.T. Seaborg (Eds.),Kirk/Othmer Encyclopaedia of Chemical Technology, vol. 2, 3rd ed., Wiley, Totonto, Ont, pp. 309/321, (1978).

O'Brien, J.; O'Dwyer, T.F.; Curtin, T. A novel process for the removal of aniline from wastewaters. *J. Hazard. Mater.* 159, 476–482, (2008).

O'Neill, F.J.; Bromley-Challenor, K.C.A.; Greenwood, R.J.; Knapp, J.S. Bacterial growth on aniline: implications for the biotreatment of industrial wastewater. *Water Res.* 34 (18), 4397–4409, (2000).

Oguz, E.; Keskinler, B.;Celik, C.; Celik, Z. Determination of the optimum conditions in the removal of Bomaplex Red CR-L dye from the textile wastewater using O_3, H_2O_2, HCO_3^- and PAC. *J. Hazard. Mater.* B131, 66–72, (2006).

Olafadehan, O.A.; Susu, A.A. Modelling and Simulation of Liquid Phase Ternary Adsorption on Activated Carbon. *Ind. Eng. Chem. Res.* 43, 8107, (2004).

OME, Ontario Ministry of Environment (OME), Environmental Aspects of Selected Aromatic Amines and Azo Dyes in Ontario, MOE Report no. ARB-TDA-83-79, Toronto, Ont., (1980).

Orshansky, F.; Narkis, N. Characteristics of organics removal by PACT simultaneous adsorption and biodegradation. *Water Res.* 31, 391–398, (1997).

Othmer, K. Hydroquinone, resorcinol, and catechol. In: Kirk-Othmer encyclopedia of chemical technology, 3rd ed. Vol.13. New York, NY, John Wiley & Sons, pp. 39–69, (1981).

Ozbelge, T A.; Onder, H.; Ozbelge,; Baskaya, S.Z. Removal of phenolic compounds from rubber–textile wastewaters by physico-chemical methods. *Chem. Eng. Process.* 41, 719–730, (2002).

Pak_u a M.; Swiatkowski, A.; Walczyk, M.; Biniak, S. Voltammetric and FT-IR studies of modified activated carbon systems with phenol, 4-chlorophenol or 1,4-benzoquinone adsorbed from aqueous electrolyte solutions. *Colloids and Surfaces A: Physicochem. Eng. Aspects.* 260, 145-155, (2005).

Pan, B.C.; Zhang, Q.X.; Meng, F.W.; Li, X.T.; Zhang, X.; Zheng, J.Z. Sorption enhancement of aromatic sulfonates onto an aminated hyper-cross-linked polymer, *Environ. Sci. Technol.* 39, 3308, (2005).

Pandit, B.; Chudasama, U. Synthesis, characterization and application of an inorgano organic material: p-chlorophenol anchored onto zirconium tungstate. *Bull. Mater. Sci.* 24, 265–271, (2001).

Parida K.M.; Pradhan, A.C. Removal of phenolic compounds from aqueous solutions by adsorption onto manganese nodule leached residue. *J. Hazard. Mater.* 173, 758-764, (2010).

Parris, G.E. Environmental and metabolic transformations of primary aromatic amines and related compounds. *Residue Rev.* 76, 1-30, (1980).

Patil, S.S.; Shinde, V. M. Biodegradation studies of aniline and nitrobenzene in aniline plant wastewater by gas chromatography. *Environ. Sci. Technol.* 22 (10), 160–1165, (1988).

Patterson, J.W. Wastewater Treatment Technology, Ann Arbor Sci., Ann Arbor, Michigan, (1975).

Peres, C.M.; Naveau, H.; Agathos, S.N. Biodegradation of nitrobenzene by its simultaneous reduction into aniline and mineralization of the aniline formed. *Appl. Microbiol. Biotechnol.* 49, 343-349, (1998).

Phadke, M. S.; Dehnad, K. Optimization of product and process design for quality and cost. *Qual. Reliab. Eng. Int.* 4, 159–169, (1988).

Phan, N.H.; Rio, S.; Faur, C.; Coq, L.L.; Cloirec, P.L.; Nguyen, T.H. Production of fibrous activated carbons from natural cellulose (jute, coconut) fibers for water treatment applications. *Carbon.* 44, 2569–2577, (2006).

Pi, Y.; Zhang, L.; Wang, J. The formation and influence of hydrogen peroxide during ozonation of para-chlorophenol. *J.Hazard. Mater.* 141, 707-712, (2007).

Pistonesi, M.; Centurion, M.E., Pereyra, M.; Lista, A.G.; Fernande, B.S. Synchronous fluorescence for simultaneous determination of hydroquinone and resorcinol in air samples. *Anal. Bioanal. Chem.* 378, 1648-1651, (2004).

Pithan, F.; Bickel, C.S.; Lichtenthaler, R.N. Synthesis of highly fluorinated copolyimide membranes for the removal of high boiling organics from process water and wastewater by pervaporation. *Desalination*. 148, 1-4, (2002).

Plessis du, B.J.; de Villiers, G.H. The application of the Taguchi method in the evaluation of mechanical flotation in waste activated sludge thickening. *Resour. Conserv. Recycl*. 50, 202–210, (2007).

Podkoscielny, P.; Laszlo, K. Heterogeneity of activated carbons in adsorption of aniline from aqueous solutions. *Appl. Surf. Sci*. 253, 8762-8771, (2007).

Poljanšek, I.; Matjaz, K. Characterization of phenol-formaldehyde prepolymer resins by in line FT-IR spectroscopy. *Acta chim. slov*. 52, 238-244, (2005).

Prager, J.C., In: Environmental contaminant reference data book, New York: Van Nostrand Reinhold, pp. 190–193, (1997).

Pulgarin, C.; Peringer, P.; Albers, P.; Kiwi, J. Effect of Fe-ZSM-5 zeolite on the photochemical and biochemical degradation of 4-nitrophenol. *J. Molecular Catal. A: Chem*. 95, 61-74, (1995).

Qi, X.H.; Zhuang, Y.Y.; Yuan, Y.C.; Gu, W.X. Decomposition of aniline in supercritical water. *J. Hazard. Mater*. 90, 51–62, (2002).

Quiroz, M.A.; Reyna, S.; Martinez-Huitle, C.A.; Ferro, S.; Battisti, A.D. Electrocatalytic oxidation of p-nitrophenol from aqueous solutions at Pb/PbO_2 anodes. *Appl. Catal. B: Environ*. 59, 259–266, (2005).

Rajkumar, D., Palanivelu, K.; Balasubramanian, N. Combined electrochemical degradation and activated carbon adsorption treatments for wastewater containing mixed phenolic compounds. *J. Environ. Eng. Sci*. 4, 1–9, (2005).

Rajkumar, D.; Palanivelu, K. Electrochemical treatment of industrial wastewater. *J. Hazard. Mater*. B113, 123–129, (2004).

Rallapalli, P.; Prasanth, K.P.; Patil, D.; Somani, R.S.; Jasra, R.V.; Bajaj, H.C. Sorption studies of CO_2, CH_4, N_2, CO, O_2 and Ar on nanoporous aluminum terephthalate [MIL-53(Al)]. *J. Porous Mater*. (2010). DOI: 10.1007/s10934-010-9371-7.

Ramade, F. Dictionnaire Encyclopédique des Pollutions, Ediscience International, (2000).

Ramirez, R.M.; Schouwenaars, R.; Duran, A.; Buitron, G. Production of activated carbon from petroleum coke and its application in water treatment for the removal of metals and phenol. *Water. Sci. Technol*. 42, 119, (2000).

Rao, M.; Parwate, A. V.; Bhole, A. G. Removal of Cr^{6+} and Ni^{2+} from aqueous solution using bagasse and fly ash. *Waste. Manage*. 22, 821-830, (2002).

Raupach, M.; Janik, L.J. Polarized Infrared Study of Anilinium-Vermiculite Intercalate. *J. Colloid Interf. Sci.* 121, 449, (1988).

Ravi, V.P.; Jasra, R.V.; Bhat, T.S.R. Adsorption of phenol, cresol isomers and benzyl alcohol from aqueous solution on activated carbon at 278, 298 and 323 K. *J. Chem. Technol. Biotechnol.* 71, 173-179, (1998).

Ravikumar, K.; Pakshirajan, K.; Swaminathan, T.; Balu, K. Optimization of batch process parameters using response surface methodology for dye removal by a novel adsorbent. *Chem. Eng. J.*105, 131–138, (2005).

Raymon, C. *Chemistry: Thermodynamic*, McGraw–Hill, Boston, (1998).

Razee, S.; Masujima, T. Uptake monitoring of anilines and phenols using modified zeolites. *Anal. Chimica Acta*. 464, 1–5, (2002).

Redlich, O.; Peterson, D. L. A useful adsorption isotherm. *J. Phys. Chem.* 63, 1024-1026, (1959).

Reichenberg, D. Properties of ion exchange resin in relation to their structure. III. Kinetics of exchange. *J. Am. Chem. Soc.* 75, 589, (1953).

Reid, M.S. Ethylene in post-harvest technology, in A. Kadar (ed.) *Postharvest Technology of Horticultural Crops*. Oakland: University of California, (1985).

Ress, N.B.; Witt, K.L.; Xu, J.; Haseman, J.K.; Bucher, J.R. Micronucleus induction in mice exposed to diazoaminobenzene or its metabolites, benzene and aniline: implications for diazoaminobenzene carcinogenicity. *Mutat Res Gen Toxicol Environ. Mutagen*. 521, 201–208, (2002).

Richard, D.; Delgado, M.L.; Schweich, D. Adsorption of complex phenolic compounds on activated charcoal: adsorption capacity and isotherms. *Chem. Eng. J. 148*, 1–7, (2009).

Ricordel, S.; Taha, S.; Cisse, I.; Dorange, G. Heavy metals removal by adsorption onto peanut husks carbon: characterization, kinetic study and modeling. *Sep. Purif. Technol.* 24, 389-401, (2001).

Rio, S.; Faur-Brasquet, C.; Coq, L.L.; Courcoux, P.; Cloirec, P. L. Experimental design methodology for the preparation of carbonaceous sorbents from sewage sludge by chemical activation-application to air and water treatments. *Chemosphere.* 58, 423–437, (2005).

Rodriguez, I.; Llompart, M.P.; Cela, R. Solid-phase extraction of phenols. *J. Chromatogr.* 885, 291–304, (2000).

Ross, P.J. Taguchi Techniques for Quality Engineering: Loss Function, Orthogonal Experiments, Parameter and Tolerance Design, New York, (1996).

Roy R.K., Design of Experiments Using the Taguchi Approach: 16 Steps to Product and Process Improvement, John Wiley & Sons, New York (2001).

Roy, R.K. A primer on the Taguchi method, Society of Manufacturing Engineers, Michigan, (1990).

Rubin, E.; Rodriguez, P.; Herrero, R.; de Vicente, M.E.S. Biosorption of phenolic compounds by the brown alga Sargassum muticum. *J. Chem. Technol. Biotechnol.* 81,1093-1099, (2006).

Sabah, E.; Çinar, M.; Çelik, M.S. Decolorization of vegetable oils: Adsorption mechanism of β-carotene on acid-activated sepiolite. *Food Chem.* 100 (4), 1661–1668, (2007).

Sabio, E.; Zamora, F.; Ganan J.; Gonzalez-Garcia, C.M.; Gonzalez, J.F. Adsorption of p-nitrophenol on activated carbon fixed-bed. *Water Res.* 40, 3053 – 3060, (2006).

Sag, Y.; Akcael, B.; Kutsal, T. Application of multicomponent adsorptionmodels to the biosorption of Cr(II), Cu(II), and Cd(II) ions on *rhizopus arrhizus* from ternary metal mixtures. *Chem. Eng. Comm.* 190, 797-812, (2003).

Sag, Y.; Akcael, B.; Kutsal, T. Ternary biosorption equilibria of chromium (VI), copper(II), and cadmium(II) on *Rhizopus arrhizus*. *Sep. Sci. Technol.* 37, 279-308, (2002).

Salame, I.I.; Bandosz, T.J. Role of surface chemistry in adsorption of phenol on activated carbons. *J. Colloid Interf. Sci.* 264, 307–312, (2003).

Sanchez, L.; Peral, J.; Domenech, X. Aniline degradation by combined photocatalysis and ozonation. *Appl. Catal. B: Environ.* 19, 59-65, (1998).

Sarasa, J.; Cortes, S.; Ormad, P.; Gracia, R.; Ovelleiro, J.L. Study of the aromatic by-products formed from ozonation of anilines in aqueous solution Water Research 36,3035–3044, (2002).

Schweigert, N.; Zehnder, A.J.B.; Eggen, R.I.L. Chemical properties of catechols and their molecular modes of toxic action in cells, from microorganisms to mammals. *Environ. Microbiol.* 3, 81-91, (2001).

Shakir, K.; Ghoneimy, H.F.; Elkafrawy, A.F.; Beheir, Sh.G.; Refaat, M. Removal of resorcinol from aqueous solutions by adsorption onto organophilic-bentonite. *J. Hazard. Mater.* 150,765, (2008).

Shapiro, A.; Stenby, E.H. Multicomponent adsorption approaches to modeling adsorption equilibria. Encyclopedia of surface and colloid science, Taylor & Francis, New York, pp. 4180-4189, (2006).

Sheindorf, C.; Rebhum, M.; Sheintuch, M.A. Freundlich-type multicomponent isotherm. *J. Colloid Interf. Sci.* 79, 136-142, (1981).

Shen, S.; Chang, Z.; Liu, H. Three-liquid-phase extraction systems for separation of phenol and p-nitrophenol from wastewater. *Sep. Purif. Technol.* 49, 217–222, (2006).

Singh, S.; Yenkie, M.K.N. Competitive Adsorption of Some Hazardous Organic Pollutants from their Binary and Ternary Solutions onto Granular Activated Carbon Columns, Water, Air, & Soil Pollution, 156 (1-4) 1573-2932 (2004).

Skelland, A.H.P. Diffusional Mass Transfer. Wiley, NY, (1974).

Smith, C.J.; Perfetti, T.A.; Morton, M.J.; Rodgman, A.; Garg, R.; Selassie, C.D.; Hansch, C. The relative toxicity of substituted phenols reported in cigarette mainstream smoke. *Toxicol. Sci.* 69, 265–278, (2003).

Sorial, G.A.; Suidan, M.T.; Vidic, R.D.; Maloney, S.W. Competitive adsorption of phenols on GAC .1. adsorption equilibrium. *J. Environ. Eng.-ASCE*, 119, 1026-1043, (1993a).

Sorial, G.A.; Suidan, M.T.; Vidic, R.D.; Maloney, S.W. Competitive adsorption of phenols on GAC. adsorption dynamics under anoxic conditions. *J. Environ. Eng.-ASCE*, 119, 1044-1058, (1993b).

Srivastava, V.C.; Prasad, B.; Mishra, I.M.; Mall, I.D.; Swamy, M.M. Prediction of breakthrough curves for sorptive removal of phenol by bagasse fly ash packed bed. *Ind. Eng. Chem. Res.* 47, 1603-1613, (2008c).

Srivastava, V.C.; Mall, I.D.; Mishra, I.M.; Optimization of parameters for adsorption of metal ions onto rice husk ash using Taguchi's experimental design methodology. *Chem. Eng. J.* 140, 136–144, (2008b).

Srivastava, S.K.; Tyagi, R. Competitive adsorption of substituted phenols by activated carbon developed from the fertilizer waste slurry. *Water Res.* 29, 483–488, (1995).

Srivastava, V. C.; Mall, I. D.; Mishra, I. M. Adsorption of toxic metal ions onto activated carbon. Study of sorption behaviour through characterization and kinetics. *Chem. Eng. Process.* 47, 1269-1280, (2008a).

Srivastava, V.C.; Mall I.D.; Mishra, I.M. Characterization of mesoporous rice husk ash (RHA) and adsorption kinetics of metal ions from aqueous solution onto RHA. *J. Hazard. Mater.* B134, 257-267, (2006b).

Srivastava, V.C.; Mall I.D.; Mishra, I.M. Multicomponent Adsorption Study of Metal Ions onto Bagasse Fly Ash Using Taguchi's Design of Experimental Methodology. *Ind. Eng. Chem. Res. 46,* 5697-5706, (2007).

Srivastava, V.C.; Swamy, M.M.; Mall, I.D.; Prasad, B.; Mishra, I.M. Adsorptive Removal of Phenol by Bagasse fly ash and Activated Carbon: equilibrium, kinetics and

thermodynamic study. *Colloid Surface A: Physicochem. Eng. Aspects*, 272, 89-104, (2006a).

Star, A.; Han, T.R.; Gabriel, J.C.P.; Bradley, K.; Gruner, G. Interaction of aromatic compounds with carbon nanotubes: correlation to the hammett parameter of the substituent and measured carbon nanotube FET response. *Nano Lett. 3*, 1421-1423, (2003).

Stoilova, A.; Krastanov, V.; Stanchev, D.; Daniel, M.; Gerginova, Z. Alexieva. Biodegradation of high amounts of phenol, resorcinol, 2,4-dichlorophenol and 2,6-dimethoxyphenol by Aspergillus awamori cells. *Enzyme Microb. Tech.* 39, 1036–1041, (2006).

Subramanyam, R.; Mishra, I.M. Biodegradation of Resorcinol (2-hydroxy phenol) bearing wastewater in an UASB reactor. *Chemosphere*. 69, 816-824, (2007).

Subramanyam, R.; Mishra, I.M. Co-degradation of catechol and resorcinol in an UASB reactor. *Bioresour. Technol.* 99, 4147-4157, (2008).

Sulaymon, A.H.; Ahmed, K.W. Competitive adsorption of furfural and phenolic compounds onto activated carbon in fixed bed column. *Environ. Sci. Technol.* 42, 392–397, (2008).

Sun, Y.; Chen, J.; Li, A.; Liu, F.; Zhang, Q. Adsorption of catechol and resorcinol from aqueous solution by aminated hypercrosslinked polym. *React. Funct. Polym.* 64-63, (2005).

Svobodova, A.; Psotová, J.; Walterová, D. Natural Phenolics in the Prevention of UV-Induced Skin Damage. A Review. *Biomed. Papers*. 147 (2), 137–145, (2003).

Swaminathan, K.; Chakrabarti, T.; Subrahmanyam, P.V.R. Substrate-substrate interaction of resorcinol and catechol in upflow anaerobic fixed film-fixed bed reactors in mono and multi substrate matrices. *Bioproc. Eng.* 20, 349–353, (1999).

Swamy, M. M.; Mall, I. D.; Prasad, B.; Mishra, I. M. Sorption Characteristics of O-Cresol on Bagasse Fly Ash and Activated Carbon. *Indian J. of Environ. Health.* 40(1), 67-78, (1998).

Swamy, M.M., Mall, I.D.; Prasad, B.; Mishra, I.M. Removal of phenol by adsorption on coal fly ash and activated carbon. *Poll. Res.* 16, 170–175, (1997).

Taguchi G., Wu Yu-in, Off-line Quality Control, Central Japan Quality Control Association, Nagaya, Japan (1979).

Taguchi, G. Introduction to Quality Engineering, Quality Resources, New York, (1986).

Tang, D.; Zheng, Z.; Lin, K.; Luan, J.; Zhang, J. Adsorption of p-nitrophenol from aqueous solutions onto activated carbon fiber. *J. Hazard. Mater.* 143, 49–56, (2007).

Tarley, C.R.T.; Kubota, L.T. Molecularly-imprinted solid phase extraction of catechol from aqueous effluents for its selective determination by differential pulse voltammetry. *Anal. Chimica Acta.* 548, 11–19, (2005).

Temkin, M. J.; Pyzhev, V. Kinetics of ammonia synthesis on promoted iron catalysts. *Acta Physiochim.* 12, 327-356, (1940).

Ten Hulscher Th.E.M.; Cornelissen, G. Effect of temperature on sorption equilibrium and sorption kinetics of organic micropollutants—a review. *Chemosphere.* 32, 609–626, (1996).

Teng, H.; Hsie, C.T. Influence of surface characteristics on liquid-phase adsorption of phenol by activated carbons prepared from bituminous coal. *Ind. Eng. Chem. Res.* 37, 3618, (1998).

Terashima, C.; Rao, T.N.; Sarada, B.V.; Tryk, D.A.; Fujishima, A. Electrochemical oxidation of chlorophenols at a boron-doped diamond electrode and their determination by High-Performance liquid lhromatography with amperometric detection. *Anal. Chem.* 74, 895, (2002).

Terzyk, A.P. Molecular properties and intermolecular forces-factors balancing the effect of carbon surface chemistry in adsorption of organics from dilute aqueous solutions, *J. Colloid Interf. Sci.* 275, 9–29, (2001).

Thepsithar, P.; Roberts, E.P. Removal of phenol from contaminated kaolin using electrokinetically enhanced

Tomei, M.C.; Annesini, M.C.; Rita, S.; Daugulis, A.J. Biodegradation of 4-nitrophenol in a two-phase sequencing batch reactor: concept demonstration, kinetics and modelling. *Appl. Microbiol. Biotechnol.* 80(6), 1105-1112, (2008).

Ugurlu, M.; Gurses, A. ; Dogar, C.; Yalcin, M. The removal of lignin and phenol from paper mill effluents by electrocoagulation. *J. Environ. Manage.* 87, 420–428, (2008).

USEPA, Federal Register, vol. 52, no. 131, USEPA, Washington, DC, pp. 25861–25962, (1987).

USEPA, method 604. Phenol and certain substituted phenols by high performance liquid chromatograph. Washington, DC, (1987).

Vasu, A.E. Removal of phenol and o-Cresol by adsorption onto activated carbon. *E-J. Chem.* 5, 224-232, (2008).

Vasudevan, D.; Stone, A.T. Adsorption of catechols, 2-aminophenols, and 1,2-phenylenediamines at the metal hydroxide/water Interface: effect of ring substituents on the adsorption onto TiO_2. *Environ. Sci. Technol.* 30, 1604-1613, (1996).

Vermeulen, T. Theory for irreversible and constant pattern solid diffusion. *Ind. Eng. Chem.* 45, 1664-1670, (1953).

Vijayalakshmi, P.R.; Raksh, V.J.; Thirumaleswara, S.G.B. Adsorption of phenol, cresol isomers and benzyl alcohol from aqueous solution on activated carbon at 278, 298 and 323 K. *J. Chem. Technol. Biotechnol.* 71, 173-179, (1998).

Villacanas, F.; Fernando, M.; Pereira, R.; Orfao, J.J.M.; Figueiredo, J.L. Adsorption of simple aromatic compounds on activated carbons. *J. Colloid. Interf. Sci.* 293, 128–136, (2006).

Viraraghavan, T.; Alfaro, F.M. Adsorption of phenol from wastewater by peat, fly ash and bentonite, J. Hazard. Mater. 57, 59-70, (1998).

Wadekar,V.V.; Sharma, M. M. Separation of close boiling substituted phenols by dissociation-extraction. *J. Chem. Technol. Biotechnol.* 31, 279, (1981).

Wang, L.; Zheng, L.X. The research of CBDS system simulation on petrochemical wastewater treatment process. *Environ. Prot.* 260 (6), 32–39, (1999).

Wang, R.C.; Yang, J.J. Competitive adsorption of bisolute phenols onto granular activated carbon. *J. Chinese Institute Chem. Eng. 28*, 185-195, (1997).

Wang, Y.; Zhou, H.; Yu, F.; Shi, B.; Tang, H. Fractal adsorption characteristics of complex molecules on particles-A case study of dyes onto granular activated carbon (GAC). *Colloid. Surface. A.* 299, 224–231, (2007).

Wang. H.; Wang. J. Electrochemical degradation of 4-chlorophenol using a novel Pd/C gas-diffusion electrode, *Applied Catalysis B: Environmental.* 77, 58–65, (2007).

Watts, M.J.; Cooper, A.T. Photocatalysis of 4-chlorophenol mediated by TiO_2 fixed to concrete surfaces. *Solar Energy*. 82, 206-211, (2008).

Weber Jr. W.J., Morris, J.C., Kinetics of adsorption on carbon from solution. *J. Sanitary. Engg. Div.* ASCE, 89(SA2), 31-59, (1963).

Weber, W.J. In: Physicochemical processes for water quality control, New York: Wiley-Interscience, pp. 211, (1972).

WHO, Guidelines for drinking water Quality vol.1. Recommendation World Health Organisation, Geneva, (1984).

Wong, Y.C.; Szeto, Y.S.; Cheung, W.H.; McKay, G. Biosorption of acid dyes on chitosan-equilibrium isotherm analyses. *Process Biochem.* 39, 693-702, (2004).

Xiao,W.; Xiao, D. Aminopyrene functionalized mesoporous silica for the selective determination of resorcinol. *Talanta.* 72, 1288, (2007).

Yalkowsky, S.H.; Dannenfelser, R.M. Aquasol Database ofAqueous Solubility, Version 5. College of Pharmacy, AZ. PC Version, (1992).

Yang, K.; Wu, W.; Jing, Q.; Zhu, L. Aqueous Adsorption of Aniline, Phenol, and their Substitutes by Multi-Walled Carbon Nanotubes. *Environ. Sci. Technol.* 42 (21), 7931-7936, (2008).

Yang, K.; Wu, W.; Jing, Q.; Zhu, L. Aqueous Adsorption of Aniline, Phenol, and their Substitutes by Multi-Walled Carbon Nanotubes. *Environ. Sci. Technol.* 42 (21), 7931-7936, (2008).

Yang, R.T. Gas Separation by Adsorption Processes, (1987).

Yildiz, N.; Gonulsena, R.; Koyuncu, H.; Calimli, A. Adsorption of benzoic acid and hydroquinone by organically modified bentonites. *Colloids and Surf. A: Physicochem. Eng. Aspects*. 260, 87, (2005).

Young, D.M.; Crowell, A. D. *Physical adsorption of gases;* Butterworths, London. (1962).

Yousef, R.I.; El-Eswed, B. The effect of pH on the adsorption of phenol and chlorophenols onto natural zeolite. *Colloid. Surf. A: Physicochem. Eng. Aspects*, 334, 92-99, (2009).

Yu, J.; Du, W.; Zhao, F.; Zeng, B. High sensitive simultaneous determination of catechol and hydroquinone at mesoporous carbon CMK-3 electrode in comparison with multi-walled carbon nanotubes and Vulcan XC-72 carbon electrodes. *Electrochimica Acta*. 54 984–988, (2009).

Yu-li, Y.; Yue-Zhong, W.; Xiao-Ying, L.; Si-Zhen, L. Treatment of wastewater from dye manufacturing industry by coagulation. *J. Zhejiang Univ SCIENCE* A, 7 (Suppl. II), 340-344, (2006).

Zhang, W.M.; Xu, Z.W.; Pan, B.C.; Zhang, Q.J.; Du, W.; Zhang, Q.R.; Zheng, K.; Zhang, Q.X.; Chen, J.L. dsorption enhancement of laterally interacting phenol/aniline mixtures onto nonpolar adsorbents. *Chemosphere*. 66, 2044-2049, (2007a).

Zheng, H.; Liu, D.; Zheng, Y.; Liang, S.; Liu, Z. Sorption isotherm and kinetic modeling of aniline on Cr-bentonite. *J. Hazard. Mater*. 167, 141-147, (2008).

Zheng, H.; Liu, D.; Zheng, Y.; Liang, S.; Liu, Z. Sorption isotherm and kinetic modeling of aniline on Cr-bentonite. *J. Hazard. Mater*. 167, 141-147, (2008).

Zhou, M.; Zucheng, Wu.; Xiangjuan, Ma.; Yanqing Cong, Qian Ye, Dahui Wang. A novel fluidized electrochemical reactor for organic pollutant abatement, Separation and Purification Technology 34, 81–88 (2003).

Zhou, Q.; Frost, R.L.; He, H.; Xi, Y.; Liu, H. Adsorbed para-nitrophenol on HDTMAB organoclay—A TEM and infrared spectroscopic study. *J. Colloid Interface Sci. 307*, 357-363, (2007).

Zhu, D.Q.; Pignatello, J.J. Characterization of aromatic compound sorptive interactions with black carbon (charcoal) assisted by graphite as a model. *Environ. Sci. Technol.* 39, 2033-2041, (2005).

Zhu, L.; Ren, X.; Yu, S. Use of cetyltrimethylammonium bromide-bentonite to remove organic contaminants of varying polar character from water. *Environ. Sci. Technol.* 32, 3374–3378, (1998).

Zierkiewicz, W.; Michalska, D.; Zeegers-Huyskens, T. Molecular Structures and Infrared Spectra of *p*-chlorophenol and *p*-bromophenol. Theoretical and Experimental Studies. *J. Phys. Chem. A.* 104, 11685-11692, (2000).

Zogorski, J.S.M.; Faust, S.D.; Haas, J.H. The kinetics of adsorption of phenols by granular activated carbon. *J. Colloid. Interf. Sci.* 55, 329–341, (1976).

Websites visited:

1. http://en.wikipedia.org/wiki/Phenol
2. http://www.the-innovation-group.com/ChemProfiles/Aniline.htm
3. www.scorecard.org/chemical- profiles/hazard-indicators [accessed June 2010]

BIO DATA

Name	:	**SURESH S.**
Father's Name	:	V. Sundaramurthy
Date of Birth	:	14-01-1982
Permanent Address	:	10, Karthar Street (Near Post office), Thirukkanur Post Puducherry PIN- 605 501
Email	:	sureshpecchem@gmail.com

Professional Profile

1. B.Tech. (Chemical Engg.), 2004 from P.E.C., Puducherry.
2. M.E. (Chemical Engg.), 2006 from Annamalai University.
3. One and half year research experience from Indian Institute of Technology Kanpur, Kanpur and Pondicherry University, Puducherry.
4. Will be joining as Assistant Professor in the Department of Chemical Engineering, Maulana Azad National Institute of Technology (MANIT), Bhopal in August 2010.

Field of Interest

Adsorption, Chemical Reaction Engg., Biochemical Engg., Industrial Pollution Abatement

Publications

- International Journal – 5
- Conferences - 7

PUBLICATION FROM THESIS

AWARD

- **"Young Scientist Award"** to ***Mr. Suresh S.*** under the discipline of 'Engineering Science and Technology' by Uttarakhand State Council for Science & Technology, Department of Science & Technology, Government of Uttarakhand for presentation of paper entitled "**Kinetic study on removal of Catechol and Resorcinol by Granular Activated Carbon**" coauthored by S. Suresh, V.C. Srivastava, I.M. Mishra at 4th Uttarakhand State Science & Technology Congress-2009 held at GB Pant University of Agriculture and Technology, Pantnagar during 10-12 November, 2009.

INTERNATIONAL PEER-REVIEWED JOURNALS

1. Suresh S., Srivastava V.C., Mishra I.M. Isotherm, thermodynamics, desorption and disposal study for the adsorption of catechol and resorcinol onto granular activated carbon. *Journal of Chemical Engineering and Data* (Communicated 2010).
2. Suresh S., Srivastava V.C., Mishra I.M. Optimization of parameters for adsorption of Aniline-catechol and Aniline-resorcinol onto GAC using Taguchi's experimental design methodology. *Chemical Engineering Research and Design* (Communicated 2010).
3. Suresh S., Srivastava V.C., Mishra I.M. Adsorption of hydroquinone in aqueous solution by granular activated carbon. *Industrial Engineering Chemistry and Research* (Communicated 2010).
4. Suresh S., Srivastava V.C., Mishra I.M. Adsorption of Aniline, Phenol, 4-Chlorophenol and 4-Nitrophenol onto Granular Activated Carbon: Isotherm, Thermodynamics and Relationship with Solvatochromic Parameter. *Chemical Engineering Communication* (Communicated 2010).
5. Suresh S., Srivastava V.C., Mishra I.M. Adsorptive removal of aniline-phenol and 4-nitrophenol-phenol binaries from aqueous solution by granular activated carbon. *Adsorption Science and Technology* (Communicated 2010).

PAPER PRESENTED IN CONFERENCES/SEMINARS

(a) International Conference

6. Suresh S., Srivastava V.C., Mishra I.M. Adsorption isotherm and thermodynamics for removal of Catechol and Resorcinol onto Granular Activated Carbon, *ICSP 2009*, IT BHU, Varanasi, India. Oct. 20-22, 2009.
7. Suresh S., Srivastava V.C., Mishra I.M. Desorption and disposal study for Aniline-loaded Granular Activated Carbon, *ICSP 2009*, IT BHU, Varanasi, India. Oct. 20-22, 2009.
8. Suresh S., Srivastava V.C., Mishra I.M. Studies on simultaneous adsorption of aniline and catechol onto granular activated carbon, *ChemBio tech' 09-10*, NUS, Singapore, Jan. 28-29, 2010.

(b) National Conference

9. Suresh S., Srivastava V.C., Mishra I.M. Kinetic study on removal of catechol (C) and resorcinol (R) by Granular Activated Carbon (GAC), *4th Uttarakhand state Council for Science and Technology (UCOST),* Pantnagar, Uttarakhand, India. Nov. 10-12, 2009.
10. Suresh S., Srivastava V.C., Mishra I.M. Kinetic study on removal of phenol and 4-chlorophenol by Granular Activated Carbon, *62st Annual Session of CHEMCON-2009*, IIChE & Andhra University, India. Dec. 27-30, 2009.
11. Suresh S., Srivastava V.C., Mishra I.M. Adsorption isotherm and thermodynamics for removal of aniline onto Granular Activated Carbon, *62st Annual Session of CHEMCON-2009*, IIChE & Andhra University, India. Dec. 27-30, 2009.
12. Suresh S., Srivastava V.C., Mishra I.M. Equilibrium modeling of binary adsorption of aniline and catechol onto granular activated carbon. *ChEmference 2010*, Indian Institute of Technology Kanpur, India. July 13-14, 2010.